Studies of Photochemical Internalisation: Mechanisms and Strategies in Cancer Therapeutics

Tzu-Wen Wang

National Medical Laser Centre
Division of Surgery and Interventional Sciences
University College London

A thesis submitted in fulfilment of the degree of
Doctor of Philosophy (Ph.D.)

2010

I, Tzu-Wen Wang, confirm that the work presented in this thesis is my own. Where information has been derived from other sources, I confirm that this has been indicated in the thesis.

Abstract

Photochemical internalisation (PCI) is a technique which enhances targeted drug delivery using light in combination with a photosensitiser. It is a modification of photodynamic therapy (PDT) which involves sub-lethal photodynamic treatment to modify the intracellular distribution of co-administered drugs and other agents which are sequestered in lyso/endosomes. In this study, PDT and PCI using a sulfonated chlorin, Amphinex^{TM} ($TPCS_{2a}$), in combination with two anti-cancer drugs, saporin or bleomycin, have been investigated both *in vitro* and *in vivo*.

In vitro experiments initially examined the cell uptake, photostability and cellular localisation of Amphinex using A431 human epidermoid carcinoma cells and HN5 human head and neck squamous cells. The cell killing effect after PDT and PCI in the presence of saporin and bleomycin were assessed. The bioavailability and therapeutic efficacy were also compared with another two PCI photosensitisers, $TPPS_{2a}$ and $AlPcS_{2a}$. The results indicate that PCI is able to induce the relocalisation of bleomycin and saporin inside cells and thereby enhance cell death.

A new porphyrin-peptide bioconjugate of a cell penetrating peptide (CPP) and tetraphenylporphine was investigated for PDT and PCI. It was found that CPP peptide conjugation renders efficient cellular delivery of the tetraphenylporphine for use as a PDT and PCI sensitiser.

The pharmacokinetics of Amphinex in normal and tumour-bearing rats was studied using quantitative fluorescence microscopy and chemical extraction. *In vivo* Amphinex PCI effects and the comparison with PDT were investigated in normal rat liver, colon and a syngeneic rat fibrosarcoma tumour models. Amphinex PCI showed a significant enhancement in inducing damage to normal tissues and tumour. The involvement of apoptosis was also established using the TUNEL assay.

This thesis has demonstrated that Amphinex has favourable properties for PDT and PCI. The consistent results from both *in vitro* and *in vivo* experiments indicate that Amphinex has the potential for further clinical utilization.

Table of Contents

List of Figures and Tables

List of Abbreviations

ALA	5-aminolevulinate
AlS_2Pc	Disulfonated aluminium phthalocyanine (mixture)
$AlPcS_{2a}$	Disulfonated (adjacent) aluminium phthalocyanine
AlPcSn	Aluminium sulfonated phthalocyanine
AMX	Amphinex
AO	Acridine orange
APAF-1	Apoptosis-activating factor-1
ATP	Adenosine triphosphate
BLM	bleomycin
BPD	Benzoporphyrin derivative
CCD	Cooled charge-coupled device
Ce6	Chlorin e6
CLE	Confocal laser endomicroscope
CPP	Cell penetrating peptides
Cre	cAMP response element
DAB	Diaminobenzidine
DMPC	Dimyristoyl phosphatidylcholine
DMSO	Dimethyl sulfoxide
DOTAP	Dioleoyltrimethylammoniumpropane
DPc	Dendrimer phthalocyanine
EGF	Epidermal growth factor
EGFP	Enhanced green fluorescent protein
EGFR	Epidermal growth factor receptor
EGP-2	Epithelial glycoprotein-2
EPR	Enhanced permeability and retention
FITC	Fluorescein isothiocyanate
GM-CSF	Granulocyte macrophage colony stimulating factor
H&E	Haematoxilin and eosin
HIV-1	Human immunodeficiency virus type I
HpD	Haematoporphyrin derivative
HRP	Horseradish peroxidise
i.c.	Intracardiac

i.m.	Intramuscular
i.p.	Intraperitoneal
IRF	Instrument response function
i.v.	Intravenous
i.t.	Intratumoural
LD_{50}	Sub-lethal dose
LDLs	Low density lipoproteins
LIFS	Light induced fluorescence spectroscopy
MDR	Multiple drug resistance
MeOD	Deuterated methanol
MeOH	Methanol
m-THPC	Meta-tetrahydroxyphenyl chlorin
m-THPP	Meta-tetrahydroxyphenyl porphine
MTT	3-(4,5-dimethylthiazol-2-yl)-2,5-diphenyltetrazolium bromide
NDP	Nanozoomer digital pathology
NIR	Near infrared
NPe6	Mono-N-aspartyl chlorine e6
OP	Optical pharmacokinetic
PAMAM	Polyamidoamine
p-gp	p-glycoprotein
Pc4	Silicon phthalocyanine
PCI	Photochemical internalisation
PDD	Photodynamic diagnosis
PDT	Photodynamic therapy
PDT_{50}	Sub-lethal PDT dose
PEG	Polyethyleneglycol
PEI	Polyethylenimine
PIC	Photosensitiser immunoconjugate
PNAs	Peptide nuclei acids
PTDs	Protein transduction domains
PTP	Permeability transition pore
PVA	Polyvinylalcohol
RIPs	Ribosome-inactivating proteins
ROS	Reactive oxygen species
SAP	Saporin

s.c.	Subcutaneous
SCC	Squamous cell carcimoma
SD	Standard deviation
siRNA	Small interfering RNA
Tat	Trans-activating transcriptional activator
TBST	Tris buffer saline tween
TCSPC	Time-correlated single photon counting
$TPCS_{2a}$	Disulfonated tetraphenylchlorin
TPP	Meso-tetraphenylporphine
$TPPS_{2a}$	Disulfonated tetraphenylporphine
TPPSn	Sulfonated tetraphenylporphine
TUNEL	Terminal deoxynucleotidyl transferse mediated dUTP nick-end labelling

Acknowledgements

This thesis was conducted at the National Medical Laser Centre, Division of Surgery and Interventional Sciences, University College London and I would like to thank all the members of the department who have assisted me with its completion. I am particularly grateful to my supervisors Professor S.G. Bown and Dr A.J. MacRobert for their enthusiasm, endless support and advice.

I would like to acknowledge the specific contributions of Dr F. Giuntini, Dr L. Bourre, Dr S. Battah and Dr M. Austwick. I also wish to thank Dr J Woodhams, Mr D. Oukrif and Professor M. Novelli for their help and advice. I would also like to thank Dr A. Høgset (PCI Biotech, Norway) and Professor K. Berg (Norwegian Radium Hospital, Norway) for their support and helpful discussions during this thesis study.

I would like to thank all my colleagues who fill my research life with their ineffable joy. Finally, heartfelt thanks to my friends and family for their constant encouragement and support.

Section A: Background and Introduction

Chapter 1: Photodynamic Therapy

1.1 General Introduction and Early History

Photodynamic therapy (PDT) is a promising treatment which induces damage to the target tissues by using photosensitive drugs with the activation of light. In the presence of sufficient oxygen, cytotoxic agents can be produced upon illumination and initiate the photodamage to tissues. Each component is essential and their combination can achieve a site-specific treatment by the fact of the limited irradiation area.

Although it was only in the last century that PDT began to be used in oncology, the attempt to combine light and certain chemicals to treat illness can be traced to thousands of years ago. Dolmans et al. have summarised the early history of PDT in this review [Dolmans et al., 2003]. In ancient Egypt, India and China, people have used light to deal with several diseases such as psoriasis, rickets, vitiligo and skin cancer. The beginning of modern 'phototherapy' is considered to be in 1903 when a Danish doctor, Niels Finsen, was awarded the Nobel Prize for his work on phototherapy [Finsen, 1901]. Sun light was proven to be beneficial for treating smallpox and cutaneous tuberculosis lesions. In fact, evidence for the therapeutic effects triggered by the combination of chemicals and light has been reported since the early 1900s. Using acridine or eosin together with light exposure could cause the killing effect on microorganisms (infusoria) or skin tumours [Raab, 1900;von Tappeiner and Jesionek, 1903]. A few years later, the term 'photodynamic action' was first mentioned by von Tappeiner and Jesionek to describe this photosensitised reaction in biological systems [von Tappeiner and Jodlbauer, 1907]. Since then, more and more studies have been carried out and haematoporphyrin, a compound with a porphyrin structure, was found to be one of the most powerful photosensitising agents [Figge et al., 1948;Meyer-Betz, 1913].

The purification of haematoporphyrin was another step forward for PDT treatment. Haematoporphyrin derivative (HpD) was isolated by Schwartz et al. [Schwartz et al., 1955] and exhibited better tumour localisation properties [Lipson et al., 1961]. Another breakthrough happened in 1975 when Dougherty and Kelly independently demonstrated that the combination of HpD and red light could eradicate tumour growth using animal tumour models [Dougherty et al., 1975;Kelly et al., 1975]. One year later, Kelly and his co-workers began the first human trial with HpD PDT in bladder cancer [Kelly and Snell, 1976]. The clinical application of PDT was soon expanded for treating many

other early-stage cancers, and PDT with Photofrin® (Porfimer sodium), a further partially purified HpD, was first approved for treatment of bladder cancer in Canada in 1993. Until now, Photofrin® is the most extensively studied photosensitiser, and has been licensed for use in lung cancer, superficial gastric cancer, oesophageal adenocarcinoma, cervical cancer, and bladder cancer among many countries [Brown et al., 2004].

However, Photofrin® is a mixture of monomers, dimers, and oligomers involving ester and ether linkages [Byrne et al., 1990]. It is difficult to reproduce the same composition and to identify the therapeutic effect attributed to individual constituents. Moreover, it has a relatively low extinction coefficient in the red light region and the problem of prolonged skin photosensitivity in patients. As a result, the need for new photosensitisers has arisen and research has aimed for the development of sensitisers with improved properties, e.g. chemically pure, with stronger absorbance at longer wavelength, better tumour specificity and less skin photosensitivity etc. These sensitisers are called second-generation photosensitisers [Moser J.G., 1998] whose basic structures include porphyrins, chlorins, bacteriochlorins and phthalocyanines.

PDT has gone through an era of rapid development since the early approaches to human cancer. The use of diode lasers certainly benefits PDT treatment in many aspects. This intensive, coherent and monochoromatic light source provides efficient and reliable light delivery. A combination with other fibre optic delivery systems also broadens the approachable locations of human disease. To date, PDT has accumulated substantial experiences either in preclinical experiments or clinical studies as a cancer therapy. There several drugs originally developed for PDT which are now clinically approved, as listed in Table 1.1: 5 in oncology, one for fluorescence diagnosis (Hexvix) and two for non-malignant disorders. Several drugs are currently under clinical trial investigation. PDT seems to be a profound modality which can deal with solid tumours appearing in almost all anatomical sites. However, the lack of standard dosimetry and the difficulty in establishing its optimum use have made PDT remain marginal [Brown et al., 2004;Zhu and Finlay, 2008]. The inherent complexity of PDT mechanism is believed to be one of the main reasons. PDT already involves light, photosensitiser and molecular

	Chemical name	Tradename	Time of approval	Indications
Oncology	Haematoporphyrin derivative (HpD), porfimer sodium	Photofrin	First approved in 1993; now approved in a number of countries	Lung cancer, superficial gastric cancer, oesophageal adenocarcinoma, cervical cancer, bladder cancer
	Meta-tetrahydroxyphenyl chlorin (m-THPC), temoporfin	Foscan	Approved in EU, Norway and Iceland in 2001	Head and neck cancer
	5-aminolevulinate (ALA)	Levulan	Approved in USA in 1999	Actinic keratosis of face and scalp
	Methyl aminolevulinate	Metvix	Approved in EU and Australia in 2001	Actinic keratosis, basal cell carcinoma
	Aluminium sulfonated phthalocyanine (AlPcS)	Photosense	Approved in Russia	Head and neck cancer
Diagnosis	Hexyl aminolevulinate	Hexvix	Approved in Sweden (2004) and EU (2005)	Fluorescence diagnosis of bladder cancer
Non-malignant disease	Benzoporphyrin derivative (BPD), Verteporfin	Visudyne	Approved in 2001 in more than 70 countries	Age-related macular degeneration

Table 1.1 Approved PDT drugs for oncology, fluorescence diagnosis and benign disorder [Berg et al., 2005b;Brown et al., 2004;Juzeniene et al., 2007].

oxygen. These components not only can change during treatment but also can influence each other. The variations are also the causes of some conflicting treatment results.

Research has focused on the understanding of the fundamental mechanisms of PDT in a view of chemistry, biology and physics. The development of nanotechnology, molecular biology and the improvement of light sources and detection techniques can certainly improve drug uptake and localisation, standardise treatment protocols and establish optimal dosimetry.

1.2 Mechanism of Actions - Photosensitisation

1.2.1 Photochemistry

The photocytotoxic effect of PDT is caused by a series of photochemical reactions including the excitation of photosensitiser under light exposure and the interaction with surroundings by energy transfer. Figure 1.1 illustrates the process of photosensitisation using the Jablonski diagram. With the absorption of light (a), photosensitisers are excited from the ground state (S_0) to a higher energy state, singlet state (S_1). The photomolecules can thereafter decay to the ground state by emitting fluorescence (b) or to the triplet state (^3S) via intersystem crossing (c). The energy transition from the singlet state to triplet state is unusual because it requires a change of electron spins. However, the fully conjugated double bond system (the macrocyclic structure) of photosensitisers allows this exception. Moreover, because the transition to return to the much lower ground state energy level from the triplet state is "quantum mechanically forbidden", photomolecules can remain in the triplet state with a longer lifetime than the singlet state. Eventually sensitisers at triplet state will slowly relax back to the ground state either via emitting phosphorescence (d) or internal conversion (g).

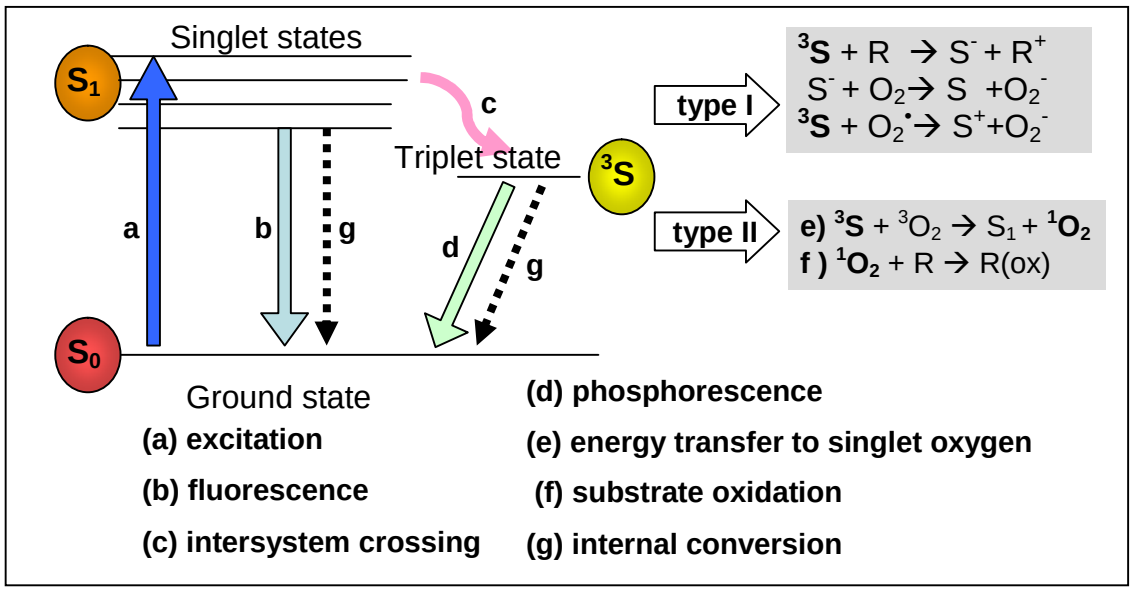

Figure 1.1 Jablonski diagram depicting the photophysical processes following photosensitiser excitation, together with Type I and Type II mechanisms. S_0: photosensitiser in a ground state, S_1: photosensitiser in a singlet excited state, ^3S: photosensitiser in a triplet excited state, R: substrate, S^-: reduced photosensitiser molecule, R^+: oxidised substrate, O_2^-: superoxide anion, $O_2^{\bullet}$: superoxide radical, $^3O_2$: triplet ground state oxygen, $^1O_2$: singlet excited state oxygen, R(ox): oxidised substrate.

Excited triplet photosensitisers (^3S) can react with neighbouring substrates (R) and generate reactive oxygen species (ROS) which lead to cytotoxic effects. This is known as the type I mechanism. In an oxygen-rich environment, ^3S can also transfers its energy to the oxygen molecule (e) to an excited state called singlet oxygen ($^1O_2$) which is highly active and can directly oxidise surrounding substrates (f). This process is classified as type II mechanism.

1.2.2 Singlet oxygen

Oxygen has a unique triplet ground state ($^3O_2$) because its two unpaired electrons reside in separate orbitals (Px* and Py*) in order to comply with the Pauli exclusion principle, resulting in three possible configurations: both spin aligned up or down or one up and one down (Figure 1.2). Two electrons can be paired together in the same orbital when the spin of one electron is inverted during the interaction with excited photosensitisers. The energy transfer produces singlet oxygen ($^1O_2$) which is not stable and thus extremely reactive.

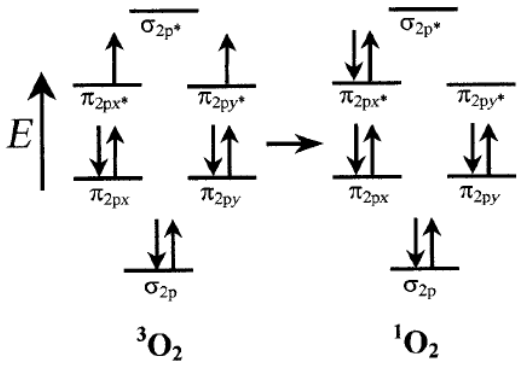

Figure 1.2 Molecular orbital diagrams of the electron distribution in triplet and singlet oxygen [MacDonald and Dougherty, 2001].

Although type I and type II mechanisms can take place simultaneously and the balance is driven by the surrounding substrates, the concentration of oxygen, as well as the sensitisers themselves, indirect or direct evidence from *in vitro* and *in vivo* experiments have proved the importance of singlet oxygen during the photosensitisation process [Juzenas and Moan, 2006;Niedre et al., 2002]. In fact, the significance of singlet oxygen in PDT treatment was already acknowledged in the early stage of PDT treatment since

1976 [Weishaupt et al., 1976]. Singlet oxygen was proposed responsible for the cytotoxicity of PDT in tumour cells.

The lifetime of singlet oxygen in organic solvents can be up to tens of μs but it is only 2-3 μs in aqueous solutions [Egorov et al., 1989], and even lower in cells which means that the reaction area inside cells is confined [Moan and Berg, 1991;Moan, 1990]. On one hand, this character restricts the photodynamic damage to the nearby region where sensitisers locate; on the other hand, it gives PDT a low probability to cause genome toxicity [Evans et al., 1997] since cell nucleus is not a favourable accumulation site for most of the photosensitisers [Moan, 1986].

1.2.3 Photosensitisers and the singlet-oxygen quantum yields

Photosensitisers are chemicals which can be activated by irradiation and then transfer the energy to other molecules. This photo-sensitive character is attributed to their back bone chemical structures. Figure 1.3 shows the structure of the most common photosensitisers used for PDT: porphyrin, chlorin, bacteriochlorin and phthalocyanine.

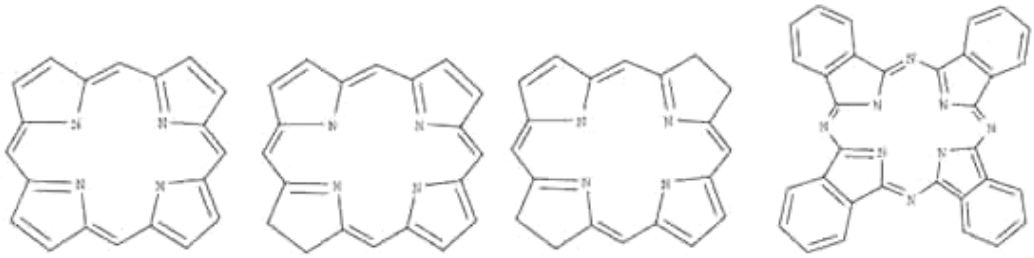

Figure 1.3 Basic structures of porphyrin, chlorin, bacteriochlorin and phthalocyanine.

These compounds are usually planar and aromatic. The core structure is called ‘macrocycle’ which is composed of four pyrroles linked by azone bridges in the case of phthalocyanine or by methine bridges for the others. They are all fully conjugated with double bones (π-electrons). The extensive aromatic (i.e. π-conjugation) structure enables photomolecules to absorb light in the visible spectrum region. The absorption spectra among these compounds are similar with a strong peak at around 400 nm called Soret band and other weaker bands between 600 nm and 800 nm called Q-bands. Generally, red light is preferable for clinical use because blue light penetrates tissue less efficiently and there is a large attenuation of the absorbance up to 580 nm by

haemoglobins. The extended π-conjugation in these molecules results in lower electronic repulsion and therefore lowers the energy of the molecular states involved. A lower transition energy (ΔE) results in longer wavelength absorption according to the equation $\Delta E = hc/\lambda$ where the energy of light is inversely proportional to the wavelength λ (h is Plank's constant and c is the speed of light). Porphyrins have more π-electrons than other photosensitisers because the others have reduced double bonds (chlorin has one double bond reduced and bacteriochlorin and phthalocyanine have two double bonds reduced). As a result, the maximum absorption of porphyrin is around 630 nm, shorter than the peak absorption of chlorin at 650nm and phthalocyanine at 670 nm. Several studies have demonstrated that the small changes in wavelength can lead to improvements in the clinical outcomes such as the increase of penetration depth and the consequent larger treatment volume [Lee et al., 1995;Pantelides et al., 1990]. Based on this advantage, among the 2nd generation sensitisers, chlorin and phthalocyanine are believed to be two of the most efficient photosensitisers for *in vivo* and clinical applications.

There have been many chemical approaches to increase the bioavailability of photosensitisers by the co-ordination with metal irons in the centre or the substitution of the peripheral pyrrole rings on the four methine carbons. These synthesised complexes are meant to have better properties for PDT in many aspects such as improved solubility and stability. For instance, the introduction of sulfonate groups to tetraphenylporphine (TPPSn) and aluminium phthalocyanine (AlPcSn) reduces the tendency of photosensitiser aggregation. Among those sulfonated sensitisers, disulfonated tetraphenylporphine ($TPPS_{2a}$) and aluminium phthalocyanine ($AlPcS_{2a}$) have the amphiphilicity which creates their cellular localisation to membranes because of the hydrophobic and hydrophilic interfaces [Margaron et al., 1996]. This feature has been exploited for photochemical internalisation (PCI) which achieves drug/gene delivery by photosensitisation [Berg et al., 2003;Hogset et al., 2004] and is also the theme of this thesis study. The details of PCI will be described later.

A good photosensitiser should not only exhibit high absorbance of light activation but also yield a high quantity of singlet oxygen after the energy transfer through its triplet state formation. This property is called singlet oxygen quantum yield (Φ_Δ) which is recognised as one of the main determinant of effectiveness of photosensitisers for PDT. A direct method to measure the singlet oxygen is to detect the phosphorescence emitted

at 1270 nm when singlet oxygen returns to the ground state. Measurements can be carried out in water or organic solvents for longer lifetimes [Tanielian et al., 1996]. In Chapter 5, this technique was also used to investigate a new porphyrin-peptide conjugate for PDT and PCI.

Although the importance of singlet oxygen in PDT has been recognised since 1976 [Weishaupt et al., 1976], early attempts to directly measure the Φ_{Δ} generated *in vivo* were not successful due to insufficient detection sensitivity [Patterson et al., 1990]. It was until the innovation of the near-infrared (NIR) photomultiplier tube by Hamamatsu that direct measurement of the singlet oxygen production *in vitro* and *in vivo* became feasible and reliable [Niedre et al., 2002]. Despite no human or clinical data being available yet, directly examining the singlet oxygen luminescence has received considerable attention as a metric for PDT dosimetry along with other traditional approaches such as measuring the photobleaching of photosensitisers or the ground-state oxygen concentration [Jarvi et al., 2006].

The whole photosensitisation process is an incorporation of the involved components: light, drug and oxygen. The therapeutic outcomes rely on how their interactions work within the biological system. For example, at a cellular scale, the site of the intracellular localisation of photosensitisers determines the location where initial photodamage takes place. In animals or human beings, more biological and physiological factors such as the pharmacokinetics of sensitisers, the light delivery and the treatment responses including cell death or triggered inflammatory reaction will certainly influence the overall efficacy of PDT treatment. The following section will discuss PDT on the basis of biology.

1.3 The Biology of Photodynamic Therapy

1.3.1 *In vitro* studies

1.3.1.1 Cellular uptake and subcellular localisation of photosensitisers

Cellular uptake of photosensitisers has been intensively studied during the past two decades. For instance, the relationship between the molecular structure of sensitisers and their extent of cellular uptake has been investigated using zinc phthalocyanines [Margaron et al., 1996] and porphyrins [Oenbrink et al., 1988] in artificial membranes and cells. The structure, charge and hydrophobicity of the photosensitiser are the factors that determine the cellular uptake, subcellular localisation and phototoxicity.

In general, longer incubation time and higher drug dose can result in higher drug accumulation in cells. Additionally, cellular uptake of photosensitisers is under the influence of various parameters such as the temperature, the pH value, and the serum concentration [Bohmer and Morstyn, 1985]. In their study, it was found that HpD exhibited higher cellular uptake in the medium with acidic pH and lower serum concentration. Lower temperature also seemed to inhibit the uptake of HpD in cells. Using the chemical nature of HpD- a complex mixture of porphyrins, Kessel also has reported the different pathways involved in the uptake of photosensitisers [Kessel, 1981]. The hydrophobic components of HpD displayed a rapid accumulation but they were readily washed off from cells, whereas the hydrophilic components of HpD presented a gradual accumulation with stronger affinity to cells. In this regard, different mechanisms may operate the cellular uptake of different sensitisers.

Many photosensitisers are believed to enter the cell through endocytotic pathway and target endo/lysosomal vesicles [Geze et al., 1993]. Based on the molecular properties, several mechanisms of the cell entry and the lysosomal targeting of hydrophobic photosensitisers were suggested. Firstly, highly hydrophobic photosensitisers such as protoporphyrin, photofrin II, and phthalocyanines display some solubility in medium containing serum. After being solubilised by binding with lipoproteins, for example LDLs, sensitisers could be carried by these lipid proteins and localised within the lysosomes. Secondly, photosensitisers with negatively charged or very polar structures, such as the sulfonates of tetraphenylporphine and aluminium phthalocyanine, could

possibly bind to the cell membrane by anionic-ionic interaction. The third group of molecules comprises naturally lysosomotropic photosensitisers, such as Nile Blue derivatives which would localise within lysosomes eventually. In fact, hydrophobic photosensitisers, such as hypericin and m-THPC, have been reported to be able to enter cells through passive diffusion when using serum free medium, whereas, in the presence of serum, these sensitisers will bond to the serum proteins and result in endocytotic cellular uptake [Friberg et al., 2003;Siboni et al., 2002].

Subcellular localisation of photosensitisers is crucial for effective PDT since the main cytotoxic agent, $^1O_2$, has a short lifetime and diffusion distance. Organelles including Golgi, endoplasmic reticulum, mitochondria, lysosomes and membranes have been reported as intracellular target sites for various photosensitisers [MacDonald and Dougherty, 2001].

An adequate accumulation of photosensitisers in cells is essential for effective PDT. The type of photodamage triggered after illumination is clearly dependent on the subcellular localisation of the employed photosensitisers. Therefore, it is important to understand the uptake and intracellular localisation of interesting photosensitisers.

Many of the sensitisers were found to be localised at lysosomes. The lysosomal localisation is the main feature of the photosensitisers used for photochemical internalisation (PCI). Amphiphilicity is the reason for this phenomenon. Details of this group of photosensitisers will be addressed in Chapter 2 and Chapter 4 in the experimental sections.

1.3.1.2 Cell death induced by photodynamic therapy

In general, there are two types of cell death: necrosis and apoptosis. The term of ‘apoptosis’ was firstly described in 1972 as a tight-regulated process of cell suicide which involves series of signalling pathways either intrinsic or extrinsic [Kerr et al., 1972]. Cells which undergo apoptosis are morphologically distinguishable by the cell shrinkage, chromatin condensation and the formation of apoptotic bodies. DNA fragmentation is also one of the features that ‘DNA ladder’ can be found upon gel electrophoresis. *In vivo*, apoptotic bodies are engulfed by phagocytes without the

participation of tissue inflammation. Apoptosis happens naturally and is a regulated process. The loss of regulatory ability (either inhibited or unrestrained) can lead to diseases such as cancer or neurodegenerative disorders [Gorman et al., 1996;Guchelaar et al., 1997]. Stresses from the outside environment such as chemicals, radiation or heat can also induce apoptosis [Robertson and Orrenius, 2000;Verheij and Bartelink, 2000;Zhuang et al., 2000].

In contrast to apoptosis, necrosis is a more acute process which causes cytoplasmic swelling, destruction of organelles and inflammation *in vivo*. After PDT treatment, it was found that cells can die through necrosis or apoptosis or the combination of both pathways, but lower dose of PDT is believed to be capable of inducing efficient apoptosis in many cases [Oleinick and Evans, 1998]. Since the first report of PDT-induced apoptosis [Agarwal et al., 1991], numerous investigations of the occurrence of apoptosis have been carried out. The initiation of this process and the engaged mechanisms differs depending on the photosensitiser, its subcellular localisation and other circumstances. Figure 1.4 shows some of the PDT-induced apoptosis pathways and the involved signalling molecules, particularly associated with mitochondria.

Mitochondria appear to be the central organelles in relation to most of the apoptotic mechanisms. Sensitisers, such as Photofrin [Wilson et al., 1997] and Pc4 (Silicon phthalocyanine) [Trivedi et al., 2000], were found to accumulate at various compartments in mitochondria and evoke mitochondria-mediated apoptosis after photosensitisation. As shown in Figure 1.4, the mechanism begins with the release of cytochrome c oxidase into cytosol, assembles a complex with dATP, APAF-1 (apoptosis-activating factor-1) and pro-caspase 9 and generates active caspase 9, which in turn cleaves pro-caspase 3 to form caspase 3. Caspases (cycteine protease acting on aspartic acid), a family of proteases, are principle enzymes in the apoptosis process. Among them, caspase 3 is the key protein which is responsible for the cleavage and activation of other downstream caspases, leading cells to apoptosis. The release of cytochrome c immediately after photoactivation has been reported in many studies using mitochondria localised photosensitisers [Granville et al., 1998;Kessel and Luo, 1999]. The collapse of mitochondria membrane potential upon PDT was also observed in the later study which might be due to the opening of a large channel called permeability transition pore (PTP) complex. Opening of the PTP complex can change

the concentration of ions (e.g. Ca^{2+}) and may associate with the release of cytochrome c [Green and Reed, 1998].

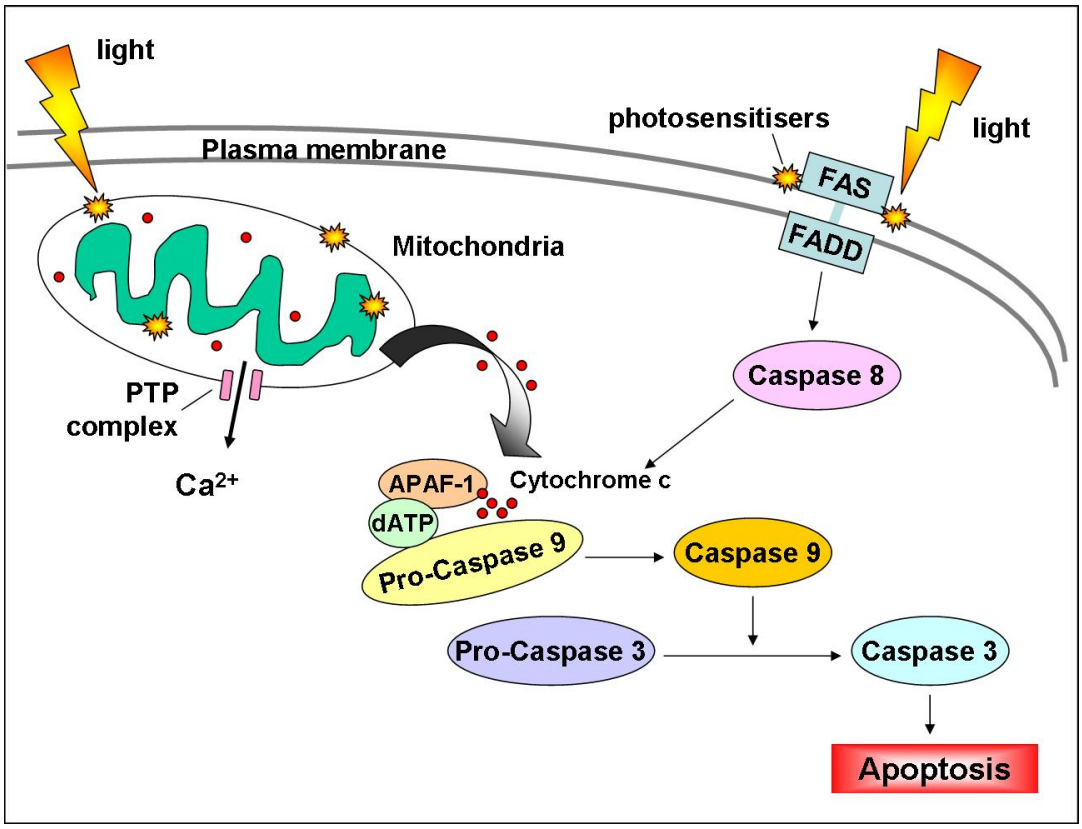

Figure 1.4 Some PDT-associated apoptosis pathways

A separate pathway through the cell surface receptor FAS also has been reported in the induction of apoptosis in response to PDT [Granville et al., 1998]. A delayed activation of caspase 8 was found whose downstream proteins can also induce the release of cytochrome c and lead to the consequent caspase 3 activation (Figure 1.4) [Granville et al., 1999].

The critical influence of the subcellular localisation of photosensitisers on the apoptotic mechanism has been demonstrated in a series studies conducted by Kessel and co-workers [Kessel et al., 1997;Kessel and Luo, 1998;Luo and Kessel, 1997]. Photosensitisers which localise in mitochondria induced rapid apoptosis upon illumination while sensitisers that bind to the plasma membrane or lysosomes displayed non-apoptotic mechanisms and resulted in less efficient killing effects. In another study, apoptosis was observed in the cells irradiated after 24hr incubation of Photofrin when most of the drugs have been internalised, in contrast, necrosis was predominant in the case of cells incubated with drugs for only 1 hr in which drugs were primarily in the cell membrane [Dellinger, 1996].

Further evidence was shown by Noodt et al. who compared the cell death mechanisms induced after PDT with four sensitisers with different degrees of lipophilicity by microscopic examination [Noodt et al., 1999]. After irradiation of sensitisers that localised mainly at mitochondria, increasing number of apoptotic cells was detected during the first 12 hr but apoptotic bodies were not observed. On the other hand, apoptotic cells were not detected until after 12 hr but with the appearance of extensive apoptotic bodies in the cases of using lysosome-localised photosensitisers. The results imply that multiple mechanisms might be involved in the PDT-induced apoptosis.

Using Rose Bengal, a plasma membrane-localised photosensitiser, Zhuang et al. showed that singlet oxygen was generated after the photosensitisation at the cell membrane and stimulated the signalling for apoptosis via FAS receptor pathway [Zhuang et al., 1999]. This is also an example that the cellular localisation of sensitisers plays an important role in the determination of apoptotic mechanisms induced after photoactivation.

There are still a number of other pathways and signalling molecules involved in the regulation of cell death in response to PDT, such as Bcl-2 family proteins [He et al., 1996;Kim et al., 1999] and lipid-derived second messengers ceramide [Separovic et al., 1997;Separovic et al., 1998]. With the development of molecular biology techniques, many convincing results have revealed the possible mechanisms participating in the killing effects of PDT [Moor, 2000;Oleinick et al., 2002]. However, many details remain unclear and require further investigations. It should be noted that some studies have shown that cells could die after PDT treatment without undergoing apoptosis or when some of the apoptotic pathways were blocked [Fisher et al., 1999;Xue et al., 2007]. These results indicate that PDT may be beneficial for some tumours resistant to certain apoptosis inducing chemotherapy or radiation therapy by providing a bypass modality *in vivo* and in clinic practice. Although the *in vivo* data of cell death mechanisms after PDT is limited, some studies have demonstrated that the situations *in vivo* were in agreement with the ones *in vitro* [Colussi et al., 1999;Whitacre et al., 2000;Whitacre et al., 2002].

Recently, another pathway was found to be associated with cell death after PDT treatment. Cells lacking pro-caspase 3 can die after PDT by undergoing a non-apoptotic or non-necrotic mechanism [Whitacre et al., 2002], known as autophagy. This process was confirmed as the dominant cell death pathway when cells are incapable of

undergoing normal apoptosis [Buytaert et al., 2006;Kessel et al., 2006]. Autophagy, which literally means 'self-eating', is also a programmed cell death with the formation of double-membrane vesicles called autophagosomes, encasing cellular constituents (e.g. damaged organelles) [Tsujimoto and Shimizu, 2005]. It was initially discovered as a survival response to nutrient depletion, but it can also provide a protective function against several diseases and infections. When damage is extensive, damaged organelles can be removed through the mechanism by the fusion of autophagosomes and lysosomes/vacuoles, resulting in the lysis of the contents. As a consequence, microscopic observation of autophagosomes (300-900 nm) is usually used as one of the methods to characterise this mechanism. Several studies have demonstrated the involvement of autophagy in response to PDT treatment [Kessel and Reiners, Jr., 2007;Xue et al., 2008]. The later authors proposed that the release of calcium ion by the damage of endoplasmic reticulum or mitochondria may initiate the pathway. Further investigations still need to be carried out.

More discussion of the *in vivo* pharmacokinetics of photosensitisers and treatment response to PDT will be shown in the next sections.

1.3.2 *In vivo* studies

1.3.2.1 Pharmacokinetics of photosensitisers - accumulation, distribution and clearance of photosensitisers in tissue/tumour

In PDT, the first generation photosensitisers haematoporphyrin derivative (HpD) and Photofrin were both found to localise preferentially in tumours in the early stage when discovered [Lipson et al., 1961] and have been well studied since then. As more and more photosensitisers (so-called 2nd and 3rd generation photosensitisers) were identified, detailed pharmacokinetics of sensitisers has been investigated and extensively reviewed [Gomer, 1991;Jori, 1996;Kessel and Woodburn, 1993]. In summary, the biodistribution patterns of photosensitisers are affected by the fundamental properties of sensitisers themselves, the delivery system (the drug formulation and administration methods), and the diverse physiological circumstances between different tissues or species etc. Among them, the hydrophobicity of sensitisers is believed to be one of the major determinants for the drug bioavailability.

Evidence has been reported of the association of hydrophobic porphyrin derivatives (first generation photosensitisers) and plasma low-density lipoprotein (LDL) [Barel et al., 1986;Jori and Reddi, 1993;Kessel, 1986]. This lipid-type transport system certainly contributes to the enhanced tissue uptake of such photosensitising compounds. Moreover, as many tumour cells and certain normal tissues including liver and kidney contain more lipoprotein receptors on the cell surface, the LDL-mediated pathway should favour the accumulation of these sensitisers in those tissues [Maziere et al., 1991;Norata et al., 1984].

Other pathways were also suggested as a few 2nd generation photosensitisers, NPe6 (mono-N-aspartyl chlorine e6), m-THPC (meso-tetraphenylporphyrin tetrasulfonate), and $AlPcS_4$ (Aluminium phthalocyanine tetrasulfonate), which are water-soluble but exert great tumour localisation, were found in strong affinity for albumin [Kessel et al., 1992;Kongshaug, 1992]. Thus, there should be multiple mechanisms for the *in vivo* uptake of sensitisers in respect of their basic features.

Another aspect to be noted is that tissue accumulation results from both localisation and retention. For instance, the initial concentration of Photofrin in malignant tissues was

found to be low but elevated values for the ratio of tumour to normal was observed with time, resulting in preferential retention [Bellnier et al., 1989]. Pottier et al. have reported the influence of tissue and cellular pH value on the biodistribution of porphyrins [Pottier and Kennedy, 1990]. Thomas and Peng have independently demonstrated that lowered pH induced by multiple injection of glucose could facilitate HpD or Photofrin retention *in vivo* [Peng et al., 1991;Thomas and Girotti, 1989]. Hyperglycemic tumours in animals with decreased pH resulted in increased photosensitiser uptake and consequent enhancement in tumour killing. In fact, the intracellular pH (pHi) was measured slightly more basic than the extracellular pH (pHe) in tumour tissues [Gerweck and Seetharaman, 1996]. It is proposed that the decreasing pHe in tumours would make drugs lose their charges and diffuse freely into cells. Further more, the relatively basic intracellular compartment would make drugs ionized again and trapped inside cells. This mechanism might explain why the acidity of tumour favours the uptake of some photosensitisers.

The administration methods would also affect the drug localisation substantially. In order to ease the skin photosensitivity caused by HpD and achieve higher uptake of drugs in tumours, Amano et al. injected drugs intratumourally (i.t.) into mouse bladder tumours, comparing the effect of intraperitoneal injection (i.p.) [Amano et al., 1988]. Several studies also have compared the PDT effect of Photofrin following these two administration modes using different animal tumour models [Brand et al., 1990;Gibson et al., 1990a]. Although, the i.t. route can in some cases be better than i.p. as the former resulted in higher photosensitiser accumulation in tumours and greater photodynamic damage to tumours, the non-uniform intratumoural distribution using i.t. will be a disadvantage.

Systemic delivery of photosensitisers is the most adopted administration routes for PDT as drugs could be distributed to tissues with sufficient amount at times regardless of their location (depth) in the body. Another approach, topical administration, is used widely for PDT in superficial skin disorders. In particular, topical application of ALA (5-aminolevulinic acid) or methyl-ALA has been successfully used for a variety of neoplastic skin diseases [Donnelly et al., 2008]. It is because the drug can be given to the areas of interest within a short interval and without undesirable cutaneous photosensitivity caused by the prolonged drug accumulation from systemic injection. In

fact, topical delivery of methyl-ALA has gained clinical approval for treating skin cancer in Europe (Table 1.1).

2nd generation of photosensitisers were introduced to overcome the drawbacks of HpD and Photofrin including the problems of impurities, low absorbance at red spectral region and prolonged skin photosensitivity. Over the past two decades, there have been numerous pharmacokinetic studies of these sensitisers using different analytic methods on various animal models or on humans. Researches also have focused on the correlation of the biodistribution photosensitisers with their biological effects and photodynamic activities [Barr et al., 1991].

For instance, m-THPC, one of the most powerful photosensitisers, has been intensively studied in animals and humans in the aspects of the biodistribution and treatment efficacy. Glanzmann et al. have compared the pharmacokinetics of m-THPC using LIFS (light induced fluorescence spectroscopy) and its PDT effect in hamster cheek pouch and human oral mucosa [Glanzmann et al., 2000]. The kinetic patterns were observed to be similar in both normal tissues where the maximum uptake is between 3-6 days. However, a quantitative difference was observed of the same drug dose (3 times higher concentration in human mucosa) as well as the different photodynamic responses in each tumour tissue. It should be noted the drug administration for hamsters was intracardiac (i.c.) and it was i.v. for humans.

Another pharmacokinetic study using ^{14}C-labelled m-THPC in transplanted fibrosarcoma in rats was carried out by Jones and her colleagues [Jones et al., 2003]. There seemed to be three half-lives of m-THPC according to the plasma pharmacokinetics and the peak drug concentration in tumours at 24hr after i.v. injection. PDT treatments at 24hr post injection induced the most tumour growth delay which is correlated to pharmacokinetic results. However, treatments at 2hr after injection also achieved significant tumour growth inhibition. Taking the kinetic results and treatment efficacy together, it is suggested that multiple mechanisms might be involved in m-THPC PDT – vascular effect dominates the early-time treatment on tumour while the majority of sensitisers were accumulated in the circulating system; direct cell killing contributes the tumour eradication in the longer-term treatment while most of the sensitiser was localised inside tumour cells.

There also have been attempts of using polymer-sensitiser conjugates to improve the bioavailability and delivery of many photosensitisers. Brasseur et al. examined the pharmacokinetics of hydrophobic aluminium phthalocyanine and its water-soluble polyethyleneglycol or polyvinylalcohol conjugates (AlPc-PEG or AlPc-PVA) by chemical extraction in tumour bearing mice [Brasseur et al., 1999]. A higher retention in the reticulo-endothelial system (liver and spleen) was found compared to other organs in all compounds. AlPc-PVA exhibited the lowest drug level in the RE system, the longest plasma half-life, and the highest concentration of tumour-to-skin ratio among the three. AlPc alone reached the peak uptake in tumour at 6-24hr after i.v. injection while AlPc-PVA was accumulated the most at 24hr and remained stable for 1 week.

This study demonstrates the influence of the conjugation with polymer on the pharmacokinetics of photosensitisers. In fact, the incorporation of carriers (e.g. dendrimers, micelles, liposomes and nanoparticles) with photosensitisers has been exploited rapidly and become one of the major branches PDT development at present [Sibani et al., 2008]. A common aim of these strategies is to perform enhanced permeability and retention (EPR) effect, resulting in better diffusion and retention of photosensitisers within tumours [Iyer et al., 2006]. Other approaches, linking photosensitising compounds to targeted ligands such as antibodies or peptides, have also been designed to achieve specificity [Schneider et al., 2006;van Dongen et al., 2004]. In chapter 5 of this thesis, a porphyrin-peptide conjugate was synthesised to benefit the cellular uptake. Another conjugate coupling photosensitiser with protein toxin was also synthesised for photochemical internalisation. More details about photosensitiser conjugates will be discussed in Chapter 5.

1.3.2.2 The anti-tumour effects of photodynamic therapy and the immune responses

The killing effect of PDT is initiated by the cytotoxic species generated from the photochemical reactions after illumination. The anti-tumour effects of PDT can be categorised into three processes: direct cytotoxicity, vascular effect and immune responses. These three factors are interdependent and together result in the overall outcome while individual contribution is difficult to define [Nowis et al., 2005].

The direct cell death following PDT *in vivo* shows similarity with the *in vitro* situation. Necrosis or apoptosis can be induced through the photodamage. It is generally believed that higher light dose or drug dose has the tendency to cause necrotic cell death. Evidence for the switch from apoptosis to necrosis under increasing PDT doses has been shown using several photosensitisers [Lavie et al., 1999;Vantieghem et al., 1998]. Strategies which manipulate the light fluence rate, the drug-light interval or other parameters have established enhanced PDT efficacy *in vivo* [Gibson et al., 1990b;Sitnik et al., 1998;Tsutsui et al., 2002]. In a study of ALA-PDT, low fluence rate (with extended irradiation or drug delivery time) was found to induce selective killing effects in rat brain tumour, i.e. apoptotic damage to tumour and no detectable damage to surrounding normal tissue [Bisland et al., 2004].

As oxygen is the key factor in PDT, reduced oxygen consumption using fractionated illumination or low fluence rate has been documented in improving treatment outcome [Foster et al., 1991]. It is suggested that the dark interval of the fractionation permits reoxygenation of tissue [Tsutsui et al., 2002]. Higher oxygen concentration was also detected using lower fluence rate PDT in mouse tumour [Busch, 2006]. However, the intratumoural oxygen level is not controlled by a single factor. The oxygen supplier, the microcirculation of the tumour, plays a critical role in the final therapeutic efficacy of PDT. In fact, the photodamage to the tumour vasculature is considered a marked contributing effect in PDT.

Tumour growth is dependent on the blood supply, and therefore, approaches to achieve vascular destruction have brought in new therapeutic opportunities for cancer therapy [Siemann and Horsman, 2009]. In addition to the direct cell kill, the vascular effect of PDT has been reported since early 1980s [Star et al., 1984]. By measuring the oxygen level in tumour, Henderson et al. observed the ‘post PDT’ tumour hypoxia which resulted in a profound tumour cure rate, and thus suggested the inactivation of tumour cells is not limited to the direct PDT effect [Henderson and Fingar, 1987]. It was further confirmed by Fingar et al. that an early photodynamic treatment (within minutes of Photophrin injection) induced vascular damage [Fingar et al., 1992].

The response of the vascular devastation after PDT have been reported similar to the inflammatory reactions after injury or infection [Korbelik, 1996]. The primary

photodamage to the endothelial cells induce downstream chain events such as vessel occlusion, the release of vasoactive molecules, leukocyte adhesion and blood flow stasis and finally lead to ischemic death of tumour cells [Fingar, 1996]. As a result, antivascular PDT has become an upcoming alternate PDT modality to induce cell death by vessel constriction [Zilberstein et al., 2001]. Further studies, focusing on the photodynamic effect in relation to the vascular perfusion and molecular extravasation, also gave more information to understand the mechanism and optimised the treatment conditions [He et al., 2008].

The immune response to PDT is another indirect anti-tumour effect which may act as a secondary cytotoxic mechanism and lead to long-term tumour control. Several researchers have demonstrated that the cure rate of PDT on tumour was lower in immunosuppressed mice than in the mice with normal immunity [Canti et al., 1994;Korbelik et al., 1996]. The resistance to tumour cell rechallenge was found in normal animals but not in immunosuppressed ones who all survived after PDT. Moreover, the curative effect was restored in the immunosuppressed mice after adoptive transfer of T-lymphocytes (from normal mice). These results together pointed out the existence and the importance of the immunity after PDT treatment.

Many studies have proved the recruitment of several immune cells and inflammatory products after PDT. The increased level of cytokines, such as IL-1β, IL-6, IL-10, TNF-α and GM-CSF (granulocyte macrophage colony stimulating factor), have been detected in the serum of animals receiving PDT [Gollnick et al., 2003]. Some of them are associated with the apoptotic killing effect on tumour cells and some are generated from the direct photodamage to the immune cells. These advantages have been applied for developing cancer vaccines – injecting PDT treated cultured cells or the lysates to tumour-bearing mice [Gollnick et al., 2002;Korbelik and Sun, 2006]. These vaccines were found to be able to induce a cytotoxic T-cell response and benefit for tumour growth inhibition, regression and cures.

Common cancer therapies such as chemotherapy and radiation therapy are often immunosuppressive but that is on condition when the doses are sufficient. Lower doses of either treatments have been shown to stimulate the immune system [Crum, 1993;Lugade et al., 2005]. An ideal cancer treatment should not only have a direct killing effect but also have some other impacts to deal with further possible tumour

recurrence or metastasis. In this regard, PDT, being a remedy able to evoke immune responses, may be more desirable for cancer treatment [Castano et al., 2006].

Photoimmunotherapy is a new approach which combines PDT and immunotherapy. It can be a simple combination of PDT and immuno-enhancers to boost specific immune responses [Golab et al., 2000]. The other branch is using photosensitiser-monoclonal antibody conjugates to achieve selective tumour cell localisation and may be useful for tumour detection [del Carmen et al., 2005;van Dongen et al., 2004]. PDT in combination with different immunobiological approaches opens another era to improve the overall therapeutic outcome [Kwitniewski et al., 2008].

1.4 Current Clinical Achievements and Future

Since early 1980s, effective photodynamic effects have been reported in clinical trials for treating cancers. Unlike the conventional chemotherapy, PDT is a site-specific modality where the ablation of tumour is confined to the area exposed to irradiation. Compared to surgery, PDT is non-invasive when treating superficial diseases, or only minimal invasive by combining endoscopy or other fibre-optic systems for treating internal cancers interstitially. The fact that PDT treatment can be repeated is one of the advantages of PDT over radiotherapy where only a limited treatment regimen can be tolerated [Brown et al., 2004]. The outstanding healing response which contributes good cosmetic results, and the greatly reduced morbidity particularly benefits the application of PDT in skin cancer and head and neck cancer [Hopper, 2000].

PDT is already a routine treatment in dermatological oncology. It has been 8-10 years since the clinical approvals of ALA (US) and methyl-ALA (EU) under the indications covering treatment of basal cell carcinoma and some pre-cancerous diseases, and m-THPC for palliative reduction of tumour volume in head and neck cancer in the Europe (Table 1.1). Since then, PDT has demonstrated promising results in treating these two groups of diseases as most of the tumours are accessible to direct light illumination. Nevertheless, there is room for improvements.

In skin cancer, non-laser light sources are usually considered more effective than lasers due to the larger illumination area [Brancaleon and Moseley, 2002]. Small size and low cost are other advantages. However, some disadvantages such as the small penetration depth, as well as the insufficient power resulting in longer treatment time should be taken into account. Long irradiation may cause hyperthermia which may be associated with more pain and burning sensation. Skin photosensitivity is another problem that needs to be improved. Researches regarding the efficacy and safety of PDT are required and will help the applications to other fields of skin diseases.

Some major problems of PDT of head and neck cancers were pointed out in a review article by Kübler [Kubler et al., 2001]. Concerning the limitation of the therapy depth, PDT on oral dysplasia or small primary tumours was only sufficient for very superficial diseases, especially using topically applied ALA PDT [Kubler et al., 1998]. In the case

of squamous cell carcinoma of oropharynx, this malignant tumour tends to spread into the regional lymph nodes of the neck; therefore, there is a risk of lymph node metastasis if patients are only treated by PDT. Up to date, surgery and radiation are still the first choice of therapies for advanced head and neck tumours. But, these tumours are able to be treated with image guided, interstitial PDT [Jager et al., 2005]. Improving the light penetration depth and reducing skin sensitivity etc are tasks for PDT treatment on head and neck cancers in the future.

PDT also has been used in many other diseases in the regions including brain, lung, gastroenterology and genitorurology and has accumulated a substantial number of promising results. Although PDT has been used widely in clinic, it has not been a mainstream therapy in oncology. As mentioned before, there is a need for standard evaluation of the efficacy of clinical PDT. In tumour ablation for instance, the extent of acute tumour necrosis, the duration and rate of this response, and the length of the tumour-free period can be considered as parameters to determine the clinical response or biological endpoint [Huang et al., 2008]. With the development of more selective and effective drugs, inexpensive and convenient light sources, and more understanding of the biology of PDT, the future prospects of PDT remain encouraging.

1.5 Combination Strategies and Photochemical Internalisation

Strategies combining PDT with other therapies have been exploited for enhancing the overall therapeutic effect. Combination with established clinical treatments such as chemotherapy [Canti et al., 1998], radiation therapy [Luksiene et al., 1999], hyperthermia [Henderson et al., 1985] or immunotherapy [Kwitniewski et al., 2008], have shown as good as or better results compared with single treatments are applied alone. This attraction of such combination strategies is that each modality will treat the diseased lesion using a different mechanism which would be expected to result in a more effective overall treatment and enable lower doses to be used. For example, the reduction of the dose of anti-cancer drugs can lower their toxicity to normal tissues. It is important also to distinguish between combinations which are merely additive in effect compared to synergistic combinations, where the combined effect is greater than the effect obtained by applying each modality separately.

PDT in combination with chemotherapy will be discussed in this section which is relevant to the following chapter on the use of Photochemical Internalisation (PCI) to enhance the delivery of anti-cancer drugs by photosensitisation, which is the theme of this thesis. An early attempt was made using HpD-PDT, together with the well known chemotherapy agents cisplatin and doxorubicin, to treat transplanted tumours in nude mice [Nahabedian et al., 1988]. No enhancement was found in the case of PDT in combination with cisplatin whereas the combination with doxorubicin resulted in enhanced anti-tumour effect. The authors suggested the increased activity of doxorubicin (compared to drug alone) may be due to the photochemical treatment. Another study using the same cytotoxic drugs but with AlS_2Pc PDT was carried out by Canti et al. to treat two murine tumours [Canti et al., 1998]. Treatments with non-therapeutic toxin doses were ineffective, whereas additive toxicity was observed in combination with PDT.

Mitomycin C is another chemotherapeutic agent which also has been used in PDT-chemotherapy in vivo. Combination treatments with PDT using Photofrin, m-THPC, or bateriochlorin showed a significant tumour growth delay, even when the light dose was considerably reduced in most of the cases [Baas et al., 1994;van Geel et al., 1995]. Moreover, according to the results of these studies, the administration timing of anti-

cancer drugs to achieve the greatest tumour responses varied when different PDT regimens were used. This finding indicates that the anti-tumour effects derived from PDT and chemotherapy are not independent, and optimising the combined treatment in terms of the administration interval and sequence is important.

The influence of the combination schedule was also found when using cisplatin and doxorubicin [Kirveliene et al., 2006;Uehara et al., 2006]. Zuluaga and Lange proposed several considerations based on the pharmacological mechanism of the anti-neoplastic drugs and their impacts on photodynamic therapy: for example chemotherapy agents can interfere in the cell replication and the subsequent cellular uptake of photosensitisers [Zuluaga and Lange, 2008].

Different techniques such as the introduction of a copolymer to link either toxins or sensitisers [Peterson et al., 2003] and the use of bioreductive anti-cancer agents [Bremner et al., 1992] also have demonstrated significant inhibition in tumour growth. The copolymer conjugates in the former study not only increased the tumour accumulation of the toxins but also prolonged the retention time which enabled multiple PDT irradiations, resulting in a better therapeutic outcome. In the later study, the PDT-induced tumour hypoxia created a favourable environment for the bioreductive anti-cancer drugs, leading to an increased tumour cure rate.

In contrast to conventional combination strategies outline above, PCI is a technology which is designed to enhance drug delivery using light in combination with a photosensitiser. Although the approach is similar to the combination treatment of PDT and chemotherapy, the role of photochemical reaction is to promote the drug delivery to its intracellular targets. The cell killing effect therefore results predominantly from the drug not the photochemical treatment, as will be discussed in more detail in the following chapter.

Chapter 2: Photochemical Internalisation

2.1 General Background

PDT is considered to be a site-specific cancer therapy because the therapeutic effects only take place in the area exposed to light. With the rapid expansion of PDT, many new drugs either chemically or endogenously synthesized have been developed and exploited in various ways. Among them, there is a group of photosensitisers with a unique intracellular distribution pattern observed under fluorescence microscopy.

These photosensitisers enter cells through endocytosis and localize at the membrane of endocytotic vesicles instead of being diffusely localised in the cytosol. Upon irradiation, the generated cytotoxic agents destroy the endosomal membrane and release the content inside these organelles (eg. lysosomal enzymes) [Berg and Moan, 1994;Moan et al., 1994]. Moreover, the redistribution of these sensitisers (i.e. an increase of fluorescence intensity and the change of distribution phenomenon to become diffuse) was also observed. This particular lysosomal photosensitisation and the membrane disruption accompanying the release of content led to the concept of photochemical internalization (PCI) – a novel photochemical technology for inducing the release of macromolecules from endocytotic vesicles [Berg et al., 1999].

Macromolecules generally refer to oligonucleotides, peptides, proteins and polymers whose sizes are normally larger than 1k Dalton. They can serve as alternatives to traditional drugs (e.g. low molecular weight chemotherapeutics) but their bioavailabilities are usually limited [Bareford and Swaan, 2007]. First of all, the cell membrane is normally impermeable to the above large molecular complexes, whereas small molecules such as glucose, ions or amino acids can quickly diffuse into cells. Secondly, even though macromolecules still can enter cells through various active internalisation mechanisms called endocytosis, escaping from endocytotic vesicles to reach the intracellular targets is another problem [Lloyd, 2000].

Lysosomes are known to be the destination of all substances taken up by cells through endocytosis. Their characteristics of storage were discovered by de Duve, one of the pioneers who related lysosomes and drug action together [de Duve, 1969]. Many approaches have been established to improve the uptake of macromolecular therapeutics [Juliano et al., 2001]. There is also growing awareness of a need to develop drug

delivery systems which can efficiently release therapeutics accumulated in endosomes and lysosomes.

The fact that macromolecules retain in intracellular vesicles and remain inactive is not ultimately a hindrance. If their biological effects can be manipulated by a delivery system, these macromolecular drugs will be superior to traditional chemotherapeutics in terms of specificity. In this regard, PCI which causes the rupture of endo/lysosomal membranes during photosensitisation can provide a site-specifically light-induced delivery of macromolecules.

As shown in Figure 2.1, after being taken up by cells, photosensitisers (S) for PCI are localised at the membranes of endo/lysosomes together with the delivered molecules (G) trapped inside the endocytotic vesicles. Upon illumination, photochemical reactions are induced which cause the membrane destruction and consequent macromolecule release.

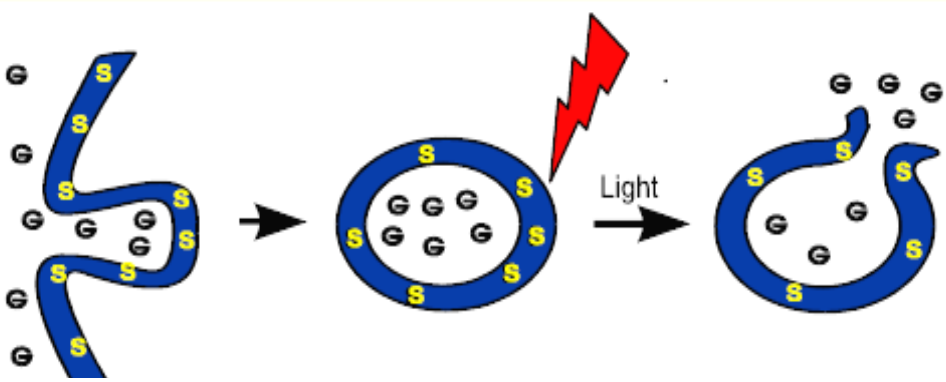

Figure 2.1 The principle of photochemical internalization (PCI) [Hogset et al., 2004]. S: Photosensitiser; G: molecules to be delivered.

It should be noted that the whole PCI process is dynamic and therefore the efficacy is highly dependent on the timing of drug (both sensitisers and macromolecules) administration and light exposure. The illumination should be carried out when sensitisers are sufficiently localised at the biomembranes and the macromolecules have been internalised in endocytotic vesicles but before being degraded by the lysosomal enzymes. As a result, understanding the kinetics of the endocytosis of both sensitisers and macromolecules is very important.

The aim of PCI is to relocalise the therapeutics - escape from the barrier of endo/lysosomal membrane and ability to reach their targets. In other words, the principal considerations are the drug delivery effects and the cytotoxicity from

macromolecules after PCI. Therefore, the light and sensitiser doses required for PCI is much lower than the ones for PDT treatment whose ultimate goal is to kill the whole cell. Moreover, because the therapeutics used for PCI are normally potent drugs but not bioavailable without efficient delivery system, the drug dose can be reduced to extremely small (compared to its LD_{50} dose) using PCI technology. For these reasons, synergistic effects are expected for PCI strategy where individual treatment (i.e. PDT and drug alone) exhibits minor effect but an enhanced killing effect can be achieved when these macromolecules are activated after photosensitisation.

This is different from most of the combination therapies which combine PDT with another treatment modality (e.g. hyperthermia, radiation therapy, antibody therapy or chemotherapy). Although a synergistic response can be obtained if one mechanism influences the other, additive effects are often the results of these combined strategies where treatments are working independently.

PCI has been established to enhance the intracellular delivery of a large variety of macromolecules including peptides, protein toxins and genes (either through viral or non-viral vectors) [Hogset et al., 2004]. It has been shown to be effective for releasing these therapeutics both *in vitro* and *in vivo* [Berg et al., 2006]. However, some details of PCI remain to be investigated such as the exact mechanism of membrane rupture at molecular scale and the optimisation of PCI in terms of the balance of photochemical treatment and drug toxicity.

The later sections in this chapter will discuss the principle, applications, current results and future of PCI.

2.2 Mechanism of PCI Action

2.2.1 Photosensitisers for PCI

2.2.1.1 Entry into the cell – Endocytotic pathway

As mentioned before, essential small molecules such as sugars, amino acids or ions can enter cells through the membrane protein pumps or channels whereas macromolecules must be carried into cells through a process termed endocytosis which involves the formation of membrane-bound vesicles derived from the plasma membrane. Endocytosis is known as a common way for the uptake of extracellular substances. It can be divided in two broad catagories: phagocytosis and pinocytosis. They both play a crucial role in the communication between cells and their environment which involves almost all the cell physiology conditions [Conner and Schmid, 2003]. Unlike phagocytosis which is restricted to specialized mammalian cells (e.g. macrophages, monocytes and neutrophils), pinocytosis, known as fluid-phase uptake, occurs in all cells and transports molecules by forming vesicles coated with a protein layer surrounding the membrane. In pinocytosis, some solutes bind to cell membrane non-specifically, but most of the pinocytic pathways involve specific high-affinity receptors. In those cases, substances are concentrated into specialized endocytotic transport vesicles and taken up into cells more efficiently. There are at least 4 mechanisms of receptor involved endocytosis: macropinocytosis, clathrin-mediated endocytosis, caveolae-mediated endocytosis and clathrin- and caveolae-independent endocytosis. The particular pathway that should be followed for entering cells is well regulated and driven by the cargo molecules themselves.

It has been well documented that many photosensitisers enter the cell through pinocytosis pathway and target endo/lysosomal vesicles, especially hydrophobic photosensitisers [Geze et al., 1993]. However, it is not expected that all endo/lysosome-localised photosensitisers are suitable to be used for PCI. The selection of PCI sensitisers is based on the property of ‘membrane’ localisation at these endocytotic vesicles.

The reason for this requisition is simply to limit the photochemical destruction to the membrane and therefore minimise the possible photo-damage to the delivered

macromolecules in the lumen compartment. As the reactive oxygen species, particularly singlet oxygen, generated from photochemical reactions have a short diffusion distance (10-20 nm) [Moan and Berg, 1991;Niedre et al., 2005], amphiphilic sensitisers are desirable to fulfil this certain criteria.

2.2.1.2 Subcellular localisation

To date, meso-tetraphenylporphine ($TPPS_{2a}$) and aluminium phthalocyanine disulfonate ($AlPcS_{2a}$) are the most efficient photosensitisers for PCI with two sulfonate groups on adjacent phthalate/phenyl rings (Figure 2.2). After being taken up by cells through endocytosis, these sensitisers localise specifically at the membrane of endo/lysomes, with a hydrophobic part inserted into the membranes and a hydrophilic part free inside the vesicle matrix. This amphiphilic feature ensures their membrane localisation and inhibits further penetration (Figure 2.3).

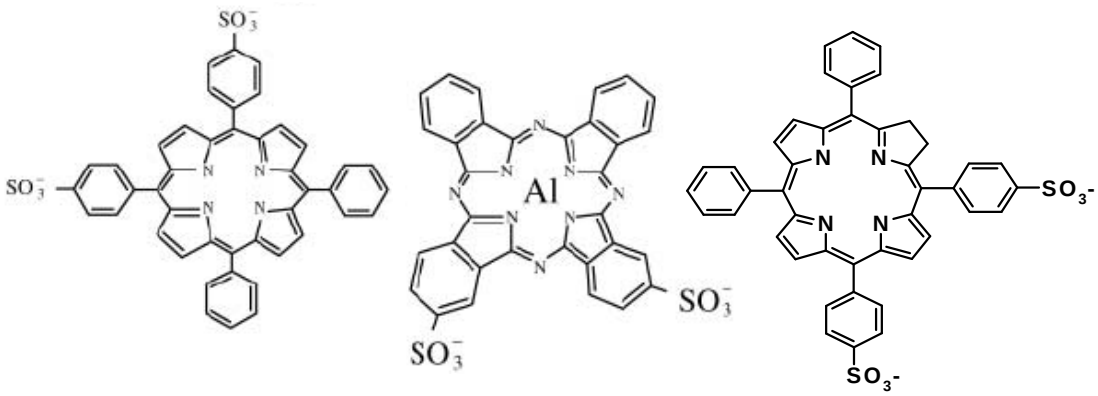

Figure 2.2 The structures and molecular weights of three PCI photosensitisers – (from the left) $TPPS_{2a}$, $AlPcS_{2a}$ and Amphinex ($TPCS_{2a}$).

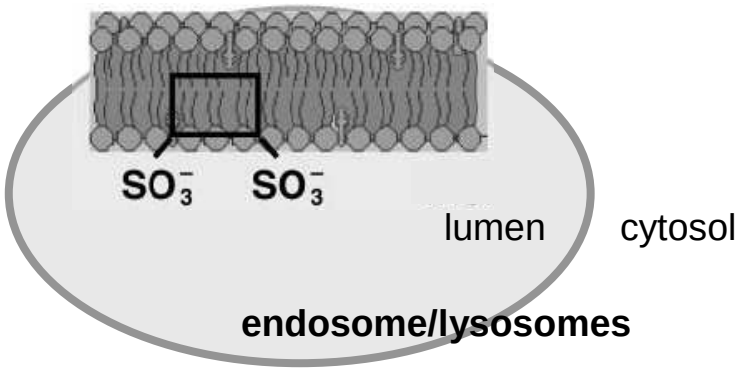

Figure 2.3 Schematic proposed localisation of sulfonated sensitisers in endocytic vesicles. (Modified from [Berg et al., 2005b])

Evidence has been shown that the exact lysosomal membrane localisation is crucial to an efficient PCI effect [Prasmickaite et al., 2001]. To study the impact of intracellular localisation of photosensitisers for PCI, several photosensitisers were tested for their ability to induce macromolecule delivery - polylysine-mediated gene transfection. This study showed that photosensitisers which are localized at the endo/lysosomal membrane (e.g. $AlPcS_{2a}$ and $TPPS_{2a}$) have the greatest effects on the transfection of plasmid encoding EGFP (enhanced green fluorescent protein). In contrast, transfection was not significantly stimulated after photoactivation of non-lysosomally localised photosensitisers (e.g. 3THPP, 5-ALA). Moreover, other hydrophilic sensitisers, such as $TPPS_4$ and Nile blue A, which localise within endocytotic vesicles displayed only weak or negligible EGFP expression after light treatment. As a result, the physical property of photosensitisers determines their intracellular localisations and amphiphilic sensitisers are the best photosensitising compounds for PCI applications.

Amphiphilic sensitisers also exhibit some advantageous photodynamic properties [Allen et al., 2002]. The cell uptake of amphiphilic photosensitisers was detected as good as hydrophobic ones but the tendency to aggregate was lower. This is an important feature as dimerised photosensitisers are less effective in inducing photochemical reactions.

The absorbance spectrum also should be considered in clinical practice since near infrared is preferable for deeper tissue penetration of light. It has been mentioned in section 1.2.3 that phthalocyanines have a porphyrin based macrocycle with four benzo rings on the pyrrol units (Figure 1.3), which results in a strong absorption in the far-red region of spectrum (> 670nm) [Spikes, 1986]. In this regard, $AlPcS_{2a}$ may be preferable

to $TPPS_{2a}$ for *in vivo* or in clinic utilisation. In fact, $AlPcS_{2a}$ is so far the only photosensitiser used for *in vivo* PCI studies.

Amphinex (tetraphenylchlorin disulfonate, $TPCS_{2a}$) is a new chlorin-based amphiphilic photosensitiser (PCI Biotech, Norway) which is designed for PCI (Figure 2.2). The chemical synthesis of Amphinex is rather simpler than $AlPcS_{2a}$ and it is proposed to be as efficient as the well known chlorin sensitiser, m-THPC, regarding the photodynamic ability. The investigation of PCI using Amphinex *in vitro* and *in vivo* will be shown in the experimental sections of this thesis.

2.2.2 Light Induced Drug Delivery

Figure 2.1 depicts the principal mechanism of photochemical internalisation. It contains three processes: the uptake of photosensitiser and macromolecules, the illumination and induced membrane rupture, and finally the release of macromolecules. After diffusing into the cytosol, macromolecules can thereby perform their pharmacological action when reaching their targets. As PCI also utilises the same photochemical reactions as PDT, the fundamental requirements, such as the presence of oxygen and sufficient photosensitisers, are also essential to PCI. The key step is the photochemically induced membrane rupture.

Although a wealth of published studies have demonstrated that PCI can release a variety of macromolecules from endosomes and lysosomes to cytosol, the detailed mechanism of membrane break is not fully understood. Some results from other photosensitisers indicate a possible mechanism of membrane destruction that the generated reactive oxygen species damage the membrane proteins rather than oxidation of membrane lipids of mitochondria and erythrocyte [Belzacq et al., 2001;Zavodnik et al., 2002]. However, whether this is also the case of PCI awaits further investigations.

The role of different endocytotic vesicles for PCI-directed gene transfection has been studied by Prasmickaite and her co-workers [Prasmickaite et al., 2000]. Using different strategies to perturb the endocytotic uptake of DNA-polymer complexes, the results showed that plasmid can also be released from early endosomes.

In contrast to the conventional concept of PCI that irradiation should be carried out when the internalisation of macromolecules and photosensitisers has been completed, another strategy called ‘light before’ PCI has been found to be as effective as or even better than ‘light after PCI’ in some cases *in vitro* [Prasmickaite et al., 2002]. The possible mechanism is shown in Figure 2.4. Photochemical treatment is performed after photosensitisers have been localised at the membrane of endocytotic vesicles. When cells are incubated with molecules to be delivered, the molecules will be taken up through endocytosis as well and the vesicles may fuse with the ones damaged by light treatment, resulting in the release of molecules.

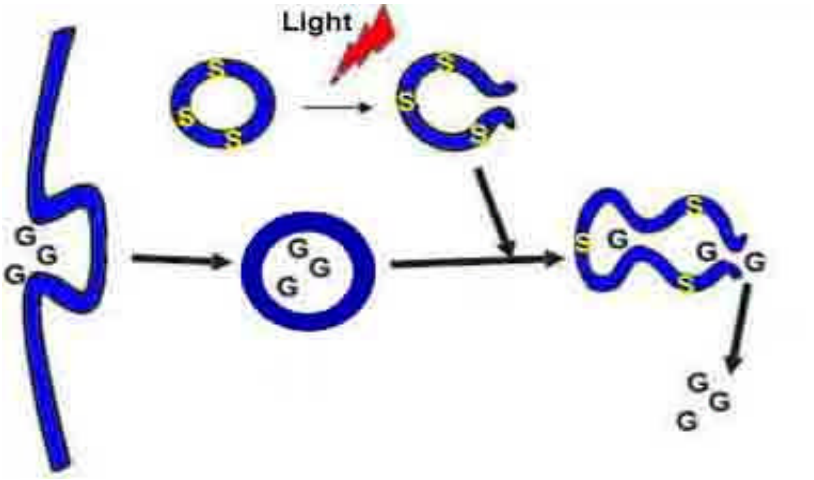

Figure 2.4 Possible mechanism for ‘light before’ PCI. Modified from [Hogset et al., 2004]. S: Photosensitiser; G: molecules to be delivered.

It is suggested that, following this ‘light before’ procedure, macromolecules can leak out immediately once the endocytotic vesicles with delivered macromolecules are fused to photochemically destructed ones. Several advantages are proposed, firstly, that the possible photochemical effects on the therapeutics should therefore be diminished as those drugs are delivered after illumination. Secondly, it may be more practical in animal models or in clinic in the case when PCI is in combination with surgery. After surgical removal of tumours, light treatment can be carried out for residual disease, followed by the administration of therapeutics. This will be difficult for ‘light after’ PCI because the period of several hours between drug application and irradiation is not appropriate during surgery.

However, no differences were observed regarding the results between both strategies when delivering transgene [Prasmickaite et al., 2002]. Therapeutics dependence is

clearly an assumption. It is not unexpected that PCI effects were also found to be cell line dependent [Hogset et al., 2004]. The uptake of photosensitisers and macromolecules varies between cell lines and so does the light sensitivity. In fact, these are all the factors which relate to the optimisation of PCI treatment conditions. Despite the unclear mechanism, the significant release of large particles such as viral vectors indicates that PCI provides a remarkable drug delivery platform. A successful PCI should be well planned and the photochemical reaction has to be efficient, precise and well timed, in respect to the incorporated therapeutics.

2.3 PCI Applications

2.3.1 Macromolecular delivery

2.3.1.1 Type I ribosome inactivating proteins

The studies of PCI-induced delivery of protein have mainly focused on ribosome-inactivating proteins (RIPs), a group of protein toxins which inhibit protein synthesis by damaging ribosomes catalytically. RIPs are usually divided into two groups (Figure 2.5A): Type II RIPs consist of an enzymatically active A chain (30 k Dalton, approx.) linked to a B chain (35 k Dalton, approx.) which contains a binding domain. Type I RIPs, however, which only consist of the A chain, are hardly taken up by cells.

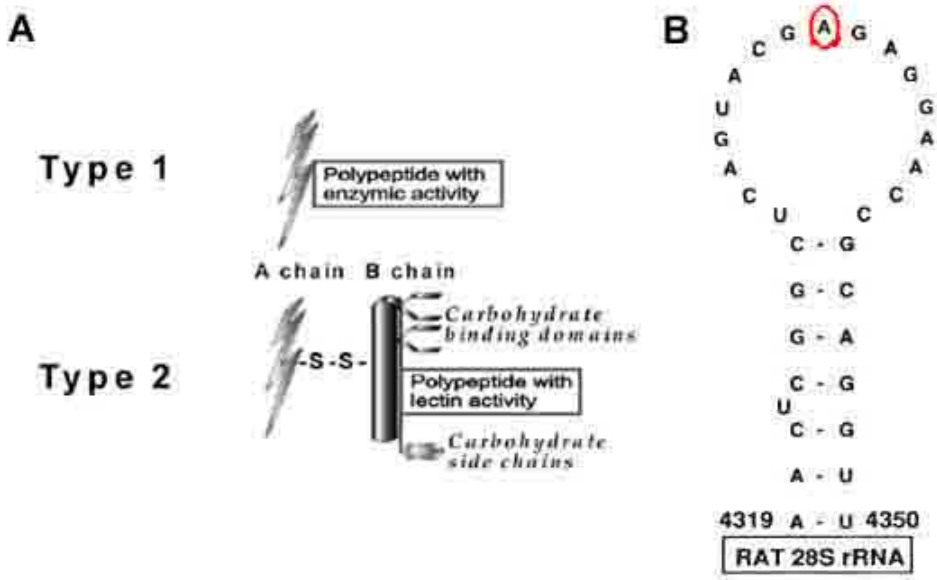

Figure 2.5 A: Schematic representation of ribosome-inactivating proteins (RIPs) [Stirpe, 2004]. B: Rat 28S rRNA loop and the site of depurination by RIPs. The red circle is the A_{4324} adenine resi due, the target of RIPs.

The toxicity of RIP toxins was discovered in the early 1970s when it was found that protein synthesis can be inhibited by ricin, one of the type II RIPs, in cells and cell-free systems [Montanaro et al., 1973;Montanaro et al., 1975]. The inhibition of the binding of elongation factor 2 (EF-2) to ribosomes by this plant toxin was identified. The detailed enzymatic activity was later confirmed by Endo and colleagues who showed that the toxin exhibits a removal of a single adenine residue (A_{4324} in rat liver rRNA) from a universally conserved loop at the top of a stem in 28S rRNA (Figure 2.5) [Endo

et al., 1987]. This phenomenon was extended to all RIPs, which all have similar activity [Stirpe et al., 1988].

The absence of a B chain with a binding domain indeed limits the entry of type I RIPs into cells and justifies their very low toxicity to cells and to animals compared to type II RIPs, with LD_{50} for mice of 40-75 mg/kg [Battelli, 2004]. However, if they are delivered into cells, they can induce efficient inhibition of protein synthesis. Several strategies have been employed to improve the cellular delivery of type I RIPs including enclosing them in drug carriers (reviewed in [Barbieri et al., 1993]), subjecting cells to shock waves [Delius and Adams, 1999] and conjugating to antibodies [Thorpe et al., 1985]. These protein toxins are ideal model proteins to evaluate and demonstrate PCI effects.

Gelonin and saporin are two type I RIP toxins which are mostly used in PCI strategy. The effect of PCI-induced delivery of gelonin has been investigated using several photosensitisers in 16 cell lines of various origins [Berg et al., 1996]. The best results were found using $TPPS_{2a}$ PCI of gelonin in NHIK 3025 cells where protein synthesis was significantly reduced by more than a factor of 300 compared to each treatment alone [Berg et al., 1999]. Co-localisation of fluorescent probe-labelled gelonin and photosensitiser, $AlPcS_{2a}$, and the re-localisation of both molecules were observed by fluorescence microscopy [Selbo et al., 2000a].

Saporin is another type I RIP which exerts much higher toxicity than gelonin [Bolognesi et al., 2000]. As a result, it is believed that saporin has the potential to affect protein synthesis and thereby induce cell death in use of PCI more efficiently. Lai et al. investigated the PCI effect using $AlPcS_{2a}$ in combination of saporin *in vitro* [Lai et al., 2008]. In addition, the introduction of polyamidoamine (PAMAM) dendrimer to saporin showed an increased cellular uptake and cytotoxicity using PCI. Interestingly, after PCI, the distribution of PAMAM-saporin conjugates was observed to be a nuclear-localisation which was different from the granular distribution in the cytosol before illumination.

To increase the uptake and specificity of protein toxins, antibody-conjugated gelonin and saporin have been developed for PCI. Details will be discussed in the section on targeted macromolecules.

2.3.1.2 Bleomycin

Bleomycins are a family of water-soluble glycopeptidic antibiotics with at least four functional domains mediating DNA breakage, ion binding and O_2 activation (Figure 2.6) [Hecht, 2000]. Since first isolated by Umezawa in 1966, bleomycins have been used in combination with several anti-cancer agents for a number of cancer chemotherapies, notably squamous cell carcinomas and malignant lymphomas [Sikic et al., 1985].

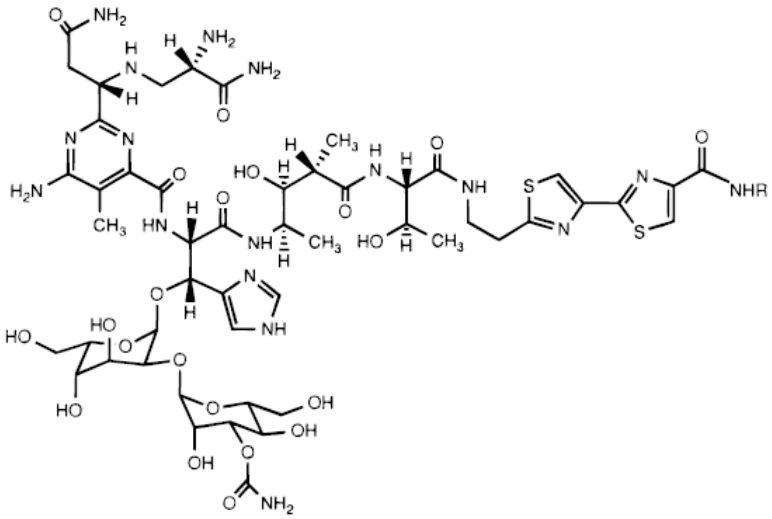

Figure 2.6 Structure of bleomycin [Hecht, 2000]. Molecular weight:1400.

With a very high cytotoxicity, as few as 500 bleomycin molecules translocated to cytosol are sufficient to kill a cell in combination with electroporation *in vitro* [Poddevin et al., 1991;Pron et al., 1999]. However, due to its hydrophilic property, bleomycin penetrates membrane structures poorly and therefore accumulates in endocytic vesicles. The sensitivity of tumour cells to this drug is accordingly variable. Although many fundamental properties of bleomycin are still unknown, its therapeutic potential could be activated if delivered and exported sufficiently into cytosol.

PCI has demonstrated enhanced cell growth inhibition in combination with bleomycin in vitro [Berg et al., 2005a]. As bleomycin is a current chemotherapy drug, *in vivo* studies of PCI of bleomycin using $AlPcS_{2a}$ also have been carried out in xenograft mice models. Details of PCI of bleomycin using animal models will be discussed in the *in vivo* section.

2.3.1.3 Targeted macromolecules - Immunotoxins

The targeting strategy was developed due to the demand of specific and efficient drug delivery system, especially in *in vivo* studies. Immunotoxins are one of the designs which link antibodies with specific binding function to therapeutics. Protein toxins are usually used for this conjugation approach and the conjugates should meet several criteria to be used in clinical practice for cancer treatment: a high toxicity, a linker modification and survival from the endocytotic process [Johannes and Decaudin, 2005]. Because the number of receptors presenting on the cell surface is usually less than 10^5 molecules per cell, it is important to have very high toxicity to kill targeted cells efficiently. To combine the antibody and the toxin, a linker is sometimes required to synthesize immunotoxins. Moreover, most toxins enter the cell through the endocytotic pathway. Therefore, the toxin must be able to survive from the acidic compartments of endo/lysosomes and the proteolytic process.

Immunotoxin therapy has been developed to treat cancer by linking tumor-targeting ligands or antibodies to toxins, which are mainly bacteria or plant protein toxins. The aims of combining targeting ligands are to achieve tumour specificity and a favourable biodistribution between normal and tumour tissues. Since cooperation of PCI and RIPs has inactivated protein synthesis efficiently, the use of immunotoxins- monoclonal antibody conjugated type I RIP is believed to be able to increase the drug uptake and specificity.

The first studies of PCI in combination with immuno-RIP conjugates were introduced by Selbo et al. coupling of monoclonal IgG_1 antibody MOC31 with gelonin [Selbo et al., 2000b;Selbo et al., 2001a]. This conjugation enables gelonin to directly bind to epithelial glycoprotein-2 (EGP-2) which is expressed on most carcinoma cells, resulting in increased uptake of the conjugates. The cell viability was significantly reduced using $TPPS_{2a}$, $AlPcS_{2a}$ and ALA PCI compared to immunotoxins alone. Moreover, the results also show that there was no difference between immunotoxin and toxin alone in the case of using PCI in EGP-2 negative cell line. The specificity might be very useful for *in vivo* application.

Epidermal growth factor receptor (EGFR) targeting is one of the most common strategies to achieve specific cancer therapies. EGFR is involved in regulating cell

proliferation, metastasis, angiogenesis and is over-expressed in a variety of tumour cell lines [El-Rayes and LoRusso, 2004]. The EGFR inhibitor, C225, has been used as an anti-cancer drug in Phase-I to Phase-III trials for several malignant diseases, most notably colorectal and head and neck cancer.

It may therefore be a good combination employing EGFR targeting system to PCI. Weyergang et al. established an EGF-saporin affinity toxin (biotin-straptavidin linkage) to investigate the PCI effects using EGFR over-expressing and EGFR-negative cell lines [Weyergang et al., 2006]. PCI of EGF-saporin enhanced the cytotoxicity about 1000-fold in NuTu-19 cells. Researchers from the same group later demonstrated increased cytotoxicity by using PCI in combination with saporin-C255 complex (via the same linking method) in EGFR-positive cells [Yip et al., 2007]. The efficacy and selectivity of this combination of PCI and EGFR targeting system indicate it can be of benefit for cancer therapies in clinic.

2.3.1.4 Multidrug resistance

Since PCI has been employed for enhancing the cellular uptake of drugs which have difficulties in entering the cell, it is predicted that PCI might be able to reverse the multiple drug resistance (MDR) of chemotherapy agents. Two main mechanisms for MDR are the overexpression of p-glycoprotein (p-gp) efflux pumps and the entrapment of anticancer drugs in endosome/lysosomes. The former leads to the extrusion of drugs from cytosol and the later induces the degradation of drugs by lysosomal enzymes [Gottesman et al., 2002]. As a result, weak base chemotherapeutics such as doxorubicin are often trapped in endocytotic vesicles due to the increased acidification of these intracellular compartments. In this respect, PCI might have the potential to deal with multiple drug resistance, which is a serious problem affecting many chemotherapy drugs.

It was firstly established by Lou et al. that successful reversal of drug resistance can be induced by PCI [Lou et al., 2006]. After $TPPS_{2a}$ PCI treatment (doxorubicin was administered after irradiation), doxorubicin was observed in the nuclei of MCF-7/ADR cells (a breast cancer cell line which is resistant to doxorubicin) and the drug dose required for 50% inhibition of cell survival was reduced to 10 times lower.

Another study using similar concepts also indicated the PCI effects on the improvement of drug resistance. The cytotoxicity of mitoxantrone (a chemotherapy agent) against its drug resistant cancer cells sensitised with hypericin (a photosensitiser) was enhanced after illumination [Adigbli et al., 2007]. The mobilisation of mitoxantrone to cell nuclei was also found after light exposure.

As mentioned before, there are many different phenotypes of drug resistance and some mechanisms may not be affected by PCI treatment. Selbo et al. reported that $TPPS_{2a}$ PCI has no influence in reducing the level of resistance to doxorubicin for MES-SA/Dx5 cells, a MDR cell line [Selbo et al., 2006]. However, PCI of gelonin successfully reduced the cell survival. The results suggest that PCI may not be able to adjust the drug sensitivity for some MDR cells, but it still can be useful as a cancer treatment when in combination with other macromolecules.

2.3.1.5 Other macromolecules

PCI also has been employed to release some peptides or small proteins efficiently. It was reported that more than 60% of endocytosed horseradish peroxidase (HRP) can be released into cytosol by using $TPPS_{2a}$ PCI. Similar findings were also obtained when it was shown that fluorescein-labelled ras peptide ($p21^{ras}$), a cancer-specific peptide was co-localised granularly with $AlPcS_{2a}$ in cells but became diffuse in cytosol after light exposure [Berg et al., 1999].

Oligonucleotides are a group of macromolecules with recognised therapeutic potential. Some of these molecules exhibit antisense effects, resulting in the replication of uncorrected DNA sequence or site-specific gene silencing from the host cell. Peptide nuclei acids (PNAs) are examples for the former action which are DNA mimics with a pseudopeptide backbone [Pooga et al., 2001]. Small interfering RNA (siRNA) molecules are the examples for the later mechanism which are able to control gene expression through the process of RNA interference [Dykxhoorn et al., 2003]. The inefficient cellular uptake is the major obstacle for both therapeutic agents [Koppelhus et al., 2002]. As a result, several strategies, including PCI, have been explored to enhance the drug delivery.

Recent studies have clearly shown that PCI represents an efficient delivery system for naked PNA conjugated with the catalytic component of human telomerase reverse transcriptase (hTERT-PNA) [Folini et al., 2003] and various cell penetrating peptides (CPPs-PNA) [Shiraishi and Nielsen, 2006]. As for siRNA molecules, substantial gene silencing was induced by PCI-mediated gene transfection of siRNA molecules against S100A4, a protein associated with the invasive and metastatic phenotype of cancer cells [Boe et al., 2007]. These promising *in vitro* results open the future applications using PCI technology for activating the biological antisense effects of oligonecleotides on animals or humans.

2.3.2 Gene delivery

The basic principle of gene therapy is that insertion of corrective genetic material into cells alleviates the symptoms of disease. However, there are some obstacles, and consequently few successes in gene therapy. The three main problems of gene therapy are the lack of efficient delivery systems, the lack of sustained expression, and the host immune reactions *in vivo* [Verma and Somia, 1997]. PCI, as a novel technology for releasing macromolecules from endosomes to cytosol, could provide efficient delivery for gene therapy.

Recent studies have shown encouraging results in gene transfection via either viral or non-viral vectors. $AlPcS_{2a}$ based PCI-induced EGFP/polylysine complex delivery was tested and the transfection efficiency reached above 50% of surviving cells [Hogset et al., 2000]. PCI using different photosensitisers has also been examined to induce EGFP transfection and a light dependent transfect efficacy was found [Prasmickaite et al., 2001].

In addition, various delivery agents have been evaluated in PCI mediated gene transfection. It was found that PCI enhanced transfection using polycationic vectors (e.g. polylysine or polyethylenimine (PEI)), but cationic lipid vector-mediated transfection (e.g. DOTAP (dioleoyltrimethylammoniumpropane) was inhibited [Prasmickaite et al., 2000]. One possible explanation suggested was that the photochemical treatment might perturb the dissociation of DNA/DOTAP complex and cause DNA inactivation. Although the exact reason is still unknown, this finding warrants further mechanistic study of both PCI and gene delivery.

PCI mediated delivery requires administration of both photosensitisers and candidate drugs or genes. There is a new design devised a complex composed of a core DNA packaged with cationic peptides and enveloped in the anionic dendrimer phthalocyanine (DPc) [Nishiyama et al., 2005].

The concept was to reduce the administration of photosensitisers and drugs into one and was thought to be more suitable for *in vivo* application due to the integration of photosentisers and DNA/polymer complex. The preliminary results showed lowered

photocytotoxicity and increased cell viability compared to $AlPcS_{2a}$ mediated PCI in gene transfection. This study is also the first success in PCI-mediated gene delivery *in vivo* with transgene expression in conjunctival tissues of rats.

Gene delivery through viral vectors is usually regarded as a very efficient process because of the natural occurrence of virus infections [Anderson, 1998]. However, after being taken up into cells through endocytosis (mostly) [Greber et al., 1993], virus-DNA complex may still be trapped inside the endocytotic system in cases of some virus vectors or in certain cell lines [Hansen et al., 2000].

PCI-mediated gene transfection by adenoviral vectors was firstly introduced by Hogset et al. using β-galactosidase-encoding adenovirus [Hogset et al., 2002]. Pronounced transduction efficiency was obtained and the amount of virus dose was significantly lowered to achieve the same results using PCI compared with conventional adenovirus transfection (no illumination).

A later study investigated the transfection efficacy of PCI-induced transduction of polycation-complex adenovirus using several cell lines [Bonsted et al., 2004]. The efficacy was found to be cell type dependent but positive transgene expression were observed in all cell lines including cells with low or without the receptors to adenovirus on the cell surface.

Altogether, PCI has the potential of being a useful technology for *in vitro* and *in vivo* gene delivery and gene therapy but optimization of PCI-mediated gene delivery is still needed.

2.3.3 *In vivo* PCI for cancer treatment

For *in vivo* PCI, most of the studies were performed in tumour using nude mice transplantation xenograft models; $AlPcS_{2a}$ is the only photosensitiser employed so far. The first *in vivo* PCI study was carried out using $AlPcS_{2a}$ PCI of gelonin in a transplanted human colon adenocarcinoma model [Selbo et al., 2001b]. PCI treatments delayed the tumour growth and resulted in complete remission in 6 out of 9 animals whereas only one of six animals in the PDT group achieved complete remission. A different strategy in which gelonin was administered after light treatment also demonstrated inhibition in tumour growth comparable to the result using gelonin before light [Berg et al., 2006].

Dietze et al continued the previous study but using the human fibrous histocytoma xenograft model in nude mice [Dietze et al., 2005]. $AlPcS_{2a}$ was observed well distributed in tumour cells with a roughly constant concentration at the time of surgery (48hrs after intraperitoneal (i.p.) injection). Gelonin also could be detected in tumour at the time of light treatment (6hrs after intratumoural (i.t.) injection) although the level in tumour was found decreasing with time after drug administration. 50% of the animals receiving the $AlPcS_{2a}$ PCI of gelonin treatment remained tumour free after more than 100 days where the complete response was only found in 10% in the PDT group. The histological results showed that PCI could induce deeper damage than PDT in this tumour treatment.

Bleomycin also has been used for *in vivo* PCI in four different xenograft tumours in nude mice [Berg et al., 2005a;Norum et al., 2009a]. A synergistic delay in the tumour growth was found in all models after PCI of bleomycin. The tumour re-growth in the peripheral zone was inhibited by PCI treatment according to histological analysis of the samples 7 days after surgery. A further study also indicated that PCI treatment could act as an adjunct to surgery, resulting in the delay of tumour growth in a human fibrosarcoma model [Norum et al., 2009b]. This finding suggests that PCI might be suitable for treating residual tumour cells after inadequate surgical resection from the clinical point of view.

2.4 Future and Clinical Application

PCI is attracting interest as a novel technology for improving macromolecular drug delivery to cells. The key advantage of PCI is the site specificity due to the light-dependent activation of a photosensitiser which is co-administered with the macromolecule. The photochemical effect only takes place in areas under light exposure.

Additionally, PCI has the potential to approach different cancer treatments when in combination with different therapeutic agents since various macromolecules have been shown to be released by PCI and their size can range from small peptides to genetic materials. Combination with specific ligand targeted drugs may therefore improve the specificity of PCI treatment *in vivo* by directing drugs to antigen presenting tumour cells through receptor-mediated endocytosis.

As described previously, synergistic effects are obtained in PCI treatment because both the PDT dose (the dose of light and photosensitisers) and drug dose are reduced. The killing effect originating from the photochemical reaction is beneficial to cancer therapy where the final goal is to kill the malignant cells, whereas it might be a disadvantage for gene therapy. The possibility of the damage to the internalized DNA following photochemical treatments might cause DNA mutations or further dysfunction which could affect normal gene expression.

Toward this point, optimization of the treatment conditions should therefore be emphasized again. The ‘light before’ method of PCI might also provide an alternative approach to minimise the potential photodamage to delivered DNA complexes. The detailed mechanisms behind PCI also need further investigations since PCI involves the participation of delivered therapeutic agents which makes the whole procedure more complicated compared with PDT.

Collectively, PCI is a promising technology to improve a cytosolic delivery of macromolecules *in vitro* and *in vivo*. It is important to point out that PCI is in the stage of its first clinical trial using Amphinex PCI in combination with bleomycin for head and neck cancers in University College London Hospital. As a cancer treatment, the challenges will be the same as what PDT faces: the benefit of its therapeutic effects

against the conventional well-established therapies, such as chemotherapy, radiation therapy and surgery. The fact that PCI seems flexible for delivering a variety of anti-cancer drugs broadens the future applications of PCI in clinic to deal with different cancers.

Chapter 3: Aims of Thesis

Aims of Thesis

This thesis firstly aims to investigate the *in vitro* PCI effect using $TPCS_{2a}$ (Amphinex), a new amphiphilic chlorin based photosensitiser, in comparison to two other photosensitisers, $TPPS_{2a}$ and $AlPcS_{2a}$, with A431 and HN5 cells. The cellular uptake, subcellular localisation/relocalisation after irradiation, phototoxicity and the ability of inducing PCI effect in combination with two anti-cancer drugs, saporin and bleomycin will be examined. The photostability and photosensitising process will be also assessed by looking at the intracellular photobleaching properties and photomodification upon exposure to light.

The next objective is to investigate the PCI effect *in vivo* starting with the biodistribution of Amphinex in healthy rats. The drug uptake in several organs at different time points after administration will be examined using quantitative fluorescence microscopy. The absorption spectrum of Amphinex will also be measured in rat liver using an optical pharmacokinetic system. The *in vivo* optical properties of Amphinex can be informative for optimising the wavelength of the light source suitable for activating Amphinex *in vivo*.

The next aim is to investigate the PCI effect with Amphinex in normal rat tissues and a transplanted tumour model. Experiments begin with the Amphinex PCI treatments in combination with saporin and bleomycin on normal rat liver/colon. The interplay between the dose of Amphinex and the light fluence, as well as the influence from the doses of toxins and their administration time points on the therapeutic efficacy will be examined by histological examination of the size of necrosis induced after treatments. Studies will later focus on the treatments on tumours using a syngeneic transplanted rat fibrosarcoma model. Further experiments will also be carried out to look at the PCI mechanisms *in vivo*.

Finally, the possibility of using new photosensitiser bioconjugates will be studied in an additional chapter to investigate the use of bioconjugation strategies for PCI applications.

Section B: *In Vitro* Studies

Chapter 4: PCI Treatment *In Vitro*

4.1 Introduction

Photochemical internalisation (PCI) has been developed as a technology to improve drug delivery to cells since the late 90s. Studies involved different photosensitisers, cell lines and in combination with a variety of anti-cancer drugs have been documented for the last years, particularly from the group from Norwegian Radium Hospital in Oslo. Høgset reviewed PCI-mediated drug and gene delivery in 2004 and concluded that PCI can induce the rupture of vesicles containing the co-administered therapeutic macromolecules and thereby display significant reduction of cell viability [Hogset et al., 2004].

As mentioned in Chapter 2, PCI has been shown to work well with anti-cancer drugs from different categories including small peptides and protein toxins. The drugs considered to be used in PCI strategy either have difficulties in entering cells or they are sequestered in lyso/endosomes after cell uptake and would be degraded eventually. In other words, PCI induces the relocalisation of those drugs inside the cell and thereby enhance cell death. Among these anti-cancer drugs, bleomycin and a group of plant toxins, type I ribosome-inactivating protein, have drawn researchers' attention in particular. As discussed in Chapter 2, these drugs would be ideal anti-cancer agents if delivered and exported sufficiently into cytosol. However, due to the nature of these molecules (i.e. the hydrophilicity of bleomycin; the lack of a binding domain of type I RIPs), their therapeutic potential are inactivated if without any modifications. Based on these facts, these two drugs should thus be candidates to demonstrate the PCI technology.

To date, the most efficient photosensitisers for PCI are meso-tetraphenylporphine ($TPPS_{2a}$) and aluminium phthalocyanine disulfonate ($AlPcS_{2a}$), which have two sulfonate groups on adjacent phthalate/phenyl rings. This amphiphilic structure with both a hydrophobic part and a hydrophilic part enables molecules to insert into biomembranes and inhibit further penetration. A new chlorin based photosensitiser with two adjacent sulfonated groups known as Amphinex^{TM}, ($TPCS_{2a}$, tetraphenylchlorin disulfonate), has been developed by PCI Biotech which was also investigated through out this thesis study.

PCI could work as a cancer treatment by acting a technology for drug delivery. PCI can deal with different cancer diseases when in combination with different drugs. Head and neck cancer is a good model for PDT treatment because it is easily accessible for treatment and follow-up. The good cosmetic outcome is one of the major advantages of PDT on head and neck cancers. As organ structures are complicated and delicate which should be well-preserved after any treatments for tumour removal, the benefit of PDT has made this site-specific treatment superior to other conventional regimens such as surgery in some cases. However, some advanced tumours of the larynx and the requirement for deeper light penetration in order to tackle potential lymph node metastasis in the case of SCC of the oropharynx are the problems that PDT has to overcome in the future [Kubler et al., 2001]. From this point of view, because PCI involves not only the sub-lethal photodynamic treatment but also the therapeutic effects caused by the combined drugs, PCI can induce more intensive damage to target tissues and thus has the potential to tackle head and neck cancers.

The *in vitro* experiments in this thesis were carried out using A431 human epidermoid carcinoma cells and HN5 human head and neck squamous cell carcinoma cells. Since both cell lines express high levels of the epidermal growth factor receptors, they are good models for cancer associated signalling pathway studies. Considering the possible introduction of targeting strategy into PCI technology in the future, as well as the future clinic applications on head and neck cancers, these two cell lines were chosen in this thesis study to investigate the PCI effect *in vitro*.

The following chapter will, therefore, assess the PCI approaches at the cellular level by examining the intracellular uptake, photostability (**4.3**) and photodynamic modification (**4.5**) of photosensitisers, conducting imaging studies of photosensitisers in cells (**4.4**), measuring the cell kill effect after photodynamic treatment (**4.7**), and also the cytotoxicity achieved by photochemical internalisation in the presence of two anti-cancer drugs, saporin and bleomycin (**4.8**).

4.2 Materials and Methods

Chemicals and drugs

$AlPcS_{2a}$ was supplied as a powder (Frontier Scientific, USA) and was dissolved in water as the stock solution (1mg/ml). The sulfonate groups are adjacently substituted on the macrocycle. In many previous studies the $AlPcS_{2a}$ preparation contained both adjacently and oppositely substituted isomers, therefore the preparation used here represents an improvement on those studies. $TPPS_{2a}$ dissolved in dimethyl sulfoxide (0.35 mg/ml) and Amphinex in Cremophor (10 mg/ml) were kindly donated by PCI Biotech (Norway). The structures and molecular weight of these three photosensitisers are shown in Figure 2.2 in Chapter 2. The stock solutions (20 μg/ml) for $TPPS_{2a}$ and Amphinex were prepared after serial dilutions in water. Sensitiser solutions (in water) were finally added into cell culture medium to make desired concentration for experiments (personal communication with Prof Berg, Norwegian Radium Hospital). Saporin was purchased from Sigma-Aldrich (UK). The stock solution of saporin (1mg/ml) was prepared by dissolving the drug power in sterile water. Saporin stock solution was then diluted to 10μg/ml (330nM) and the aliquotes was kept at -20ºC until use. Bleomycin (Kyowa Hakko, Mayne) was provided as powder (15 IU per vial according to the U.S. standard equivalent to 15,000 IU according to the European Pharmacopeia. 5.1), and was dissolved in 0.5ml 0.9% NaCl (30 IU/ml). The stock solution of bleomycin was prepared at a concentration of 0.14 IU/ml after serial dilutions with 0.9% NaCl. Alexa Fluor®488 was purchased as a protein labelling kit from Molecular Probes (UK).

Cell line and cultivation

A431 human squamous carcinoma cell line was purchased from ECACC (UK) and cultured in Minimal Essential Medium which was supplemented with 10% fetal bovine serum (FBS) (Sigma, UK), 100μM nonessential amino acid, 2mM Glutamine (GIBCO BRL, UK) and 500μg/ml Gentamycin (GIBCO BRL, UK). The HN5 human squamous cell carcinoma cells were obtained from Prof. MJ O'Hare (Ludwig Institute for Cancer Research, London, UK). Cells were cultured in Dulbecco's Modified Eagle's medium containing 10% FBS (Sigma, UK), 100μM nonessential amino acid, 2mM Glutamine (GIBCO BRL, UK) and 500μg/ml Gentamicin (GIBCO BRL, UK). All cells were incubated at 37 °C in a humidified atmosphere containing 5% CO_2.

Synthesis of Saporin-AlexaFluor488 conjugates

The linkage of saporin and Alexafluor488 followed the protocol provided by the supplier Molecular Probes. Briefly, saporin was dissolved by adding 1M sodium bicarbonate to the protein concentration of 2 mg/ml. The protein solution was then transferred to the vial of reactive AlexaFluor488 dye containing a magnetic stirrer bar. After 1 hour (or more) stirring at room temperature, the reaction mixture was carefully loaded to a column filled with resin. An elution buffer was then added slowly to the column. The absorbance of the protein conjugates was measure at 280nm (for proteins) and 494nm (for the dye) in a cuvette with a 1cm pathlength. The protein concentration was calculated followed the equation:

$$\text{Protein concentration (M)} = \frac{[A_{280} - (A_{494} \times 0.11)] \times dilutionfactor}{24000}$$

where 24000 $cm^{-1}M^{-1}$ is the molar extinction coefficient of saporin and 0.11 is a correction factor to account for absorption of the dye at 280nm.

$$\text{Moles dye per mole protein} = \frac{A_{494} \times dilution\_factor}{71000 \times protein\_concentration(M)}$$

where 71,000 $cm^{-1}M^{-1}$ is the approximate molar extinction coefficient of Alexa Fluor®488 dye at 494nm.

Light irradiation equipment

The light source for excitation of $TPPS_{2a}$ and Amphinex for the *in vitro* experiments was a blue lamp, LumiSource® (PCI Biotech, Norway), emitting light uniformly from four fluorescence tubes in the spectral region 375-450nm. The fluence rate was 7 mW cm^{-2} (Figure 4.1).

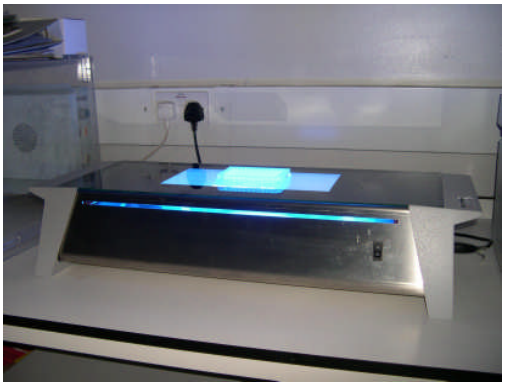

Figure 4.1 LumiSource®. It consists of a bank of 4 fluorescence tubes. Plates are covered with light-impermeable material during exposure from the plate base.

$AlPcS_{2a}$ was activated with laser excitation at 670nm (Hamamatsu Photonics, Japan). Irradiation from below is required because cells are cultured in well plates with the lid in place. This method was used because condensation tends to collect on the inside surface of the lid which would scatter light delivered from above the plate. A 400 micron diameter fibre terminated with a microlens was used to deliver a uniform beam of light for irradiating the whole of a 96 well-plate. The setup of laser irradiation equipment for well-plate experiments (i.e. photobleaching, phototoxicity and PCI with anti-cancer drugs) is shown in Figure 4.2. The fluence rate was 0.88 $mWcm^{-2}$ measured on the bottom of plates.

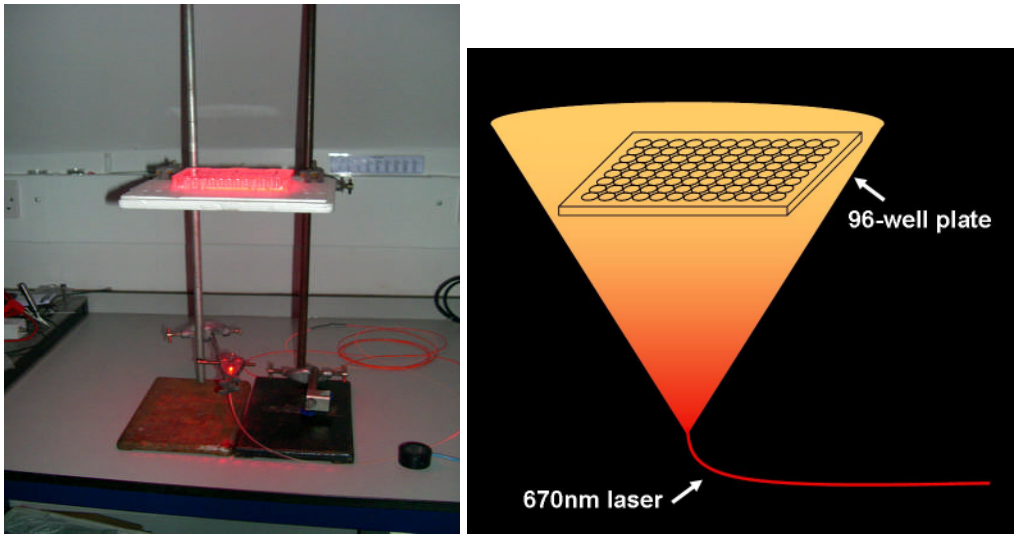

Figure 4.2 Laser devices setup of $AlPcS_{2a}$ PCI for well-plate experiments

The 670nm laser was also used for activating $AlPcS_{2a}$ on stage in the microscopic imaging study of light-induced $AlPcS_{2a}$ redistribution. As shown in Figure 4.3, the light was delivered from above using a 400 micron diameter fibre terminated with a microlens. A uniform beam of light produced an irradiation area with about 1cm diameter which covered the whole round coverslip. The fluence rate was 19.1 $mWcm^{-2}$ measured on the platform of microscope.

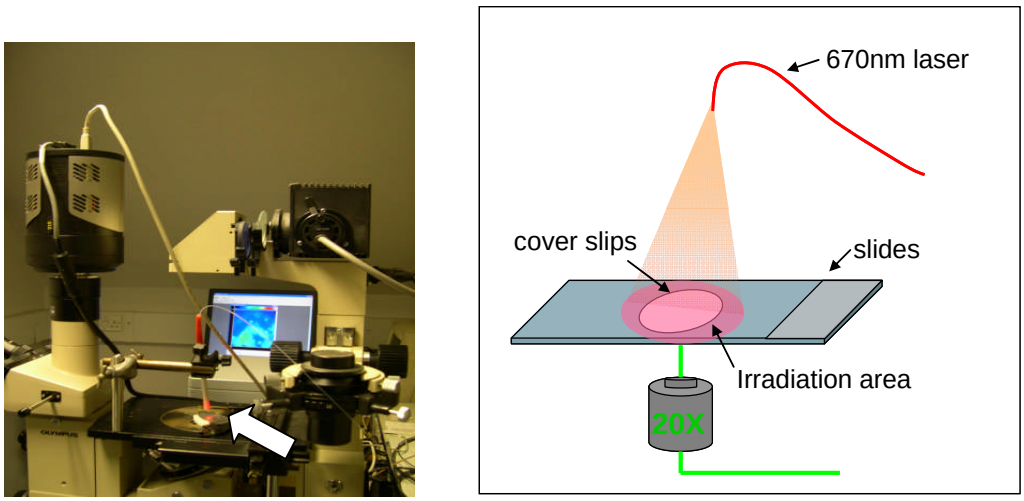

Figure 4.3 Laser setup for activating $AlPcS_{2a}$ on stage. The laser fibre is pointed out by the inset white arrow.

Spectroscopic measurements

The absorption spectrum measurement was carried out on a Perkin-Elmer Lambda 25 UV/Vis spectrometer (Perkin-Elmer, UK) using a 1 cm path length quartz cell. The absorption spectrum of Amphinex was measured with samples prepared from the stock solution diluted to 5 μg/ml in water. The fluorescence spectrum of Amphinex was examined in aqueous solution (diluted in distilled water to the concentration of 0.5 μg/ml) and also within A431 cells using a LS50B Perkin-Elmer spectrofluorimeter (Perkin-Elmer, UK). Cells were incubated with 0.1 μg/ml Amphinex for 18 hrs and the medium was replaced with clear medium before fluorescence measurement.

Cellular uptake and photostability detection by fluorescence spectrometer

A431 cells were plated onto 96-well plate at 2-2.5x10^4 cells/well overnight and then incubated with $TPPS_{2a}$ or Amphinex in different concentrations for 18 hours. Thrice washing of cells and a 4-hour further incubation with fresh medium was the recommended protocol to avoid photosensitiser molecules remaining bound on the plasma membranes which might affect fluorescence measurements or photosensitisation [Selbo et al., 2000a]. Then the medium was replaced with clear medium (no phenol red; no serum), and cellular uptake of photosensitisers was excited at 420nm and detected at 655nm using a LS50B Perkin-Elmer Spectrofluorimeter (Perkin-Elmer, UK). For photobleaching experiments, the fluorescence was detected using the spectrometer after different light dose irradiation by LumiSource® (PCI Biotech, Norway). Photobleaching curves were constructed from normalised fluorescence intensities against irradiation time. The fluorescence measurement itself did not induce any measurable

photobleaching**.** Each data point of the experiments was carried out by using 96-well plates in triplicate as the average of 6 wells.

Observation of the intracellular distribution of photosensitisers and the redistribution after illumination using fluorescence microscopy

Cells were seeded on glass coverslips in 6-well plates overnight and were then incubated with 2.5μg/ml $TPPS_{2a}$ or $AlPcS_{2a}$ and 0.1μg/ml Amphinex for 18 hours, washed three times with fresh medium and then incubated for further 4 hours. After that, DMEM medium with neither serum nor phenol red was replaced for microscopy study.

The subcellular distribution was observed using fluorescence microscopy. A 633nm laser was used to activate $AlPcS_{2a}$ and a 532nm laser was for $TPPS_{2a}$ and Amphinex. The first fluorescence imaging system was used in cells with $AlPcS_{2a}$, using a slow-scan liquid nitrogen cooled charge-coupled device (CCD) camera (Model 1, Wright Instrument Ltd, UK) and a combination of bandpass (Omega Optical Inc.USA) and longpass (Schott RG55) filters to record the images. The studies of $TPPS_{2a}$ and Amphinex were carried out with an upgraded fluorescence imaging system using a Peltier-cooled charge-coupled device (CCD) camera (Princeton Instruments Ltd., UK).

Co-localisation studies using fluorescence microscopy or confocal microscopy

In order to identify the subcellular distribution of photosensitisers and saporin, cells treated with either photosensitisers or Alexa488-labelled saporin were exposed to lysosomal probes before imaging analysis. A431 or HN5 cells overnight seeded onto glass bottom dishes FluoroDish^{TM} (WPI, UK) were incubated with 0.1 μg/ml Amphinex or 300nM Alexa488-labelled saporin for 18 hours. After thorough washing and further incubating with fresh medium for 4 hours, LysoTracker Green or LysoTracker Red (Molecular Probes, UK) was added to medium (final concentration 100nM) for 30min for lysosomes labelling. Following incubation, clear medium with neither serum nor phenol red was replaced for live-imaging. Experiments were initially conducted using fluorescence microscope attached a CCD camera. Confocal imaging was later carried out by confocal microcopy using a laser-scanning confocal microscope (FLUOVIEW FV1000, 60x magnification, NA 1.20, Olympus, Japan).

Co-localisation of Alexa488-labelled saporin and Amphinex and their redistribution after irradiation on stage by confocal microscopy

HN5 cells seeded onto FluoroDish were co-incubated with 0.1μg/ml Amphinex and 300 nM Alexa488-labelled saporin for 18 hours. After thorough washing and incubation with fresh medium for at least 4 hours, clear medium was replaced for live-imaging by confocal microscopy. Light treatment was carried out on stage using the 405nm laser of the microscope.

Observation and detection of photodynamic modification

HN5 cells were plated onto FluoroDish overnight and incubated with either 10 μg/ml $AlPcS_{2a}$ or 0.1 μg/ml Amphinex for 18 hours. Cells were washed three times and incubated with fresh medium for a further 4 hours. Clear medium was replaced before imaging studies.

A 670nm laser (Hamamatsu Photonics Ltd, UK) was used for the irradiation of $AlPcS_{2a}$. The laser setup is shown in Figure 4.3 as described before. A uniform beam of light was produced with a microlens to give an irradiation area of about 1.9 cm^2 which covered the glass bottom of the dish. The fluence rate was 10.9 $mWcm^{-2}$ measured on the platform of microscope. For activating Amphinex and for fluorescence microscopy, a green 543 nm laser module was used (Edmund Optics Inc., UK). The laser irradiation power measured on the platform of the microscope was 50 $mWcm^{-2}$. In each case the exposure time used to record the fluorescence image was short (3 s) in comparison to the light exposures needed to induce the photomodification process. Thus there was negligible perturbation induced by the fluorescence measurement itself on the overall fluorescence dynamics.

The irradiation was switched on and off sequentially and the fluorescent images were captured at pre-set times using a Peltier-cooled charge-coupled device (CCD) camera (Princeton Instruments, UK). Fluorescence intensities at set times were analyzed by ImageJ, a Java-based image processing software developed by NIH.

Phototoxicity of $TPPS_{2a}$, $AlPcS_{2a}$ and Amphinex in A431 cells and HN5 cells

The phototoxicity of $TPPS_{2a}$, $AlPcS_{2a}$ and Amphinex in A431 and HN5 cells was examined and compared. The PCI effect in combination with anti-cancer drugs, saporin and bleomycin, was further investigated using these two cell lines.

Cells were seeded at 5000 cells/well in 96-well plates overnight. After 18 hour incubation with either $TPPS_{2a}$, $AlPcS_{2a}$ or Amphinex, cells were washed off trice and incubated further 4 hours with fresh full medium. Irradiation was carried out up to 5 or 10 min for photosensitisers at a range of concentrations ($TPPS_{2a}$: 0-0.2 μg/ml; $AlPcS_{2a}$: 0-10 μg/ml; Amphinex: 0-0.5μg/ml in A431 cells and 0-0.2μg/ml in HN5 cells). The light source for $TPPS_{2a}$ and Amphinex was LumiSource® (PCI Biotech, Norway) and $AlPcS_{2a}$ was activated by a 670nm laser. The cell viability was measured by means of standard MTT (3-(4,5-dimethylthiazol-2-yl)-2,5-diphenyltetrazolium bromide) assay 48 hours after light treatment. Cultured medium was replaced with fresh medium containing MTT (1mg/ml) (Sigma, UK) and the plates were returned to the CO_2 incubator for 2 hours. The mitochondrial dehydrogenase in the remaining live cells converts MTT to fomazan crystals with purple colour in the base of each well. After removing the medium, dimethyl sulfoxide (DMSO) (Sigma-Aldrich, UK) was added to dissolve the crystal. The plates were shaken for 20 min and then the absorbance was then read at 570nm by an MRX_{II} Microtiter® Plate Reader (Dynex Technologies, Inc., USA). Each data point of the experiments was carried out by using 96-well plates in triplicate as the average of 6 wells**.**

PCI treatment schedules

This treatment schedule was based on previous PCI studies by Berg and co-workers in other cell lines. To summarise, the photosensitiser was incubated with the cells for 18 hours and then washed off thoroughly (3 times) so as to minimise plasma membrane levels of the photosensitiser so that the PDT effect of the photosensitiser is maximised in the intracellular organelle membranes. The 18-hour incubation was chosen by Berg et al. based on the optimum endo/lysosomal localisation; however, in this work independent confirmation was also carried out for the sensitisers used.

For PCI experiments, saporin was co-incubated with the photosensitiser whereas bleomycin was added after the photosensitiser was washed off. The reasons for the different incubation conditions are discussed later in this section. Light irradiation was carried out at the 22 hour timepoint in each case. The cell viability of the cells treated with saporin was measured by the MTT assay 2 days after light treatment and up to 4 days for cells treated with bleomycin, as discussed later.

The detail of PCI treatment schedule is shown below in Figures 4.4 A and B.

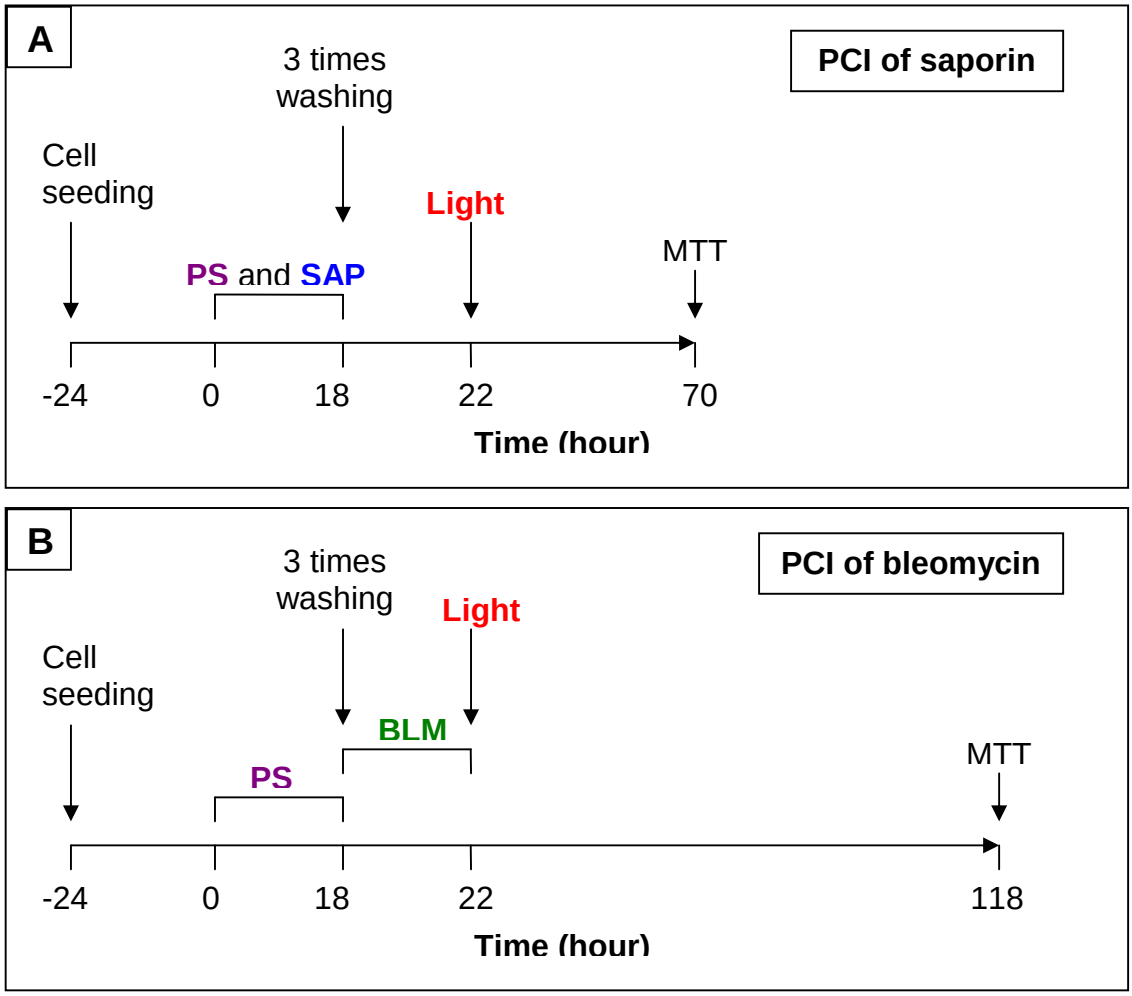

Figure 4.4 PCI treatment schedules. A: PCI of saporin. B: PCI of bleomycin. PS: photosensitiser; SAP: saporin; BLM: bleomycin.

Statistical analysis

Results are presented as mean ± standard deviation (SD). Significant differences were assessed by one tailed Student's t-test analysis. $P \leq 0.05$ was considered statistically significant.

4.3 Comparison of Cellular Uptake and Photostability of $TPPS_{2a}$ and Amphinex

4.3.1 Introduction

The therapeutic effect of PDT or the initiation of PCI comes from the photochemical reactions that take place following light absorption by the photosensitiser. This process involves the production of cytotoxic reactive oxygen species that induce oxidative biological damage and cell death. The other factors determining the efficacy of the treatment are the rate at which the photosensitiser is taken up by cells and then delivered into endo-lysosomes, which are related to the intracellular accumulation. However another factor to consider is the photostability of the photosensitiser once inside the cells since photodegradation (or photobleaching) would reduce the amount of photosensitiser present for PCI treatment. Therefore measuring the uptake and the photostability of sensitisers within cells are the key starting points to estimate their potential efficacy on photodynamic therapy or photochemical internalisation.

$TPPS_{2a}$, $AlPcS_{2a}$ and $TPCS_{2a}$ (Amphinex) are photosensitisers used in PCI which are water-soluble second generation photosensitisers, as summarised in Chapter 2. Unlike the first generation photosensitisers such as Photofrin®, $AlPcS_{2a}$ and $TPCS_{2a}$ have many improved chemical and biological properties, for instance, the stronger absorption at longer wavelengths. Moreover, amphiphilicity is another common feature among these three PCI sensitisers.

In general lipophilic, hydrophobic photosensitisers display higher cell uptake than hydrophilic ones because they can partition more easily to the cell membrane and thus enter the cell. However, hydrophobic photosensitisers also tend to aggregate in solution, thereby decreasing their photoactivity because of the excited state self-quenching effects induced by dimerization [Berg et al., 1990;Moan et al., 1992]. Amphiphilic photosensitisers with both hydrophilic and hydrophobic characteristics within the same molecule, on the other hand, exhibit favourable physical and pharmacokinetic properties for PDT [Allen et al., 2002]. Chemical synthesis of adjacent sulfonated tetraphenylporphines, phthalocyanines, and tetraphenylchlorins is one of the most common ways to make amphiphilic photosensitisers which are particularly effective for

PCI owing to the membrane localisation [Kunz et al., 2007], as previously outlined in Chapter 2.

Photobleaching refers to the process of photochemically induced destruction or photodegradation in which the molecular structure of the molecule is degraded following light absorption. Photostability can be estimated by measuring the bleaching of absorption or fluorescence after light exposure. Each fluorophore has its own photobleaching characteristics depending on its photophysicochemical properties and the rate at which it reacts with reactive oxygen species. Photobleaching can also take place under anaerobic conditions but in most cases is studied under air-saturated conditions. The mechanisms of photobleaching have been reviewed by Bonnett and Martinez [Bonnett and Martinez, 2001]**.** In the case of porphyrin-type photosensitisers, it is believed that photobleaching takes place mainly by destruction of the porphyrin macrocycle or ring following reaction with reactive oxygen species such as singlet oxygen, resulting in smaller molecular fragments that do not absorb in the visible range.

The term 'photomodification' is often used in the same context but generally refers to other photoinduced processes which result in the chromophore being retained in a modified form. For example, the production of a photoactive photoproduct, or the photoinduced monomerisation of weakly fluorescent fluorophore aggregates. The influence of this process will also be considered in following sections.

The situation will be more complex for treatments *in vivo* than *in vitro* because of the heterogenous environment, but in practical terms, it is essential to study both accumulation and photostability of photosensitisers in order to establish the dosimetry of PDT and PCI treatments in clinic.

In this section, we will only focus on the sensitisers used in PCI. The cellular uptake of $TPPS_{2a}$, and Amphinex and their photobleaching induced after irradiation were determined and compared in A431 cell line using spectrofluorimetry. Detailed photodynamic modification of $AlPcS_{2a}$ and Amphinex in HN5 cells demonstrated by fluorescence microscopy will be discussed in section **4.5**.

4.3.1.1 Results

Spectroscopic studies of Amphinex

The spectroscopic properties of both $TPPS_{2a}$ and $AlPcS_{2a}$ have both been well studied. However since Amphinex is a newly available photosensitiser, spectroscopic properties of Amphinex were assessed then prior to the cellular studies in aqueous solution. One advantage of Amphinex over $AlPcS_{2a}$ is that there are only three regioisomers present (personal communication with K. Berg) whereas there are far numerous regioisomers present in commercially available preparations of $AlPcS_{2a.}$

Figure 4.5 shows the absorbance of 5 μg/ml Amphinex diluted in distilled water. The peak absorption of Soret absorption band was found at 418 nm. The weaker series of Q bands were measured at 520 nm, 546 nm, 595 nm and 649 nm (Figure 4.5, inset). Peak absorption in the red is at 649 nm. A slight red-shift of this peak is observed in tissue as described later in Chapter 6. Its molar extinction coefficient in water can therefore be estimated as $\varepsilon_{418nm} = 1.6 \times 10^5\ M^{-1}cm^{-1}$ which is similar to the value for m-THPC (in ethanol) as $\varepsilon_{418nm} = 1.9 \times 10^5\ M^{-1}cm^{-1}$ (measured in our laboratory).

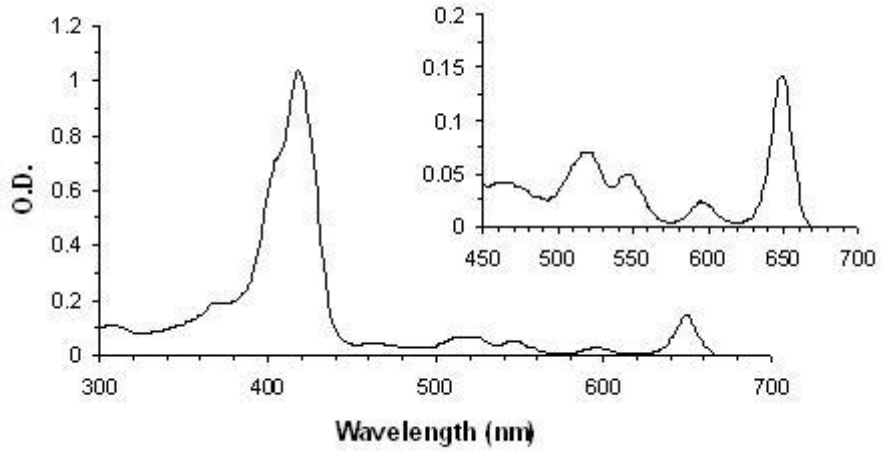

Figure 4.5 Absorption spectrum of 5 μg/ml Amphinex diluted in distilled water. Inset: the Q band region from 450 nm to 700 nm.

The fluorescence spectra of 0.5 μg/ml Amphinex diluted in distilled water are shown in Figure 4.6A. Two peaks of fluorescence emission were detected at 655 nm and 718 nm when excited at 415nm; the maximum excitation was at 413 nm ($\lambda_{emission}$ 655 nm). The fluorescence spectra of Amphinex were also measured within A431 cells sensitised with

0.1 μg/ml Amphinex for 18 hrs (Figure 4.6B). Medium was washed off and replaced with clear medium for fluorescence measurement. Two peaks of fluorescence emission were detected at 655 nm and 725 nm when excited at 420 nm; the maximum excitation was at 421 nm ($\lambda_{emission}$ 655 nm).

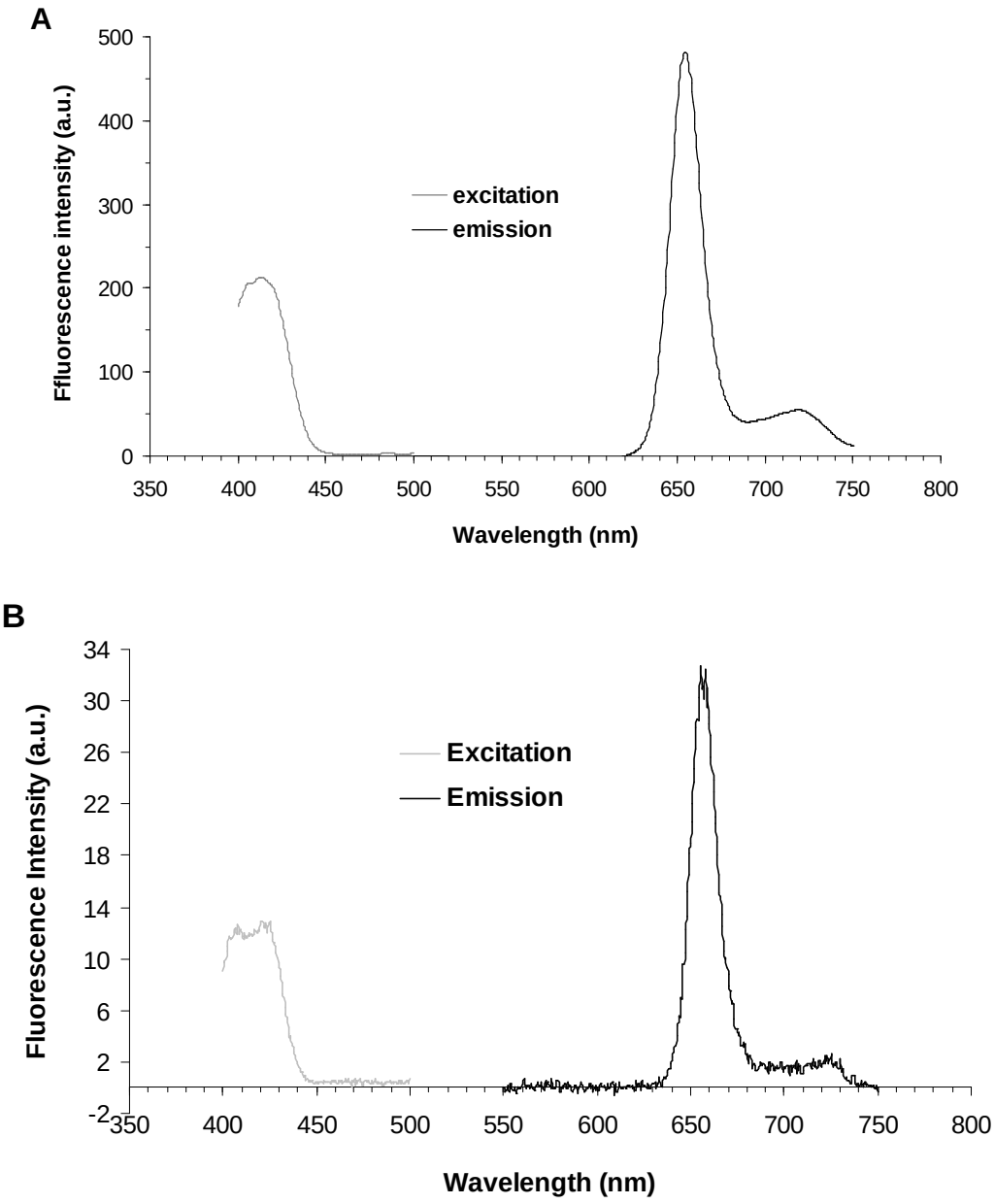

Figure 4.6 Fluorescence emission and excitation spectra of Amphinex detected in distilled water (A) and within cells (B). A: The spectra in aqueous solution were measured with the concentration of 0.5 μg/ml diluted in distilled water ($\lambda_{excitation}$ 414 nm and $\lambda_{emission}$ 655 nm). B: The signal was detected within A431 cells sensitised with Amphinex (0.1 μg/ml) for 18hrs. The spectrum was corrected for the variation of detector sensitivity with wavelength.

Cellular uptake of $TPPS_{2a}$ and Amphinex in A431 cells

The cellular uptake of photosensitisers was determined by measuring the fluorescence intensity in cells following an 18 hour incubation. A431 cell monolayers were incubated with increasing concentrations of sensitisers and following washing the fluorescence from the cells was measured using fibre-optic spectrofluorimeter with the detection/excitation fibre placed above each well in a 96 well plate. A concentration dependent cellular uptake was found in using $TPPS_{2a}$ and Amphinex. As shown in Figure 4.7 and 4.8, the fluorescence intensity linearly increased against different concentrations (R^2>0.99) and no saturation was observed. The fluorescence intensity is not comparable between two photosensitisers as experiments were carried out on different days with different cell confluency. However, a similar uptake pattern was found in using both sensitisers when comparing to the fluorescence signals between concentrations of 0.1μg/ml and 0.5μg/ml. The fluorescence intensity using Amphinex increased linearly, ie the intensity increased by a factor of 5 higher when a 5 times higher concentration was used. Likewise using $TPPS_{2a}$ a near-linear dependence between fluorescence intensity and sensitiser concentration was observed. Since this detection technique measures fluorescence from whole cells the possibility of fluorescence quenching effects (e.g. due to self-quenching induced by dimerization) cannot be ruled out, but the fact that a near linear increase with concentration is observed would be consistent with relatively little interference from dimerization effects in this concentration range.

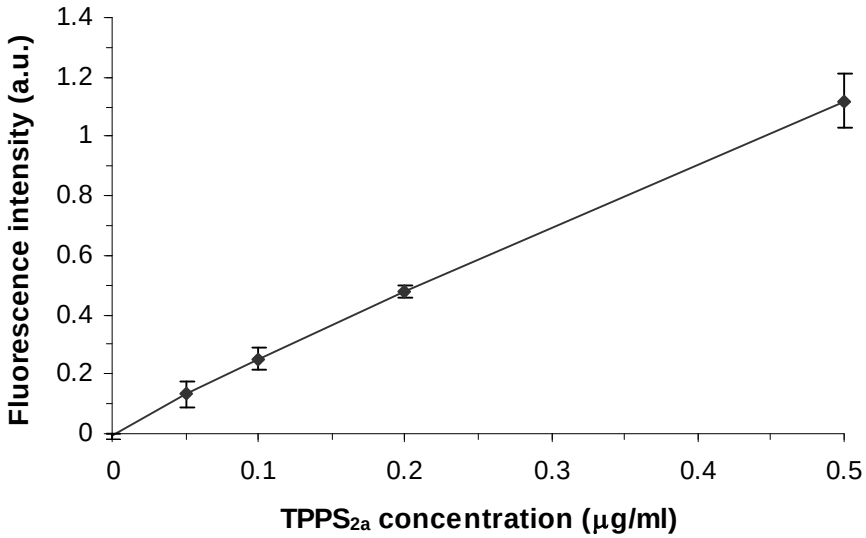

Figure 4.7 Cellular uptake of $TPPS_{2a}$ in A431 cells using spectrofluorimetry. Cells were incubated with $TPPS_{2a}$ with various concentrations for 18 hrs previously. Fluorescence

measurements were carried out when cells were incubated with clear medium. Detailed procedures can be found in the section of Materials and Methods.

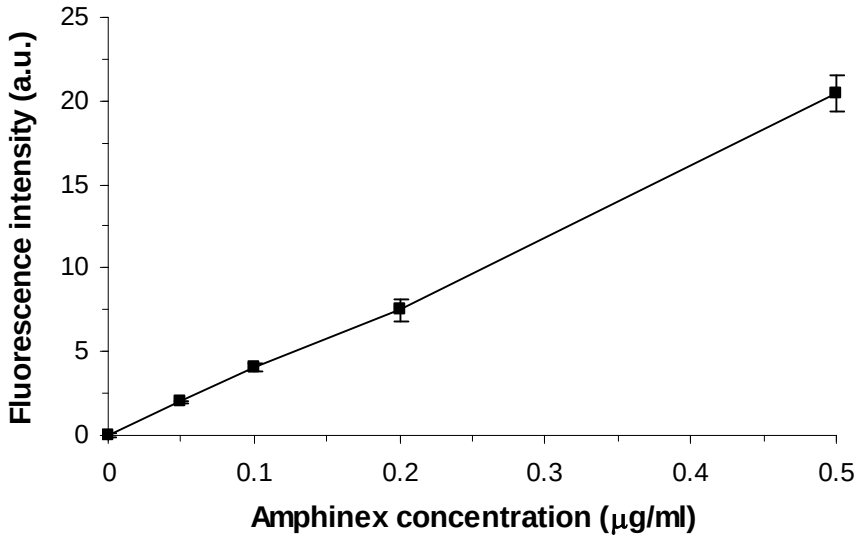

Figure 4.8 Cellular uptake of Amphinex in A431 cells using spectrofluorimetry. Cells were incubated with Amphinex with various concentrations for 18 hrs previously. Fluorescence measurements were carried out when cells were incubated with clear medium. Detailed procedures can be found in the section of Materials and Methods.

Photo-induced changes in fluorescence of $TPPS_{2a}$ in cells

All photosensitising dyes are susceptible to photodegradation, which is also known as photobleaching, and this process can limit the efficacy of the photosensitiser. In order to evaluate the relevance of this process to PCI, the changes in fluorescence of $TPPS_{2a}$ in cells were studied using fluorescence spectroscopy following different light exposures with blue light. The results are presented in Figure 4.9. The fluorescence intensity in the cells treated with higher photosensitiser concentrations (0.2 and 0.5 μg/ml) increased upon light exposure, displayed the maximum fluorescence intensity after a light dose of 4.2 J/cm^2 and decreased afterwards. The cells incubated with lower concentration of $TPPS_{2a}$ (0.05 and 0.1 μg/ml) had a reduction of fluorescence signal at the beginning of illumination. The fluorescence intensity then went up upon irradiation, followed by a photobleaching after the light dose of 4.2 J/cm^2. In the cell-free system, it was observed that the fluorescence intensity kept declining during the process of light irradiation and dropped to approximately 50% of its initial value after a light dose of 2.1 J/cm^2.

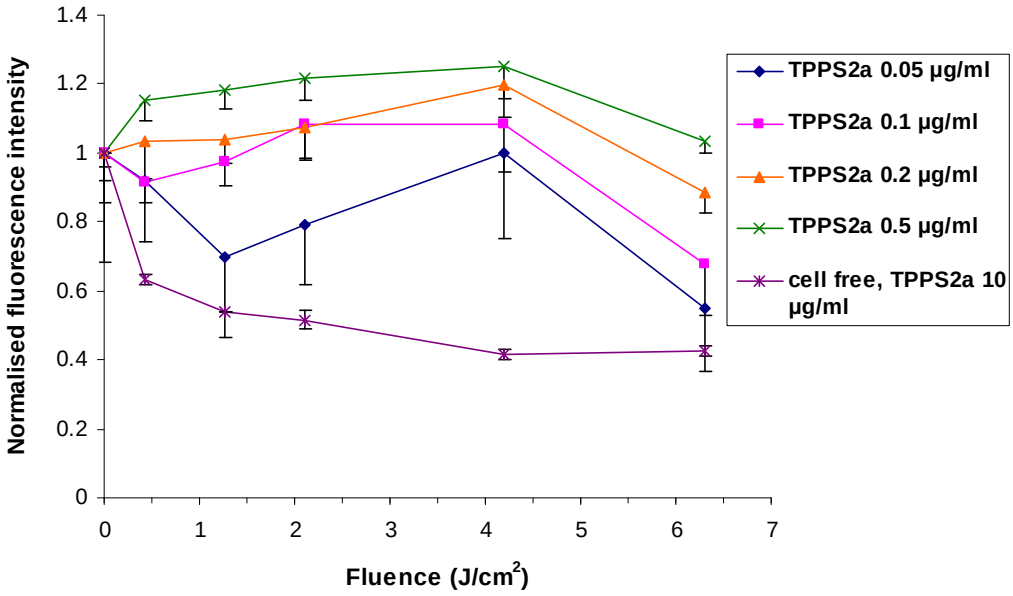

Figure 4.9 Normalised changes in fluorescence of $TPPS_{2a}$ in A431 cells as a function of fluence. Cells were incubated with $TPPS_{2a}$ with various concentrations for 18 hrs previously. Fluorescence measurements were carried out when cells were incubated with clear medium. Detailed procedures can be found in the section of Materials and Methods.

Photo-induced changes in fluorescence of Amphinex in cells

Similar experiments were carried out but using Amphinex as the photosensitiser (Figure 4.10). In contrast to $TPPS_{2a}$, the fluorescence signals detected within A431 cells were continuously falling but with a slower photobleaching rate after expose to light regardless of the Amphinex concentration. The fluorescence decayed less than 5% after 1.26 J/cm^2 (3 min irradiation) and remained above 90% after 4.2 J/cm^2 (10 min irradiation). At the longest irradiation time point (i.e. 12.6 J/cm^2, in this experiment), 80% of the original fluorescence intensity was still detectable in the cells with higher concentrations. There was only a loss of about 13% of fluorescence in the cells treated with 0.05µg/ml Amphinex. Unlike the case of using $TPPS_{2a}$, there is less variation in the photobleaching rate between cells incubated with different concentrations of Amphinex.

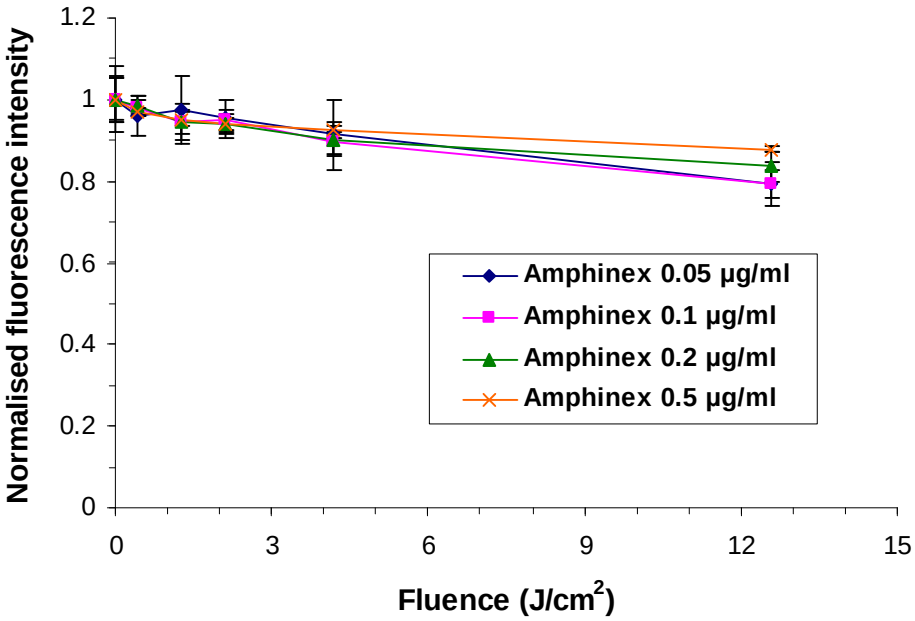

Figure 4.10 Normalised changes in fluorescence of Amphinex in A431 cells as a function of fluence. Cells were incubated with Amphinex with various concentrations for 18 hrs previously. Fluorescence measurements were carried out when cells were incubated with clear medium. Detailed procedures can be found in the section of Materials and Methods.

4.4 Subcellular Distribution of Photosensitisers, Co-localisation with Organelles and Redistribution after Illumination

4.4.1 Introduction

As addressed in Chapter 2, photosensitisers used in PCI should enter cells via pinocytosis and possibly follow clathrin-mediated pathway because of their amphiphilic structures. It is believed that photosensitisers would be directed to further stages along the endo-lysosomal system and ended in late endosomes or lysosomes, the major compartments of material degradation. Because photochemical internalisation takes place during this trafficking process, it is important to investigate the cellular distribution and the possible co-localisation with other intracellular organelles.

There are many approaches to demonstrate intracellular lysosomal localisation of photosensitisers. In 1989, Moan and his colleagues used differential ultracentrifugation and electron microscopy to look at the intracellular localisation of photosensitisers [Moan et al., 1989]. In another of their studies, the release of the lysosomal enzymes (i.e. β-N-acetyl-D-glucosaminidase and cathepsin) was detected after treating $TPPS_n$-sensitised NHIK 3025 carcinoma cells with light. This funding indicated a lysosomal disruption caused by illumination and lysosomes are surely photochemical targets [Berg and Moan, 1994]. Similar results were obtained in the experiment using $AlPcS_4$ or $AlPcS_2$; moreover, the cellular distribution of sensitisers were found identical to the lysosomotropic dye acridine orange (AO) by a co-staining method using fluorescence microscopy [Moan et al., 1994].

Using inhibitors or generating a cold environment to stop or slow down the metabolism of cells is also a way to examine the relationship between photosensitisers and endolysosomal vesicles. Prasmickaite reported the role of endosomes in gene transfection by conducting pulse-chase experiments, lowering the temperature to inhibit endocytosis, or using endocytosis inhibitors [Prasmickaite et al., 2000]. The outcome indicated that early endosomes are involved in this light-dependent transfection.

Since many photosensitisers are reasonably fluorescent in the red region, nowadays, co-staining cells with chemically synthesized specific organelles probes is a common way

to trace the cellular uptake and identify the subcellular distribution of photosensitisers. By carefully choosing dyes with suitable absorption and emission spectra, the imaging results from fluorescence microscopy or confocal microscopy can demonstrate the cellular location of photosensitisers. Therefore, in this section, the subcellular distributions of the photosensitisers and their redistribution after light exposure will be examined using fluorescence microscopy. A lysosomal probe emitting fluorescence in the range around 515 nm will be used to demonstrate the co-localisation studies. Cells co-incubated with Amphinex and a synthesized green fluorescent probe-labelled saporin will be analyzed by fluorescence microscopy. Another experiment co-staining lysosomal probes to cells treated with this fluorescence labelled protein will also be carried out to present the subcellular distribution of the protein toxin.

4.4.2 Results

Subcellular distribution of $TPPS_{2a}$, $AlPcS_{2a}$ and Amphinex and their redistribution after illumination

After treating with 2.5μg/ml $AlPcS_{2a}$ for 18 hours, intracellular distribution of $AlPcS_{2a}$ was observed in A431 cells by fluorescence microscopy. Following 670nm laser irradiation on stage, the distribution of $AlPcS_{2a}$ became diffuse accompanied by an increase in intensity, and thereafter photobleaching with a decrease of the fluorescence signal (Figure 4.11). Peak fluorescence levels were observed after 40sec exposure in both cases, and thereafter declined due to photobleaching. The same phenomenon was also observed using a lower dose of $AlPcS_{2a}$ (0.5μg/ml) (data not shown). This transient increase in fluorescence phenomenon is studied in more detail in section 4.5.

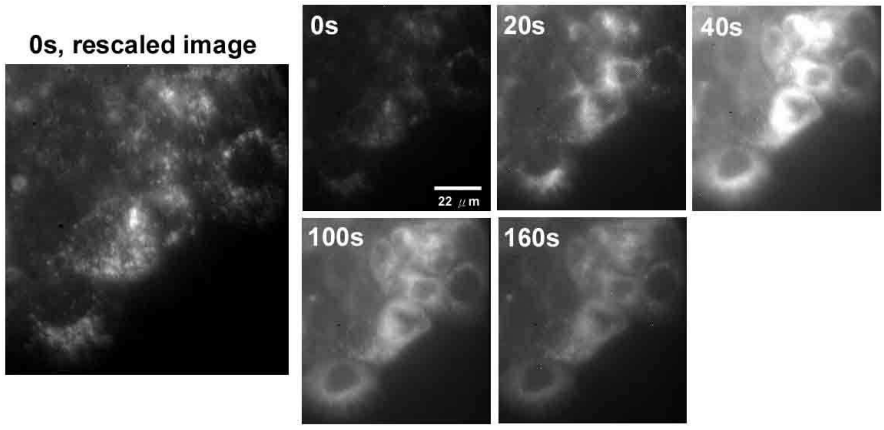

Figure 4.11 Fluorescence studies of $AlPcS_{2a}$ light-induced relocalisation in A431 cells using fluorescence microscopy. Cells were treated with 2.5 μg/ml $AlPcS_{2a}$ for 18 hours. The light exposure was up to 160s.

A431 cells were incubated with 2.5μg/ml $TPPS_{2a}$ or 0.1μg/ml Amphinex for 18hrs. A granular cellular distribution was found in both cases by fluorescence microscopy (Figure 4.12A and 4.13A). The distribution of photosensitisers became diffuse following 5 min light exposure on stage or by the blue lamp respectively (Figure 4.12B and 4.13B). After light exposure, a distinct fluorescence in the cell membrane was also observed. Further experiments using confocal microscopy are needed to clarify whether this is the result of photo-induced relocalisation of photosensitiser or is due to the limitation of CCD fluorescence microscopy in which images are taken from the whole thickness cells.

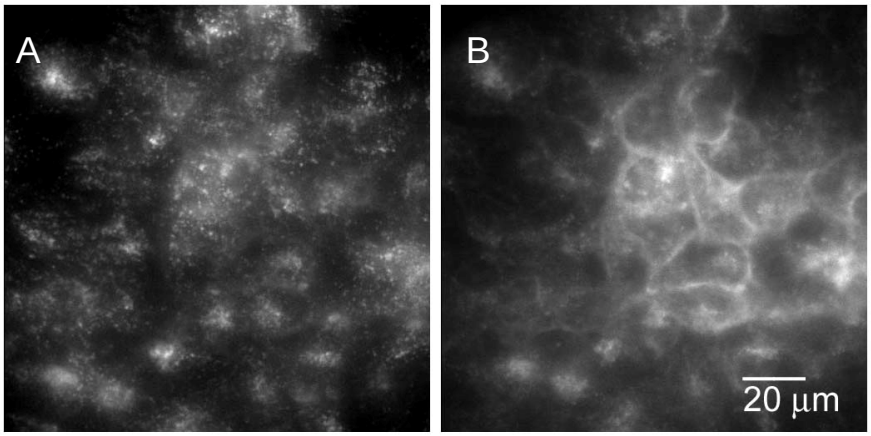

Figure 4.12 Cellular distribution of $TPPS_{2a}$ in A431 cells and the redistribution after 5 min irradiation on stage images by fluorescence microscopy. Cells were incubated with 2.5 μg/ml $TPPS_{2a}$ for 18 hours.

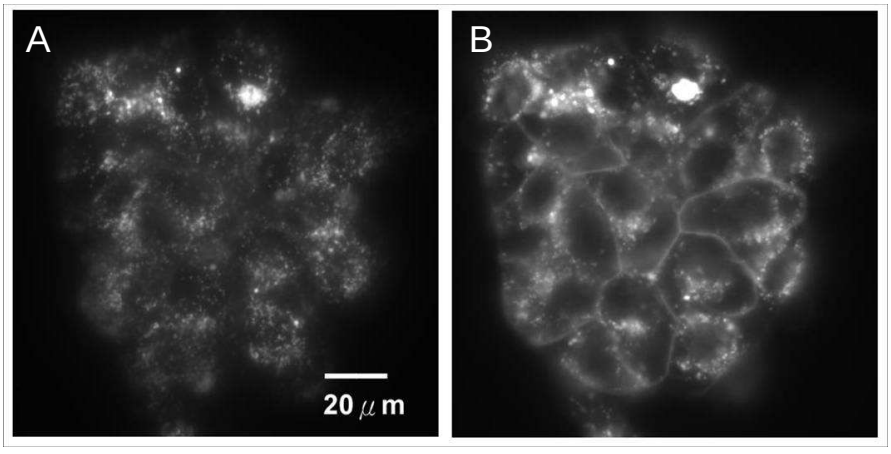

Figure 4.13 Cellular distribution of Amphinex in A431 cells and the redistribution after 5 min irradiation by blue lamp using fluorescence microscopy. Cells were incubated with 0.1 μg/ml Amphinex for 18 hours.

Synthesis of saporin-AlexaFluor488 conjugates

The final concentration of saporin-AlexaFluor488 conjugates was 41 μM and the ratio was 1.5 moles dye per more of protein. Comparing the spectrum of AlexaFluor488 to the conjugate, there is only a slight blue shift in the emission spectrum after the conjugation (Figure 4.14). The saporin conjugate was then used in co-localisation experiments.

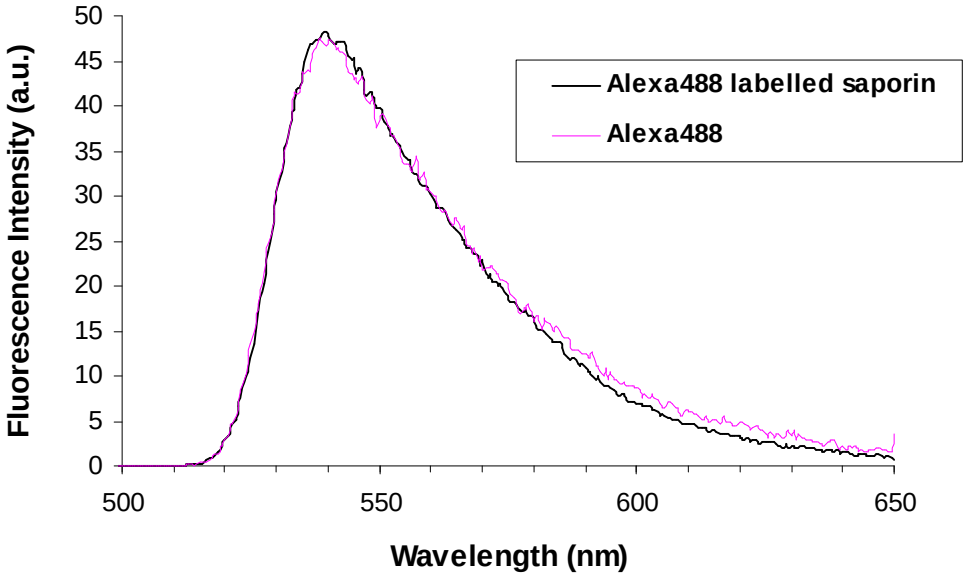

Figure 4.14 Normalised emission spectra of AlexaFluor488 (pink line) and saporin-AlexaFluor488 conjugates (black line) using 488 nm excitation.

Co-localisation of Amphinex/TPPS$_{2a}$ and Alexa488-labelled saporin in A431 cells using fluorescence microscopy

Photosensitisers (Amphinex or TPPS$_{2a}$) and Alexa488-labelled saporin were co-incubated in A431 cells for 18hrs. Their subcellular distributions without light exposure were observed using fluorescence microscopy. Fluorescence imaging results demonstrated good intracellular co-localisation of either photosensitisers with Alexa488-labelled saporin in A431 cells (Figure 4.15). The yellow colour in the overlay image (Figure 4.15C) indicates that a significant amount of Amphinex was localised in lysosomes after 18 hours cellular uptake.

Due to the rotation of the CCD camera after changing filters manually for detecting different fluorescent probes, the merged fluorescent image of TPPS$_{2a}$ and LysoTracker Green is not in exactly the same alignment(data not shown) and therefore an overlay image is not available in this experiment (Figure 4.15D and 4.15E). However, a well-

matched cellular distribution was still observed by comparing the individual fluorescent image (inset arrows).

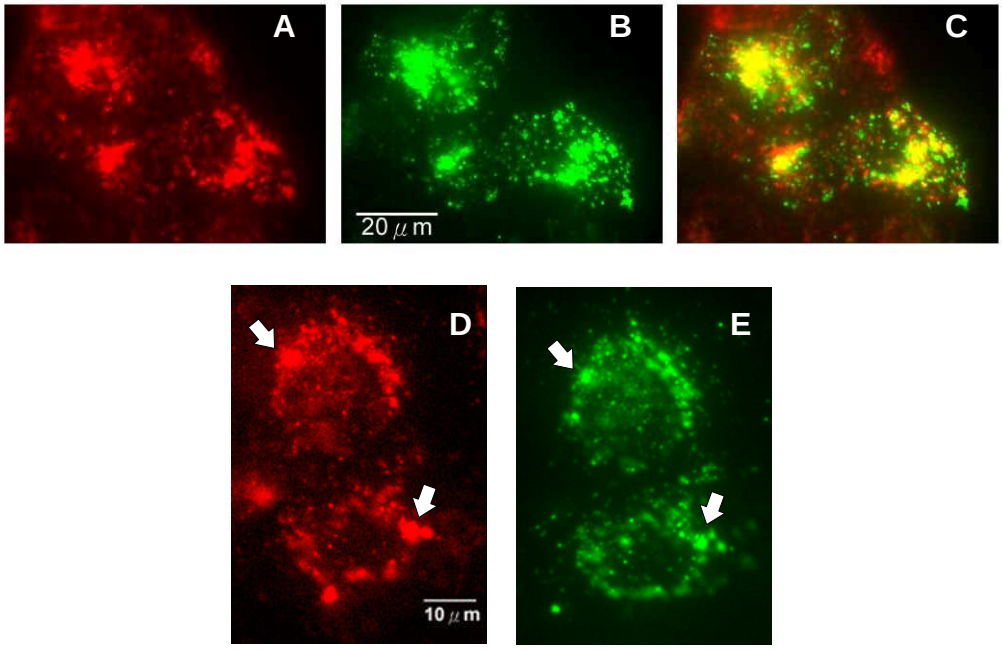

Figure 4.15 Amphinex or $TPPS_{2a}$ co-localised with Alexa488-labelled saporin in A431 cells by fluorescence microscopy. A: Amphinex; B&E: Alexa488-labelled saporin; C: Merged image of A and B; D: $TPPS_{2a}$. Cells were co-incubated with Amphinex (0.1 μg/ml)/$TPPS_{2a}$ (2.5 μg/ml) and Alexa488-labelled saporin (300 nM) for 18 hours.

Identification of the subcellular distribution of Amphinex and Alexa488-labelled saporin using lysosome probes in HN5 cells by confocal microscopy

In order to identify the subcellular distribution of Amphinex and saporin, HN5 cells were treated with 0.1 μg/ml Amphinex or 300 nM Alexa488-labelled saporin for 18hrs and then incubated with 100 nM LysoTracker Green or LysoTracker Red for 30 mins before imaging using confocal microscopy. As shown in Figure 4.16, Amphinex (red) and LysoTracker Green (green) were well co-localised (yellow) in HN5 cells. Similar results were found in cells treated with green fluorescent saporin and LysoTracker Red (Figure 4.17). The merged yellow colour showed that saporin were localised at lysosomes after cell uptake.

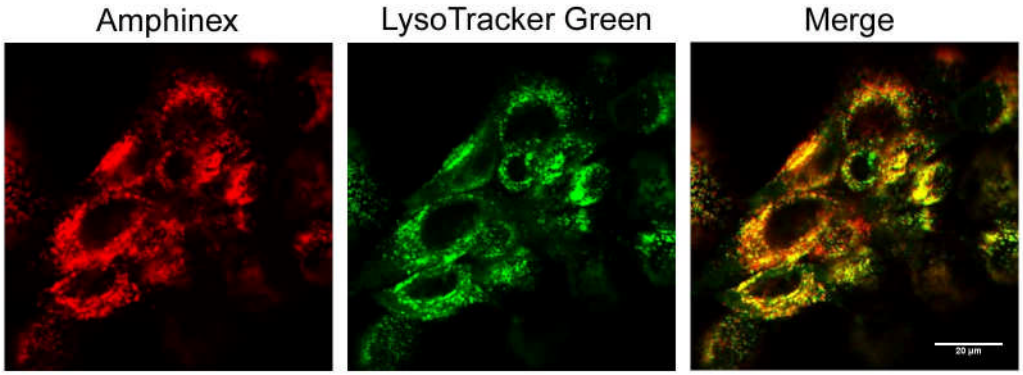

Figure 4.16 Co-localisation of Amphinex and LysoTracker Green in HN5 cells by confocal microscopy. Red: Amphinex; green: LysoTracker Green; yellow: merged image. Cells were incubated with 0.1 µg/ml Amphinex for 18 hours. LysoTracker Green (100 nM) was applied to cells 30min prior to imaging.

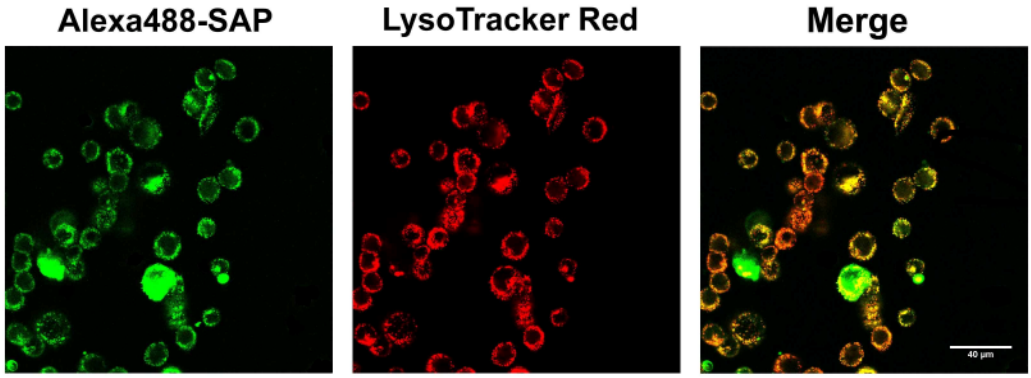

Figure 4.17 Co-localisation of Alexa488-labelled saporin and LysoTracker Red in HN5 cells by confocal microscopy. Green: Alexa488-labelled saporin; red: LysoTracker Red; yellow: merged image. Cells were incubated with 300 nM Alexa488-labelled saporin for 18 hours. LysoTracker Red (100 nM) was applied to cells 30min prior to imaging.

Imaging the PCI action in vitro - Co-localisation of Alexa488-labelled saporin and Amphinex and their redistribution after irradiation on stage in HN5 cells by confocal microscopy

The PCI action *in vitro* was observed using this live-imaging confocal microscopy system. HN5 cells were co-incubated with 0.1 µg/ml Amphinex and 300 nM Alexa488-labelled saporin for 18 hours. The results are shown in Figure 4.18. The images taken before light exhibit good intracellular co-localisation of Amphinex and saporin in HN5 cells (Merged-before light). A 90-second light treatment was carried out on stage using the microscopic 405nm laser through the objective. After 90 seconds irradiation, Amphinex became diffuse accompanied by a decreased fluorescence intensity (AMX-

90 sec light) which is consistent to previous studies. Minor changes in the distribution of saporin were found after the 90-second light exposure (SAP-90 sec light, arrow). Light treatment was not carried on as blebbing cells were observed (data not available). Long-term changes of the intracellular distribution of saporin were continuously monitored after irradiation. Images taken 7 min after light exposure show that the distribution of saporin has changed but not radically (SAP-7 min after light, white arrow). There is not much difference in the fluorescence intensity of Amphinex since no further irradiation was applied.

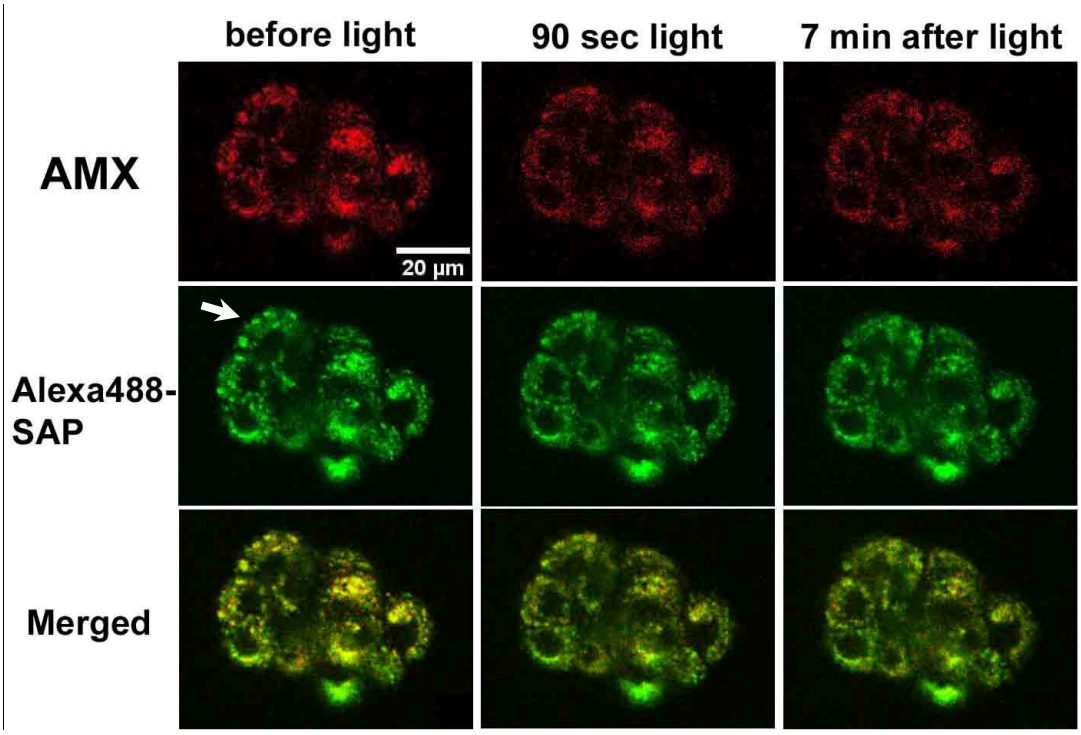

Figure 4.18 Co-localisation of Alexa488-labelled saporin and Amphinex and their redistribution after irradiation on stage in HN5 cells by confocal microscopy. Green: Alexa488-labelled saporin; red: Amphinex; yellow: merged images. Light source: 405nm laser of the confocal microscope. Cells were co-incubated with Amphinex (0.1 µg/ml) and Alexa488-labelled saporin (300 nM) for 18 hours.

4.5 Fluorescence Imaging of Photodynamic Modification and Bleaching of $AlPcS_{2a}$ and Amphinex in HN5 cells

4.5.1 Introduction

The term 'photomodification' is often used in the same context as photobleaching or photodegradation but generally refers to other photoinduced processes such as the photoinduced monomerisation of weakly fluorescent fluorophore aggregates, or the production of a photoactive photoproduct, as previously discussed in section 4.3. The fluorescence of photosensitisers makes it feasible to determine their concentration by measuring the fluorescence intensity. However, it is known that photosensitisers tend to aggregate at higher concentrations which can result in self-quenching of the fluorescence signal in its dimeric or in higher aggregated forms. In the case of disulfonated aluminum phthalocyanine (AlS_2Pc) only the monomer is fluorescent, as shown in several studies [Kunz et al., 2007]. For example, decreasing fluorescence and triplet quantum yields were found when the concentration of AlS_2Pc was increasing [Dhami et al., 1997].

Previous studies have demonstrated the photodynamic modification of AlS_2Pc fluorescence using a macrophage cell line by fluorescence microscopy [Kunz et al., 2007]. The AlS_2Pc fluorescence intensity was increased after a short irradiation period (1 min). It was found to continue to rise for more then 10 minutes in the absence of irradiation. Photobleaching, corresponding to the decay in fluorescence signal, was then observed after the second longer irradiation at 15 min. Moreover, an oxygen dependence was found when cells were incubated in deoxygenated solution, with the observation of slow photobleaching instead of transient increased fluorescence intensity.

The fluorescence quantum yield of a photosensitiser can be affected by its aggregation state, as well as its primary photophysics [Boyle and Dolphin, 1996]. Since sulfonated phthalocyanines can be complex mixtures, chemically well-characterised $AlPcS_{2a}$ obtained from Frontier Scientific Inc., with the sulphonate groups on adjacent phthalate rings, will be used instead to investigate the photomodification properties in this section. The photomodification properties of the new chlorin based Amphinex was studied in comparison to AlS_2Pc using quantitative fluorescence microscopy both to image and

measure fluorescence levels in cells following light exposure.

4.5.2 Results

The fluorescence intensities of $AlPcS_{2a}$ from four random HN5 cells in the field were measured over the experiment (Figure 4.19 images). A transient increase was found during the first 3min irradiation period (Figure 4.19 graph). As shown in the images, $AlPcS_{2a}$ was granularly distributed inside cells but became diffuse after 2min light exposure. After switching off the laser, the fluorescence signals continued to increase 2 min after but remained the same level afterwards. The second irradiation was performed at the 13 min time-point for 1 min and the effect of photobeaching was observed onwards. The laser was switched on again at 30min for 1 min and the fluorescence signal continued to decrease. The effect of the excitation light used for fluorescence detection was negligible on the photobleaching observed. Similar results using A431 cells were found using different concentrations of $AlPcS_{2a}$ as shown in Figure 4.11 where the relocalisation of $AlPcS_{2a}$ occurred in parallel to a transient increase in fluorescence.

Different results were found in the studies using Amphinex. The fluorescence intensity started decreasing and continued falling after several light-on-light-off procedures (Figure 4.20 graph). As shown in the pictures in Figure 4.20, the cellular distribution of Amphinex became diffuse after light exposure but only with incremental changes of the fluorescence intensity.

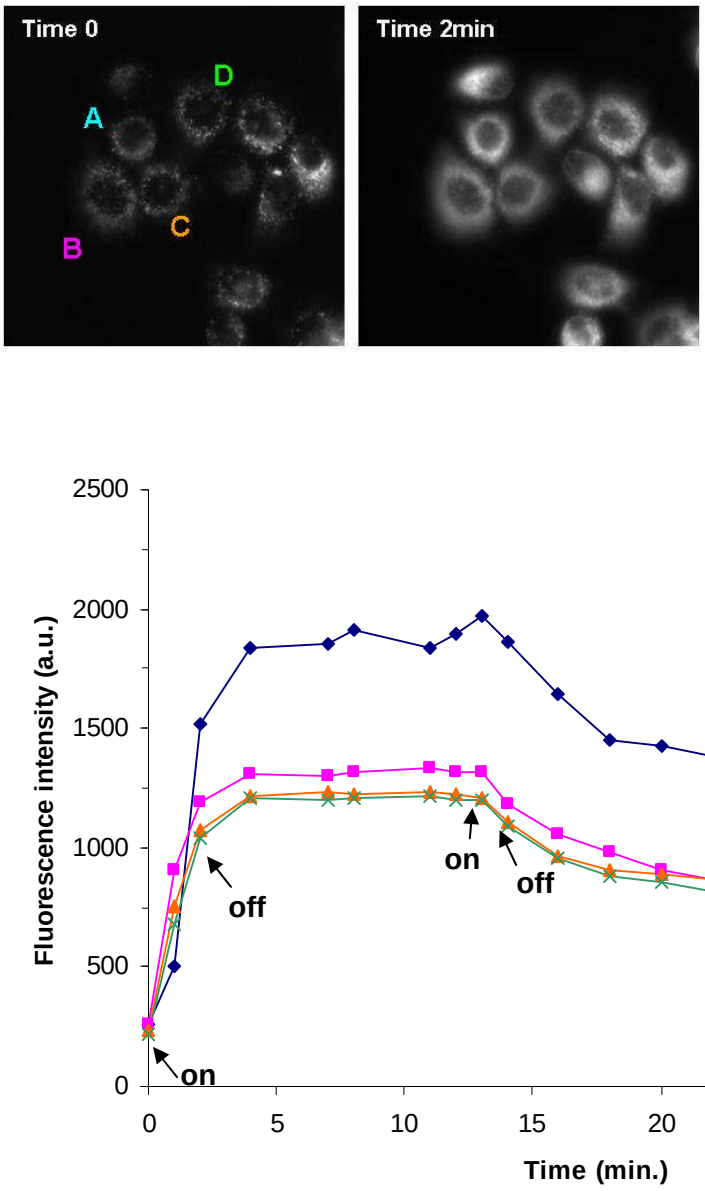

Figure 4.19 Photoinduced changes in integrated intracellular $AlPcS_{2a}$ fluorescence intensities measured in HN5 cells at set times. Cells were incubated with 10 μg/ml $AlPcS_{2a}$ for 18 hours and irradiated using a 670 nm laser. Images: $AlPcS_{2a}$ fluorescence images of cells before and 2 min after light exposure. Four cells were randomly chosen for fluorescence intensities analysis. Graph: Monitoring the changes of fluorescence intensity after several short irradiations (on: laser on; off: laser off, shown by arrows).

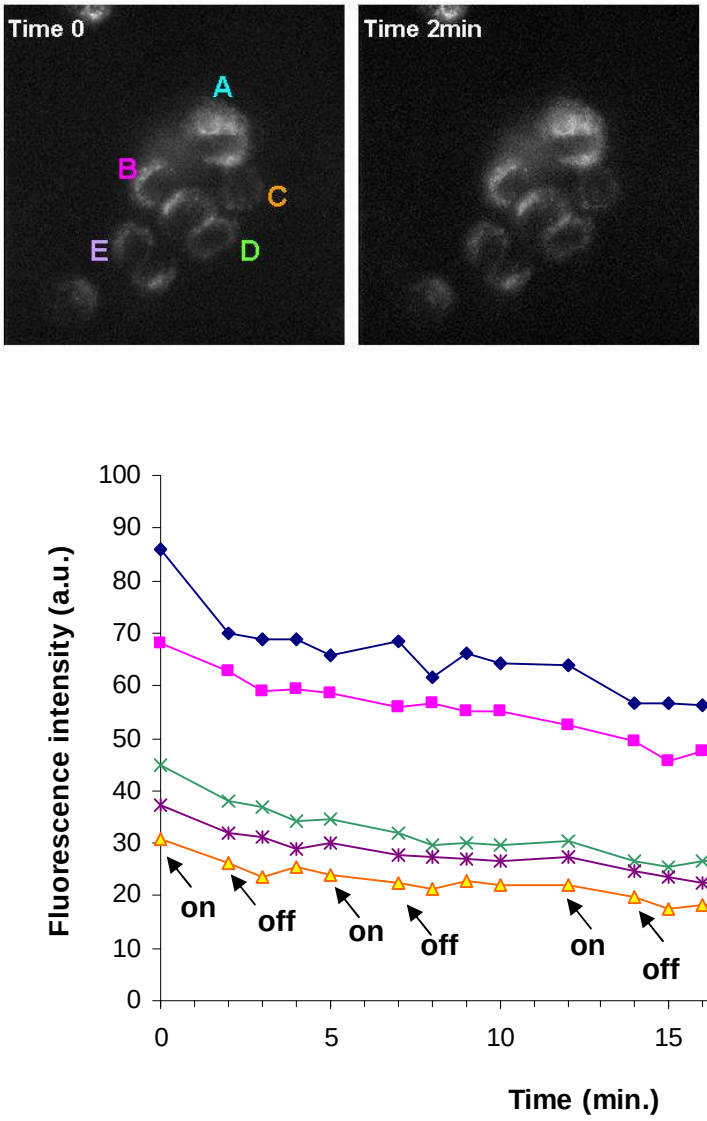

Figure 4.20 Photoinduced changes in integrated intracellular Amphinex fluorescence intensities measured in HN5 cells at set times. Cells were incubated with 0.1 µg/ml Amphinex for 18 hours and irradiated using a 543 nm laser. Images: Amphinex fluorescence images of cells before and 2 min after light exposure. Five cells were randomly chosen for fluorescence intensity analysis. Graph: Monitoring the changes of fluorescence intensities after several short irradiations (on: laser on; off: laser off, shown by arrows).

4.6 Discussion

4.6.1 Comparison of cellular uptake and photostability of $TPPS_{2a}$ and Amphinex

Cellular uptake is the process by which photosensitising molecules are incorporated and accumulated by living cells. The cell uptake of sulfonated alumimum phthalocyanines and meso-tetraphenylporphines has been investigated by comparing their different degrees of sulfonation [Berg et al., 1989b;Berg et al., 1990;Paquette et al., 1988]. The results showed that the derivatives bearing a reduced number of sulfonate groups exhibit better cell uptake and higher phototoxicity. This is consistent with the effect of sulfonate groups on decreasing the lipophilicity of the photoseisitising compounds. However, high hydrophobicity of photosensitisers will increase their tendency to aggregate and thereby reduce the photosensiticing activity. This might explain the observation that $AlPcS_1$ was found to be less toxic than $AlPcS_2$ [Berg et al., 1989a]. As a consequence, sensitisers with two sulfonate groups seem the most effective among sulfonated photosensitising agents for the use in PDT or PCI.

In this study, we found both $TPPS_{2a}$ and Amphinex displayed similar cellular uptake in A431 cells, as might be expected since the molecular structures are virtually identical. The drug concentrations used were the same as employed in the PCI studies described in the following section. A linear regression analysis of the results for fluorescence intensity versus increasing drug doses indicated a constant cellular uptake rate in a drug concentration dependent manner. No plateau was found for both drugs dose up to 0.5μg/ml. Higher doses could be applied to check for any plateauing of the cellular uptake, but there is the potential problem of increased toxicity induced when using higher concentration of photosensitisers which should be taken into account.

It is essential to determine the cell uptake and photobleaching in cells in order to evaluate the effectiveness of photosensitisers. Researchers so far have not successfully established *in vitro* mathematical kinetic models for the cellular uptake and photobleaching of different photosensitisers yet. Measuring photobleaching properties is important when carrying out PDT or PCI since it is possible that the light doses used would significantly affect the mean cellular levels of the photosensitiser. It is also important that a very low excitation light dose is used when using fluorescence detection so that there is minimal perturbation to the fluorescence measurements of

photobleaching or photomodification [Bastogne et al., 2007]. In this great care was taken to use low light doses combined with sensitive detection techniques. Measuring the changes of fluorescence intensity of photosensitisers during or after expose to light by spectrofluorimetry may not be ideal but is still the most straight-forward method to observe the photobleaching/photomodification processes in cells.

Photobleaching is the chemical destruction of fluorophores induced by light activation. $TPPS_{2a}$ and Amphinex display somewhat different photobleaching properties in A431 cells although their cell uptake and light absorption properties are comparable. The same blue light source for cell illumination was used in each case and fluorescence was detected using exactly the same excitation/detection setup. Fluorescence intensity was found increased at the beginning of irradiation and decreased after longer light exposure when using higher concentrations of $TPPS_{2a}$ (0.2 and 0.5 μg/ml). Using lower $TPPS_{2a}$ concentrations (0.1 and 0.05 μg/ml), the fluorescence signal within cells was decreased first upon illumination, then increased and decreased again after longer exposure time. In contrast to $TPPS_{2a}$, photobleaching of Amphinex was observed with continuously decreasing fluorescence intensity when irradiation started regardless the concentrations used (0.05-0.5 μg/ml). However, Amphinex bleached slowly in A431 cells and therefore displayed a higher fluorescence signal (80% of the original intensity) after longer light exposure in comparison with $TPPS_{2a}$. The results indicate that Amphinex is more photostable than $TPPS_{2a}$ in cells following light exposure.

The results here also give information about the suitable window of the light dose used for activating photosensitisers for PCI. The fluorescence intensity was similar to the original intensity after 10 min irradiation and remained within 90% of the original intensity in the case of $TPPS_{2a}$ and Amphinex respectively. Since the light dose used for PCI experiments in the following section described are within the range of light doses used here it can be inferred the effect of photobleaching on the PCI results is minimal.

4.6.2 Subcellular distribution of photosensitisers, co-localisation with organelles and redistribution after illumination

As mentioned before, amphiphilic photosensitisers are believed to display more ideal physical and pharmacokinetic properties compared to hydrophilic or hydrophobic

sensitisers [Allen et al., 2002]. Synthesis is carried out by chemical modification of the photosensitiser with two ionic sulfonate groups on adjacent sites of the periphery of the macrocycle. This polarity from the structure favours lipid membrane penetration and therefore makes amphiphilic sensitisers particularly suitable to be used in PCI which required a co-accumulation of sensitiers and anti-cancer drugs.

The optical properties of three photosensitisers ($AlPcS_{2a}$, $TPPS_{2a}$ and Amphinex) *in vitro* were examined in this section. Experiments including their intracellular distribution, redistribution after light, and the co-localisation with lysosomes and co-administered protein toxin were carried out using two squamous cell carcinoma cell lines, A431 and HN5 cells.

In general, all photosensitisers displayed a granular cellular distribution after cell uptake. Moreover, a light-induced redistribution was observed after light exposure using either a blue lamp for Amphinex and $TPPS_{2a}$ (Soret band absorption) or 670 nm laser irradiation for $AlPcS_{2a}$. As shown in Figure 4.11, the $AlPcS_{2a}$ fluorescence pattern inside cells was changed to a more diffuse distribution after a 20s light exposure. The increased intensity after the first 40s irradiation is believed to be caused by the monomerization of the sensitiser following disruption of intracellular vesicles [Kunz et al., 2007], which was also observed in the photomodfication studies (Figure 4.19). The diffuse pattern following light exposure is consistent with the process of photodynamic reactions which induces the rupture of endo-lysosomes membranes. This significant change also indicated that PCI could achieve sufficient release of macromolecules by using a very low light dose.

Since most of the hydrophobic or lipophilic sensitisers were found to favour lysosomes as their final targets after cell uptake [Geze et al., 1993], photosensitisers used in PCI strategy were assumed to follow this endocytotic pathway because of their amphiphilic properties. As a result, experiments imaging the intracellular distribution of photosensitisers together with LysoTracker Green labelled lysosomes were carried out to study further whether this particular subcellular distribution is indeed related to the distribution of lysosomes. According to the results of the co-localisation experiments, most of the red fluorescence produced from Amphinex is co-localised to lysosomes which are labelled with LysoTracker Green fluorescence (Figure 4.16).

PCI is a technology to release the co-administered anticancer agent retained within endo/lysosomal compartments after taken up via endocytosis by shining the light. The PCI effect in combination with different anticancer drugs has been well documented by analysing the cell viability after treatments but only few studies presented the PCI action by fluorescence microscopic studies. A conjugation strategy was used by Selbo and his colleagues who coupled a green fluorescence probe to gelonin and imaged its changes of cellular localisation after PCI in a melanoma cell line using epi-fluorescence microscopy [Selbo et al., 2000a]. In this study, we synthesized Alexa488-labelled saporin and carried out fluorescence imaging using an inverted confocal microscope with cells seeded in a glass-bottom dish for live and higher resolution image analysis. Therefore, we were able to examine the subcellular localisation of saporin and monitor the PCI action in sensitised cells by visualising photosensitiser and fluorescence labelled saporin at the same time.

The fluorescence spectrum of the saporin-Alexa488 complex was measured in comparison with AlexaFluor488 alone (Figure 4.14). The maximum emission is almost the same after conjugation but the possibility of perturbing the enzymatic activity of saporin after conjugation to Alexa488 should be considered. A relatively high concentration was used in these studies and some cell morphological changes were noted with more cells detaching from the base (Figure 4.17 and 4.18). As shown in the figures, the overlapping fluorescence images indicate the lysosomal localisation of Alexa488-labelled saporin and its co-localisation with photosensitisers. The PCI effect was visualised in the cells co-incubated with Amphinex and labelled saporin after expose to 90s at 405nm by the confocal laser microscope (Figure 4.18). Cells were also found to exhibit blebbing at this time point. A slow re-localisation of saporin was then observed 7 min after irradiation accompanying the redistribution of Amphinex with a diffuse pattern of distribution evident with lower fluorescence intensity.

This section has demonstrated the subcellular distribution of $TPPS_{2a}$, $AlPcS_{2a}$ and Amphinex by co-staining cells with lysosomal probes. Also, the re-localisation of these sensitisers was observed after light exposure. The PCI effect, the light-induced re-localisation of saporin, was visualised using Alexa488-labelled saporin in sensitised HN5 cells after irradiation on stage. Further studies to elucidate the photochemical reaction and to investigate the PCI effect in combination with anticancer agents will be illustrated in the following sections.

4.6.3 Fluorescence imaging of photodynamic modification of $AlPcS_{2a}$ and Amphinex in HN5 cells

Previous work done by Kunz and colleagues investigated photodynamic modification processes by imaging the fluorescence of disulfonated aluminium phthalocyanine in a macrophage cell line [Kunz et al., 2007]. The aim of the experiments here was the same but using purer $AlPcS_{2a}$ from a commercial source to carry out a comparison with Amphinex in HN5 squamous carcinoma cells. The drug concentrations and incubation times used were similar to those employed in the PCI studies.

$AlPcS_{2a}$ and Amphinex are both amphiphilic photosensitisers with a phthalocyanine and chlorin macrocycle respectively. Both of them exhibit efficient cell uptake in HN5 cells according to the results in previous sections. Using $AlPcS_{2a}$, similar results to the previous study were obtained where the fluorescence inside cells increased after a short irradiation, increased slightly and retained the intensity in the absence of light. The second irradiation was carried out when the fluorescence remained constant for 10 min after the first irradiation (Figure 4.19). Unlike the previous study by Kunz [Kunz et al., 2007], smaller light doses were used initially in order to resolve the induced fluorescence increase more clearly. However, it still resulted in a decline of fluorescence signal due to photobleaching. Amphinex, on the other hand, exhibited a different photomodification pattern in this experimental setting. No increase of fluorescence intensity was found after the first irradiation. Nevertheless, photobleaching was observed from the beginning when cells were exposed to light. Of course different light sources were used for each photosensitiser so it is difficult to compare the relative light doses absorbed by the cells for each photosensitiser. However it is clear that the fluorescence dynamics observed from the start of illumination are different

The aggregation of photosensitisers at high concentrations may explain the increase of $AlPcS_{2a}$ fluorescence after the first short illumination. Dimeric or aggregated $AlPcS_{2a}$ could be naturally formed when concentration is high which would result in self-quenching of the fluorescence signal [Berg et al., 1990;Moan et al., 1992]. This conclusion is supported by time-resolved fluorescence lifetime studies in cells [Kelbauskas and Dietel, 2002]. With light activation, lysosomal rupture occurs which results in release and dilution of the dimers which are then converted to monomers and this monomerisation results in an increase of fluorescence intensity which was observed

and detected in the early stage of photochemical reactions. In the previous study by Kunz, the transient increase of fluorescence intensity was only found when cells were treated with higher concentration of AlS_2Pc (10μM) for longer incubation time. Similar results were obtained in this study using 10μg/ml $AlPcS_{2a}$ in HN5 cells for 18 hours. In contrast, cells were treated with a much lower dose of 0.1μg/ml Amphinex for 18 hours. This was partly because Amphinex was easier to detect probably as result of more efficient cellular uptake and the fact that a much lower concentration of Amphinex can be used for PCI compared to $AlPcS_{2a}$.

The photomodification imaging studies using $AlPcS_{2a}$ also showed a transient increase in fluorescence which was ascribed to dimer monomerization. The fluorescence dynamics of $TPPS_{2a}$ in cells during irradiation therefore parallels to the intracellular photomodification of $AlPcS_{2a}$, but are different from Amphinex where only slow photobleaching was observed. The results obtained using Amphinex are also consistent with the earlier photobleaching study (Section 4.4) in a different cell line (A431) using fluorescence spectroscopy of cell monolayers. The fluorescence intensity of $TPPS_{2a}$ (higher concentrations) in cells increased initially and then decreased during illumination, whereas, the signal from Amphinex declined throughout the light exposure process (Figure 4.9 and 4.10). Therefore it appears that Amphinex under these incubation conditions (the same as employed for PCI) only undergoes slight photobleaching without any noticeable photomodfication processes such as light-induced monomerization.

Taking the results together from Sections 4.3 and 4.5, Amphinex has appears to exhibit distinct photobleaching properties from $TPPS_{2a}$ and $AlPcS_{2a}$. It should be noted however that whereas the same concentrations of $TPPS_{2a}$ and Amphinex were used (0.1 μg/ml) a much higher concentration of $AlPcS_{2a}$ was used which would favour dimerization. The lack of any transient fluorescence increase when using Amphinex could indicate that this compound undergoes less dimerization in cell membranes, which may be of benefit to its photoactivity. Resistance to aggregation may be a consequence of its tetraphenyl chlorin structure but further experiments comparing different photosensitisers in a range of doses should be conducted to unravel the exact mechanisms.

We did not attempt to investigate the role of oxygen in the photodynamic modification of photosensitisers here, but, oxygen dependence is an essential characteristic of photodynamic reactions. Considering the oxygen supply, cells were seeded in chamber slides instead of using conventional coverslips for microscopic observation. For the later photomodification studies glass-bottom ‘FluoroDishes’ which also enable live cell imaging were used to guarantee a sufficient oxygen supply. Therefore in all these studies the oxygen supply should not have been a limiting factor.

4.7 Determination of the Optimal Treatment Conditions of PCI - Analysis of the Phototoxicity Induced after PDT

4.7.1 Introduction

The overall cytotoxicity of PCI using a cytotoxic agent is combination of the phototoxic effect of PDT from the photosensitiser and the enhanced toxicity from the released cytotoxic agent. However, the 'photodynamic dose' (the product of the light dose and photosensitiser dose) employed in PCI for inducing breakdown of the membranes of intracellular organelles is much less than that required for PDT treatment itself which aims to kill the whole cell. In other words, only a sub-lethal PDT dose is required for the PCI strategy. The aim of this study was to establish the optimum combination of light dose and photosensitiser dose for PCI treatment in cells for sub-lethal treatment.

Based on studies carried out previously by Berg and co-workers to deliver several therapeutic agents with the size ranging from peptides, protein toxins to genetic materials [Berg et al., 1999], it was found that the efficacy of PCI was clearly dependent on the light dose which in turn is related to the PDT dose. For instance, in the study using $AlPcS_{2a}$ PCI to deliver pEGFP-N1/p(Lys) DNA complex, the maximum transfection was achieved at light doses which killed about 50% of the cells with the photosensitiser alone [Hogset et al., 2000].

Optimal PCI treatment conditions may vary when combining different sensitisers and therapeutic agents using different cell lines. It is essential therefore to study the PDT effect prior to subsequent PCI experiments in order to make sure that a sub-lethal PDT dose is employed in the PCI studies. This section will, therefore, investigate the PDT-induced phototoxicity induced by $TPPS_{2a}$, $AlPcS_{2a}$ and Amphinex in A431 and HN5 cells. From these data the sub-lethal phototoxic threshold (i.e. 50% cell death) combination of light and photosensitiser can then be established. The abbreviation 'PDT_{50}' will be used to describe the sub-lethal photodynamic dose that kills 50% of the cells.

4.7.2 Results

Phototoxicity of $TPPS_{2a}$ and $AlPcS_{2a}$ in A431 cells

The phototoxicity induced by $TPPS_{2a}$ and $AlPcS_{2a}$ was investigated in a range of drug concentrations under different light exposure time with A431 cells. Cell viability was dependent on light does and drug dose in both cases (Figure 4.21 and 4.22). The PDT_{50} caused by $TPPS_{2a}$ with A431 cells was at the concentration of 0.1 μg/ml and 3 min light exposure. Determination of treatments conditions corresponding to the PDT_{50} is important when selecting the optimum treatment parameters for PCI where a sub-lethal PDT effect is the aim. Using a 5 μg/ml concentration and 3 min light treatment 50% cell death of A431 cells was induced after $AlPcS_{2a}$ PDT. After 10min irradiation, less than 4% cells were viable when incubated with $AlPcS_{2a}$ for all drug concentrations in this experimental condition.

A negligible dark toxicity was measured in the cells treated with $TPPS_{2a}$. Compared to $TPPS_{2a}$, $AlPcS_{2a}$ induced some dark toxicity, but the cell viability was still more than 50% after the 18 hour-incubation of 10μg/ml $AlPcS_{2a}$.

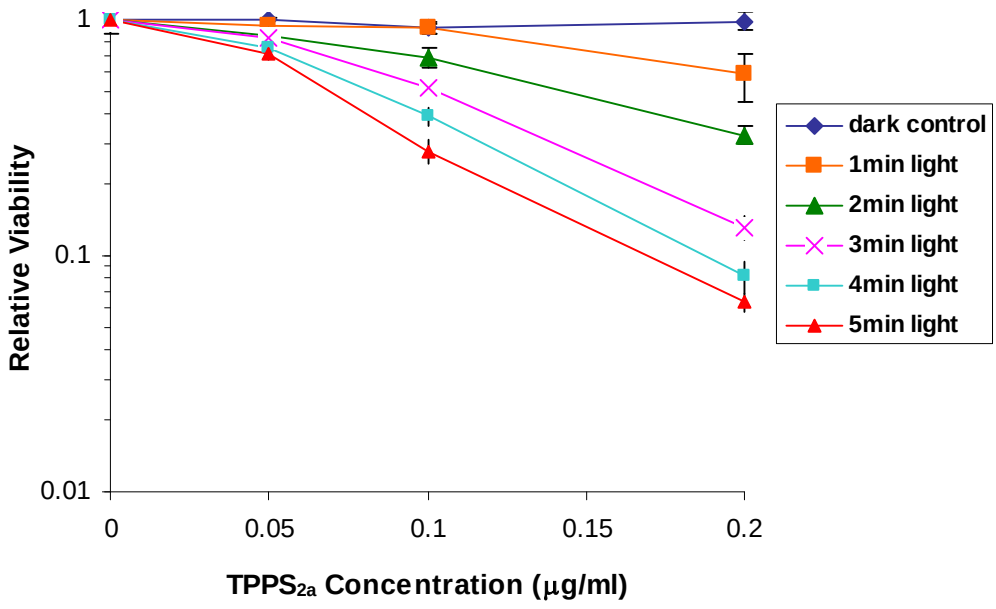

Figure 4.21 Phototoxicity of $TPPS_{2a}$ in A431 cells. Cells were incubated with $TPPS_{2a}$ with a range of concentrations for 18 hrs. Cells were irradiated using a blue lamp for up to 5 min. Cell viability was examined by the MTT assay 48hrs after irradiation.

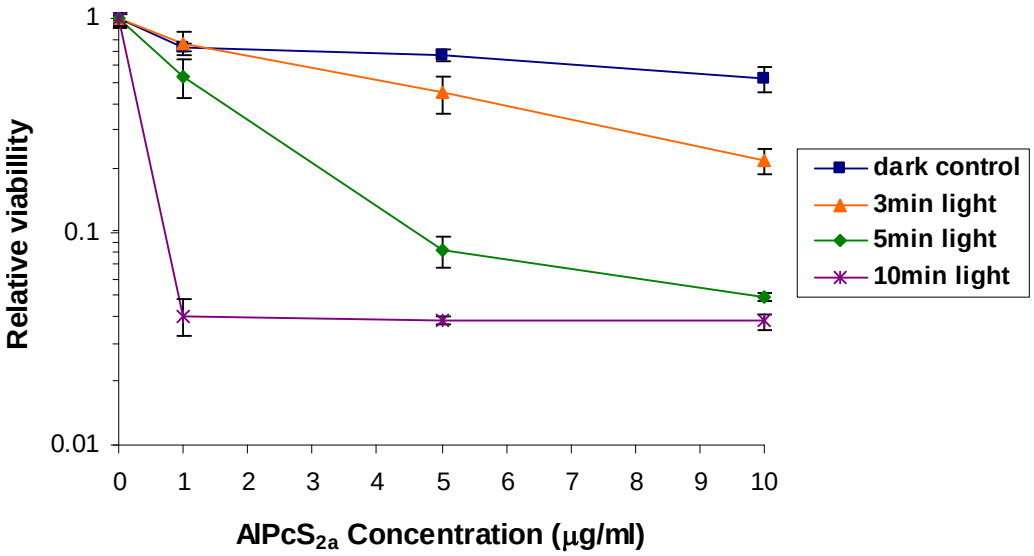

Figure 4.22 Phototoxicity of $AlPcS_{2a}$ in A431 cells. Cells were incubated with $AlPcS_{2a}$ with a range of concentrations for 18 hrs. Cells were irradiated using a 670nm laser for up to 10 min. Cell viability was examined by the MTT assay 48hrs after irradiation.

Phototoxicity of Amphinex in A431 and HN5 cells

The phototoxicity induced by Amphinex was investigated in a range of drug concentrations under different light exposure with A431 cells and HN5 cells. Light dose and drug dose dependent cell killing was found in both cell lines (Figure 4.23 and 4.24). Moreover, the phototoxicity of Amphinex in A431 and HN5 cells was very much similar. It was reduced to about a quarter using 0.1μg/ml Amphinex after 3 min light treatment. The PDT_{50} for both cell lines was achieved with a combination of 0.1 μg/ml Amphinex and 1-3min irradiation or 0.05 μg/ml drug and 3-5 min light exposure.

The cytotoxicity produced by Amphinex was very low without light exposure. It was only 15% and 6.5% in A431 or HN5 cells respectively when the drug concentration was 0.05 μg/ml. The cell viability was 86% in HN5 cells which were observed to be less sensitive to Amphinex compared to A431 cells.

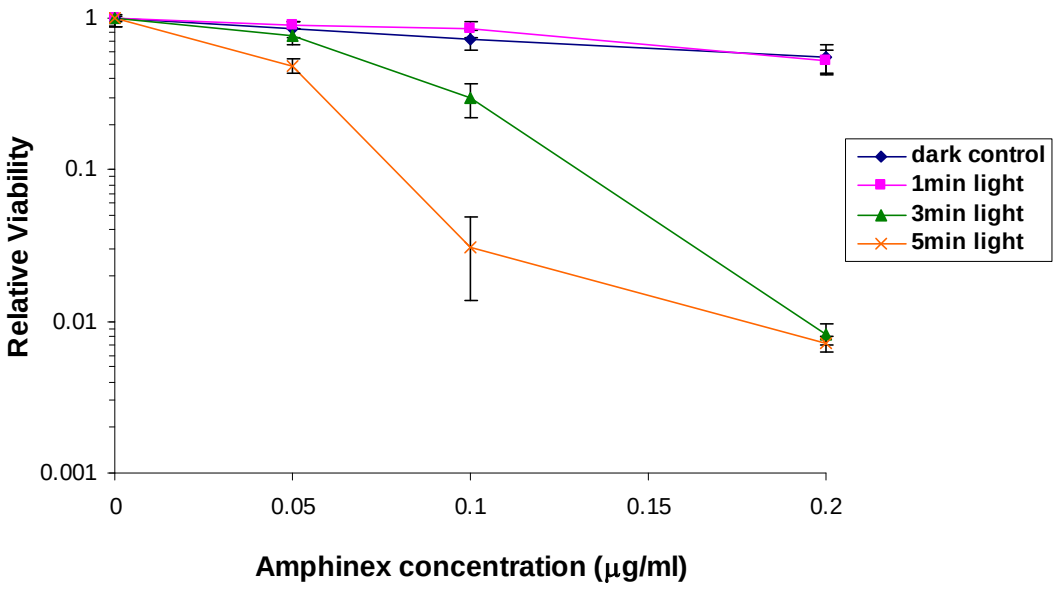

Figure 4.23 Phototoxicity of Amphinex in A431 cells. Cells were incubated with Amphinex with a range of concentrations for 18 hrs. Cells were irradiated using a blue lamp for up to 5 min. Cell viability was examined by the MTT assay 48hrs after irradiation.

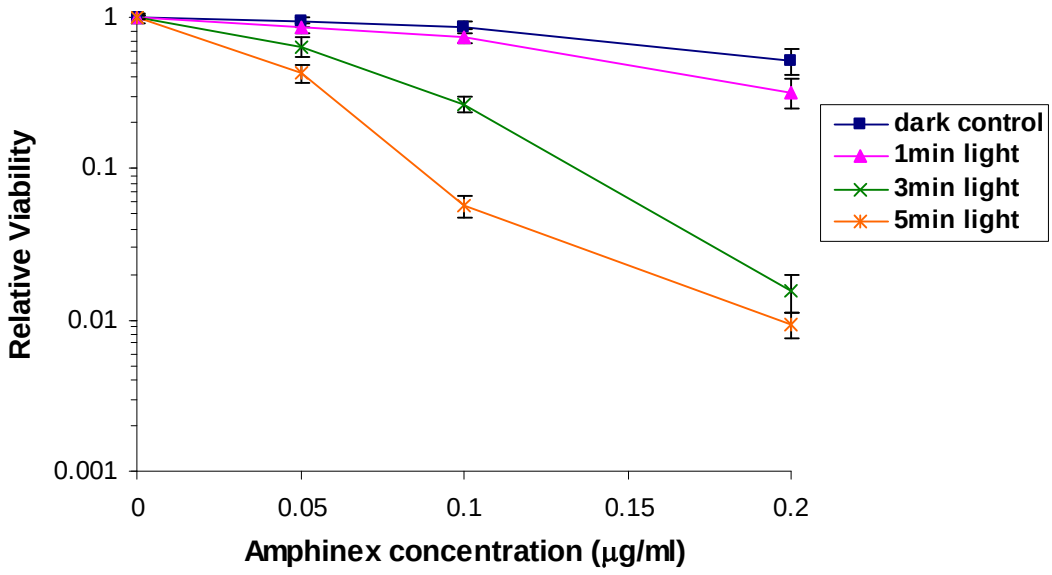

Figure 4.24 Phototoxicity of Amphinex in HN5 cells. Cells were incubated with Amphinex with a range of concentrations for 18 hrs. Cells were irradiated using a blue lamp for up to 5 min. Cell viability was examined by the MTT assay 48hrs after irradiation.

4.7.3 Discussion

PDT efficacy differs when used photosensitisers, light doses and cell lines are not the same. Effective PDT relies on an efficient cell uptake of photosensitisers and also an appropriate light source to induce the photodynamic reactions. The results in this section clearly show the drug dose and light dose dependence of PDT treatments – higher drug concentration or longer light exposure result in less cell survival.

Cells were treated with either sensitiser for 18 hours to make sure there is sufficient amount of drug taken up by cells. Due to the very low drug concentration window, the dark toxicity produced from either photosensitiser was relatively low in comparison with the treatments involving light exposure. This low dark toxicity therefore indicates the significant cell kill effects produced after irradiation were mainly from the photodynamic reaction.

In the experiments using $TPPS_{2a}$ or $AlPcS_{2a}$ in A431 cells, $AlPcS_{2a}$ induced a more appreciable enhancement of the PDT effect than $TPPS_{2a}$; however, $TPPS_{2a}$ is effective at a much lower concentration. This may be due to the more efficient excitation of $TPPS_{2a}$ by the blue lamp - the light dose delivered by the blue lamp is 1.26 Jcm^{-2} and is 0.16 Jcm^{-2} by the 670nm laser (for excitation of $AlPcS_{2a}$) after 3 min irradiation. The absorption of the two drugs at these respective wavelengths is similar.

Using the same blue lamp, Amphinex displayed a more effective PDT toxicity than $TPPS_{2a}$ on A431 cells. After 3 min irradiation, the cell viability was reduced to a half using 0.1μg/ml $TPPS_{2a}$ PDT but was less than one third using 0.1μg/ml Amphinex PDT. Exactly the same Amphinex PDT experiments were carried out but using HN5 cells. The cell kill effect was found similar to the results using A431 cells.

Many studies have indicated that the sub-lethal dose of PDT is the optimal condition for PCI treatments [Selbo et al., 2000a;Weyergang et al., 2006]. The results of this section show that either $TPPS_{2a}$, $AlPcS_{2a}$ or Amphinex could induce efficient PDT effect using very low drug concentration in A431 or HN5 cells. Marked cell kill effects were found after several minutes' light exposure. The findings, therefore, make an assumption that effective PCI effects using these three photosensitisers could be achieved if under appropriate combinations of therapeutic agents.

4.8 Photochemical Internalisation of Anti-Cancer Drugs

4.8.1 Introduction

The concept of photochemical internalisation (PCI) is based on the therapeutic effects of sequestered macromolecules and other bioactive agents through their release from vesicular compartments after the membrane-associated PDT treatment. The PCI effect is therefore a combination result of PDT effect and the drug toxicity. PCI has been used to relocate various types of macromolecules inside cells. These have been reviewed in more detail in Chapter 2 but among them, PCI in combination type I ribosome-inactivating proteins has been the most well-studied, in particular gelonin. Gelonin was the first type I RIP used in PCI which has exhibited synergistic cytotoxicity under this combined modality in many studies [Berg et al., 1996;Berg et al., 1999;Selbo et al., 2000a]. Further approaches using antibody-coupled gelonin displayed enhanced cytotoxicity in PCI strategy due to the increased cellular uptake of gelonin [Selbo et al., 2000b;Selbo et al., 2001a]. Saporin, one of the anti-cancer drugs used in the PCI studies in this thesis, is also a type I ribosome-inactivating protein but exerts much higher toxicity compared with gelonin [Bolognesi et al., 2000]. In two recent papers, PCI of saporin linked with epidermal growth factor (EGF) or the antibody against EGF receptor induced increased killing effects on EGFR positive cancer cells [Weyergang et al., 2006;Yip et al., 2007].

Another anti-cancer drug used in this thesis study is bleomycin. Bleomycins are a family of water-soluble glycopeptidic antibiotics which have been used in combination with several chemotherapy agents for cancer treatments in clinic [Sikic et al., 1985]. Bleomycin has been tested for whether its therapeutic effect could be improved by PCI *in vitro* using hamster lung fibroblasts and a human colon cancer cell line [Berg et al., 2005a]. Further details are given in Chapter 2. Although these two cell lines have different sensibilities to bleomycin, the synergistic inhibition of cell growth after PCI treatments was found in both cell lines treated with bleomycin.

Amphinex is a new photosensitiser designed for PCI technology. The aim of the studies in this section is to investigate the PCI effect using Amphinex by combinations with saporin or bleomycin in A431 human epidermoid carcinoma cells and HN5 human head

and neck squamous cell carcinoma cells. There are no published studies to date on Amphinex either for PDT or PCI in cells. The results of present study will be compared with $TPPS_{2a}$ and $AlPcS_{2a}$ which are so far the most common two PCI photosensitisers whose properties are better understood.

4.8.2 Results

Cytotoxicity of bleomycin and saporin in A431 and HN5 cells

The cytotoxicity induced by two anti-cancer drugs, saporin and bleomycin, with and without light exposure was examined prior to the combination with PDT treatment. In control cells without any applied drug but with exposure no change in viability was noted. Saporin produced similar toxicity in A431cells and HN5 cells either with light or without light treatment (Figure 4.25). The cell kill effect induced by bleomycin was also measured in both cell lines (Figure 4.26). The suitable drug dose for further PCI application is chosen when sub-lethal cell killing was induced. Therefore, up to 50 nM of saporin and 0.0007-0.007 IU/ml of bleomycin would be used to investigate the PCI effect in comparison with PDT treatment and in the presence of anti-cancer drugs only.

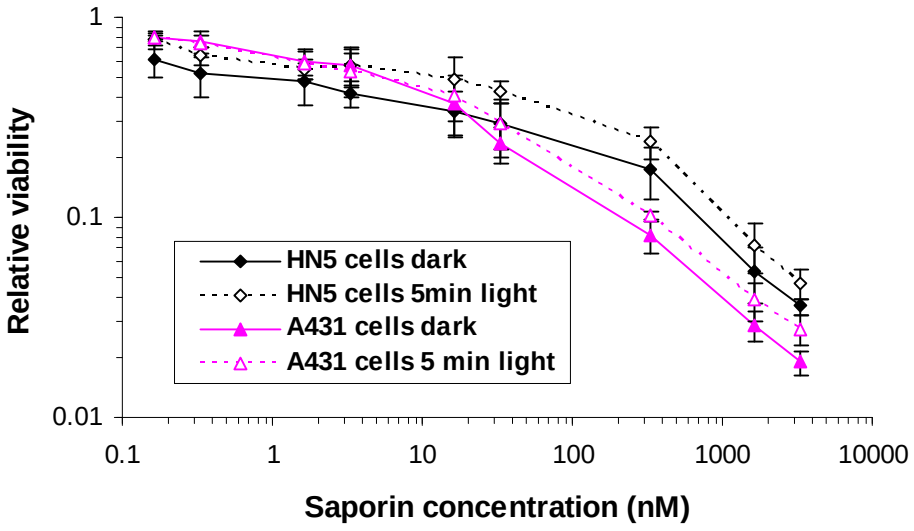

Figure 4.25 Cytotoxicity of saporin in A431 and HN5 cells with or without light exposure. Cells were incubated with saporin with a range of concentrations for 18 hrs. Cells were irradiated using a blue lamp for 5 min. Cell viability was examined by the MTT assay 48hrs after irradiation.

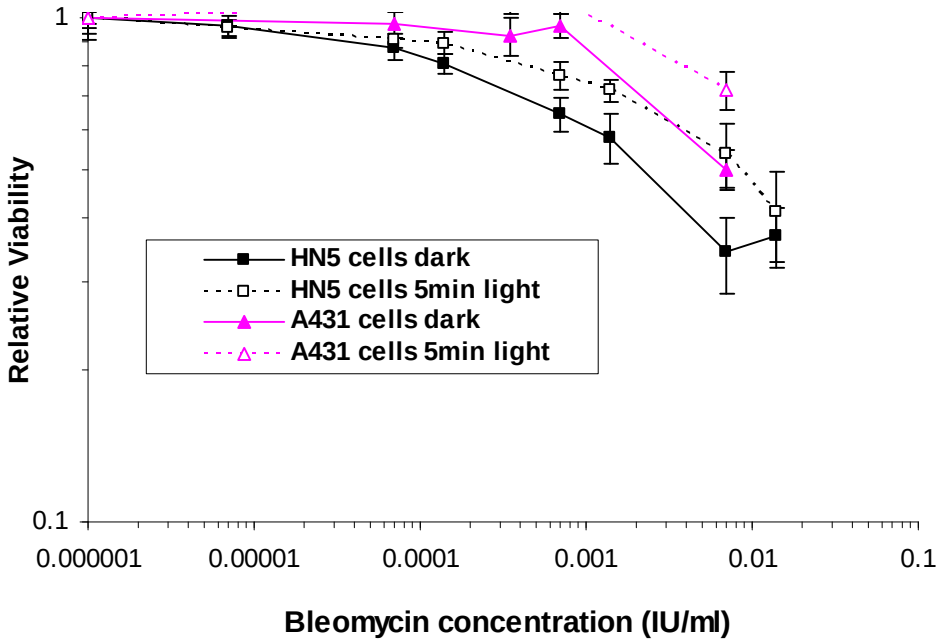

Figure 4.26 Cytotoxicity of bleomycin in A431 and HN5 cells with or without light exposure. Cells were incubated with bleomycin with a range of concentrations for 4 hrs. Cells were irradiated using a blue lamp for 5 min. Cell viability was examined by the MTT assay 4 days after irradiation.

Cytotoxicity of $TPPS_{2a}$ and $AlPcS_{2a}$ PCI combing saporin in A431 cells

The PCI effect combining saporin or bleomycin in A431 cells was investigated using $TPPS_{2a}$ and $AlPcS_{2a}$ with approximately the PDT_{50} doses. Light exposures of 3 minutes were employed in each case, and incubation times of toxins are given in section 4.2. Control measurements for light plus photosensitiser alone (i.e. PDT alone) are shown by the intercept values for zero concentrations of the cytotoxin. In each case the toxicity induced by PDT alone was about 50% (the exact values are shown in Table 4.1 in the Discussion at the end of this section). Enhanced cell killing was observed in combination with saporin or bleomycin after either $TPPS_{2a}$ or $AlPcS_{2a}$ PCI treatment (Figure 4.27-29). Figure 4.27 shows the effect of $TPPS_{2a}$ and $AlPcS_{2a}$ PCI in combination with saporin (0 to 5 nM) after 3 min light exposure. Cells treated with 0.1 μg/ml $TPPS_{2a}$ and 3 min irradiation exhibited about 50 percent survival. The cell survival by treatment with saporin alone was above 55 percent in this range of concentration but the cell viability was reduced to less than one fifth using 5 nM saporin in $TPPS_{2a}$-treated cells after 3 min light treatment ($p < 0.001$).

Comparable results were obtained using $AlPcS_{2a}$ PCI in combination with saporin. About 60 percent cells could survive from the PDT treatment with 5μg/ml $AlPcS_{2a}$ and 3 min light exposure. The cell viability was reduced to 6 percent in combination with 0.5 nM saporin after irradiation ($p < 0.001$) and was only 5 percent in the presence of 1nM saporin ($p < 0.001$).

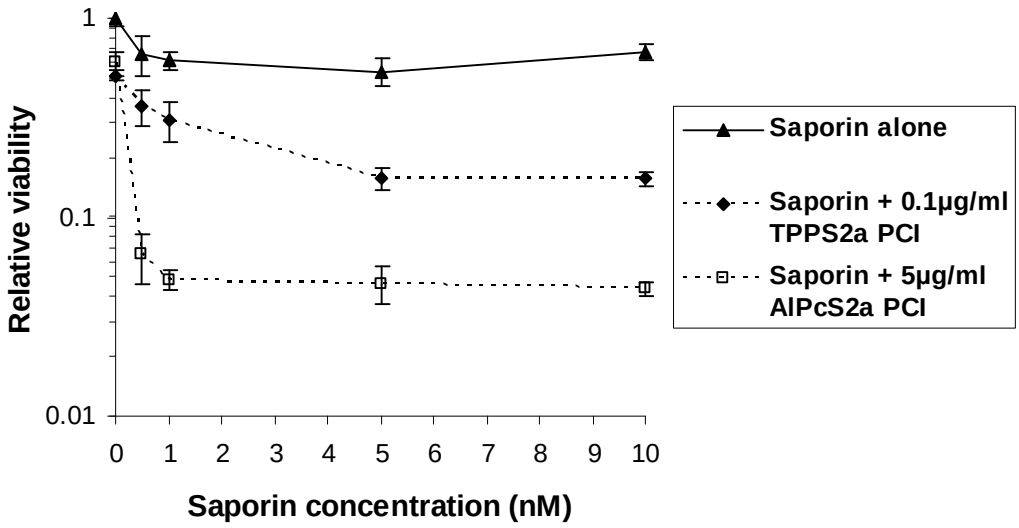

Figure 4.27 $TPPS_{2a}$ and $AlPcS_{2a}$ PCI of saporin in A431 cells after 3min light exposure. Cells were coincubated with $TPPS_{2a}$ (0.1 μg/ml) /$AlPcS_{2a}$ (5 μg/ml) and saporin (up to 10 nM) for 18 hrs. Cells were irradiated for 5 min using a blue lamp for activating $TPPS_{2a}$ and a 670 nm laser for $AlPcS_{2a}$. Cell viability was examined by the MTT assay 48hrs after irradiation.

Cytotoxicity of $TPPS_{2a}$ and $AlPcS_{2a}$ PCI combing bleomycin in A431 cells

An interesting finding was observed in the PCI treatments combing bleomycin; therefore, separate graphs are used to present the results. As shown in Figure 4.28 and 4.29, there is not much difference in the cell viabilities between cells treated with PCI upon shorter irradiation time and cells treated with bleomycin alone or with photosensitisers in the dark. Significantly enhanced cytotoxic effects induced by PCI were only found when longer light exposure was carried out using 5min irradiation for $TPPS_{2a}$ PCI and 10min light exposure for $AlPcS_{2a}$ PCI. These data are further analysed later in this section.

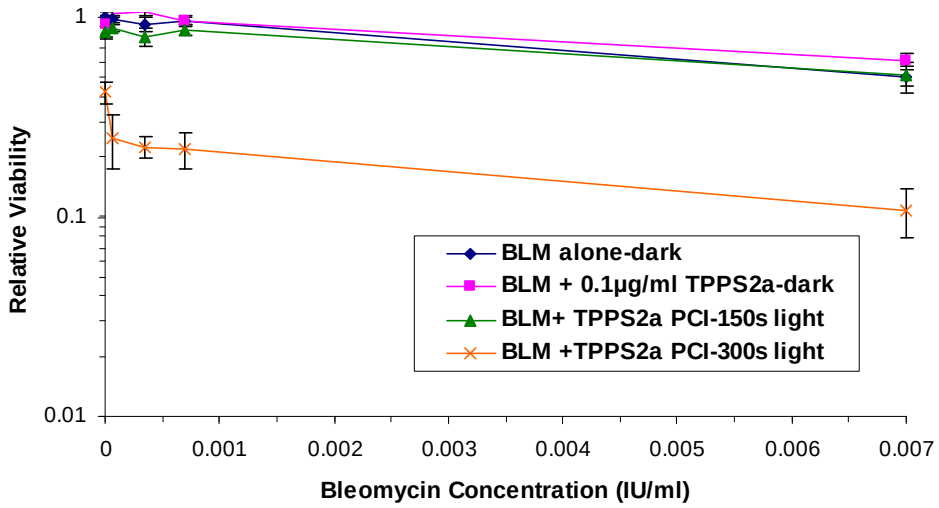

Figure 4.28 $TPPS_{2a}$ PCI of bleomycin in A431 cells. Cells were incubated with $TPPS_{2a}$ (0.1µg/ml) for 18hrs. Bleomycin (up to 0.007 IU/ml) was applied to cells 4 hrs before irradiation using a blue lamp. Cells were exposed to light for 150s or 300s. MTT assay was carried out to measure the cell viability 4 days after irradiation.

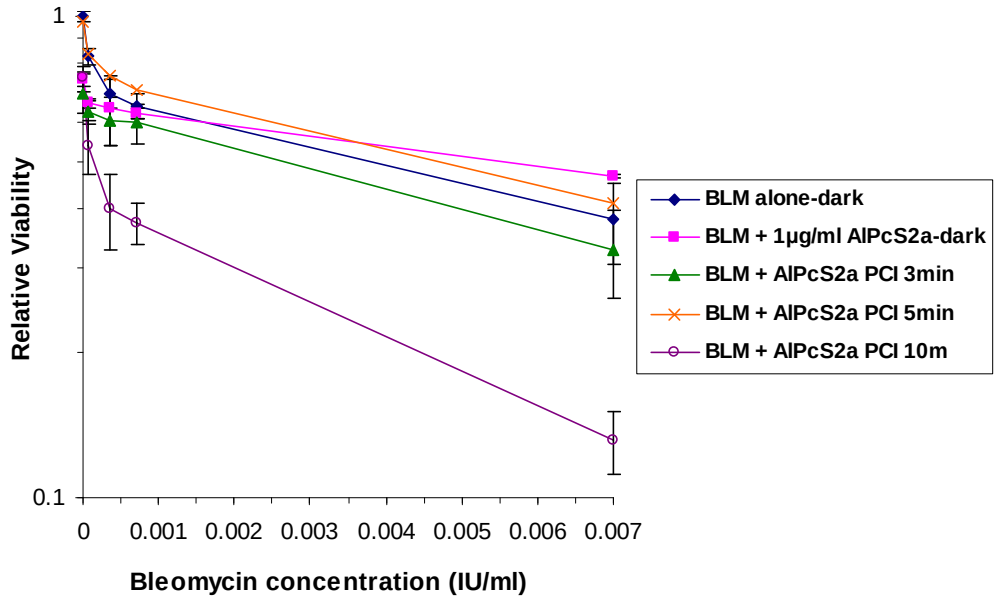

Figure 4.29 $AlPcS_{2a}$ PCI of bleomycin in A431 cells. Cells were incubated with $AlPcS_{2a}$ (1µg/ml) for 18hrs. Bleomycin (up to 0.007 IU/ml) was applied to cells 4 hrs before irradiation using a 670 nm laser. Cells were exposed to light for up to 10 min. MTT assay was carried out to measure the cell viability 4 days after irradiation.

Cytotoxicity of Amphinex PCI combing saporin and bleomycin in HN5 cells

This study was carried out after completion of the studies using $TPPS_{2a}$ and $AlPcS_{2a}$ (which were already available) since Amphinex only became available later in the

course of the project. By then a clinical trial of head and neck cancers using PCI was being considered therefore it was thought to be important to assess Amphinex PCI in a human head and neck cancer cell line. The human HN5 squamous cell carcinoma cell line derived from a head and neck tumour was available in our department, therefore experiments were conducted in this cell line. The Amphinex PCI effect on HN5 cells in combination with saporin and bleomycin was evaluated using the PDT_{50} photosensitiser and light dose combination.

Control measurements for the cytotoxic effects of saporin and bleomycin alone without light are given by the intercept values for zero light exposure. Enhanced cell killing was observed using 10-50 nM saporin concentrations. With saporin (25nM) and Amphinex (0.1μg/ml) PCI, the cell viability was significantly reduced by a factor of 29 after 3 min light exposure compared to saporin treatment alone (Figure 4.30). The results presented here were plotted as the cell viability versus light exposure because more light doses were used and fewer toxin doses were employed. This method of plotting the data was adopted from the PCI studies carried out by Berg et al. in which the PCI effect in relation to the illumination time can be seen clearly. Results of the later study in Chapter 5 using bioconjugates for PCI strategy are also presented in the same way.

Enhanced cell killing effects also could be found using bleomycin with Amphinex PCI. The survival rate became less than a half after 3 min light treatment if compared to the PDT group, whereas the cell viability remained steady irrespective of a longer irradiation time (5 min) (Figure 4.31).

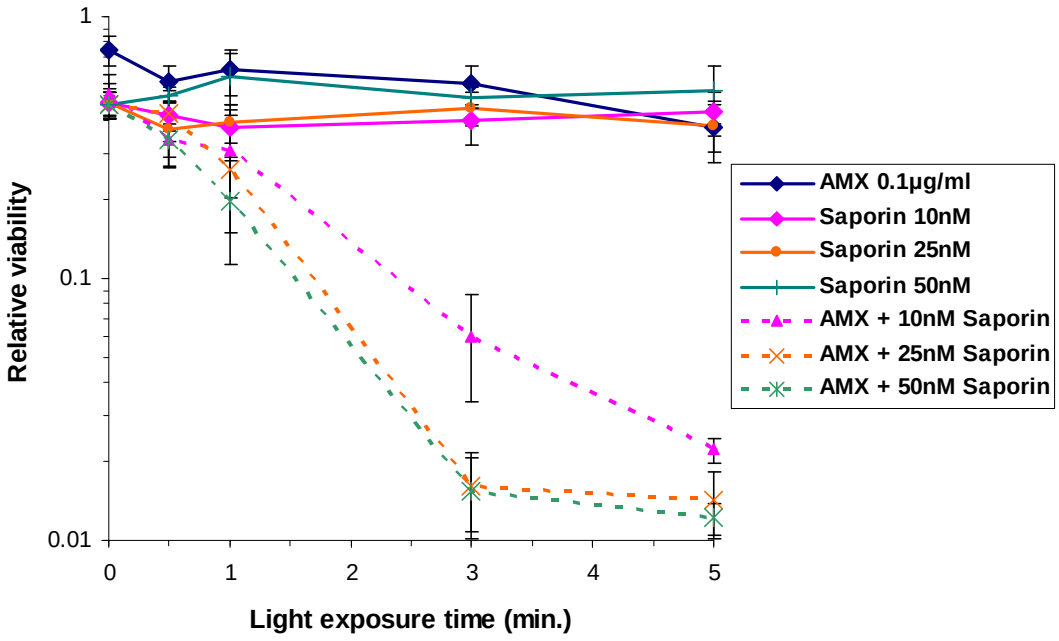

Figure 4.30 Amphinex PCI of saporin in HN5 cells as a function of light dose using different concentrations of saporin. Cells were coincubated with Amphinex (0.1 µg/ml) and saporin (up to 50 nM) for 18hrs. Irradiation was carried out up to 5 min using a blue lamp. Cell viability was examined by the MTT assay 48 hrs after exposure to light.

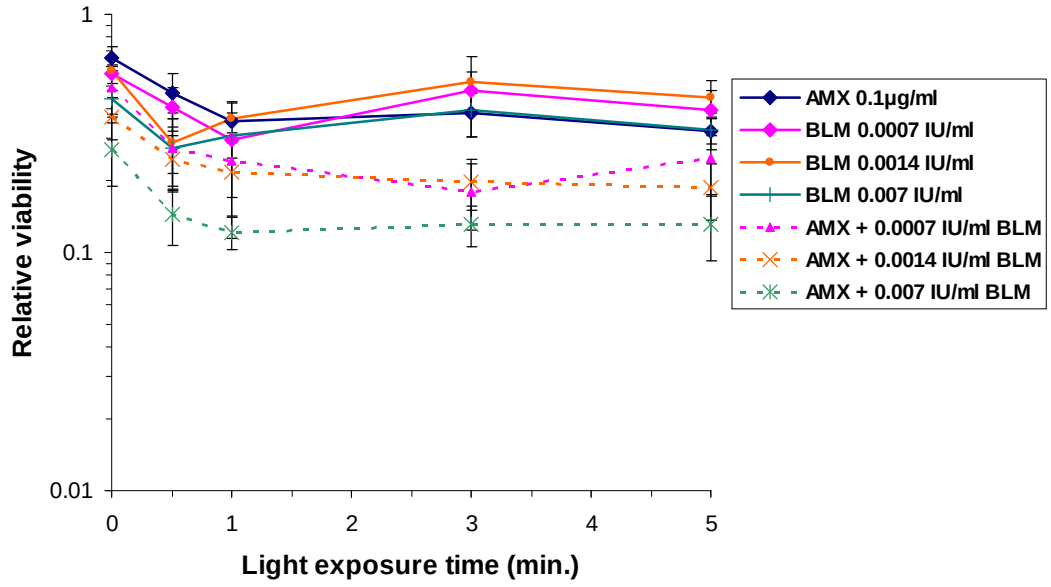

Figure 4.31 Amphinex PCI of bleomycin in HN5 cells as a function of light dose using different concentrations of bleomycin. Cells were incubated with Amphinex (0.1 µg/ml) for 18hrs and bleomycin (up to 0.007 IU/ml) for 4 hrs. Irradiation was carried out up to 5 min using a blue lamp. Cell viability was examined by the MTT assay 4 days after exposure to light.

4.8.3 Discussion

PCI is a technology which involves sub-lethal treatment of PDT to modify the intracellular distribution of co-administered drugs and other agents sequestered in lyso/endosomes [Berg et al., 1999;Hogset et al., 2004]. This section investigated whether an enhanced delivery of saporin and bleomycin to their intracellular target sites, and in turn their therapeutic efficacy, could be achieved by photochemical internalisation.

After receiving either $TPPS_{2a}$, $AlPcS_{2a}$ or Amphinex PCI treatment using the saporin and light does which induced 50% cell death, cell viability was reduced significantly ($p < 0.001$). Synergistic effects were found combining saporin in all PCI treatments. Synergistic cell killing corresponds to a loss of cell viability greater than the additive effects arising solely from toxin toxicity and PDT toxicity.

Table 4.1 summarises the optimal parameters of the PCI treatments which achieved enhanced cytotoxicity combining saporin or bleomycin in this section. The calculated additive effect is the multiplication of the toxicity observed from toxins (A) alone and from sub-lethal PDT alone (B) (A, B stand for the values of relative viability (e.g. A = 0.5 for 50% viability etc.). The PCI effect (C) represents the measured viability from the overall combination of light, photosensitiser and toxin. The ratio (A x B) / C can therefore indicate whether a synergistic enhancement or a purely additive effect is obtained from the treatment: i.e. a value of 1 would therefore correspond to purely additive effects whereas a value greater than one would correspond to a synergistic effect and a value less than one would correspond to an antagonistic effect.

The greatest synergistic enhancement was achieved by Amphinex PCI of saporin in HN5 cells in which the cell viability was reduced by a factor of 16 compared to the additive toxicity from sub-lethal PDT and saporin under the same light exposure. $AlPcS_{2a}$ PCI of saporin and bleomycin in A431 cells also reduced the cell viability by a factor of 7 and 2.6 respectively compared to the combination effect from PDT and toxins. The PCI effect using $TPPS_{2a}$ enhanced the toxicity in A431 cells by a factor of 2 in combination with both toxins. In contrast, Amphinex PCI of bleomycin in HN5 cells only induced moderate toxicity in which the overall effect was about the sum of Amphinex PDT and bleomycin.

	Cells	A431			
	Photosensitiser	**$TPPS_{2a}$ 0.1 µg/ml**		**$AlPcS_{2a}$**	
				5 µg/ml	**1 µg/ml**
Treatment viability (%)	**Toxins only** (A)* (dose and light exposure time)	**SAP 5 nM** (3min light)	**BLM 0.007 IU/ml** (5min light)	**SAP 5 nM** (3min light)	**BLM 0.007 IU/ml** (10min light)
		54.0±8.6	50.1±4.7	54.0±8.6	46.6±0.3
	PDT only (B) (no toxins)	51.6±2.8	42.2±5.1	59.6±8.6	74.4±4.6
	PCI (C) (with same light dose)	15.7±1.8	10.8±2.9	4.6±0.9	13.1±1.9
Ratio of effect of PCI over toxin only (A/C)		3.4	4.6	11.7	3.6
Synergistic effect - ratio of (A x B)/C		1.8	2.0	7.0	2.6

	Cells	HN5	
	Photosensitiser	**Amphinex 0.1 µg/ml**	
Treatment viability (%)	**Toxins only** (A) (dose and light exposure time)*	**SAP 25nM** (3min light)	**BLM 0.007 IU/ml** (3min light)
		47.1±6.3	44.3±7.3
	PDT only (B) (no toxins)	55.5±9.6	35.5±6.6
	PCI (C) (with same light dose)	1.6±0.5	13.1±2.6
Ratio of effect of PCI over toxin only (A/C)		29	3.4
Synergistic effect - ratio of (A x B)/C		16	1.2

Table 4.1 Optimisation of PCI. Cell survival (%) after $TPPS_{2a}$/$AlPcS_{2a}$ /Amphinex PCI in combination with saporin/bleomycin with A431 cells or HN5 cells. The errors are presented as ± SD. The synergistic effect is presented as the ratio of the calculated additive effect (A x B) and measured PCI effect (C). The comparison of the PCI effect and toxicity from toxins alone is shown as the ratio A/C. PS: Photosensitiser; SAP: saporin; BLM: bleomycin. * with light but no photosensitiser

In fact, the variable PCI effects in combination with bleomycin using different cell lines and sensitisers reflect some aspects found in these series of experiments where the experimental protocol was the same as the PCI treatments using saporin. First of all, bleomycin was found to be relatively more toxic than saporin; since not many cells

could survive after 18 hrs drug incubation with bleomycin. Therefore, a shorter drug incubation time where cells were only treated with bleomycin for 4 hours before irradiation was employed through out all experiments, as shown Figure 4.4. Secondly, it also has to be noted that the end time point of cell viability measurement differs from that in the saporin experiment either. The survival of bleomycin-treated cells was measured 4 days after light treatments. This is because no distinct PCI effect was observed when the cell survival was measured 2 days after irradiation (data not shown). This effect was also pointed out by the pioneering paper which evaluated the potential of $AlPcS_{2a}$ based-PCI of bleomycin [Berg et al., 2005a]. Using other measurements to examine the cell viability instead of changing the experiment termination time could also be options. The MTT assay is the most common method to determinate the cell viability but will not be suitable for every circumstance especially when experiments may have influence on cell mitochondria. The protein synthesis assay which measures the total protein amount which would be appropriate for saporin or the clonogenic assay and gives a measure of the long-term cell survival are other possibilities although time-consuming.

Nevertheless, a modified protocol which extended the exposure time but reduced the dose of photosensitisers seemed to work better in combination with bleomycin since more efficient PCI effects (i.e. significant cell killing; $p<0.05$) were only observed when longer irradiation treatments were carried out. A summary is shown in Figure 4.32. The results indicate that the optimal PDT condition for photoactivating bleomycin may not be at the PDT_{50} condition of photosensitisers and light doses. This finding shows that it is necessary to optimize the treatment conditions as it may vary because of the different pharmacokinetics of the drugs and also the cell lines used.

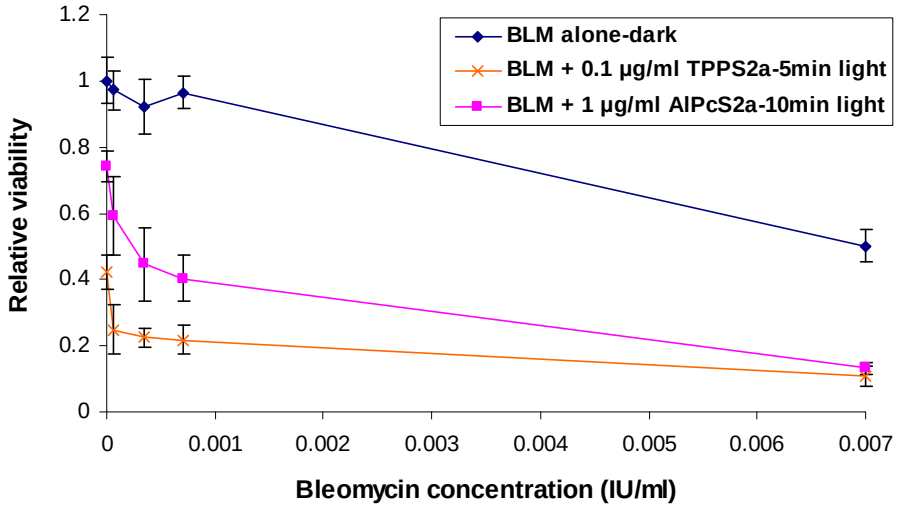

Figure 4.32 $TPPS_{2a}$ and $AlPcS_{2a}$ PCI of bleomycin in A431 cells. Cells were incubated with $TPPS_{2a}$ (0.1 µg/ml) /AlPcS2a (1 µg/ml) for 18hrs. Bleomycin (up to 0.007 IU/ml) was applied to cells 4 hrs before irradiation using a blue lamp for activating $TPPS_{2a}$ (5 min)and a 670 nm laser for $AlPcS_{2a}$ (10 min). MTT assay was carried out to measure the cell viability 4 days after irradiation.

The most encouraging finding from these series experiments is the very low doses of saporin used in the PCI treatments i.e. < 25 nM. It has been proven that PCI strategy using $TPPS_{2a}$ and $AlPcS_{2a}$ could enhance the therapeutic effects of gelonin [Berg et al., 1999;Selbo et al., 2000a]. With similar experimental settings, the results in this study show that saporin is more effective than gelonin. Massive cell killing was achieved using Amphinex PCI in combination with less than 50 nM of saporin after 3 min light exposure (Table 4.1). Comparable results also have been reported in recent two studies which saporin was photoactivated using $TPPS_{2a}$ in other cell lines [Weyergang et al., 2006;Yip et al., 2007]. Increased drug and light doses may result in further reduction of the cell viability. The results obtained in this and the previous section also warrant that Amphinex can induce efficient photosensitisation and Amphinex PCI of saporin is feasible for future tumour treatments *in vivo* and in the clinic.

4.9 Summary

The results in this chapter have demonstrated the PCI action *in vitro*. The intracellular distribution and the light-induced relocalisation of photosensitisers was observed using fluorescence microscopy. From the results shown in section 4.4, the changes from granular to diffuse distribution correspond to the process of photochemical reactions which induced the rupture of endo/lysosomes. This significant difference also indicated that PCI could achieve sufficient release of macromolecules by using a very low light dose. Moreover, the intracellular distribution of Alexa488-labelled saporin was also observed to become more diffuse following light exposure, consistent with lysosomal rupture occurring during PCI

To investigate the efficacy of the cell uptake and the photobleaching of photosensitisers after light treatment, cells were incubated with the photosensitisers and the fluorescence intensity was measured by a spectrometer (Section 4.3). Further experiments to study the detailed fluorescence changes within cells were carried out by imaging the photodynamic modification inside cells (Section 4.5). The differences of the cellular uptake and the photobleaching after irradiation between sensitisers are primarily caused by their different physiochemical properties and the local concentration inside endo/lysosomes. When cells were treated with relatively high concentrations of $AlPcS_{2a}$, the photochemical reactions leading to endo/lysosomal rupture induced an increase in fluorescence intensity at the beginning of light exposure. This is most likely due to the presence of photosensitiser dimerization at high concentrations and the dimerized photosensitisers are weakly or non-fluorescent. Upon endo/lysosmal rupture these dimers are converted to monomers which are fluorescent Sensitisers all underwent photobleaching after longer light treatment.

Two anti-cancer drugs, saporin and bleomycin, exhibited enhanced cytotoxicity in combination with $TPPS_{2a}$, $AlPcS_{2a}$ and Amphinex based PCI (Section 4.8). Sub-lethal PDT and toxins doses were generally the optimal condition to induce efficient PCI. It may however be necessary to modify the treatment protocols to adapt to different therapeutic drugs because of their different pharmacokinetic properties. Under optimal treatment conditions, PCI can relocate bleomycin and saporin inside cells and thus enhance cell death.

In addition to photosensitisers, light source and the presence of molecular oxygen, the three required elements for PDT treatment, the other participant in PCI is the therapeutic macromolecule. As mentioned before, the size range of the internalized drugs is very broad. For example: even though the molecular weight of bleomycin is 1400 but 30 kD for saporin, both chemotherapy drugs produced significant enhancement of cytotoxicity after PCI procedure. The drug doses in this study were calculated in different ways based on the information from the drug suppliers and the conventional usage. Saporin doses were measured in molar concentration whereas bleomycin was presented in IU/ml (IU – International Unit). The conversion between different units is shown in Table 4.2.

	Molecular weight/Da	**Doses used in this study**	**Molar concentration**
$TPPS_{2a}$	**775**	0.1 μg/ml	130 nM
$AlPcS_{2a}$	**770**	5 μg/ml	6.49 μM
Amphinex	**777**	0.1 μg/ml	129 nM
saporin	**30K**	Up to 25 nM	
bleomycin	**1400**	Up to 0.007 IU/ml	Up to 3.36 μM

Table 4.2 Conversion of drug concentration.

It can be seen that saporin is effective using much lower doses than bleomycin. Studies in this chapter have attempted to investigate the versatility of PCI by using three photosensitising compounds in combination with two different anti-cancer drugs in two cell lines. Promising results were obtained that PCI could induce significant enhancement in combination with saporin and bleomycin *in vitro*. Furthermore, the results also indicate that Amphinex has the properties deemed favourable for PDT and PCI. *In vivo* studies to evaluate the efficacy of Amphinex PCI in combination with these two toxins were carried out in normal rat liver/colon and subcutaneous rat tumour models. Results will be presented in the following chapters.

Chapter 5: Studies of Bioconjugates for PDT and PCI

5.1 Investigation of a Tat Peptide-Photosensitiser Bioconjugate for Photodynamic Therapy and Photochemical Internalisation

5.1.1 Introduction

Pharmaceutical agents should be internalised into cells and delivered to their target sites to exert the therapeutic action. However, low bioavailability due either to poor cell membrane penetration and/or the lack of water solubility is one of the key problems in drug delivery. Porphyrins are well known photosensitising agents but their low water solubility in many cases has limited their biomedical application. Meso-tetraphenylporphine (TPP) is one example of non-water soluble photosensitisers, which cannot be used without a suitable delivery system. There have been several approaches to overcome this problem. For instance, the introduction of conventional pharmaceutical carriers, such as liposomes [Postigo et al., 2004] or micelles [Roby et al., 2006], improves the bioavailability by delivering the photosensitiser in a water-soluble formulation. Another approach to improving bioavailability is the use of conjugating drugs with cell penetrating peptides (CPP) which can enhance the water solubility and cellular uptake of drugs. In this section, a new peptide-tetraphenylporphine conjugate is described, using the cell penetrating 'Tat' peptide, derived from the human immunodeficiency virus type I (HIV-1). These photophysical and photobiological properties of this bioconjugate were investigated to see whether it is suitable as a photosensitising compound for both photodynamic therapy and photochemical internalisation.

In 1988, Green and Frankel independently reported the cell membrane translocation ability of the trans-activating transcriptional activator (Tat), a protein from human immunodeficiency virus type I (HIV-1) [Frankel and Pabo, 1988;Green and Loewenstein, 1988]. Green chemically synthesized the 86-mer Tat protein and Frankel used the purified Tat protein. Both Tat proteins were able to enter cultured cells and induce the trans-activation of the viral promoter. The full-length protein was soon characterized as a protein with multiple functional domains [Kuppuswamy et al., 1989;Ruben et al., 1989] and the highly basic region which contains six arginine (Arg)

and two lysine (Lys) in nine residues is assigned to the protein translocation activity [Vives et al., 1997a].

Since the 1990s, other proteins or peptides also demonstrated the property of translocation. One group is derived from natural proteins (penetratin (Antp), derived from *Drosophila* Antennapedia [Joliot et al., 1991]; VP22, the transcription factor of herpes simplex virus type 1 [Elliott and O'Hare, 1997]; pVEC, from murine vascular endothelial cadherin [Elmquist et al., 2001]). Other groups include designed peptides (transportan, a fusion peptide of neuropeptide galanin and mastoparan [Pooga et al., 1998] or synthetic polyarginines [Futaki et al., 2001]. These proteins and peptides all contain the highly positive charged protein transduction domains (PTDs) or cell penetrating peptides (CPPs) that are responsible for protein transduction, i.e. the translocation process across the cell membrane.

Several approaches to link pharmaceutical cargos to Tat peptides or other CPPs to overcome the cell membrane barrier have been carried out over the past two decades. Up to date, Tat peptides have been proven to facilitate the cell entry of various molecules ranging from peptides [Gius et al., 1999] with hundreds of daltons molecular weight to liposomes [Torchilin et al., 2001] with massive structure whose diameter up to 200nm. The remarkable success of Tat peptides in drug delivery has drawn lots of attention to researchers to study the mechanisms involved in the internalisation and intracellular delivery. A reduction of cellular uptake was found when Tat peptides were modified with single deletion or substitution of the core sequence ‘GRKKRRQRRR’ in the basic domain resulted in the change of charges [Vives et al., 1997b;Wender et al., 2000]. Diminished cellular uptake indicated the unique highly cationic nature of Tat peptides certainly plays a key role in the cell uptake process. The direct electrostatic interaction between the positively charged Tat peptides and the negatively charged proteoglycans or glycosaminoglycans on the cell surface is required in the internalisation [Console et al., 2003;Sandgren et al., 2002]. Despite earlier misinterpretations of the uptake mechanism resulting from artificial uptake and nuclear localisation caused during the cell fixation procedures endocytotic uptake is the recognized mechanism for Tat peptides and most of other CPPs mediated drug delivery [Richard et al., 2003].

However, no specific import pathways could be concluded for the Tat-peptide-mediated biological cargo deliveries. Both lipid raft-mediated caveolar endocytosis and the clathrin-mediated endocytosis were identified as endocytotic routes of Tat-fusion proteins [Fittipaldi et al., 2003;Vendeville et al., 2004]. Tat-protein conjugates was also found entering cells via macropinocytosis, a rapid non-specific lipid raft cell uptake pathway [Wadia et al., 2004]. Tat-Cre (cAMP response element) fusion protein successfully entered cells and recombined DNA through macropinocytosis. Additionally, in the same study, because of the observation that most of the Tat-Cre proteins remain trapped in macropinosomes, another strategy was used to trigger the endosomal escape of Tat fusion protein. Co-treament with dTat-HA2 which Tat peptide conjugated to a fusogenic peptide, the N-terminus domain of the influenza virus hemagglutinin protein HA2, was able to drop the pH in mature endosomes, release the Tat fusion proteins into cytoplasm, and thereby achieve their nuclear localisation. Therefore, the mechanism of Tat peptide mediated endocytic uptake may be dependent on the attached cargo; this cargo-orientation manner was also suggested in the case of other CPPs [Maiolo et al., 2005].

To date, more than 20 Tat-derived short peptides with various modifications at either the N-terminal or the C-terminal ends have been used for delivering drugs into cells [Brooks et al., 2005]. The advantages and versatility of the Tat peptide-mediated drug delivery are not limited *in vitro*. The most well-known *in vivo* study was conducted by Schwarze and his colleagues in 1999 using a Tat fusion protein (120 kD) in which β-galactosidase (116 kD) was ligated to the protein transduction domain [Schwarze et al., 1999]. After intraperitoneal injection in mice, Tat-β-Gal was found to distribute into virtually every organ and even cross the blood brain barrier in 4 hours. Moreover, the β-Gal enzyme activity was assayed by X-Gal staining and found to remain strong in most of the tissue sections except kidney which is presumably due the clearance from the blood stream. The promising results from this study opened the possibility of Tat peptides as tools for *in vivo* drug delivery.

Porphyrin-type photosensitisers constitute the major class of photosensitising agents in photodynamic therapy. Conjugation strategies that modify sensitisers by linking to certain peptides or proteins with targeting function have been used to improve the selectivity of photosensitiser delivery since 1994 [Chaloin et al., 2001;Hamblin and Newman, 1994]. For example, penetratin coupled to 5-aminolevulinic acid was shown

to be taken up by cells and could be successfully converted to photoporphyrin IX via the haem biosynthetic pathway [Dixon et al., 2007]. CPPs-porphyrin conjugates also have been synthesized as photoactive compounds. Sibrian-Vazquenz at al. synthesized different porphyrin-peptide conjugates bearing PEG linkers to several targeting sequences including the Tat peptide (48-60) to compare their cellular uptake, subcellular localisation and the phototoxicity *in vitro* [Sibrian-Vazquez et al., 2006] . Sehgal et al., from the same group, examined the cell uptake and phototoxicity of five porphyrin-peptide conjugates using a prostate cancer cell line [Sehgal et al., 2008]. Among these bioconjugated photosensitisers, the Tat peptide-porphyrin conjugate exerted favourable *in vitro* cellular uptake and phototoxicity, and also the biodistribution in tumour bearing SCID mice.

In view of the recent literature reviewed above, enhancing the biological efficacy of porphyrin sensitisers by conjugation with a Tat peptide appears to be a promising approach. In the studies described below, a Tat peptide-tetraphenylporphine bioconjugate (Tat-TPP) was carefully designed and its capability for photodynamic therapy was investigated. The schematic structure is shown in Figure 5.1 with a hydrophobic porphyrin macrocycle linked to a 'Tat' peptide, which is cationically charged since the peptide contains several amino groups which will be protonated at physiological pH. The full chemical structure is shown in Figure 5.2. With this amphiphilic structure the bioconjugate should in principle localise well in membranes with the hydrophobic porphyrin localised within the lipid membrane and the cationic Tat sequence residing at the anionic membrane surface. Based on this reasoning it was hypothesized that this bioconjugate would be effective for PCI.

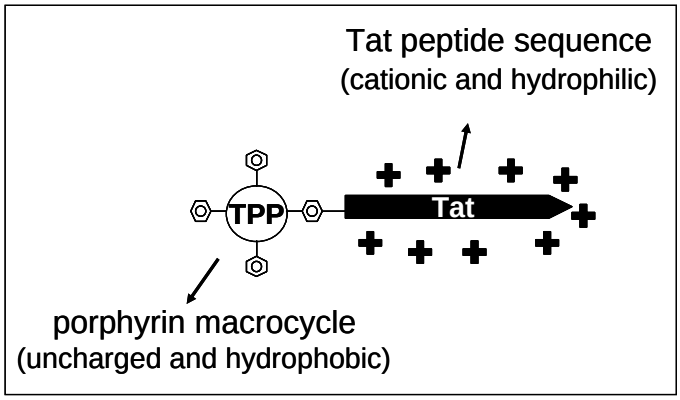

Figure 5.1 Tat-tetraphenylporphine (Tat-TPP) bioconjugate

Study aims:

It is hypothesized that a Tat-TPP conjugate could be suitable for photochemical internalisation because of the amphiphilicity produced by the hydrophilic and cationic Tat peptide sequence and the hydrophobic porphyrin. Experiments detailed below cover the assessments of its photophysical properties (absorption/fluorescence spectra, fluorescence lifetime and singlet oxygen production) and its photobiological properities such as cellular uptake, subcellular localisation and phototoxicity, and finally the PCI effect in combination with the cytotoxin saporin using HN5 cells.

5.1.2 Materials and methods

Synthesis of Tat-TPP conjugates

The synthesis of the Tat-TPP conjugate was done by Dr Francesca Giuntini from the Department of Pharmacy and Pharmacology, University of Bath. Details on the synthesis and characterization are shown in Appendix I. The structure of Tat-TPP conjugate is shown in Figure 5.2. The conjugate composes of three parts: tetraphenylporphine, a linker to couple one of the TPP phenyl rings and the peptide, and then the Tat peptide sequence. The role of the linker is to physically separate the porphyrin from the Tat peptide and minimised the spatial interference between these two components.

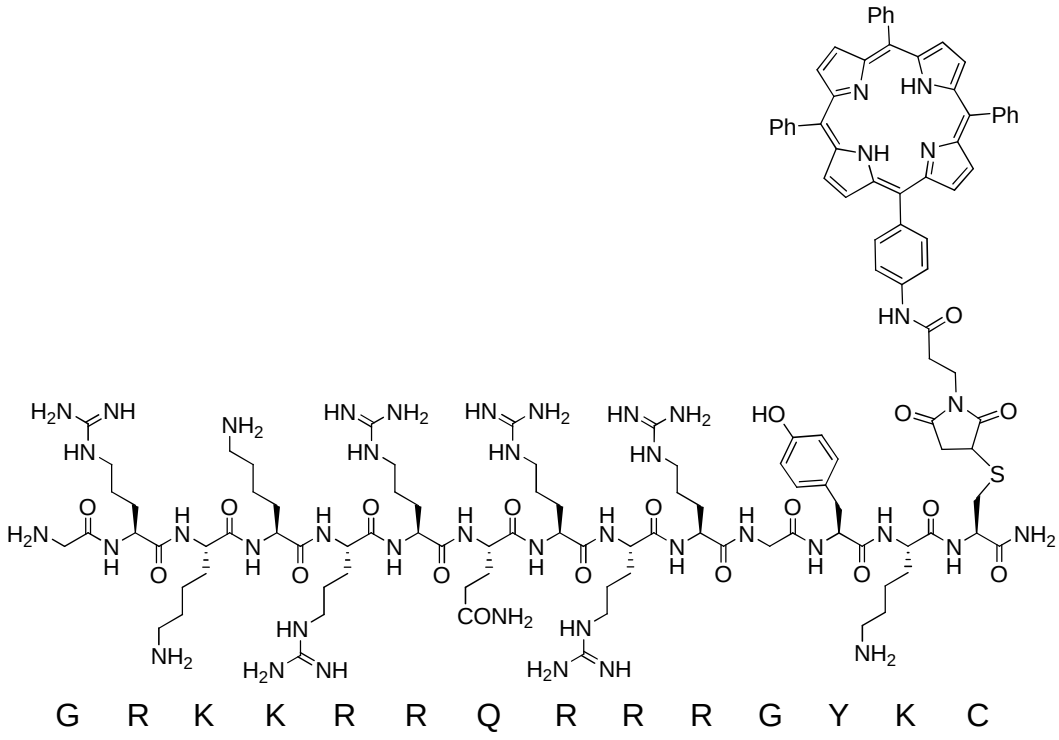

Figure 5.2 The structure of Tat-tetraphenylporphine (Tat-TPP) bioconjugates. The molecular weight is 3869.22.

Cell line and cultivation

The experiments in this section were carried out using HN5 cells. The cell culture conditions have been described in the previous chapter.

Preparation of Tat-TPP conjugate solutions

The stock solution of the Tat-TPP conjugate was made by dissolving the powder in water at the concentration of 100 μM.

The aqueous dispersions of DMPC (dimyristoyl phosphatidylcholine) liposomes were prepared according to the procedure described by Hope et al. [Hope et al., 1992]. A film of lipid (total 20 μ moles) was prepared on the inside wall of a round bottom flask by evaporation of $CHCl_3$ solutions containing the required amount of DMPC to obtain the molar percentage mixture. The obtained films were stored in a dessicator overnight under partial evacuation and were then admixed with 1 ml of PBS buffer solution in order to obtain lipid dispersions (12.5 mM). The solutions were vortex-mixed and then freeze-thawed six times from liquid nitrogen to 313 K (40ºC). Dispersions were then extruded (10 times) through a 100 nm polycarbonate membrane (Whatman Nucleopore, UK). The extrusions were carried out at 307 K (34ºC), well above the transition temperature of DMPC (297.2 K), using a 2.5 ml extruder (Lipex Biomembranes, Vancouver, Canada).

Spectroscopic measurements

The absorption spectrum measurement was carried out on a Perkin-Elmer Lambda 25 UV/Vis spectrometer (Perkin-Elmer, UK) using a 1cm path length quartz cell. The absorption spectrum was measured with samples prepared from the stock solution using different solvents, e.g. water, methanol, or deuterated methanol (CH_3OD) (Sigma-Aldrich, UK). The fluorescence emission spectra of the Tat-TPP conjugate in aqueous and liposomal solution were measured using a LS50B Perkin-Elmer spectrofluorimeter (Perkin-Elmer, UK).

Fluorescence lifetime measurements

Fluorescence lifetimes were measured using the time-correlated single photon counting method (TCSPC). A Tat-TPP conjugate solution in methanol at a concentration of 0.5 μM was placed in a 1 cm path length quartz cuvette. The light source was a 405 nm pulsed laser diode (EPL-405, Edinburgh Instruments Ltd., UK) with a pulse duration of 90 picoseconds, and 5MHz repetition rate. The fluorescence was detected using a fast multialkali photomultiplier module (model H5773-04, Hamamatsu Photonics K.K., UK) via a longpass filter (OG510, Schott, UK) and a monochromator (model M300, Bentham Instrument Ltd, UK).

TCSPC was carried out using a PC-mounted board (TimeHarp100, PicoQuant GmbH, Germany) and lifetimes were derived using FluoFit software (PicoQuant GmbH,

Germany). The Instrument Response Function (IRF) was obtained from a non-fluorescent scattering Ludox® solution (Sigmal-Aldrich, UK). Counts rates were maintained at approximately 1% of the laser repetition rate to ensure single photon counting statistics, and fluorescence decays were acquired with peak count of c. 2 x 10^4. Optimum fitting with minimisation of the residuals was confirmed using a Chi-squared value $\chi^2 < 1.4$.

Singlet oxygen measurements

The singlet oxygen phosphorescence at 1270 nm using time-resolved photon counting from photo-excited solutions in 1 cm square quartz cuvettes. Deuterated solvents (e.g. CH_3OD) were employed here, which is the standard method since the decay lifetime is much longer than water and thus easier to analyse.

For the detection in the near-IR, a specially designed thermoelectrically cooled photomultiplier (model H10330-45, Hamamatsu Photonics Ltd, UK) was used which has a quantum efficiency of 3% at 1270 nm and a rise time of 0.5 ns. The signal was collected via a series of lenses from the cuvette in combination with a long-pass and a band-pass filter centred at 1270 nm (Infrared Engineering Ltd, UK).

The solutions were excited using a 532 Nd:YAG laser (Lumanova GmbH, Germany) with the beam axis aligned orthogonally to the collection optics. The laser was pulsed at a repetition rate of 3 kHz and a pulse length of 3 ns, giving a mean power of 8mW, and a fast photodiode (1 ns rise time, Becker-Hickl, Germany) was used to synchronize the laser pulse with the photon counting detection system. A series of neutral density filters was used to attenuate the laser power.

The photon counting equipment consisted of a PC-mounted multiscaler board (model MSA-300, Becker-Hickl, Germany) and a pre-amplifier (Becker-Hickl, Germany) which gave a resolution of 5 ns per channel. Time-resolved phosphorescence measurements were accumulated by the multiscaler board for 100, 000 laser pulses, over a 30 s integration time. No photobleaching of the signal was apparent. The traces were analysed using the FluoFit software (PicoQunat GmbH, Germany) to extract the singlet oxygen decay lifetime. To calculate the quantum yield the standard zero-time intercept analysis was used where the intercept corresponds to the pre-exponential factor governing the singlet oxygen decay.

$TPPS_4$ (tetrasulfonated tetraphenylporphine) was chosen as the reference whose singlet oxygen quantum yield is known [Redmond and Gamlin, 1999;Tanielian et al., 1996].

Cellular uptake of Tat-TPP in HN5 cells

HN5 cells were plated onto 96-well plate at $2.5x10^4$ cells/well one day before drug application. For the time-dependent cell uptake experiment, cells were treated with 1μM Tat-TPP for various time periods up to 8 hrs. For temperature-dependent experiments, all protocols were the same except the incubations of sensitisers were performed at 4ºC or 37 ºC for 1hour. For the dose-dependent uptake measurement, cells were incubated with Tat-TPP with different concentrations from 0.1μM to 5μM for 16 hrs or 18 hrs. Comparison studies were carried out followed the same protocols but cells were treated with 1μg/ml (1.3μM) $TPPS_{2a}$ instead. At the end of uptake time points, cells were washed with PBS and incubated in clear DMEM medium (no phenol red; no serum) for fluorescence measurement using a LS50B Perkin-Elmer spectrofluorimeter (Perkin-Elmer, UK).

Subcellular distribution, post-light redistribution and co-localisation studies using confocal microscopy

HN5 cells overnight seeded onto glass bottom dishes FluoroDish™ (WPI, UK) were incubated with 2.5μM Tat-TPP for 18hrs. After thoroughly washed and incubated with fresh full medium for further 4 hours, cells were incubated with clear DMEM for microscopy study. The cellular distribution and redistribution after light irradiation (up to 10 min) were observed by confocal microscopy. The light treatment was carried out on stage by shining the light from the 543nm laser of the microscope. Fluorescence images were taken during the irradiation process at several time points. The changes of fluorescence intensity during irradiation was quantitatively estimated using the ImageJ software (NIH, USA)

For co-localisation studies, after the 18hr-incubation with the Tat-TPP conjugate (2.5μM), several times wash and another 4hr-incubation with fresh full medium, cells were incubated 30min with 50nM LysoTracker Green for lysosomes labelling or MitoTracker Green (Molecular Probes, UK) for mitochondria labelling. Clear medium was later replaced for live-imaging using a laser-scanning confocal microscope (FLUOVIEW FV1000, 60x magnification, NA 1.20, Olympus, Japan).

Phototoxicity of Tat-TPP and its PCI effect in combination with saporin in HN5 cells

HN5 cells were seeded at 5000 cells/well in 96-well plates overnight. Cells were treated with the Tat-TPP conjugate (0.05, 0.1 and 0.2 μM) or saporin ((10, 25 or 50 nM)) for 18hrs separately. Another three groups of cells were co-incubated with saporin (10, 25 or 50 nM) and 0.1μM Tat-TPP. Cells were then washed off trice with PBS and incubated further 4 hours with fresh full medium. Irradiation was carried out up to 5 min using LumiSource® (PCI Biotech, Norway). Cell viability was determined using the MTT assay 2 days after the light exposure.

5.1.3 Results

Spectroscopic analysis of Tat-TPP

Figure 5.3 shows the absorbance of 5 μM Tat-TPP conjugate in water. The peak absorption of Soret absorption band was found at 418 nm. The weak series of Q bands were measured at 518 nm, 556 nm, 588 nm and 642 nm (Figure 5.3, inset).

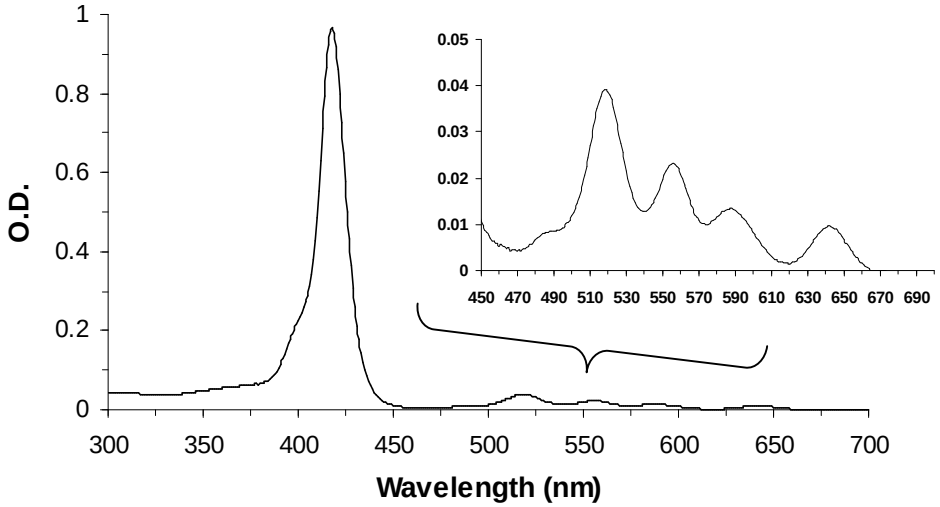

Figure 5.3 Absorption spectrum of 5 μM Tat-TPP conjugate in water. Inset: the Q band region from 450 nm to 700 nm.

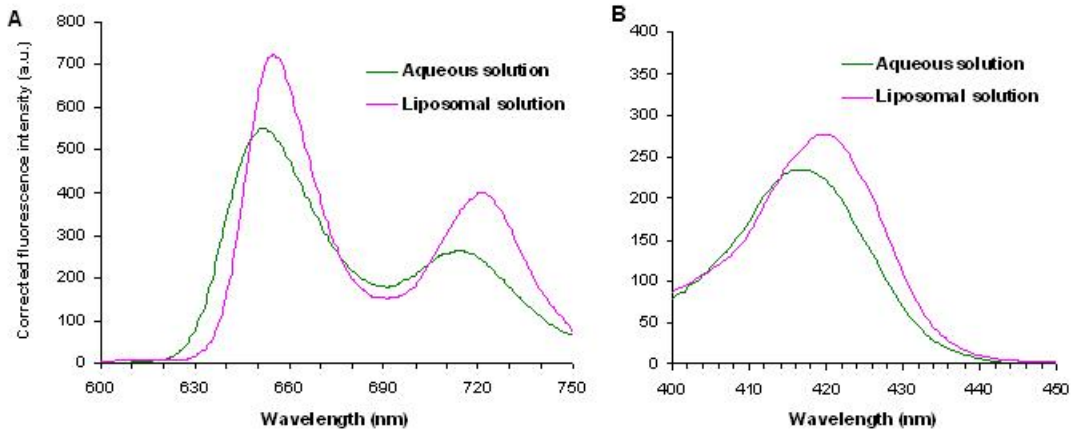

Figure 5.4 Fluorescence spectrum of 2.5 μM Tat-TPP in aqueous and DMPC liposomal solution. A: Emission spectra ($\lambda_{excitation}$ 420 nm); B: Excitation spectra ($\lambda_{emission}$ 651 nm). The spectrum was corrected for the variation of detector sensitivity with wavelength.

The fluorescence spectra of 2.5 μM Tat-TPP conjugate in aqueous and DMPC liposomal solution are shown in Figure 5.4. Two peaks of fluorescence emission in

aqueous solution were detected at 652 nm and 714 nm when excited at 420nm; the maximum excitation was at 417 nm ($\lambda_{emission}$ 651 nm). Red-shifted fluorescence spectra were observed in the liposomal solution. The peaks of fluorescence emission are at 655 nm and 721 nm while the maximum excitation is at 420 nm.

Time-solved spectroscopic studies

In order to minimise dimerisation, methanol was chosen as the solvent for the fluorescence lifetime measurement. For the determination of singlet oxygen quantum yield, deuterated methanol (CH_3OD) was used. To confirm that the methanolic solutions at the concentrations studied were monomeric, absorption spectra were recorded as a function of concentration. It was necessary to check for the presence of any aggregation because aggregated porphyrins exhibit lower fluorescence lifetimes and lower singlet oxygen quantum yields.

The absorption spectra of the Tat-TPP conjugate in methanol and deuterated methanol are shown in Figure 5.5A. It should be noted that both solutions contained 0.5 % H_2O which is derived from the stock solution. Both solutions at the same concentration displayed similar absorbance intensity and pattern. The peak absorption of the samples at 414 nm against different concentrations is demonstrated in Figure 5.5B. The peak absorbance performed as a function of the sample concentration is in agreement with the Beer's law. This also emphasizes the stability and disaggregation of the Tat-TPP conjugate in deuterated methanol within this range of concentrations.

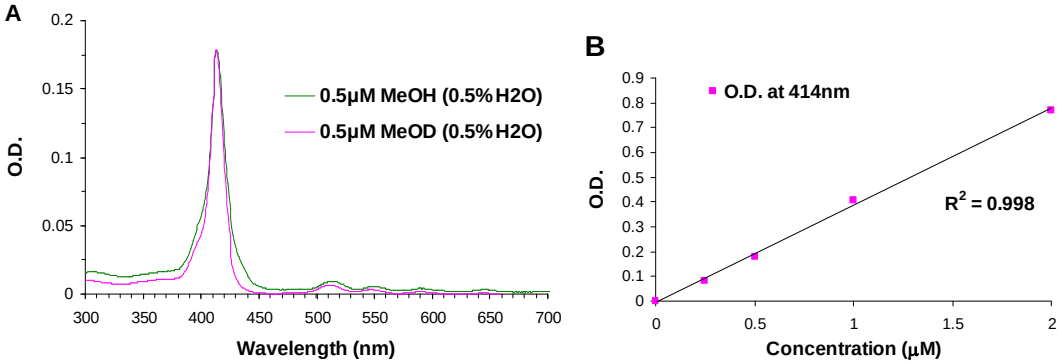

Figure 5.5 Absorption spectrum of Tat-TPP and $TPPS_4$ in methanol (MeOH) or deuterated methanol (MeOD). A: 0.5 μM Tat-TPP conjugates in MeOH and MeOD. Both solutions contained 0.5% H_2O. B: The absorbance of the Tat-TPP conjugate in MeOD at 414nm versus concentration.

a. Fluorescence lifetime measurement of Tat-TPP conjugates

Figure 5.6 shows the fluorescence lifetime of Tat-TPP in methanol (0.5 μM). The lifetime curve exhibits good mono-exponential decay fitting (χ^2<1.2) with the value for the fluorescence lifetime measured as 8.7 ns. A slightly longer value was observed in deuterated methanol (10.7 ns) as expected due to the isotope effect on the porphyrin.

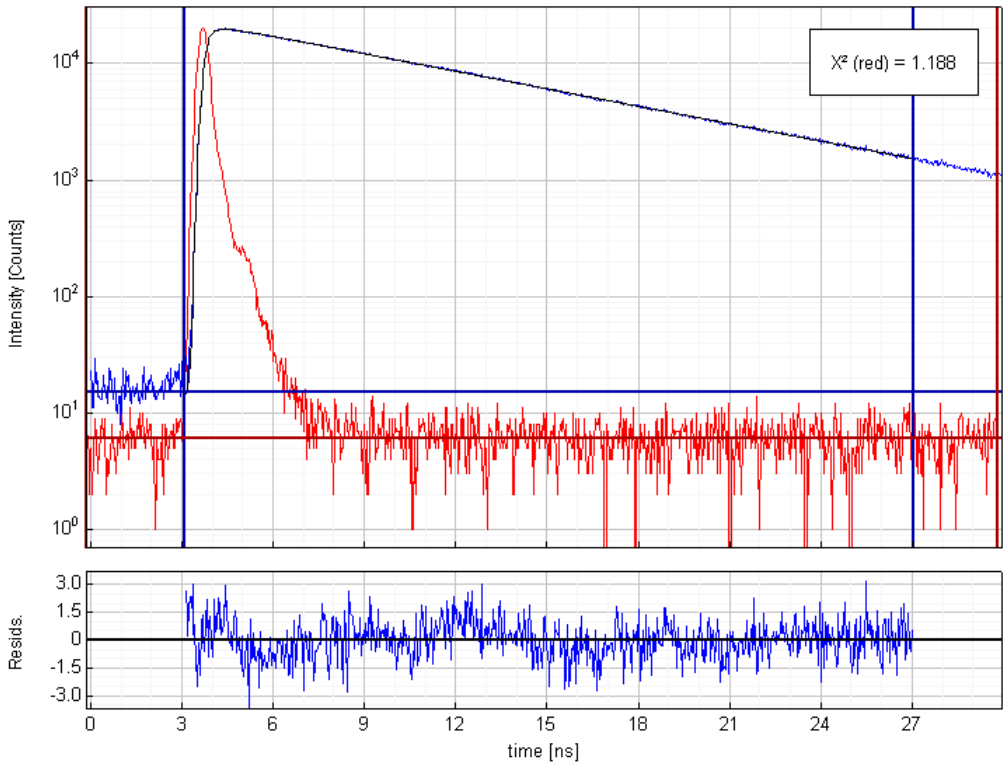

Figure 5.6 Time-resolved intensity decay of 0.5 μM Tat-TPP conjugate in methanol (with 0.5% H_2O) and the instrument response function (top). Residuals for fitting (bottom).

b. Singlet oxygen production measurement of Tat-TPP conjugates

It is widely considered that direct observation of singlet oxygen emission in the infra-red (IR) region of the spectrum provides the most accurate determination of $^1O_2$ quantum yields (Φ_Δ).

The quantum yields of the Tat-TPP conjugate were estimated in comparison with the known reference, $TPPS_4$ (Φ_Δ = 0.7 in CH_3OD) [Redmond and Gamlin, 1999;Tanielian et al., 1996]. The sample and the reference solution were with optically matched weighted lifetimes (28 μs, data not shown) and similar absorbance (Figure 5.7B) at the laser wavelength of 532 nm: 1.36 μM of Tat-TPP in CH_3OD (with 2% H_2O) and 1.97 μM of $TPPS_4$ in CH_3OD (with 1.3% H_2O). Figure 5.7A depicts the time-resolved

phosphorescence profile of the Tat-TPP conjugate. The initial fast spike represents short-lived fluorescence followed by a mono-exponential singlet oxygen phosphorescence decay over a hundred microseconds. The decay lifetime was measured as 28 µs which is the expected value for deuterated methanol containing 2% water.

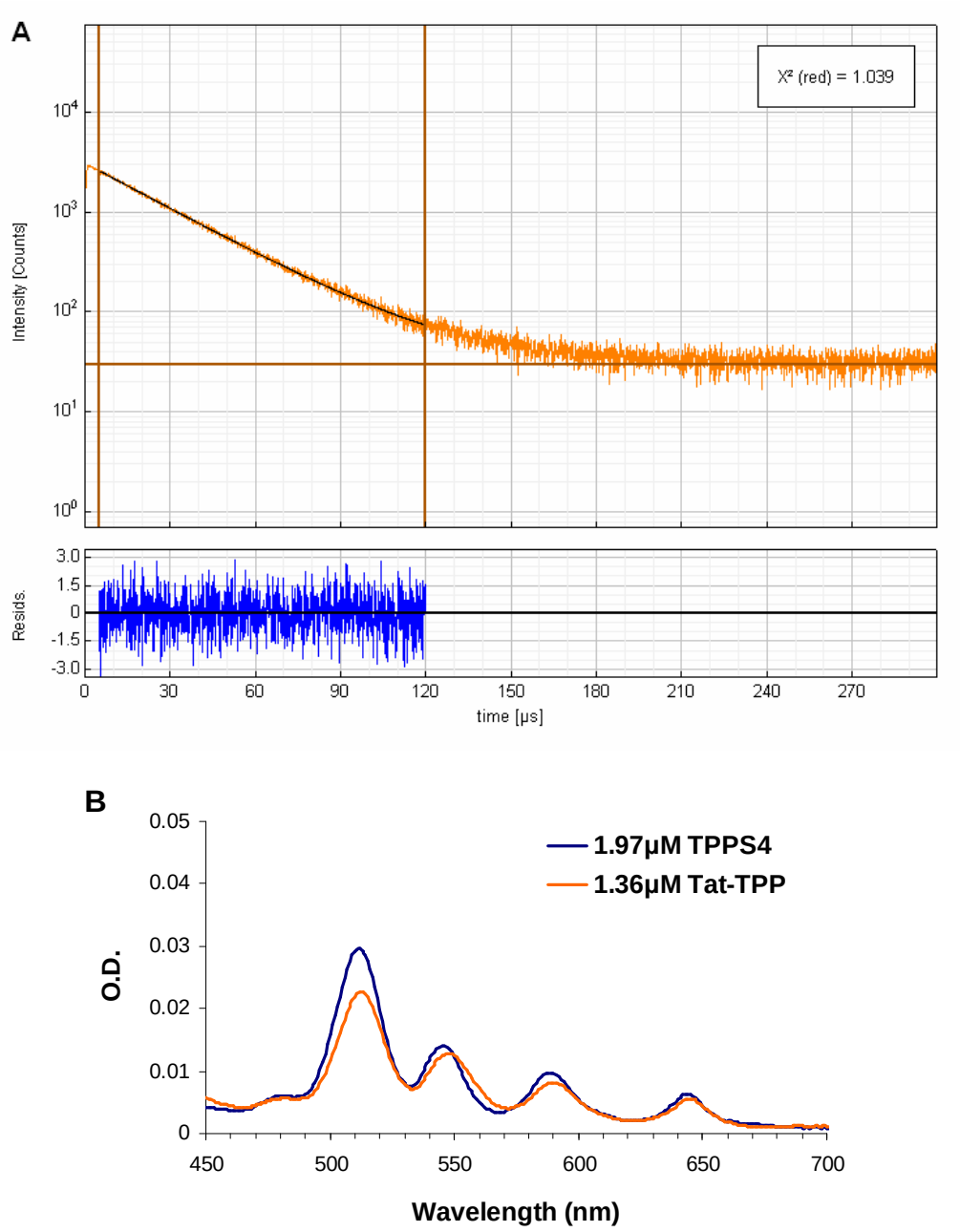

Figure 5.7 A: Tme-resolved phosphorescence decay at 1270nm plotted on a logarithmic scale of singlet oxygen sensitised by Tat-TPP in MeOD using a pulsed 532 nm laser, together with a plot of the residual deviations from the fitted monoexponential decay. B: The Q bands absorbance of Tat-TPP and $TPPS_4$ in MeOD solution with similar absorbance and optically matched lifetimes at 532nm.

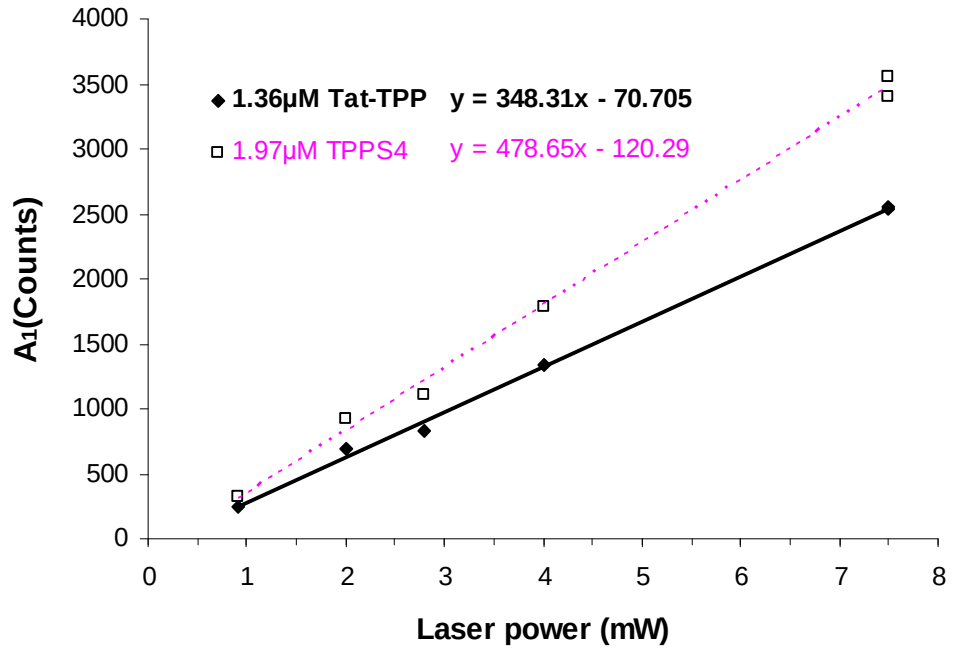

Figure 5.8 Phosphorescence signal intensity at 1270nm versus laser power (mW) at 532nm.

Using various attenuation filters, the phosphorescence intensities (I) were found to be in proportion to the laser power (P). The results are plotted in Figure 5.8. The individual gradients (G) were then obtained by the slopes from the linear distribution, yielded 348.31 for Tat-TPP and 478.65 for $TPPS_4$.

Equation (1) relates the parameters involved in the generation of singlet oxygen [Cantau et al., 2007]:

$$I = \kappa \times P \times \Phi_{\Delta} \times \left(1 - 10^{-A}\right) \qquad (1)$$

where k is a constant incorporating the efficiency of light collection and detection sensitivity, A is the absorbance of solutions at the laser wavelength, Φ_{Δ} is the singlet oxygen quantum yield, and P is the laser power. Therefore a plot of the intensity *I* versus the laser power should be linear and the gradient G equates to:

$$G = \kappa \times \Phi_{\Delta} \times \left(1 - 10^{-A}\right) \qquad (2)$$

Since near optically matched solutions have been employed, the absorbance factors are virtually identical and only a very small corrections is required.

The A_{532} values of both solutions have been measured (inset, Figure 5.7): $A_{532}^{TPPS_4}$ =0.0076; $A_{532}^{Tat-TPP}$ =0.00718. Therefore, taking Φ_Δ for $TPPS_4$ as 0.7, the quantum yield of Tat-TPP was calculated from equation (3), resulting in the value of 0.54.

$$\Phi_\Delta^{sample} = \Phi_\Delta^{ref} \times \frac{G_{sample}}{G_{ref}} \times \frac{1-10^{-A_{ref}}}{1-10^{-A_{sample}}} \quad (3)$$

Table 5.1 summarises the physical chemistry properties of the Tat-TPP conjugate.

- **Photophysical properties**

Absorption wavelength maxima[a]	Soret band: 418 nm
	Q bands: 518, 556, 588, and 642 nm
Fluorescence wavelength maxima[a]	Excitation: 417 nm
	Emission: 652 and 714 nm
Fluorescence lifetime[b]	8.7 ns
Singlet oxygen quantum yields (Φ_Δ)[b]	0.54

Table 5.1 A summary of the photophysical properties of the Tat-TPP conjugate. a: in H_2O; b: in MeOD

Subcellular distribution of Tat-TPP and its redistribution after illumination in HN5 cells

The intracellular distribution of the Tat-TPP conjugate was observed in HN5 cells by confocal microscopy. A granular subcellular distribution was found and it became diffuse following light exposure (Figure 5.9). The results of quantitative measurements show that the fluorescence signals increased after 1 min irradiation and declined afterwards (Figure 5.10). The fluorescence intensity dropped about one third of the highest signals detected (i.e. 1 min light) after 10 min light exposure.

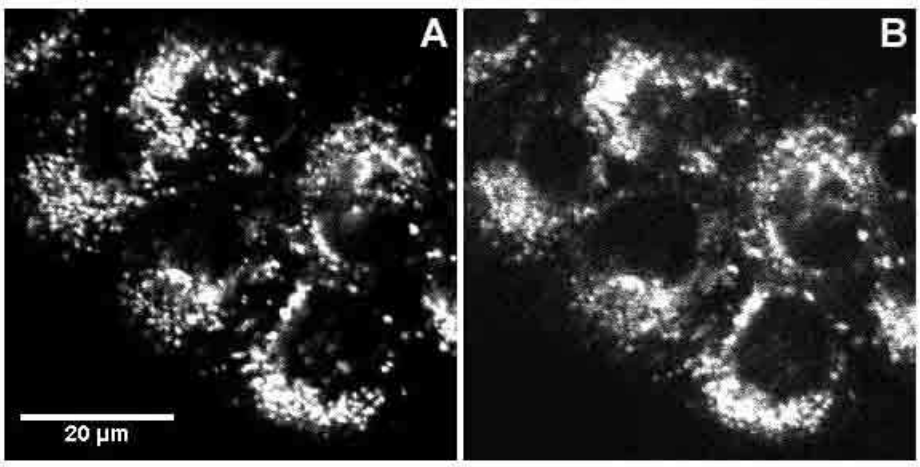

Figure 5.9 Cellular distribution of Tat-TPP in HN5 cells (A) and the redistribution after 10 min irradiation on stage by confocal microscopy (B). Light source: 543nm laser of the confocal microscope. Cells were incubated with 2.5µM Tat-TPP for 18hrs.

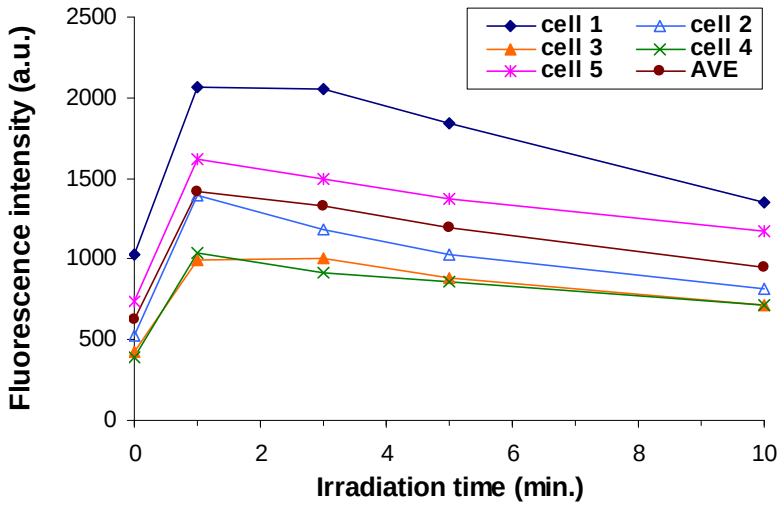

Figure 5.10 Photoinduced changes in integrated intracellular Tat-TPP fluorescence intensities measured in HN5 cells at set times. Five cells were randomly chosen from Figure 5.9 for fluorescence intensities analysis. AVE: the average intensity.

Identification of the subcellular distribution of Tat-TPP using lysosome and mitochondria probes in HN5 cells by confocal microscopy

The subcelllular localisation of Tat-TPP was investigated by co-labelling LysoTracker Green or MitoTracker Green in HN5 cells using confocal microscopy. As shown in Figure 5.11, most Tat-TPP was found co-localised with lysosomes and mitochondria but some non-lysosome or –mitochondria co-localised Tat-TPP (red dots in the merge images) were also observed.

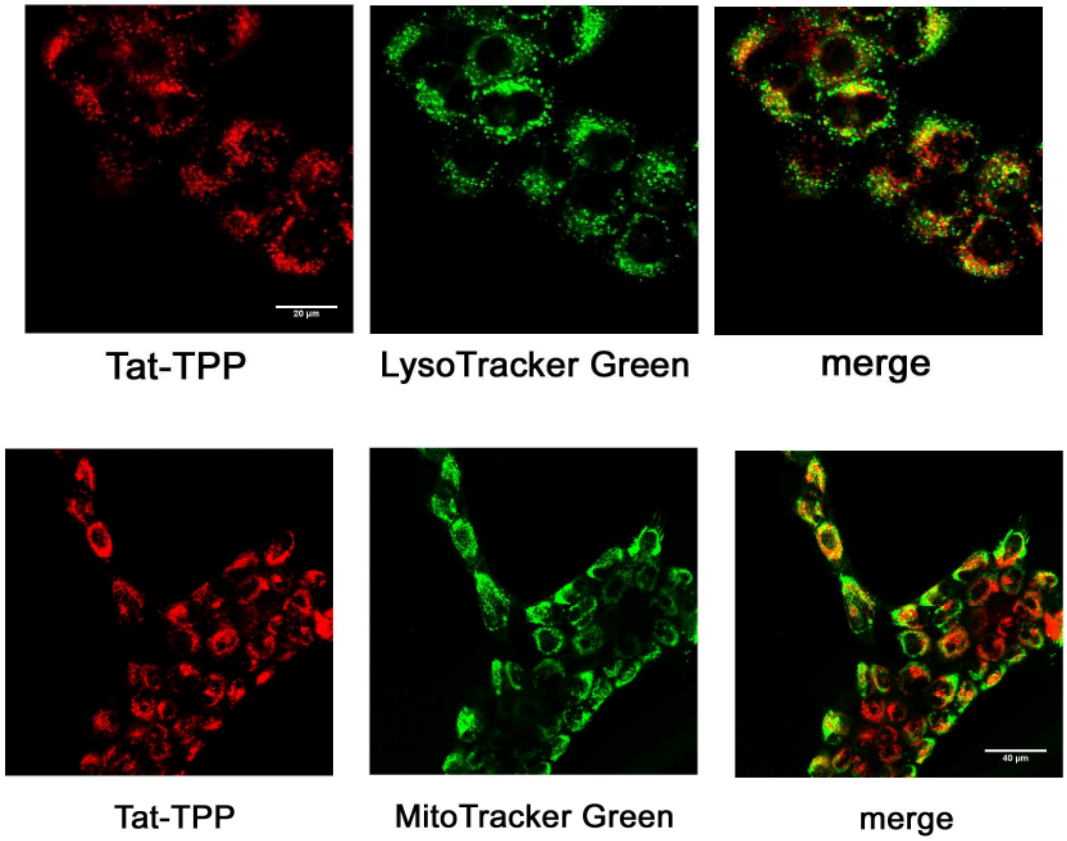

Figure 5.11 Co-labelling Tat-TPP with LysoTracker Green or MitoTracker Green in HN5 cells by confocal microscopy. Cells were incubated 2.5 μM Tat-TPP for 18hrs. 50 nM of LysoTracker Green or MitoTracker Green was applied to cells 30min before imaging.

Short-term time-dependent and temperature-dependent cellular uptake of Tat-TPP in HN5 cells

HN5 cells were incubated with 1 μM Tat-TPP or 1.3 μM $TPPS_{2a}$ and their cellular uptake were measured at up to 8 hours. As shown in Figure 5.12, the Tat-TPP conjugate steadily accumulated within HN5 cells and produced measurable fluorescence signal. Time-dependent cell uptake was found in both sensitisers. Higher fluorescence intensity was measured in cells treated with Tat-TPP compared to $TPPS_{2a}$ even though the concentration of Tat-TPP was slightly lower.

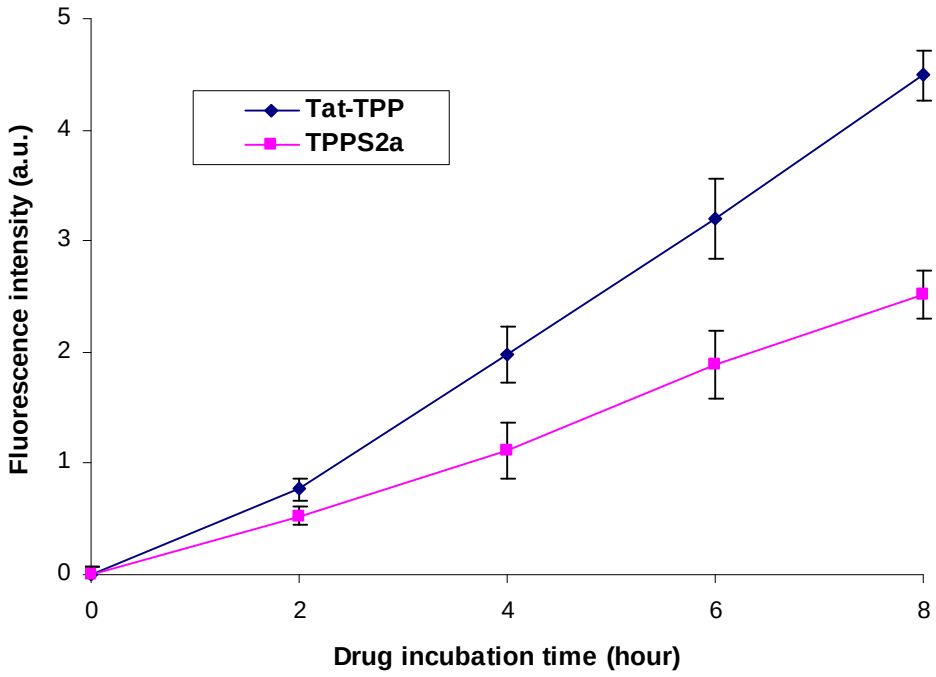

Figure 5.12 Time-dependent cellular uptake of Tat-TPP (1 μM) and $TPPS_{2a}$ (1.3 μM) in HN5 cells after 18 hr incubation.

To further study the uptake mechanism of Tat-TPP and the involvement of endocytosis, experiments with drug incubation at low temperature were performed. Endocytosis can be inhibited in a cold environment as the metabolism of cells stops or slows down.

The cell uptake of Tat-TPP showed a temperature-dependent manner. In Figure 5.13, incubation at 4ºC resulted in an inhibition of cellular uptake where lower fluorescence signal was detected compared to the incubation at 37ºC.

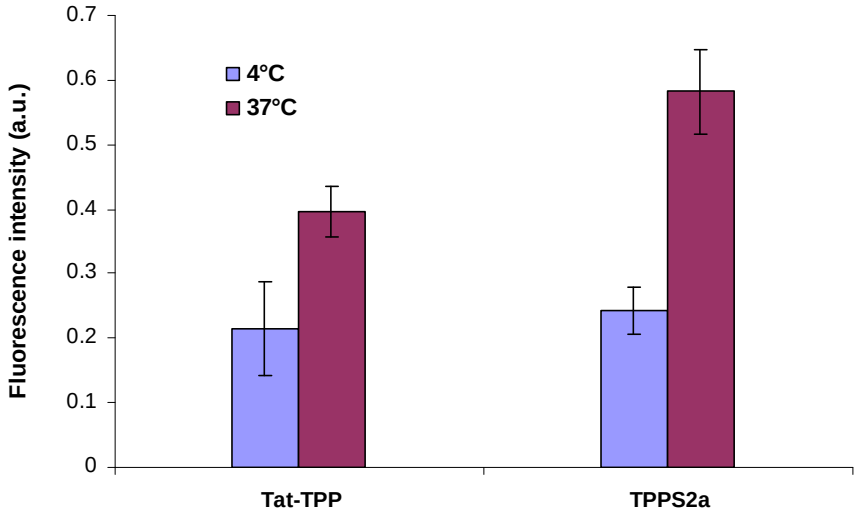

Figure 5.13 One hour cellular uptake of Tat-TPP (1 μM) and $TPPS_{2a}$ (1.3 μM) at 4ºC or 37 ºC in HN5 cells.

Long-term dose-dependent cellular uptake of Tat-TPP in HN5 cells

Long-term cellular uptake was observed with the drug concentrations ranged from 0.13 μM to 5 μM (Figure 5.14). After 18 hours incubation of 0.13 μM Tat-TPP in HN5 cells, the fluorescence signal was higher than the cells treated with 0.13 μM $TPPS_{2a}$ by a factor of five. Higher fluorescence intensity was detected when cells were incubated with higher Tat-TPP doses. Rapid increase of fluorescence intensity was observed when conjugates concentration is less than 1 μM, whereas the increase rate slowed down if compared the conjugate concentrations at 5 μM and 1 μM.

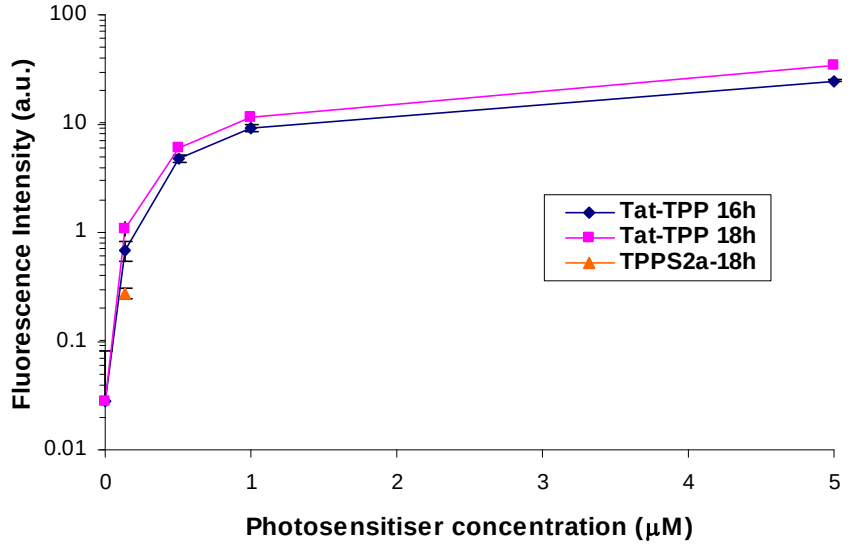

Figure 5.14 Dose-dependent cellular uptake of Tat- TPP and $TPPS_{2a}$ in HN5 cells. Cells were incubated with Tat-TPP or $TPPS_{2a}$ (up to 5 μM) for up to 18hrs.

Cytotoxicity of Tat-TPP PCI combing saporin in HN5 cells

The phototoxicity of the Tat-TPP conjugate was estimated in HN5 cells. The cell viability results showed Tat-TPP produced little dark toxicity (Figure 5.15). The toxicity induced by Tat-TPP was found in a light dose and drug dose dependent manner. Cell viability reduced to less than 40 percent using the conjugate at the concentration of 0.1 μM after 3 min light treatment. The IC_{50} (the concentration of drug or light that kills 50% of cells) was achieved in combination of 0.1 μM Tat-TPP and 1-3 min irradiation.

The PCI effect of Tat-TPP was investigated in combination with saporin. With 25 nM saporin and 0.1 μM Tat-TPP, PCI significantly enhanced the cell kill and reduced the cell viability by a factor of 7.7 and 6.8 compared to saporin and Tat-TPP alone respectively after 3 min light exposure.

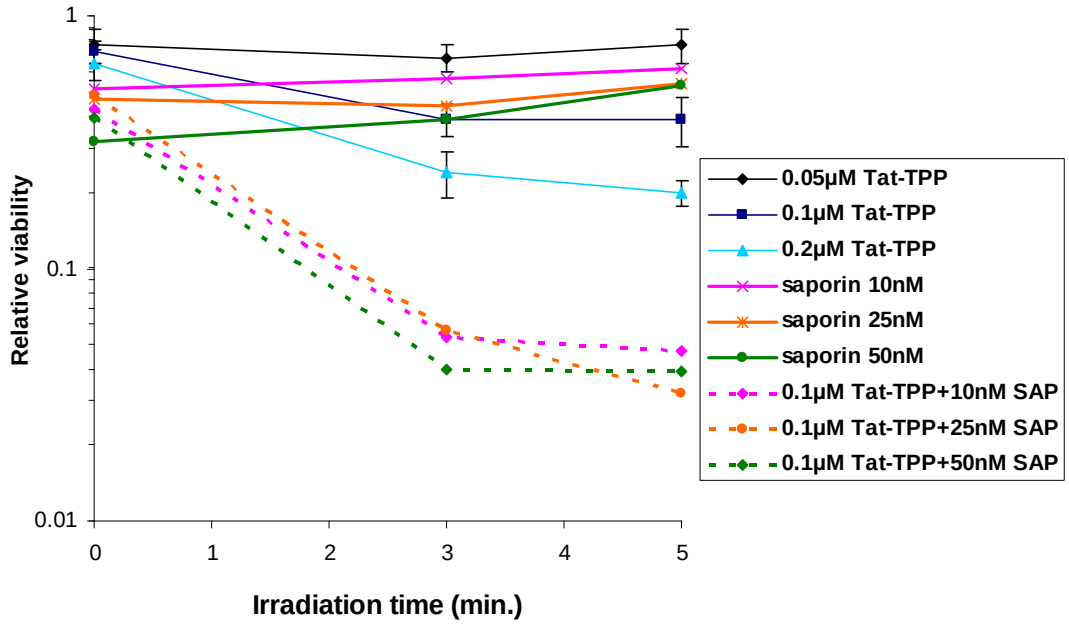

Figure 5.15 Tat-TPP PDT and PCI effect in combination with saporin in HN5 cells. Cells were incubated with Tat-TPP (up to 0.2 μM) or incubated with 0.1 μM Tat-TPP and saporin (up to 50 nM) for 18hrs. Irradiation was carried out up to 5 min using a blue lamp. Cell viability was examined by the MTT assay 48 hrs after exposure to light.

5.1.4 Discussion

It is more than 20 years ago since the protein translocation ability of the Tat activator of HIV was first reported [Frankel and Pabo, 1988;Green and Loewenstein, 1988]. Since then, several CPPs/PTDs have been recognised as proteins with membrane translocation properties and described as promising tools to transport biologically active cargos and induce efficient intracellular deliveries. Studies regarding the fundamental aspects such as endocytosis mechanism, the interaction between Tat-peptides themselves and the cargos, as well as the influence of the environment have been well documented, and were summarised in the Introduction to this section.

According to the absorption and fluorescence spectra from spectroscopic studies (Figure 5.3), the Tat-TPP conjugate displayed typical photophysical properties of porphyrins, i.e. an intense Soret band (λ_{max} = 390-415 nm) and four weaker Q-bands in the 450-700 nm region. The absorption spectra of Tat-TPP conjugates in methanol and deuterated methanol (both contain 0.5% H_2O) were also assessed (Figure 5.5) as solutions prepared with these solvents were used for fluorescence lifetime and singlet oxygen quantum yield measurements. The molar extinction coefficient of the Tat-TPP conjugate in different solvents can therefore be calculated using the Beer's Law: $A = \varepsilon \times c \times L$, where A is the absorbance, ε is the molar extinction coefficient, c is molar concentration and L is 1 when using 1cm width cuvettes. In this present study, the molar extinction coefficient of the Tat-TPP conjugate was measured lower than TPP (4.05 x 10^5 $M^{-1}cm^{-1}$ in toluene) [Du et al., 1998]. Among these three solvents, the value in water was found to be the lowest (1.94 x 10^5 $M^{-1}cm^{-1}$) compared to other polar solvents (2.65 x 10^5 $M^{-1}cm^{-1}$ in deuterated methanol and 2.92 x 10^5 $M^{-1}cm^{-1}$ in methanol). This may be attributed to the dimerisation of the Tat-TPP conjugate when dissolved in water, resulting in a lower molar extinction coefficient. The aggregation of compounds is also evident as a second short lifetime was detected in the freshly-made solution (data not shown).

The Tat-TPP conjugate displayed a significant fluorescence emission with two bands in aqueous solution, but a red shift was observed in DMPC liposomal solution in both excitation and emission spectra (Figure 5.4). The optical properties of photosensitisers in relation to lipid membranes have been reported by many studies [Kessel and Rossi,

1982;Ricchelli, 1995]. The finding here is therefore consistent with the binding of the Tat-TPP conjugate to a liposomal lipid membrane which leads to the changes in fluorescence spectra. This result would imply that the bioconjugate should also bind to cellular/oraganelle membranes.

The fluorescence lifetime of Tat-TPP in methanol was measured 8.7 ns which is shorter than the value for $TPPS_4$ as 9.7 ns (data not shown). The fluorescence lifetime of $TPPS_4$ measured in this study is similar to the result from another group [Castriciano et al., 2009]. The isotope effect was also observed after the replacement of the solvent with deuterated methanol where the substitution of hydrogen to deuterium led to a longer fluorescence lifetime of 10.68 ns (data not shown). $TPPS_4$ was used as a reference to determine the singlet oxygen yields of the Tat-TPP conjugate. The value of Φ_Δ for Tat-TPP was found 0.54, very close to the value of 0.59 for m-THPC in oxygen-saturated methanol [Bonnett et al., 1999] which is the most promising photosensitiser approved in clinic. Nevertheless, it was lower to the value of 0.66 for Amphinex [Mojzisova et al., 2009], a PCI sensitiser, although an indirect measurement was performed.

The subcellular distribution of the Tat-TPP conjugate was also observed similar to $TPPS_{2a}$ in a granular pattern and was redistributed to become diffuse after light exposure (Figure 5.9). Quantitative fluorescence measurements based on the imaging results show that the fluorescence signals inside cells began with an increase while irradiating and photobleaching was observed after longer light exposure (Figure 5.10). Moreover, in the co-localisation studies co-labelling with lysosome and mitochondria probes, the Tat-TPP conjugate appears to accumulate in lysosomes and mitochondria (Figure 5.11). Most of the conjugates were found localised in lysosomes, possibly as a consequence of endocytotic cellular uptake.

The cellular uptake of the Tat-TPP conjugate was then investigated by comparison with $TPPS_{2a}$ which has structural similarity and also a common PCI photosensitiser. The results shown in Figure 5.12 illustrate that Tat-TPP was taken up by cells efficiently where the fluorescence signals were comparable to the signals produced from $TPPS_{2a}$. Incubations in 4ºC seemed to inhibit the uptake of both sensitisers which also suggests the possible energy-dependent endocytotic mechanism of cellular uptake (Figure 5.13). However, low fluorescence signals were measured due to the low drug doses which might result in a misreading from the spectrometer, especially the incubation time is as

short as only one hour. Further experiments to verify the influence of temperature in the cellular uptake should be carried out using higher drug doses.

Since the molecular weight of the Tat-TPP conjugate is approx. 4000 Dalton, endocytotic uptake would be expected for a molecule of this size. Collectively, the experimental results presented here are in agreement with the data published by Vicente's group that Tat-porphyrin conjugates display a lysosomal intracellular localisation [Sehgal et al., 2008;Sibrian-Vazquez et al., 2008]. Therefore, the results support the conclusion that endocytotosis is the main uptake mechanism of Tat-porphyrin conjugates.

To test whether the Tat-TPP conjugate has the potential for PDT, its phototoxicity and was examined *in vitro*. As shown in Figure 5.15, Tat-TPP induced appreciable phototoxicity under very low drug concentration. The remarkably enhanced cell killing achieved combing saporin under sub-lethal PDT dose indicated that the Tat-TPP conjugate is also a favourable PCI sensitiser.

The first attempt in using a Tat peptide in PDT was demonstrated by Sibrian-Vazquez et al. using a PEG spacer to link a Tat peptide and porphyrins [Sibrian-Vazquez et al., 2006]. The enhanced cellular uptake indicated that the Tat peptide-conjugation strategy is able to increase the biological efficacy of porphyrins. The study in this section is the first attempt to incorporate the use of a Tat peptide into photochemical internalisation strategies.

The results demonstrate that the conjugation to a Tat peptide enables the tetraphenylporphine to become bioavailable which results in three advantages of the Tat-TPP conjugate: 1) The membrane permeability due to the increased solubility. 2) Efficient cellular uptake contributed by the translocation ability of the Tat peptide. 3) The specific subcellular localisation due to the amphiphilic structure (Figure 5.1 and 5.2). Other features such as low dark cytotoxicity, and intrinsic photosensitising capability furthermore make the Tat-TPP conjugate a potent photoactive therapeutics for photodynamic therapy. Last but not least, the marked enhancement of cell killing in combination with saporin even implies that the Tat-TPP conjugate has a potential for being a PCI photosensitiser. The hypothesis of the cellular uptake and endocytosis of the Tat-TPP conjugate is shown in Figure 5.16. Due to the amphiphilic structure and the

positive-charged Tat peptide end, the Tat-TPP conjugate enters cells via endocytotic pathway or through direct plasma membrane penetration. According to the co-localisation imaging results, the Tat-TPP conjugate remains in the membrane of endocytotic vesicles (e.g. endo/lysosomes) or target other organelles such as mitochondria. Photochemical internalisation could be initiated following the light activation of Tat-TPP and therefore result in the rupture of the membranes and the release of the endocytosed therapeutic macromolecules.

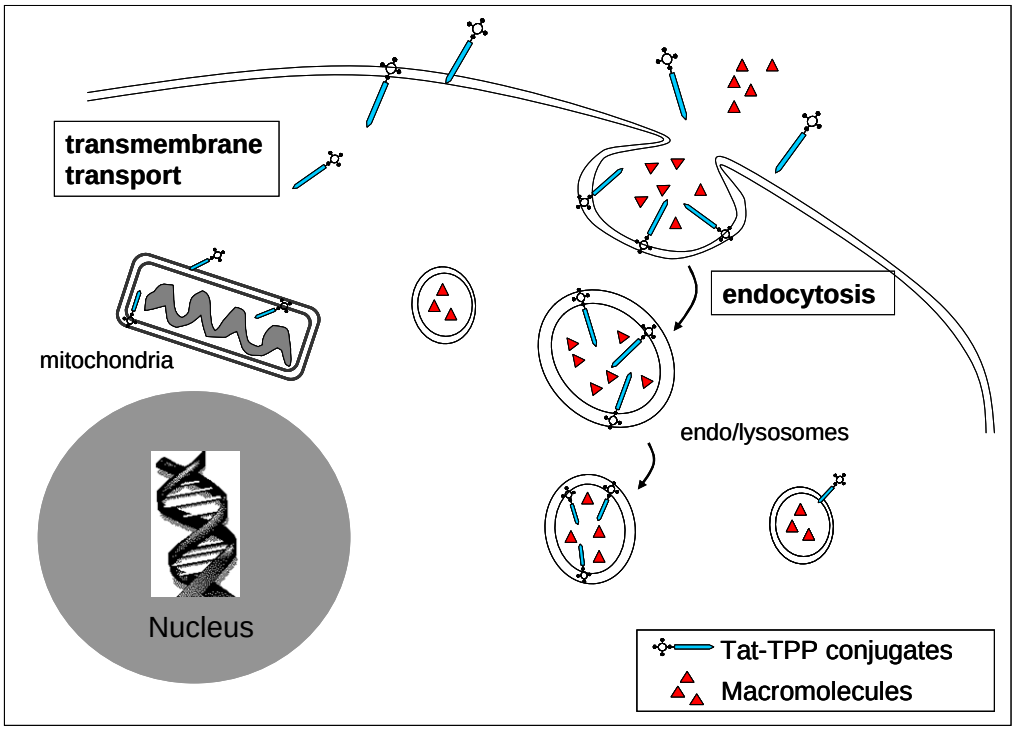

Figure 5.16 Hypothesis of the cellular uptake of the Tat-TPP conjugate.

The results here demonstrate the feasibility for an enhanced bioavailability by linking Tat peptides to other photosensitisers, particularly water soluble sensitisers with restricted cell entry ability. Future studies to investigate the PCI effect of the Tat-TPP conjugate will focus on either co-administrating or covalent biding to different therapeutic agents. Studies using different cell lines and the *in vivo* application will be carried out.

List favourable properties for PCI:

- Good photophysical properties and comparable singlet oxygen quantum yields
- Water soluble yet amphiphilic: lysosomal membrane localisation
- Efficient cellular uptake and low dark toxicity

- PCI effect: synergistic cytotoxicity in combination with saporin

Based on many promising results as reviewed elsewhere [Brooks et al., 2005;Vives, 2003], it seems that these unique peptides can achieve unrestricted delivery [Bogoyevitch et al., 2002;Schwarze et al., 2000]. However, this view has been challenged by some other recent studies.

Koppelhus and his colleagues tested the translocation ability of a Tat peptide and penetratin, and relatively poor or no cell uptake in five different cell lines were found [Koppelhus et al., 2002]. Several studies also reported this cell-dependent phenomenon of Tat peptides as distinct differences of cell uptake efficacy were found between 'leaky cells' and 'non-leaky cells' [Kramer and Wunderli-Allenspach, 2003;Trehin et al., 2004;Violini et al., 2002;Zhang et al., 2004]. Leaky cells like HeLa (cervical carcinoma) demonstrated a greater cell uptake of Tat peptides, whereas tight junction forming epithelial cells like MDCK (canine kidney) or CaCo-2 (human colonic carcinoma) restricted their entry into cells. Not surprisingly, some studies have pointed out that Tat peptide bioconjugates might behave differently *in vitro* and *in vivo* [Caron et al., 2001;Niesner et al., 2002]. However, these seemingly negative results do not dispute the biomedical potential of the Tat peptide-mediated drug delivery. In contrast, in order to achieve successful therapeutic application of Tat peptide conjugates, future studies need to carefully consider the differences in experimental settings.

A successful drug delivery should require both efficient uptake and specific targeting. On one hand, the ubiquitous cell translocation ability of CPPs has resulted in numerous impressive applications in the peptide-mediated drug delivery [Dietz and Bahr, 2004]. On the other hand, little cell specificity has therefore become a controversy feature for most of the CPPs. Tat peptides are no exception. This might become the foremost obstacle for their clinical utilities [Vives, 2005]. Nevertheless, the results shown in this section have proved that it is unlikely a problem for the PDT or PCI applications. Selectivity can be achieved by the site specificity of PDT and PCI that the therapeutic effects only take place in the area exposed to light which therefore could alleviate the 'drawbacks' of the Tat peptide-mediated cellular deliveries, the ubiquity of their translocation activity.

5.2 Investigation an $AlPcS_{2a}$-Saporin Conjugate for Photochemical Internalisation

5.2.1 Introduction

As mentioned in Chapter 1, several studies have demonstrated that the synergistic effect or at least additive effect can be induced using PDT in combination with chemotherapy. In most of the cases, administration of photosensitisers and anti-cancer drugs are separately, followed by irradiation. There is also a different approach in which chemotherapeutic agents are conjugated with photosensitisers via a polymer carrier [Peterson et al., 2003]. In fact, strategies of using photosensitiser-based bioconjugates have been extensively studied where the concept is to increase the bioavailability, solubility and targeted specificity [Sibani et al., 2008]. The study in the previous section is indeed an example showing that the linkage to a cell penetration peptide, Tat, makes tetraphenylporphine become water soluble and confers preferable properties for PDT and PCI.

Conjugation of photosensitisers and proteins provides another platform of photosensitiser-based bioconjugates in which specificity can be achieved when using known ligands against cancer-specific receptor or antibodies. For instance, a complex which comprises the anti-EGFR antibody (cetuximab) and a photosensitiser, BDP Verteporfin was synthesized through PEGylation and termed PIC (photosensitiser immunoconjugate) to combine immunotherapy and PDT. Compared to the use of unconjugated sensitiser, PIC induced the synergistic effect on the inhibition of tumour growth, indicating that targeted photosensitisers can improve the PDT treatment [del Carmen et al., 2005].

Bioconjugation enables creation of a composite which couples several molecules of interests together for multiple functions. It may be particularly beneficial to PCI, a drug delivery system with the interplay of photosensitiser and delivered macromolecules. Evidence has been shown by Nishiyama and co-workers as described previously in Chapter 2 that a complex enclosing dendrimeric phthalocyanine (anionic) and DNA packaged with cationic peptides can facilitate PCI-mediated gene delivery both *in vitro* and *in vivo* [Nishiyama et al., 2005]. In this strategy, two components of PCI, the

photosensitiser and the employed macromolecules, are assembled into one structure. The fact that the complex can be administered at one time is especially an advantage for PCI application *in vivo* or in clinic.

The design of the experiments in this section is derived from the same concept. It seems to be a possible way to integrate a photosensitiser and its employed macromolecule for PCI-directed drug delivery. In this chapter, a bioconjugate which consists of $AlPcS_{2a}$ and saporin was synthesized. Two molecules were separately modified and conjugated together through the linkers attached to the adjacent disulfonate groups of $AlPcS_{2a}$. Its bioavailability including cellular uptake and intracellular distribution was investigated, and the ability to induce PCI effect was examined in comparison with the photochemical enhancement led by conventional $AlPcS_{2a}$ PCI of saporin using HN5 cells.

5.2.2 Materials and methods

Synthesis of $AlPcS_{2a}$-saporin conjugate

The synthesis of $AlPcS_{2a}$-saporin conjugates was done by Dr Sinan Battah in our group and the detailed synthesis process is shown in Appendix I. The schematic structure of the conjugates is illustrated in Figure 5.17. $AlPcS_{2a}$ was conjugated via a linker with two free sulfhydryl (-SH) group which can react with disulfide bridge-modified saporin. The $AlPcS_{2a}$-linker with two –SH free terminals, is expected to bind to two adjacent protein molecules (Figure 5.17A) or one protein molecule (Figure 5.17B). The later conjugate is more likely to be formed because the size of protein is much larger than the photosensitiser. It is hypothesized that the hydrophobic side of phthalocyanine macrocycle will be localised to the endo/lysosomal membrane and the hydrophilic protein side will insert into the aqueous compartment.

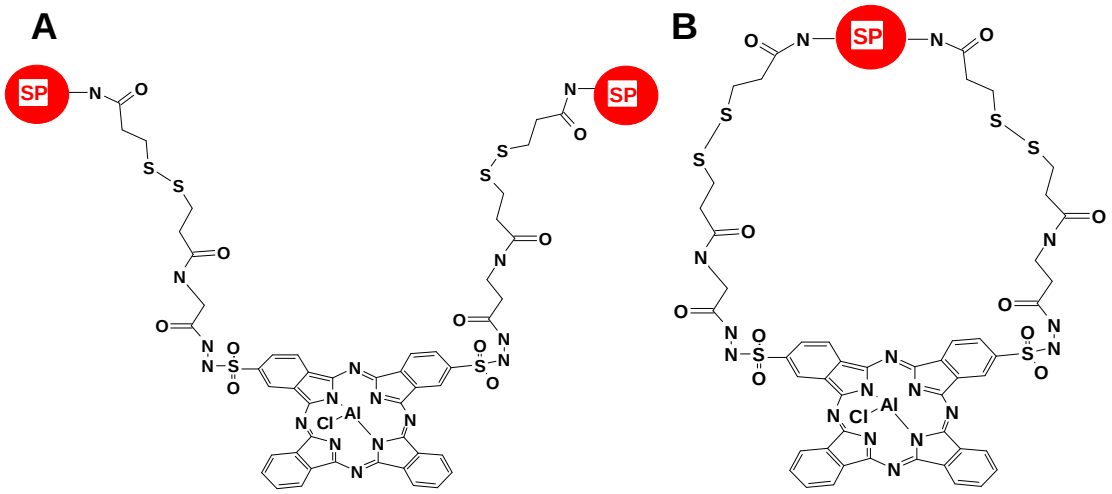

Figure 5.17 The schematic structure of $AlPcS_{2a}$-saporin conjugates. A: One $AlPcS_{2a}$ molecule links to two saporin protein molecules. B: One $AlPcS_{2a}$ links to one saporin protein molecule.

Cell line and cultivation

The experiments in this section were carried out using HN5 cells. The cell culture conditions have been described in the previous chapter.

Spectroscopic measurements

The absorption spectrum measurement was carried out on a Perkin-Elmer Lambda 25 UV/Vis spectrometer (Perkin-Elmer, UK) using a 1cm path length quartz cell. The absorption spectrum was measured with samples prepared from the stock solution and

diluted in distilled water. $AlPcS_{2a}$-saporin conjugate solution was prepared by 50x dilution of the stock solution with distilled water. The absorption spectrum of the conjugate was compared with 1 μg/ml $AlPcS_{2a}$ solution diluted in methanol. The concentration of conjugate was then estimated using Beer's law, assuming the extinction coefficient of both compound are similar (the value for $AlPcS_{2a}$ is known)

Cellular uptake of $AlPcS_{2a}$ and $AlPcS_{2a}$-saporin conjugate in HN5 cells

HN5 cells were plated onto 96-well plate at $2.5x10^4$ cells/well one day before drug application. In order to improve the solubility, $AlPcS_{2a}$-saporin conjugate solution was adjusted to be slightly alkaline by adding few drops of sterile NaOH. Cells were then treated with up to 10μM alkaline conjugate or 10 μg/ml $AlPcS_{2a}$ for 18 hrs. At the end point, cells were washed with PBS and incubated in clear DMEM medium (no phenol red; no serum) for fluorescence measurement using a LS50B Perkin-Elmer spectrofluorimeter (Perkin-Elmer, UK).

Subcellular distribution and localisation of $AlPcS_{2a}$-saporin conjugate in HN5 cells using confocal microscopy

HN5 cells overnight seeded onto glass bottom dishes FluoroDish™ (WPI, UK) were incubated with 10 μM $AlPcS_{2a}$-saporin conjugate for 18hrs. After thoroughly washed and incubated with fresh full medium for further 4 hours, cells were incubated with clear DMEM for imaging using confocal microscopy (FLUOVIEW FV1000, 60x magnification, NA 1.20, Olympus, Japan). For localisation studies, cells were incubated with 50 nM LysoTracker Green (Molecular Probes, UK) for 30min, and imaged by confocal microscopy.

PCI effect of $AlPcS_{2a}$-saporin conjugate in comparison with $AlPcS_{2a}$ PCI of saporin in HN5 cells

HN5 cells were seeded at 5000 cells/well in 96-well plates overnight. Cells were treated with 100 nM $AlPcS_{2a}$ alone or $AlPcS_{2a}$-saporin conjugate (20, 50 and 100 nM) for 18hrs separately. Another two groups of cells were co-incubated with saporin (50 nM and 100 nM) and 100 nM $AlPcS_{2a}$. Cells were then washed off trice with PBS and incubated further 4 hours with fresh full medium. Irradiation was carried out up to 10 min using a 670nm laser (Hamamatsu Photonics, Japan) as described in Chapter 4 (Figure 4.2). Cell viability was determined using the MTT assay 2 days after the light exposure.

5.2.3 Results

Spectroscopic analysis of $AlPcS_{2a}$-saporin conjugate

Figure 5.18 shows the absorbance spectra of 1 µg/ml $AlPcS_{2a}$ and the $AlPcS_{2a}$-saporin conjugates solutions diluted 50 times from stock solution in distilled water. The peak absorption was found at 676 nm. The O.D. value for $AlPcS_{2a}$ at this wavelength was measured 0.36 and it was 0.15 for the conjugate. As the extinction coefficient of $AlPcS_{2a}$ is 2.56 x $10^5 M^{-1}cm^{-1}$ at 676 nm, the relative concentration of $AlPcS_{2a}$ of the conjugate was then calculated as 0.6 µM. The dimerisation of photosensitisers due to the aggregation in water was observed with the shoulder peaks beside the main peak at 676 nm.

The average ratio of $AlPcS_{2a}$ to saporin can be obtained from the measurement of the relative saporin concentration. However, for these experiments, the supplier of saporin, Sigma-Aldrich, was unable to provide reliable purity which made it difficult to measure protein absorption at 280 nm. Since this is a preliminary study to conjugate photosensitiser with protein toxin, the conjugate concentration was taken to be equivalent of the calculated $AlPcS_{2a}$ concentration in the later experiments, assuming the ratio of $AlPcS_{2a}$ and saporin is 1.

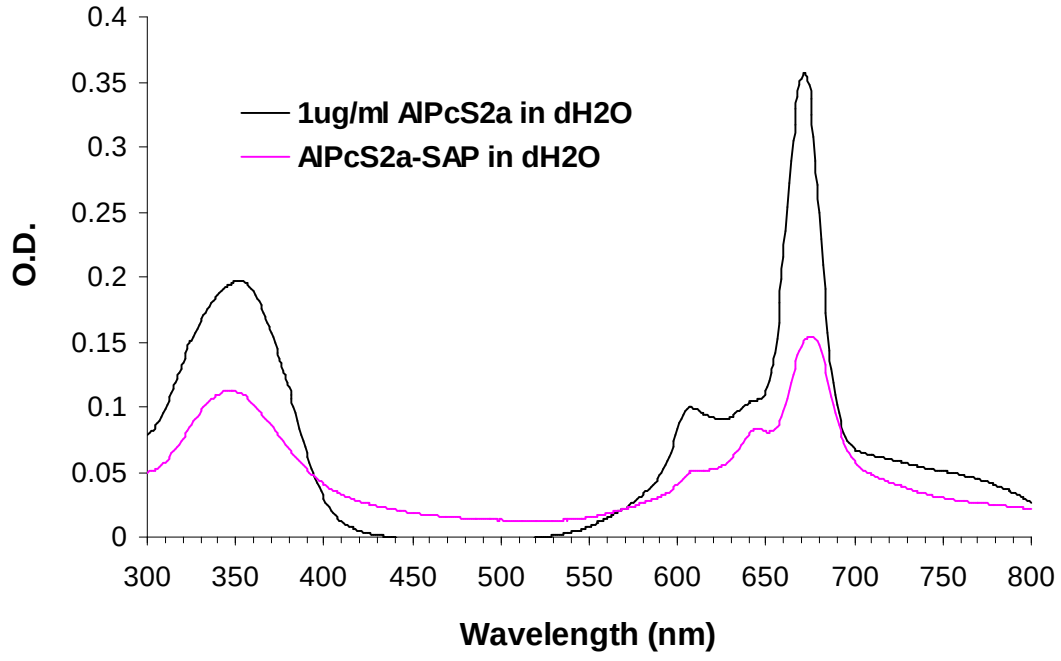

Figure 5.18 Absorption spectra of 1 µg/ml $AlPcS_{2a}$ in water and the $AlPcS_{2a}$-saporin conjugate solutions in distilled water (dH_2O).

Cellular uptake of $AlPcS_{2a}$ and the $AlPcS_{2a}$-saporin conjugate in HN5 cells

The cellular uptake $AlPcS_{2a}$-saporin conjugate was determined and compared with $AlPcS_{2a}$ by measuring the fluorescence intensity in cells following an 18 hour incubation. HN5 cell monolayers were incubated with increasing concentrations of compounds. Following washing, the fluorescence from the cells was measured using fibre-optic spectrofluorimeter with the detection/excitation fibre placed above each well in a 96 well plate.

A clear drug concentration dependent cellular uptake of the conjugate was observed in HN5 (Figure 5.19). The fluorescence intensity linearly increased against drug concentration and no saturation was found up to the drug concentration of 10 μM. However, much lower fluorescence signals of the conjugate were detected in comparison to $AlPcS_{2a}$ using similar concentrations, suggesting its cellular uptake is not as efficient as $AlPcS_{2a}$.

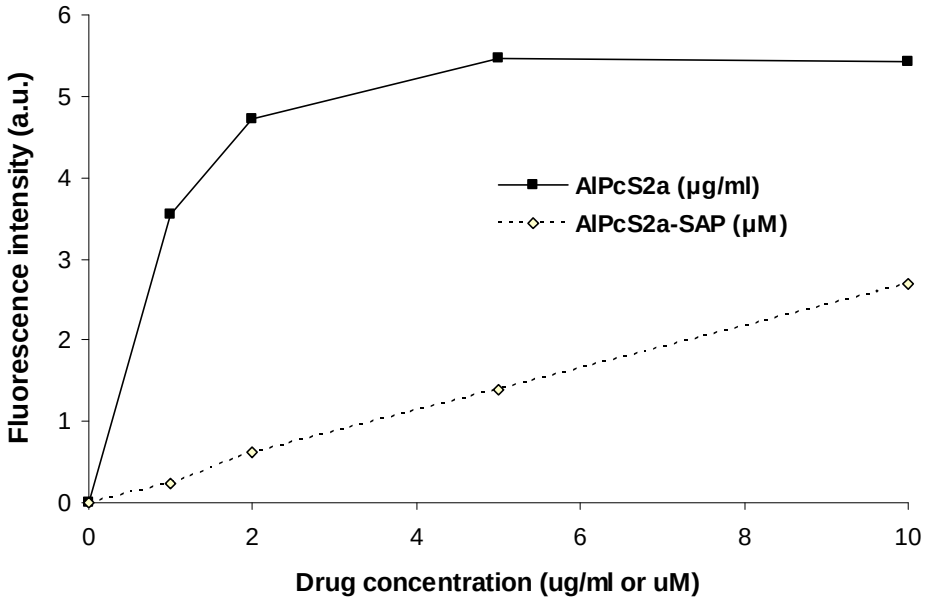

Figure 5.19 Cellular uptake of $AlPcS_{2a}$-saporin conjugate and $AlPcS_{2a}$ with increasing drug concentrations (up to 10 μg/ml or μM) in HN5 cells after 18 hr incubation.

Subcellular distribution of $AlPcS_{2a}$-saporin conjugate in HN5 cells

HN5 cells seeded onto FluoDish plates were incubated with 10 μM $AlPcS_{2a}$-saporin conjugate for 18hr and imaged using confocal microscopy. Figure 5.20 shows the intracellular distribution of the conjugate in HN5 cells. A granular distribution was

observed in which the granular particles were mainly found in the cytosol but some of them were in or overlying the nuclei (the white arrow inset).

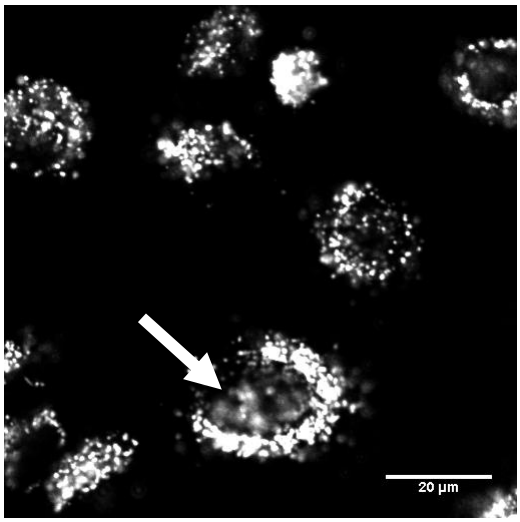

Figure 5.20 Cellular distribution of $AlPcS_{2a}$-saporin conjugate in HN5 cells. Cells were incubated with 10 µM $AlPcS_{2a}$-saporin conjugate for 18 hours and imaged by confocal microscopy. Inset arrow: nuclear localisation.

The subcellular localisation of the $AlPcS_2a$-saporin conjugate was examined by comparison with a lysosomal probe, LysoTracker Green (50 nM), which was applied to cells 30min before imaging. As shown in Figure 5.21, most of the conjugate (red) appeared to be localised at lysosomes (green), resulting in the yellow colour presented in the merged image.

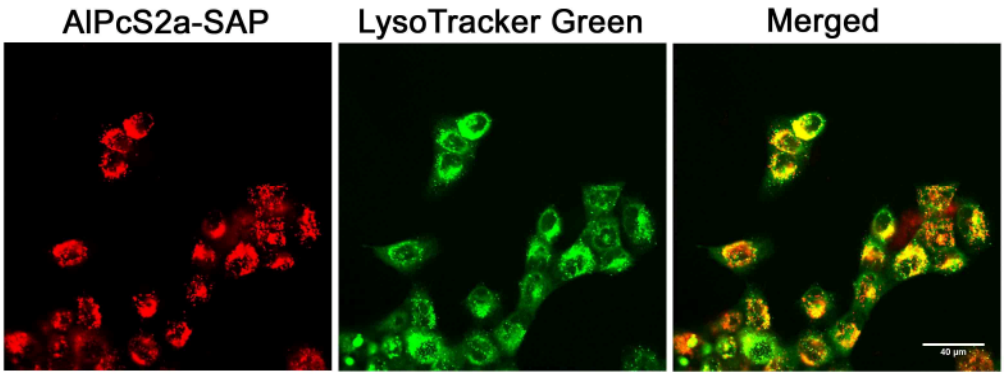

Figure 5.21 Co-localisation of $AlPcS_{2a}$-saporin conjugate and LysoTracker Green in HN5 cells by confocal microscopy. Red: $AlPcS_{2a}$-saporin; green: LysoTracker Green; yellow: merged image.

PCI effect of $AlPcS_{2a}$-saporin conjugate in comparison to $AlPcS_{2a}$ PCI of saporin in HN5 cells

The PCI effect of $AlPcS_{2a}$-saporin conjugate was investigated in comparison to $AlPcS_{2a}$ PCI in combination with saporin using the same concentrations in HN5 cells. Cells were either incubated with conjugate (20-100 nM), $AlPcS_{2a}$ (100 nM) or co-incubated with $AlPcS_{2a}$ (100 nM) and saporin (50 and 100 nM) for 18 hrs. As shown in Figure 5.22, the cell viability remained about 80% in the cells sensitised with 100nM $AlPcS_{2a}$ upon increased light exposure. It was not unexpected that no phototoxicity could be observed in this case since the dose of $AlPcS_{2a}$ used for *in vitro* PDT studies is usually more than 5 μg/ml (6.49μM) (see Section 4.7). In contrast, the PCI effect was observed in the cells incubated with the conjugate with the concentration as low as 20 nM after 10 min light exposure.

The PCI effect was much more clearly shown in the cases of using higher concentration of conjugates (50 and 100 nM), in that a dramatic drop of cell viability was measured after 10 min irradiation. It was also apparent that the conjugate itself exerted slight toxicity in which half of the cells were killed without exposure to light (the intercept at zero irradiation time). Nevertheless, after 10 min irradiation, the killing effects were only found to be as good as the usual PCI strategy in which photosensitiser and toxin were together added to cells.

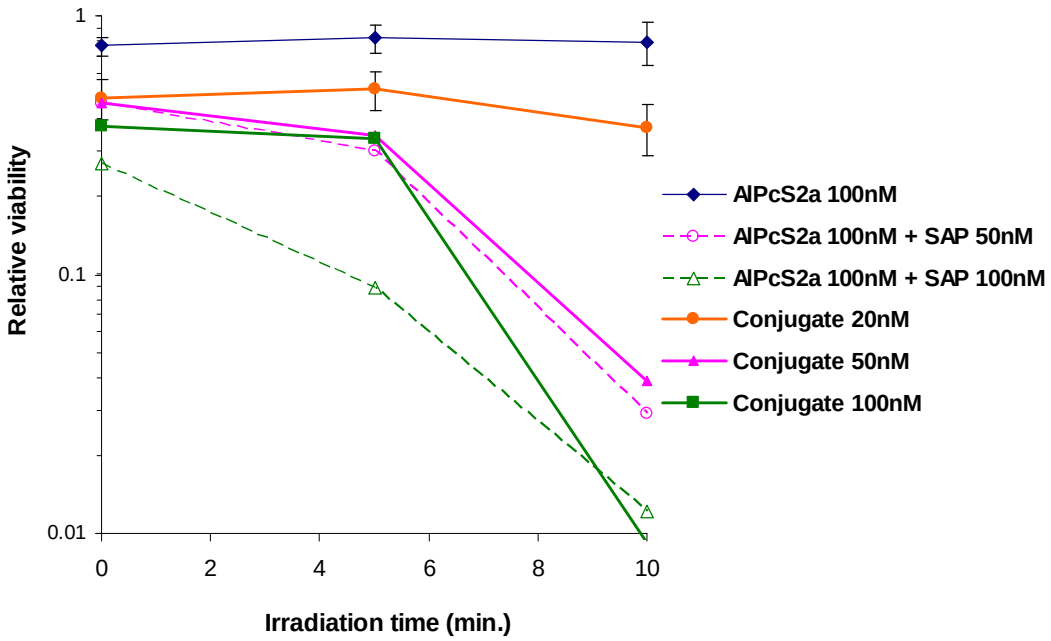

Figure 5.22 PCI effect of $AlPcS_{2a}$-saporin conjugate in comparison with $AlPcS_{2a}$ PCI of saporin in HN5 cells.

5.2.4 Discussion

The study in this section focused on the feasibility of using a photosensitiser-protein toxin bioconjugate for PCI technology. The absorption spectrum of conjugate was found to be similar to unconjugated $AlPcS_{2a}$ with the typical peak absorption of phthlocyanine around 670nm (Figure 5.18). The results indicate that the conjugate can still be activated using the same light source. The relative concentration of $AlPcS_{2a}$ was therefore obtained using Beer's Law since the extinction coefficient of $AlPcS_{2a}$ is known.

The cellular uptake of the conjugate was compared with $AlPcS_{2a}$ by measuring the fluorescence intensity inside cells. When cells were incubated with similar concentration of both compounds, the results show that the cellular uptake of the conjugate was found to be much lower than $AlPcS_{2a}$ but displayed a concentration dependent manner (Figure 5.19). The lower rate of uptake may be due to the larger size of the bioconjugate. As shown in Figure 5.20, the conjugate displayed a granular distribution in HN5 cells and it was found to be well localised with lysosomes (Figure 5.21). The distribution of the conjugate is consistent with the results of either $AlPcS_{2a}$ or saporin observed in experiments in Chapter 4 (Figure 4.11 and 4.17).

Upon illumination, the $AlPcS_{2a}$-saporin conjugate was found to be able to induce a PCI effect in HN5 cells (Figure 5.22). The killing effects induced by the conjugate at the concentration of 50 nM and 100 nM were as good as using 100 nM $AlPcS_{2a}$ PCI of saporin with the same toxin doses after 10 min light exposure. These chosen concentrations of saporin are slightly higher than the ones used for conventional PCI studies in which cells were co-incubated with unconjugated $AlPcS_{2a}$ and saporin. According to the results from Chapter 4, the sub-lethal dose of saporin is only about 25 nM for HN5 cells, whereas, the dose of $AlPcS_{2a}$ required for inducing PDT or PCI effect is at least 5 μM (Table 4.1). Since one conjugate molecule composes one $AlPcS_{2a}$ and two saporin in theory, when using the conjugate with nano-Molar concentrations, the equivalent concentrations of photosensitiser may not be able to induce efficient photochemical reactions and the consequent PCI effect. However, surprisingly, although little phototoxicity was induced in the cells incubated with 100 nM $AlPcS_{2a}$, significant enhancement in cell kill was observed in combination with saporin (50 nM

and 100 nM) under the light exposure up to 10 min. The results suggest that saporin may still be released and induce significant cytotoxicity.

Prior to the study presented in this section, attempts also had been made to synthesize different bioconjugates for PCI by conjugating saporin to porphyrin with various functional groups and linkers. Most of the conjugates remained typical porpyrin fluorescence spectrum but displayed inefficient cellular uptake probably due to the hydrophilicity or other interferences derived from their chemical structures. Some of the conjugates exhibited light dose and drug dose dependent phototoxicity; however, unfortunately, none of them demonstrated a PCI effect in which synergistic cytotoxicity should be involved.

These unsuccessful results show that there are still difficulties in making an ideal conjugate which is not only bioavailable but also able to induce a PCI effect. Care should be taken especially for the protein-involved conjugation that the structure of protein moiety must be preserved during the synthesis to retain the protein function. The results of this section also point out that the ratio of photosensitiser and protein toxin should be concerned for the conjugate used for PCI.

In recent years, there has been significant development on the molecules with nanostructures (liposomes, micelles or dendrimers) for their biomedical applications such as the delivery of drugs, imaging agents, or gene transfection. For PCI, there is always a hope to synthesise a complex which combines the targeting system (e.g. antibodies), drugs (e.g. protein toxins), and photosensitisers together. The study using a complex enveloped dendrimeric phthalocyanine and DNA to achieve efficient PCI-mediated gene delivery is a good example. However, the complexity of the nanostructures needs more delicate plans and further investigation. The study in this section was the first attempt to use a photosensitiser-protein toxin bioconjugate, $AlPcS_{2a}$-saporin conjugate, designed for a PCI strategy. Although the preliminary results show that this conjugate can be taken up by cells and induce PCI effects upon irradiation *in vitro*, further studies on the chemical structure characterization, the detailed cellular uptake mechanism and the optimisation of the treatment conditions for PCI remain to be carried out.

5.3 Summary

The aim of the studies described in this chapter was to investigate the PCI efficacy of bioconjugates for drug delivery. It was hypothesised that the use of bioconjugates will have several advantages: firstly for more efficient cellular delivery of the photosensitiser in the case of peptide-photosensitiser bioconjugates; and secondly, the co-delivery of the photosensitiser and toxin in the case of photosensitiser-toxin conjugates. The fact that the complex can be administered at one time is especially an advantage for PCI application *in vivo* or in clinic. Finally, in the longer term, such bioconjugates could enable more efficient targeting with the inclusion of targeted ligands.

In the first section of this chapter, a new porphyrin-peptide bioconjugate of a cell penetrating peptide, Tat sequence (Tat) and tetraphenylporphine (TPP) was synthesised. This Tat-TPP conjugate exhibited favourable optical properties for PDT and PCI (Table 5.1). In the *in vitro* studies, the conjugate displayed efficient cellular uptake and lysosomal and partly mitochondria localisation due to the membrane-translocation ability of Tat sequence and the amphiphilic structure derived from TPP (hydrophobic) and Tat sequence (hydrophilic). As a photosensitiser, the conjugate showed efficient light dose and drug dose dependent phototoxicity. In combination with saporin, the conjugate was found to be able to induce a significant PCI effect with the enhanced cytotoxicity after photosensitisation.

A photosensitiser-protein toxin bioconjugate, $AlPcS_{2a}$-saporin, was synthesised and designed for PCI application for the studies of the second section. After conjugation, optical properties of the conjugate in terms of absorption and fluorescence spectra remained similar to $AlPcS_{2a}$. The cellular uptake was found to be dependent on the drug concentration but the overall efficacy was not as efficient as $AlPcS_{2a}$. Using confocal microscopy, the granular distribution of the conjugate, the typical intracellular distribution for PCI photosensitisers, was still observed. This conjugate also showed to be able to induce PCI effect after illumination, resulting in the comparable increased cell kill to the PCI effect using unconjugated $AlPcS_{2a}$ and saporin.

The studies in this chapter demonstrated the use of bioconjugation to synthesise photo-products from available materials for PCI technology. The linking of a Tat peptide

sequence significantly improves water solubility and the consequent bioavailability of TPP to be an efficient photosensitiser for PDT and PCI. The $AlPcS_{2a}$-saporin conjugate has similar photophysical properties to the parent $AlPcS_{2a}$ and is also able to induce PCI effect in combination with light. Further investigations are needed for the future applications *in vivo*.

Section C: *In Vivo* Studies – Evaluation of Amphinex

Chapter 6: Biodistribution of Amphinex in Normal Rats

6.1 Introduction

Investigating the biodistribution or localisation of drugs is always a necessary task for any treatment. For drug treatments of cancer, the efficacies often rely on the drug concentration in the cancerous sites and also the tumour selectivity - the ratio of drug concentration in tumour to normal tissue. Amphinex displayed an efficient uptake by cancer cells *in vitro* according to the results from Chapter 4. In this chapter, the biodistribution of Amphinex in rats will be studied for further *in vivo* utilisation, e.g. photodynamic therapy and eventually photochemical internalisation.

As mentioned before in Chapter 1, most of the photosensitisers form a biodistribution preferential to tumours, although the mechanisms involved are not fully understood. Unlike the 1^{st} generation photosensitisers, the 2^{nd} generation photosensitisers tend to be pure compounds, which facilitate pharmacokinetic studies from the structure-localisation point of view. To investigate the biodistribution of Amphinex, it is worth looking at the distribution pattern of its fellow sensitisers as the biodistribution is heavily influenced by their fundamental chemical properties. AlS_nPc (sulfonated aluminium phthalocyanines) and m-THPC (tetra(m-hydroxyphenyl) chlorin) are two photosensitisers which are structurally similar to Amphinex. Both of them have well documented PDT effects and *in vivo* pharmacokinetics, using different analytic methods and models.

A comparative study of the biodistribution of di- and tetra-sulfonated aluminium phthalocyanines (AlS_2Pc and AlS_4Pc) in rat colon has been carried out in our lab using chemical extraction and fluorescence microscopy [Chatlani et al., 1991]. A good correlation was found between both methods for both dyes that sensitisers were eliminated with time, but the elimination of AlS_2Pc was more rapid. Microscopic distribution of the drug also gave more information about the drug localisation at the cellular level. Peak fluorescence signals were measured 1h after i.v. injection in all cases, except in the mucosa where the highest uptake of AlS_4Pc was observed at 5hr after administration. The microscopic biodistribution of AlS_2Pc has also been investigated in the canine prostate where the maximum drug concentration was measured at 5-24hr after i.v. injection [Chang et al., 1997].

Another study to compare the biodistribution of $AlPcS_2$ in mice liver and muscle after different administration routes (i.v., i.p., intramuscular (i.m.) and subcutaneous (s.c.)) was evaluated by chemical extraction and light-induced fluorescence spectroscopy (LIFS) [Lee et al., 2001]. Despite the high level of drugs measured following i.v. application, both analysis methods resulted in similar biodistribution patterns of the drug in liver with the peak value at 1-4 hrs. The drug concentration appeared much lower in muscle compared to liver by all measures. However, the i.v., i.m. and i.p. deliveries produced higher drug uptake, particularly soon after injection when measured using the LIFS method. This study indicates that different administration methods will result in different biodistribution of drugs.

As for m-THPC which is a chlorin like Amphinex, Peng et al. investigated by chemical extraction the uptake and localisation of m-THPC and m-THPP in tumour bearing mice after i.p. injection [Peng et al., 1995]. The highest uptake of m-THPC was found 24-48hrs after injection and the concentration in tumours were higher than most of the normal tissues except liver, urinary tract and skin. Different intratumoural localisations of drugs were observed by confocal microscopy where m-THPC was distributed in vascular interstitium and neoplastic cells but m-THPP was localised in the stroma of tumours.

m-THPC kinetics in normal rat liver and the implanted colon carcinoma in liver were analysed by Rovers et al. using chemical extraction and LIFS methods to examine PDT of liver metastases [Rovers et al., 1999]. Results from both methods showed that m-THPC reached the peak concentration in normal liver at 4hrs after i.v. administration and started to decrease in time. However, a different kinetic pattern was observed in tumours; here the drug concentration remained high up to 48hrs after injection. The tumour-to-liver ratio was measured at more than 5 using both methods which indicated m-THPC is accumulated more in intrahepatic tumours. Another study using pegylated m-THPC (m-THPC-PEG) was carried out to investigate the influence of drug formulation [Rovers et al., 2000]. The results showed that pegylation of m-THPC resulted in prolonged plasma half-life and higher uptake in tumours than in normal liver at up to 75hrs. However, the concentration of m-THPC-PEG in liver tissue continued to increase and it became higher than tumours when measured at 125 hrs after injection.

Blant et al. demonstrated the comparison of the biodistribution of ^{14}C-labelled m-THPC in a hamster tumour model using three different methods- LIFS, fluorescence microscopy and chemical extraction [Blant et al., 2002]. Results were consistent between three methods, showing that the highest concentration of drug was found at 12-24hrs post i.c. (intracardiac) injection in most of the tissues, including advanced neoplasia.

Reports suggest that the pharmacokinetics of sensitisers is informative for determining the timing of optical treatment during PDT. In most of the studies, most efficient PDT outcomes were obtained while they were carried out at the timing chosen based on the pharmacokinetic results i.e. when there was the sufficient photosensitiser concentration in targeted tissues and lower drug concentration in the surrounding normal tissue, or the highest ratio of drug concentration between tumour and normal tissue. Barr et al. have discussed the correlation of the biodistribution photosensitiser with its biological effects [Barr et al., 1991]. As stated before, the pharmacokinetics of sensitisers differs when different administration modes, analysis methods or target models are employed.

The aim of this chapter is to investigate the biodistribution of Amphinex in Wistar rats for further PDT and PCI treatment in normal liver and colon (the next chapters). Two methods, quantitative fluorescence microscopy and chemical extraction, will be compared and used for measuring the tissue uptake of Amphinex. To identify the tissue localisation of Amphinex, H&E stained adjacent tissue sections will be used to compare to the corresponding images collected with fluorescence microscopy.

The last experiment of this chapter describes the use of an optical pharmacokinetic (OP) system to measure the absorption spectrum of Amphinex in rat liver. The technique has been established in our laboratory [Austwick et al., 2009] and the acquired *in vivo* optical properties of Amphinex can provide information on the optimum wavelength of the light source suitable for activating Amphinex *in vivo*.

6.2 Materials and Methods

Chemicals

Amphinex in Cremophor (10 mg/ml) was kindly donated by PCI Biotech (Norway). Amphinex was diluted in phosphate-buffered saline (PBS) to a concentration of 2.5 mg/ml for intravenous injection. Solvable^{TM}, a standard tissue solubilizer and chemical extraction agent containing dodecyldimethylamine oxide, secondary alcohol ethoxylate and sodium hydroxide, was purchased from Perkin-Elmer (UK) [Kascakova et al., 2008].

Animal models

All animal experiments were conducted under the authority of project and personal licences granted by the Home Office and the UKCCCR Guidelines. Normal, female Wistar rats (180-200g, Harlan, Oxon, UK) were used for both quantitative fluorescence microscopy and chemical extraction studies. Female Hooded Lister rats (180-220g) were additionally used for chemical extraction studies as future PDT treatments on the subcutaneous tumour model are transplanted to Hooded Lister rats. Inhaled Halothane or Isoflurane was used to maintain a state of general anaesthesia for drug administration.

Pharmacokinetic Studies Using Quantitative Fluorescence Microscopy

14 Wistar rats received 2.5mg/kg Amphinex intravenously via tail vein. Tissues of 4 organs (liver, colon, muscle (thigh) and skin (abdominal)) were obtained from seven groups of animals (2 rats each) killed 1, 3, 6, 15, 24, 48, 96 hours after sensitisers injection. In order to evaluate the skin photosensitivity, skin samples from another two rats were taken 8 days after sensitiser administration. Two additional rats with no sensitiser administration were used for control study. Fresh surgical specimens were cut into suitable sizes, snap-cooled in isopentane for 10 sec. Excess liquid was removed with a paper tissue and the tissues were placed into vials in a liquid nitrogen container. Frozen tissues were stored in liquid nitrogen until sectioning. 10 μm sections were cut from tissue blocks mounted with OCT Embedding Medium (Raymond A. Lamb, UK) and picked up on poly-lysine coated slides. The cryosections were allowed to air dry for at least 1 hour and then kept at -20°C in the dark until additional use.

Sectioning was performed under minimal ambient light conditions to avoid photobleaching of the photosensitiser. Five consecutive sections were prepared from each sample for quantitative fluorescence microscopy. From each section, five images were recorded in three different regions of the slice to avoid photobeaching.

The Amphinex fluorescence signal from frozen sections was detected using fluorescence microscopy and the light source was a 532 nm laser (10mW). Fluorescence was detected at 660 nm with a 50 nm bandpass filter. Images were taken using a Peltier-cooled charge-coupled device (CCD) camera (Princeton Instruments, UK) and the fluorescence intensity was analyzed using NIH Image J software. To determine the exact histological localisation of Amphinex, one of the sections from each sample was stained with haematoxilin and eosin (H&E) after recording the fluorescence images. The H&E images were taken at an identical position. The subtraction procedure was carried out for each measurement by subtracting the autofluorescence from the sections of non-injected control animals.

Chemical extraction of Amphinex

8 Wistar rats and 6 Hooded Lister rats were given Amphinex 2.5mg/kg intravenously via tail vein. Using two animals in each group, liver and colon tissues from Wistar rats were collected at 3, 6 and 24hr after drug injection. Each time point has two animals including the control group (no drug administered). Tissue samples were cut into small pieces and frozen at -80 ºC.

Three fully defrosted samples (0.1g wet weight) from each animal (organ) were immersed in 2ml Solvable in tubes and placed into a shaking water bath at 50 ºC for 2 hours until clear solution was observed. 0.15ml tissue solution from each tube was diluted with 3ml Solvable and cooled to room temperature before measuring the fluorescence. A standard curve of Amphinex in Solvable was established by making up Amphinex solution of series concentrations with control tissue-containing Solvable. Each sample solution was plated onto 4 wells of a dark 96-well plate. A standard curve was obtained from the mean fluorescence intensity measured at 655 nm and the corresponding concentrations of Amphinex in each sample could thereby be calculated.

Optical pharmacokinetic (OP) measurement of the absorption spectrum of Amphinex in liver

The spectroscopic technique used in these experiments enables measurement of the in vivo absorption spectrum of the administered chromophore. All animals (except control groups) were sensitised with 2.5 mg/kg Amphinex through the tail vein injection, followed by the OP measurement carried out at laparotomy 6 hrs after drug administration. The same dose was used in the fluorescence pharmacokinetic studies.

OP data were collected from liver using a pair of fibres (delivery and collection) inside a catheter. The tip of catheter was pressed lightly against the liver surface. 10 separate positions were chosen with 4 OP measurements being taken at each position. The delivery fibre (400 μm in diameter) and the collection fibre (200 μm in diameter) are 1.8 mm apart. The light was delivered from a pulsed Xenon arc lamp (model LS 1130/FX1100, Perkin Elmer Optoelectronics, UK) and the signal scattered back was analysed by a CCD spectrometer (model S2000, Ocean Optics Inc.,USA). The system was calibrated before each experiment using a reference spectrum collected from white Spectralon (Labsphere, USA), a spectrally flat diffuse-reflecting polymer.

The data analysis was carried out with help from Dr Austwick. The detailed optical absorption data collection and further analysis methods can be found here [Austwick et al., 2009].

6.3 Results

6.3.1 Biodistribution of Amphinex in normal rats using quantitative fluorescence microscopy

Pharmacokinetic studies using quantitative fluorescence microscopy showed highest uptake of Amphinex in liver at 6hrs after drug administration (Figure 6.1). The excretion of Amphinex from the liver slowed down after 24hrs, and a retention phase was observed between 24 hrs and 48 hrs.

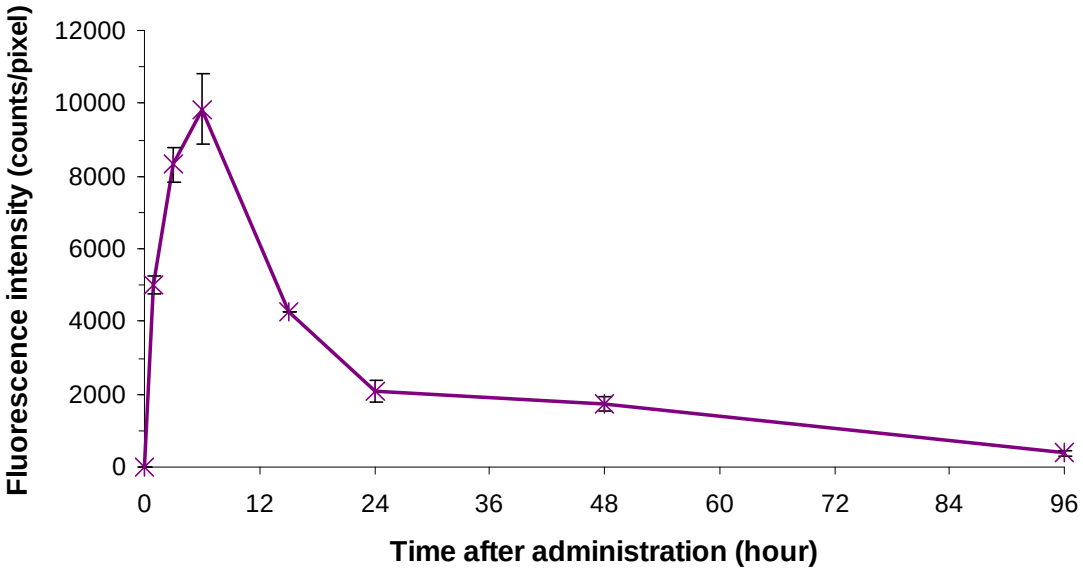

Figure 6.1 Kinetics of Amphinex in Wistar rat liver (control rats subtracted) after i.v. injection of 2.5 mg/kg Amphinex examined by fluorescence microscopy.

Figure 6.2 illustrates a comparison of the uptakes of the other 4 organs after measuring their fluorescence quantities. These 4 organs displayed, overall, a much lower uptake of Amphinex compared to the liver. Similar pharmacokinetic patterns were found as the uptakes were highest at 24 hrs after administration in the mucosa of colon, skin and muscle, and at 48 hrs in the muscle in colon. A clear decrease was observed in skin up to 8 days after injection indicating minimum skin photosensitivity.

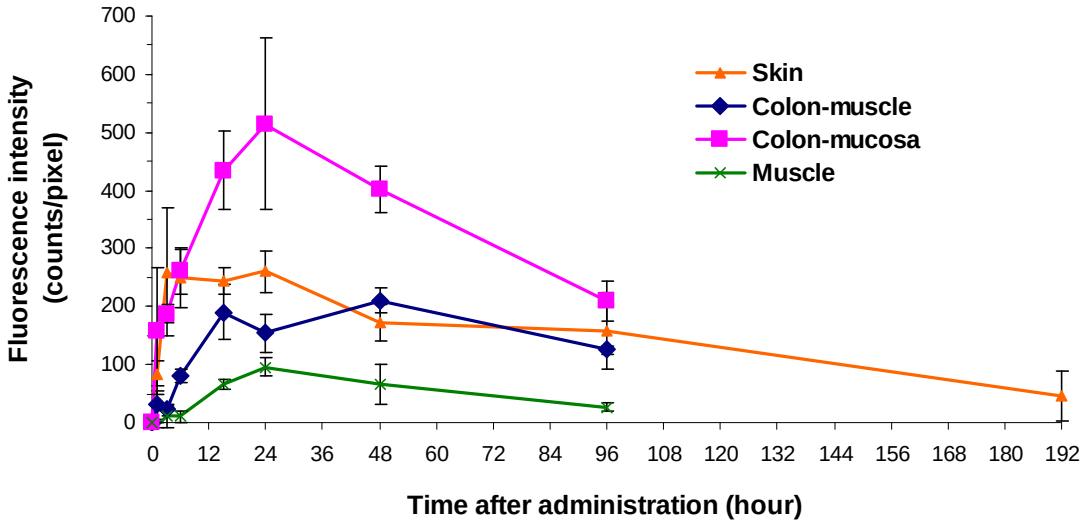

Figure 6.2 Comparative fluorescence kinetics examined by quantitative fluorescence microscopy of Amphinex in skin, colon and muscle of Wistar rats (control rats subtracted) after i.v. injection of 2.5 mg/kg Amphinex.

6.3.2 Quantitative microscopic biodistribution of Amphinex

The fluorescence microscopy imaging results of the uptake of Amphinex 1hr after administration in liver, colon and skin are shown in Figure 6.3A, B and C respectively. The corresponding histology results (H&E stain) are shown in the right column of Figure 6.3. The average fluorescence intensity was about 5000 counts/pixel in liver and 157 counts/pixel in the colon mucosa. It can be seen that Amphinex has spread throughout the colon mucosa within 1hr after injection, and there is a distinct difference in the uptake between the mucosa and muscle in the colon - the fluorescence signal was only 37 counts/pixel in the muscle structure. A significant drug accumulation in submucosa blood vessel wall was also observed with the fluorescence intensity around 1300 counts/pixel (Figure 6.3B, green arrow). Compared to the other tissues, the signals from skin were very low; the drug level in the thigh muscle is even lower (images not shown).

The highest uptake of Amphinex in liver and colon are shown in Figure 6.4. The maximum drug accumulations in liver and colon were measured at 6 hrs and 24 hrs after drug administration respectively. As these images were plotted on the same scale of fluorescence intensity as the 1hr images, the larger number of areas presented in white and yellow indicate the higher drug uptake in these two tissues. It should be noted that the colon submucosa blood vessel wall still exhibits excellent drug uptake and the drug level was slightly higher (1600 counts/pixel) compared to the 1hr data. The serosa layer was on the edge of the section which usually folds up and results in multiple layers. This could be the cause of the particularly high signals detected from the outer colon wall.

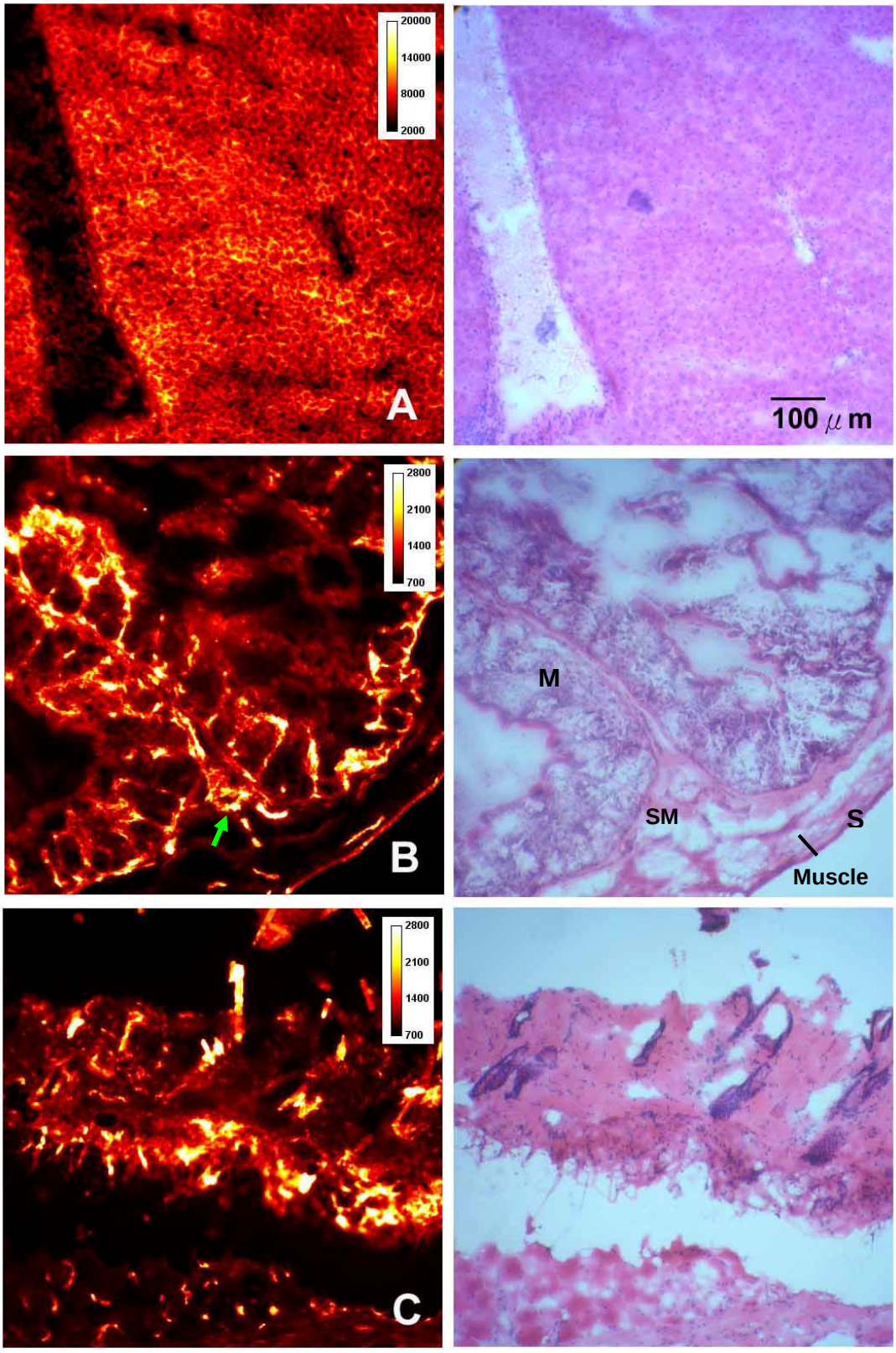

Figure 6.3 Fluorescence (left) and corresponding H&E stained (right) micrographs of frozen sections of Wistar rat liver (A), colon wall (B) and skin (C) sampled 1h after i.v. injection of 2.5mg/kg Amphinex. Individual colour scale bar refers to the relative fluorescence intensity. Arrow: submucosa blood vessel; M: mucosa; SM: submucosa; S: serosa.

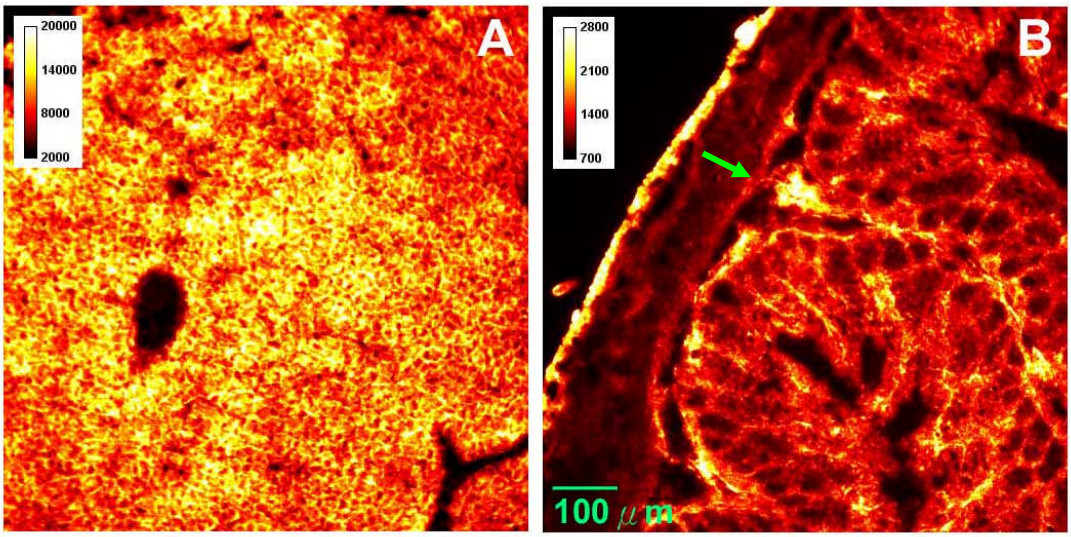

Figure 6.4 Fluorescence images of maximum uptake of Amphinex in Wistar rat liver (A) and colon wall (B). Liver and colon was sampled at 6hr and 24hr after i.v. injection of Amphinex 2.5mg/kg respectively. Green arrow: submucosa blood vessel.

6.3.3 Quantification of Amphinex concentration in rat liver and colon using chemical extraction

Pharmacokinetics of Amphinex in liver and colon of Wistar rats were also assessed by chemical extraction. As shown in Figure 6.5, liver displayed a much higher Amphinex uptake compared to colon. For the times studied, the highest concentration in both tissues was detected at 6hrs after administration although the concentration in colon at 6hrs and 24hrs were similar. Good correlations were noted between the Amphinex concentration measured by chemical extraction and the fluorescence intensity from fluorescence microscopy. Using both techniques the levels observed in liver at 24 hrs were significantly lower compared to 6 hrs as shown in Figure 6.1 and 6.5.

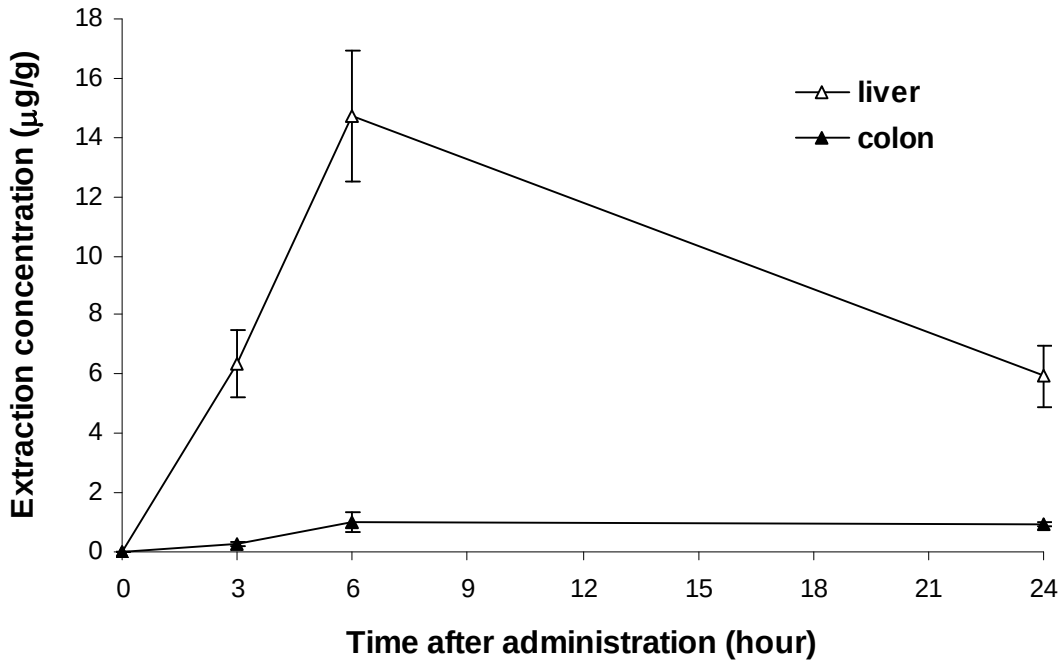

Figure 6.5 Concentration of Amphinex extracted from the liver and colon of Wistar rats as a function of the time after i.v. injection of 2.5 mg/kg Amphinex.

6.3.4 Optical pharmacokinetic measurement of Amphinex from rat liver

The mean tissue reflectance spectrum of Amphinex in liver measured by OP system is illustrated in Figure 6.6. A low signal corresponds to weak diffuse reflectance as a result of strong absorption by chromophores present in the tissue. The strong absorption of haemoglobin can be seen in the region 520-600 nm. The absorption spectrum of Amphinex in water has been measured with a strong peak lying close to 655 nm (Figure 4.5). The data obtained here also show a peak absorption in this region (red circle inset).

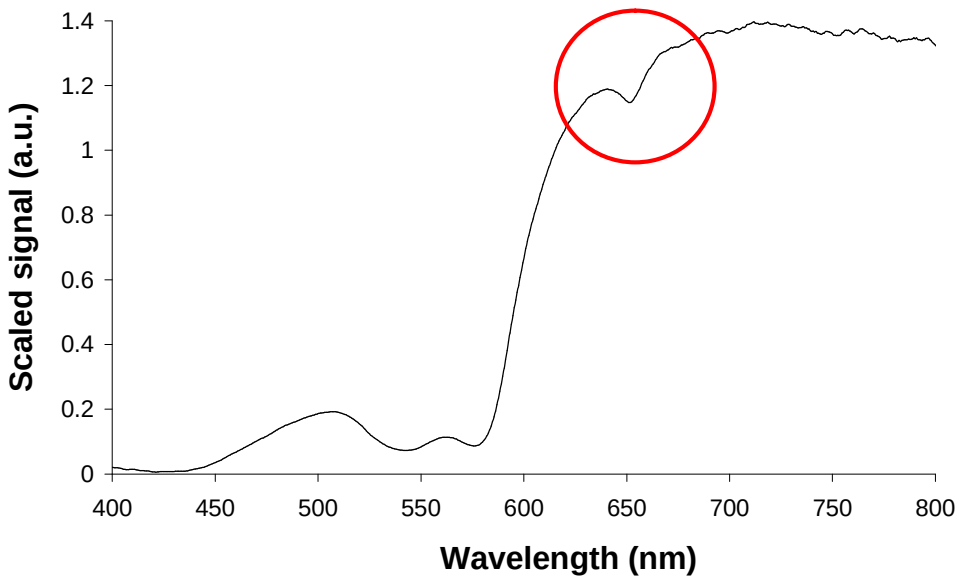

Figure 6.6 Mean OP measurement of Amphinex signal from rat liver. Animals were sensitised with 2.5mg/kg Amphinex (i.v.) for 6 hr. Red circle inset: peak absorption of Amphinex in liver.

After haemoglobin spectrum removal, linear interpolation was then carried out within the region from 635 nm to 665 nm which represents the baseline at the peak (Figure 4.6).

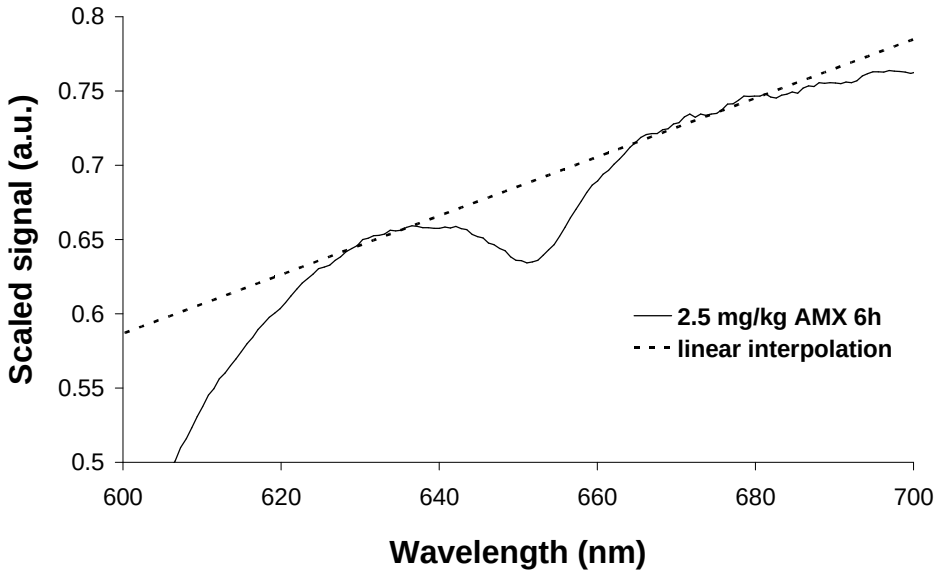

Figure 6.7 Linear interpolation of mean OP measurement of Amphinex signal from rat liver. Animals were sensitised with 2.5mg/kg Amphinex (i.v.) for 6 hr.

After the above fitting processes, the peak absorption of Amphinex measured in liver is identified and shown in Figure 6.8. The maximum absorbance was measured to be at 652 nm. The result here is close to the peak absorbance of Amphinex measured from aqueous solution but with a slight redshift of 3 nm.

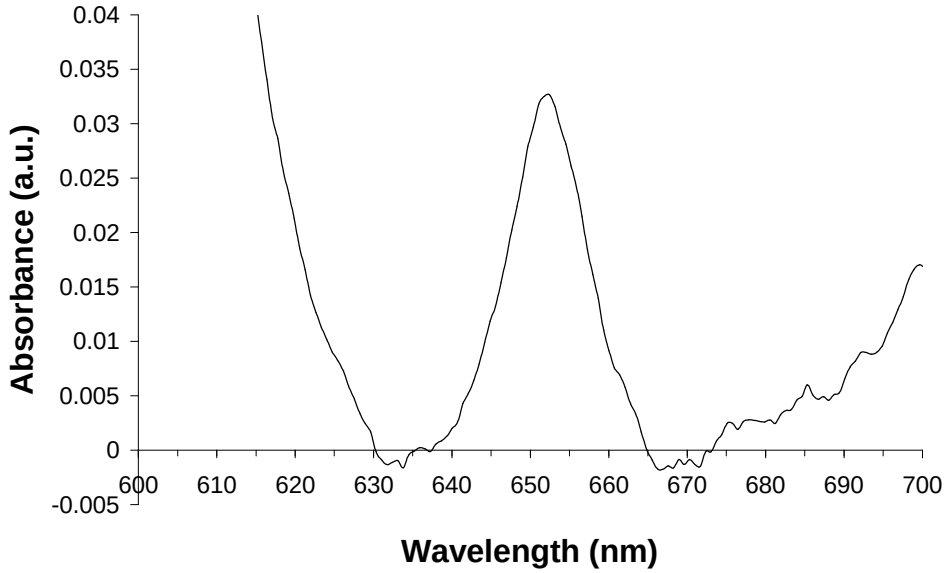

Figure 6.8 Mean absorption peak position of Amphinex from rat liver. Animals were sensitised with 2.5mg/kg Amphinex (i.v.) for 6 hr.

6.4 Discussion

In this chapter, the biodistribution of Amphinex in rats was analysed using fluorescence microscopy and chemical extraction methods. The drug kinetics in several chosen tissues was examined and should offer useful information for further PDT or PCI treatments.

Higher uptake of Amphinex in rat liver was measured compared to other organs using both quantitative fluorescence measurement and chemical extraction methods. According to the results from fluorescence microscopy, the drug concentration rises quickly in the first 6 hrs after injection and a decline appears afterwards (Figure 6.1). The same pattern was obtained using chemical extraction (Figure 6.5). The stable and low drug concentration observed after 24hr indicate a good drug and light interval for treatment in the liver.

In contrast to the liver, the peak values of the Amphinex level in other peripheral tissues were found to be much lower (Figure 6.2). The highest was measured in the colon mucosa followed by skin, colon muscle and muscle from thigh. The Amphinex concentration in the colon wall was also examined by chemical extraction (Figure 6.5). The fluorescence intensity was measured to be higher in colon mucosa than in colon muscle, which suggests a higher drug uptake by the mucosa. However, this difference could not be detected by chemical extraction, as the extraction data represents the drug concentration within all colon structures.

Concerning the skin photosensitivity, the kinetics of Amphinex in rat skin were examined and followed up to 8 days after drug application. The Amphinex level in rat skin was observed to be low when using fluorescence microscopy with the highest uptake measured during 3-24 hrs and a decline up to 8 days after injection. A high level of photosensitisers distributed to skin will cause problems when patients are exposed to ambient natural or artificial light. As prolonged cutaneous phototoxicity is still one of the major side effects of PDT treatments in clinic [Mlkvy et al., 1998;Wagnieres et al., 1998], the clear decrease of Amphinex in the longer term times which reduce the skin sensitivity will certainly benefits the clinical utility of Amphinex. Further studies are required to test the possible skin phototoxicity induced by Amphinex.

It is an interesting finding that higher Amphinex uptake was measured in the smooth muscle in colon wall, and the drug level was about a half that in the striated muscle from the thigh. A similar result has been reported by Blant et al. - ^{14}C-labelled m-THPC exhibited significant higher drug concentration in smooth muscle (uterus) than in striated muscle (skeletal) during the first 48hrs interval after injection [Blant et al., 2002]. It was suggested that this difference could be an advantage from a clinical point of view. When interstitial PDT for advanced SCC of unfavourable locations such as the base of tongue or treatment of middle to lower oesophagus where smooth muscle is the major component, the unwanted photodynamic damage to the muscle and the consequent complications can be therefore reduced.

The main conclusion from these studies is that Amphinex accumulates in normal tissues within a few hours of i.v. administration but then clears over a period of days. The kinetics appear to be similar to those found for sulfonated aluminium phthalocyanines in our laboratory also using Wistar rats, where liver uptake is also high but is cleared over several days [Barr et al., 1991;Chang et al., 1997;Chatlani et al., 1991]. Further studies using a tumour model are presented later in Chapter 8.

Quantitative fluorescence microscopy and chemical extraction were used to investigate the biodistribution of photosensitisers in this study. In fact, based on the optical properties of photosensitisers, there is another approach also often to be used to quantify the drug concentration in tissues with time: fibre-based light-induced fluorescence spectroscopy (LIFS). The LIFS technique quantifies the photosensitiser levels in tissues by measuring the corresponding fluorescence spectra. The *in vivo* system particularly provides a rapid, real-time and non-destructive measurement of drug concentration in tissue. However, the tissue optical properties would certainly affect the light penetration. Panjehpou has reported that the signal detected from muscle could be 5 times higher than from liver when given the same concentration of phthalocyanine to two tissues [Panjehpour et al., 1993]. This is due to the absorption of the excitation light by haemoglobins in the more vascularised liver. Also, it was found that different composition of epithelial layers could lead to changes in the shape and intensity of the predicted spectra [Pavlova et al., 2008]. Therefore, in order to avoid misinterpretation, it is important to understand the changes in the optical properties of photosensitisers when they are in different biological environments.

It is well known that UV light can only pass through 200μm at oral mucosa due to the strong absorption from haemoglobins. In this regard, the light penetration depth would limit the application of LIFS. Chemical extraction does not suffer from this problem as it measures the fluorescence intensity from the digested tissue solution. In spite of its intensive and time-consuming nature, chemical extraction has the advantage that it gives quantitative analysis in terms of mass of drug per mass of tissue. Also, the requirement of a large amount of tissue gives chemical extraction a better accuracy and makes it a gold standard method for pharmacokinetic studies. An obvious disadvantage turns out to be the loss of detailed information from the separate substructures of tissues. For some tissues like colon with complex composition, it is impossible to virtually dissect the colon wall into mucosa and submucosa layers. Another problem is that, ideally, photosensitising compounds will all become monomers after chemical extraction. As a result, the extraction data might not reflect the actual amount of the photosensitisers with photosensitising ability when sensitisers have the tendency to aggregate and exhibit negligible fluorescence. However, some studies have shown that e.g. AlS_2Pc can remonomerise during PDT [Kunz et al., 2007]. Therefore, LIFS, which can be carried out during treatment, might be more suitable in this circumstance.

Fluorescence microscopy can yield drug biodistribution at the cellular level. It also requires series sample preparation procedures but the pharmacokinetic details regarding the drug localisation and the levels of accumulation could be observed at the same time. Moreover, the fluorescence intensity detected by fluorescence microscopy should be from the monomerised photosensitisers which are able to induce photochemical interaction upon irradiation. In this case, the pharmacokinetics obtained from fluorescence microscopy might be more correlated with the efficacy of further photodynamic treatments. However, several things also need to be taken into account. Firstly, the measured fluorescence intensity is a relative value which does not represent the absolute drug concentration. Secondly, the sample size of fluorescence microscopy is small compared to chemical extraction. The thickness of a frozen section is usually about 8-10μm and one fluorescence image covers an area of less than 0.02 mm^2 of tissues when using a 60x objective. Also, a good section is required as non-flat sections would result in inaccurate fluorescence measurements.

There is no one analytic method that is superior to the others. Each has its own advantages and limitations. Hence, it is necessary to use more than one method to

compare and determine the drug pharmacokinetics *in vivo*. In this chapter, good correlations between the kinetics pattern of Amphinex in rat liver and colon using quantitative fluorescence microscopy and chemical extraction were obtained. Fluorescence images provided the detailed drug localisation at the cellular level. Chemical extraction results yielded the actual drug concentrations in tissue.

The separate experiment of optical pharmacokinetic measurement of Amphinex in liver gives therapeutically relevant information about the tissue absorption spectrum of Amphinex. The OP system is a non-invasive method to quantify drug concentrations using white light spectroscopic measurement [Mourant et al., 1999] and has been recently applied to measure topical m-THPC (liposomal mTHPC-gel) in the skin of albino hairless mice [Johansson et al., 2007] and AlS_2Pc in various organs in rats through i.v. injection [Austwick et al., 2009]. The figures from present study show that the peak absorbance of Amphinex in liver is at 652 nm which is similar to the value measured from aqueous solution (649 nm, Figure 4.5). The variation between the two is tiny and, in fact, its peak absorbance from liver is closer to the available light source used for m-THPC, a 652 nm laser. The results warrant the use of the 652 nm laser for activating Amphinex *in vivo*. In the subsequent PDT and PCI studies presented here a 652 nm laser has been used.

Further PDT and PCI treatments using Amphinex in normal rat tissues and tumours will be shown in the following chapters.

Chapter 7: Amphinex PDT and PCI in Normal Rat Liver and Colon

7.1 Introduction

Photochemical internalisation (PCI) is a novel technology which enhances the therapeutic effects of macromolecules by releasing them from vesicular compartments after sub-lethal PDT treatment. The results in Chapter 4 have proven that Amphinex PCI is able to improve the therapeutic effect of saporin and bleomycin resulting in the enhancement of cell killing *in vitro*. In this chapter, the *in vivo* efficacy of Amphinex PCI of saporin and bleomycin would be investigated on normal rat liver and colon.

As mentioned before, PCI has been shown to be effective for *in vitro* release of drugs and genes [Berg et al., 1999;Hogset et al., 2004]. While PCI action at the cellular level has been well studied, it is not always possible to directly translate the mechanisms into animal models. The involvement of some elements such as the vascular system would certainly make the *in vivo* situations different from the ones *in vitro*. In the past few years, PCI using $AlPcS_{2a}$ has exploited its utilisation in releasing gelonin or bleomycin *in vivo*, particularly using animal tumour models in nude mice [Berg et al., 2005a;Dietze et al., 2005;Norum et al., 2009b;Norum et al., 2009a;Selbo et al., 2001b].

Previous study has shown that AlS_2Pc PCI could induce the intracellular relocalisation of gelonin and therefore enhance its cytotoxic effect on normal liver [Woodhams et al., 2009]. The study looked at the importance of treatment parameters (the sensitiser dose and the administration timing for gelonin), demonstrating a qualitative and quantitative analysis to compare the PDT and PCI effect. The volume of necrosis in liver was increased by a factor of 2.5 when using a very low dose of gelonin intravenously 1hr before light delivery compared to the corresponding PDT treatment. The relocalisation of gelonin was also observed by staining gelonin before and after illumination using immuhistochemistry.

The present study adopted the same experimental design as the previous study but involved more aspects such as the influences of different anti-cancer agents and the target organs employed in the PCI treatment.

First of all, bleomycin and saporin were chosen to be used in the PCI strategy. Bleomycin has been used clinically in combination with a number of other drugs for

treating several types of cancers [Sikic et al., 1985]. Saporin and gelonin are both type I ribosome-inactivating proteins but saporin exhibits higher toxicity than gelonin [Stirpe and Battelli, 2006]. As a consequence, immunotoxins and bioconjugates of saporin have been developed for cancer treatments [Stirpe and Battelli, 2006]. The promising *in vitro* results in Chapter 4 also indicated the feasibility of using Amphinex PCI combining saporin and bleomycin *in vivo*.

Secondly, liver and colon are the organs of interests in this study. Previous studies at the National Medical Laser Centre have used normal liver to investigate HpD and AlSPc PDT effects [Bown et al., 1986;Woodhams et al., 2004;Woodhams et al., 2009] and the colon model for m-THPC, AlSPc, porfimer sodium, 5-ALA and WST09 PDT treatments and mechanism studies [Barr et al., 1990;Chatlani et al., 1991;Curnow et al., 1999;Messmann et al., 1995;Tsutsui et al., 2002;Woodhams et al., 2006]. It is suggested that the relative homogeneity of liver, its sufficiently large size, easy accessibility and the well-characterised photochemical responses make it a good model for investigating the biological effect of PDT treatments [Bown et al., 1986]. Colon, unlike liver, is a hollow and relatively pale organ. The colon wall is thin but anatomically more complicated than liver with layers of different tissues. The treatment responses from those substructures of the colon wall might be different. Hence, the differences of these two tissues in terms of their optical properties which affect the light delivery, the photosensitiser levels that liver displays a much higher uptake of Amphinex (results from previous chapter), as well as the amount of bleomycin or saporin would certainly provide valuable information for investigating PCI treatment *in vivo*.

The scheme of Amphinex PDT or PCI treatment using normal rat liver and colon models is shown in Figure 7.1.

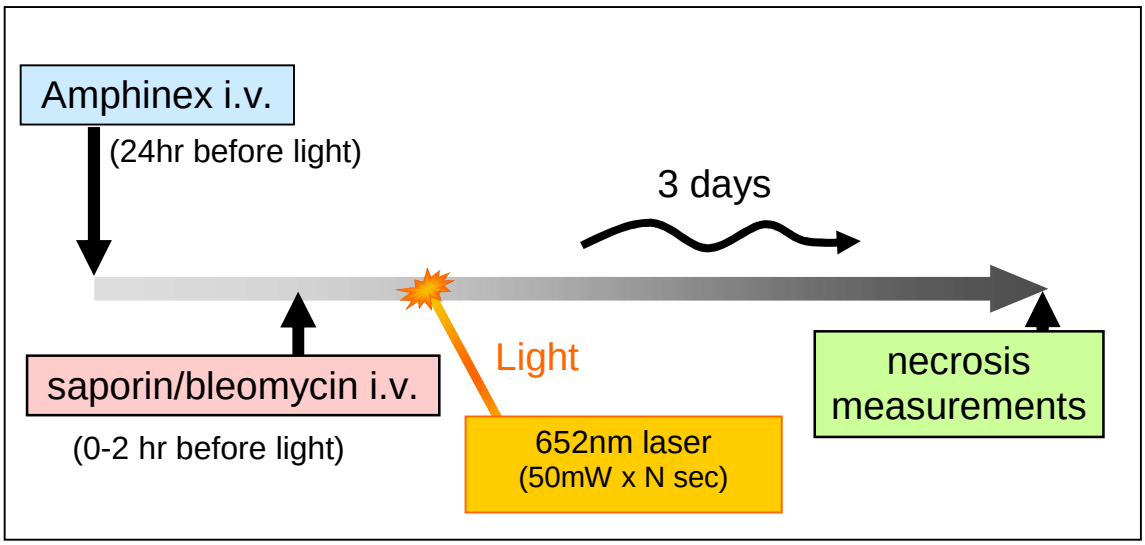

Figure 7.1 Scheme of Amphinex PDT and PCI treatments in combination with saporin and bleomycin on normal rat liver and colon models.

To optimize the treatment conditions for PCI, experiments began with looking at the PDT effect with the interplay between different amounts of Amphinex and a range for the excitation light dose. Thereafter, the PCI effect with the application of saporin and bleomycin were investigated. Experiments of PCI using $AlPcS_{2a}$ in combination with saporin were also carried out to compare with the previous study.

This chapter is a cross-comparison study to compare PDT alone and PCI of saporin and bleomycin in normal rat liver and colon using the photosensitiser Amphinex. Under the optimal PDT treatment conditions with fixed Amphinex dose and sensitisation time, studies would focus on how varying the dose of anti-cancer agents and drug application time would influence the PCI treatment efficacy on the liver and colon.

7.2 Materials and Methods

Chemicals

Amphinex in Cremophor (10 mg/ml) was kindly donated by PCI Biotech (Norway). $AlPcS_{2a}$ was purchased as a powder from Frontier Scientific (USA). Amphinex was diluted in phosphate-buffered saline (PBS) to a concentration of 0.25 mg/ml for intravenous (i.v.) injection. $AlPcS_{2a}$ was dissolved in 0.1M NaOH, and then diluted in PBS at pH 7.4 to a concentration of 5 mg/ml for i.v. injection. Saporin was purchased from Sigma-Aldrich (USA). Stock solution of saporin (1mg/ml) was prepared by dissolving the drug power in sterile water. Aliquotes of saporin stock solution were kept at -20ºC until use. The saporin solution for injection (0.5 mg/ml) was prepared by diluting the stock solution with PBS. Bleomycin (Kyowa Hakko, Mayne) was provided as a powder (15 IU per vial according to the U.S. standard equivalent to 15,000 IU according to the European Pharmacopeia. 5.1), and was dissolved in 0.9% NaCl which is ready for injection.

Animal models

All animal experiments were conducted under the authority of project and personal licences granted by the Home Office and the UKCCCR Guidelines. Normal, female Wistar rats (180-200g, Harlan, Oxon, UK) were used for all PDT and PCI treatment experiments. Inhaled Halothane or Isoflurane was used to maintain a state of general anaesthesia for drug administration. Analgesia was administered subcutaneously 30 minutes before surgery.

Light source

The light source used for Amphinex PDT and PCI treatments was a diode laser emitting at 652nm (Diomed Ltd, UK). An attenuator (FVA-UV fibreoptic variable attenuator, World Precision Instruments Ltd, UK) was used when the laser power needed to be 50mW. For $AlPcS_{2a}$ PDT and PCI treatments, the light source was a diode laser emitting at 670nm (Hamamatsu Photonics K.K., UK). Lasers were calibrated and the power at the tip of the fibre was measured using a wavelength-independent pyroelectric power meter (TPM-300, Gentec Inc, Canada) before each treatment.

Amphinex PDT effects on normal rat liver

For PDT experiments, Amphinex was administered via a tail vein at various drug doses (0.1, 0.25, 0.5, 1 and 2.5mg/kg) 24 hrs before light delivery. At laparotomy, a cleaved tip 400 μm laser fibre was placed gently touching the surface of the liver. The laser power was 100mW for providing the light doses of 15J and 25J or 50mW for 5J and 10J.

Animals were killed by cervical dislocation 3 days after surgery and the livers were removed immediately. At post mortem, the dimensions of the necrotic lesion were measured on the surface of the treated lobe using an electronic slicing caliper. The depth of necrosis was measured after cutting through its centre along the long axis. The necrotic surface area was then calculated using the formula $\pi LW/4$, where L =the maximum length of the lesion, and W = the width of the lesion, perpendicular to the line of L. The volume of necrosis was estimated using the formula $\pi LWD/6$ instead, where D is the depth measured from the centre on the surface. The tissues were then fixed in 4% formalin for 24 hrs. The samples were wax-embedded and sectioned at 4μm thickness onto poly-lysine coated slides after being placed in a tissue processing machine for further fixation. Sample slides were stained using the conventional Haematoxylin and Eosin (H&E) stains for histological examination.

H&E stained sections were examined using the Hamamatsu Nanozoomer Digital Pathology (NDP) scanner (Hamamatsu Photonics K.K., UK) where high-resolution digital images of the whole section were recorded. This microscopy imaging system uses a time delay integration (TDI) camera instead of the traditional CCD camera to scan images in lines, resulting in high-speed and high resolution (approx. 1 min 40s for 1.9 billions pixels at 20x magnification) scanning. The highest resolution obtainable is 0.23 μm per pixel. Thus one can view both the whole section and/or examine selected sites at high resolution within the section.

Treatments with drug (2.5 mg/kg) or light (10J and 25J) alone were also carried out as control studies. The rat given 2.5 mg/kg Amphinex was monitored up to 4 days until sacrificed. Animals receiving light treatment only without sensitisers were examined for possible necrotic lesions in the liver 3 days after a 25J light dose delivery (animal number = 1) or 10J light delivery (animal number = 2).

Figure 7.2 is a photograph of the light treatment on liver.

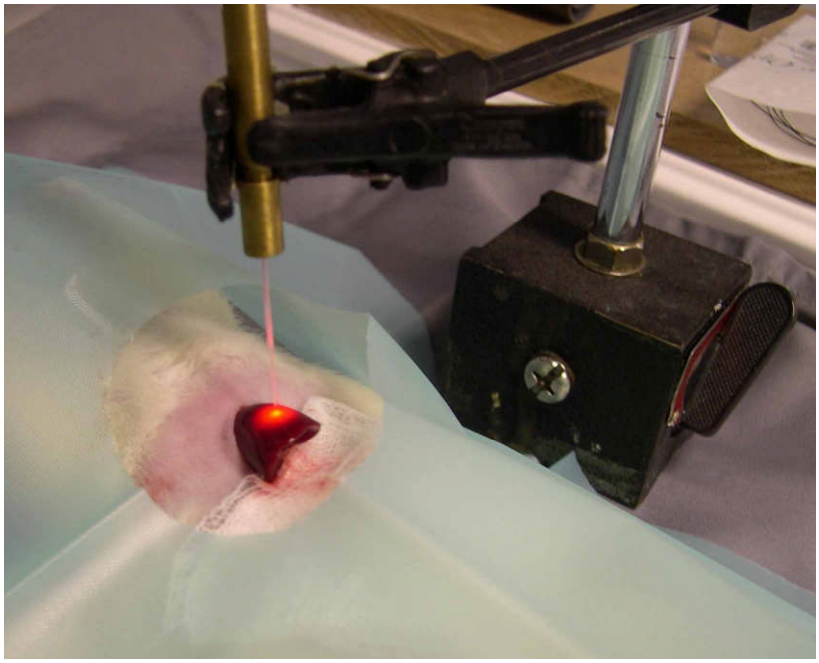

Figure 7.2 The light treatment on the rat liver.

Amphinex PCI in combination with saporin or bleomycin in rat liver and colon

All animals were sensitised with Amphinex through the tail vein injection at a dose of 0.25 mg/kg 24hrs prior to light irradiation. Two strategies were carried out to investigate the optimum effect achieved by Amphinex PCI in combination with saporin or bleomycin in liver or colon: varying the dose of toxins or varying the administration time of toxins.

For PCI of saporin, 250 μg/kg saporin was either administered intravenously 2 hrs, 1 hr or 30 min before light treatment or injected to rats at a range of doses of saporin (50, 100 or 250 μg/kg) 1hr prior to light delivery. For PCI of bleomycin, rats were given 30 IU/kg bleomycin 2 hrs, 1 hr or 30 min before light treatment or received bleomycin (15, 30 and 60 IU/kg) 1hr prior to light treatment.

For the treatments in colon, at laparotomy, the tip of the laser fibre was inserted at the antimesenteric side of the colon, 25-30mm from the pole of the caecum and placed just touching the surface of the mucosa on the opposite side to the entry point. The rest of the abdominal viscera were shielded from forward light scattering by covering pieces of opaque paper soaked in PBS. The light dose of 10J was used with the laser power of 50mW for 200 seconds. Animals were killed 3 days after treatment. The treated section of colon was removed and opened along the long axis, exposing the mucosal surface,

which was then gently flattened out for macroscopic inspection. The lesions were often yellow with irregular shapes. Macroscopic measurements were made by recording the maximum length (L) of the lesions. Sections were fixed in 4% formalin and then run through the same procedures as the liver samples for histological analysis.

The setting for the treatment in colon can be seen in Figure 7.3.

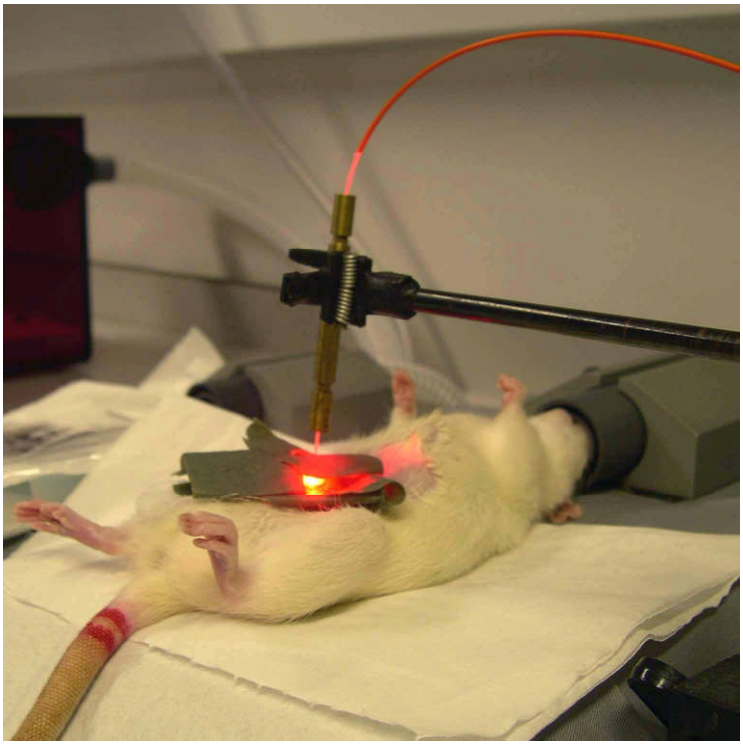

Figure 7.3 The light treatment on the rat colon.

Treatments in liver were carried out followed the same protocols described before. The light dose of 10J (50mW, 200sec) was chosen throughout all Amphinex PCI experiments. Control groups include animals receiving toxins alone, light only, sensitisers only, and sensitisers with toxins but no light as well as toxins with light treatment. Animals were killed 3 days after treatment and followed by macroscopic measurements, sample fixation and histological analysis whose details have been mentioned previously.

$AlPcS_{2a}$ PDT and PCI in combination with saporin on normal rat liver

Using AlS_2Pc as a PDT/PCI sensitiser has been investigated in our lab previously [Woodhams et al., 2009]. In this thesis study, commercially purchased pure $AlPcS_{2a}$ was used instead to compare the treatment efficacy with Amphinex. Animals were sensitised by tail vein injection of $AlPcS_{2a}$ (0.1 mg/kg) 24 hrs prior to light delivery. According to the results from previous studies, the optimum $AlPcS_{2a}$ PCI condition on

normal rat liver model was found when gelonin was given 1 hour prior to light treatment. Therefore, the dose of saporin at 0, 50 or 250 μg/kg was given 1 hour before in combination with various light doses (5J, 10J and 25J). Experiments in which animals received saporin 1 hour after 25J illumination were also carried out. All animals were killed 3 days after surgery. Macroscopic measurements, sample fixation and histological examination were conducted followed the same protocols as described before.

Statistical analysis

All data were presented as mean ± SD. Significant differences between PDT and PCI treatments were assessed by one tailed Student's t-test analysis. $P \leq 0.05$ was considered statistically significant.

7.3 Results

7.3.1 Amphinex PDT effects on rat liver

PDT effects on normal rat liver in combination with 1mg/kg AlS_2Pc and 25J light irradiation have been previously investigated in our laboratory [Woodhams et al., 2009]. The present study expanded the picture, examining the PDT effects induced by Amphinex using various light and drug doses. Sub-lethal doses induced appropriate size necrotic lesions in liver suitable for PCI applications.

Animals in control groups were all observed to be healthy throughout the study without weight loss. No necrosis was found in liver when rats were treated with Amphinex or light only (Figure 7.4). Amphinex, with the dose up to 2.5 mg/kg, produced no toxicity in rat liver in the absence of light.

In figure 7.4, the necrotic lesions induced after PDT treatments were all of ellipsoid shapes and the size was measured 3 days after surgery. The size of necrosis induced after Amphinex PDT treatment increased when higher drug or energy doses were applied. The maximum lesion size was found under the 2.5 mg/kg Amphinex and 25 J light treatment condition which was 43.5 mm^2 with full thickness necrosis. A drug dose dependent manner was well displayed in the group with 15J light treatment. The size of lesions was more than 4 times larger on average using 1 mg/kg Amphinex compared to 0.1 mg/kg Amphinex.

The volume of necrosis induced after Amphinex PDT is displayed in Figure 7.5. Some measurements in volume are underestimated as full thickness necrosis was caused due to high drug dose or light dose. Three groups with rats having full thickness necrosis (0.5 or 1 mg/kg Amphinex with 15J light irradiation and 2.5 mg/kg Amphinex with 25J light) were marked with stars in Figure 7.5.

The optimum PDT treatment conditions for further PCI application was chosen combining a dose of 0.25 mg/kg Amphinex and 10J light which caused a suitable size of necrosis (no full thickness necrosis involved) and reduced the possible thermal effects of light delivery. An example of the corresponding H&E stained histology results of Amphinex PDT in rat liver is shown in Figure 7.12A.

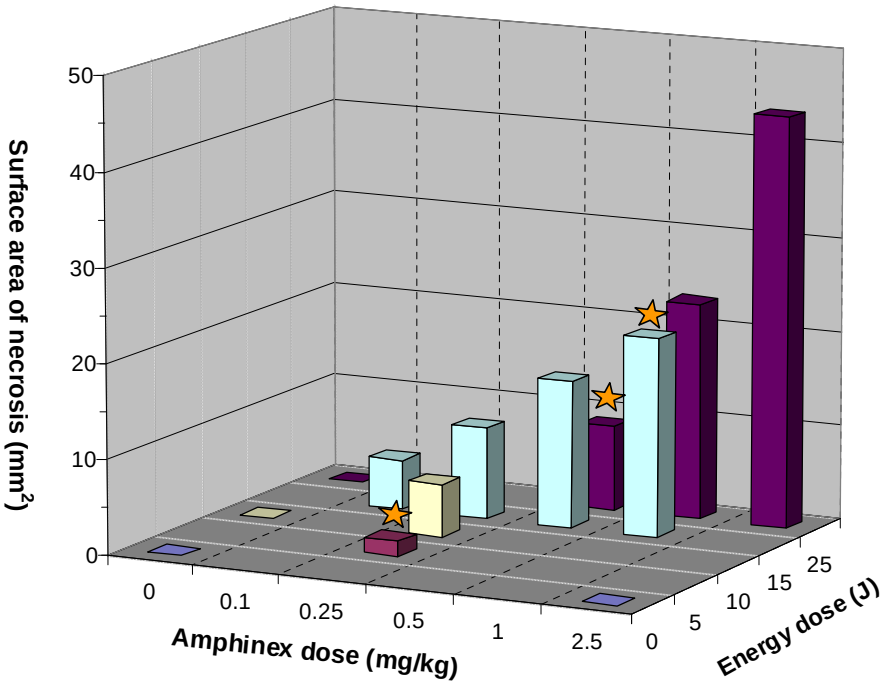

Figure 7.4 Mean surface area of necrosis induced by Amphinex PDT in normal rat liver. The necrotic lesions induced after PDT were measured 3 days after surgery. Stars mark the animal number of non-control PDT groups which is only one. At least 2 animals were investigated for other PDT treatment groups.

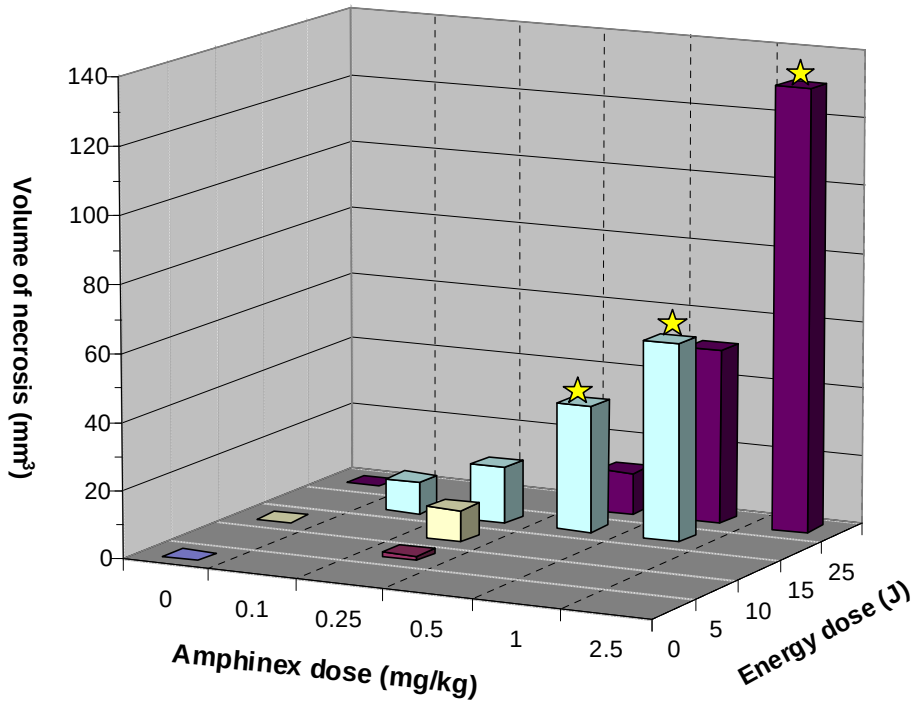

Figure 7.5 Mean volume of necrosis induced by Amphinex PDT in normal rat liver. Stars mark the groups with the involvement of full thickness necrosis in liver induced after light treatments.

7.3.2 Amphinex PCI in rat liver

Direct comparison studies of AlS_2Pc PDT alone and PCI in combination with a ribosome inactivating protein toxin, gelonin, using normal rat liver have been investigated in our lab previously [Woodhams et al., 2009]. This present study followed the same methods but using Amphinex as the sensitiser. The PCI effects combining saporin, another member of type I RIP, and bleomycin, a chemotherapeutic in clinic, was investigated in the same rat liver model.

In order to clarify the PCI effects applied to PDT, various saporin and bleomycin doses were used in the optimum PDT condition in this model (i.e. Amphinex: 0.25 mg/kg; light dose:10J; drug light interval: 24 hrs; saporin or bleomycin given 1hr prior to light treatment). The mean surface area of necrotic damage in liver was increased but not significantly when animals received 50-100 μg/kg saporin or 15-60 IU/kg bleomycin 1 hour before light delivery if compared to PDT alone (Figure 7.6). The mean surface area of necrosis increased significantly by a factor of 2.4 when a dose of 250 μg/kg saporin was injected to animals (t-test, $p<0.01$). The corresponding H&E stained histology results of the maximum liver damage induced after PCI treatment are shown in Figure 7.12.

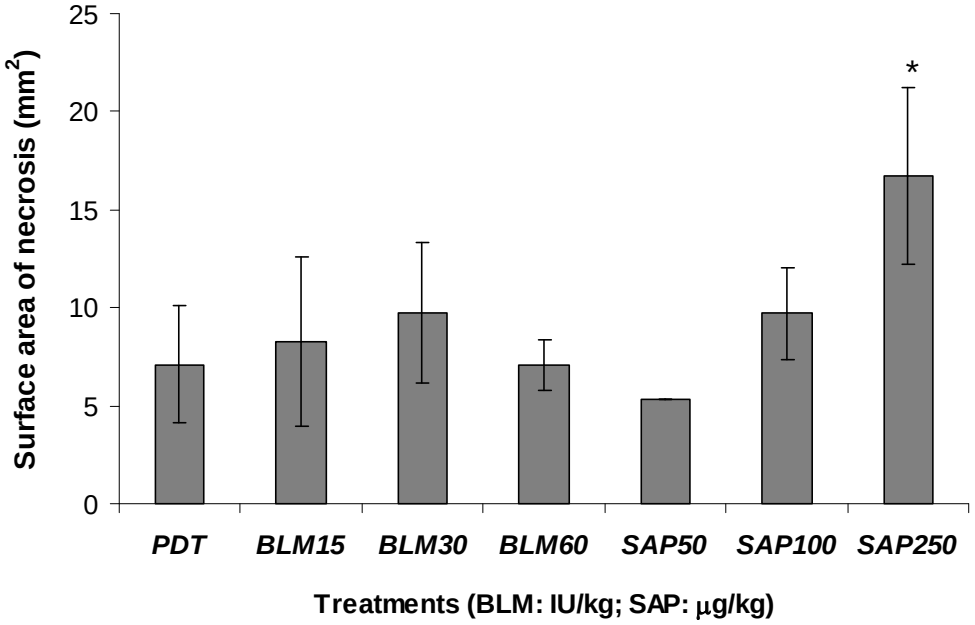

Figure 7.6 Mean surface area of necrotic lesions in liver at three days after light treatment in animals treated with 0.25 mg/kg Amphinex (i.v.) 24 hrs before light against various doses of saporin and bleomycin given 1 hour before light treatment. (*: $p<0.01$)

Figure 7.7 shows the mean surface area of necrosis induced 3 days after light treatment against different administration intervals of 250 μg/kg saporin or 30 IU/kg bleomycin prior to the light irradiation. The maximum enhancement was found when saporin was injected 1 hour before light delivery where the necrotic area increased by a factor of 2.4 compared to the PDT alone treatment ($p<0.01$). The mean surface area of necrosis was about doubled compared with the lesions in PDT treated animals when saporin was injected 30min prior to the light treatment ($p=0.02$). The maximum PCI damage combining with bleomycin was found when the drug was injected 15-30min before light so that the mean necrotic area increased significantly by a factor 1.8. The results of the animals treated with bleomycin just before light irradiation (T=0) showed an increase in the necrosis size on average but not significant with a wide variation. Examples of H&E stained histological analysis of liver sections after PCI treatments combining saporin and bleomycin are shown in Figure 7.12B and C.

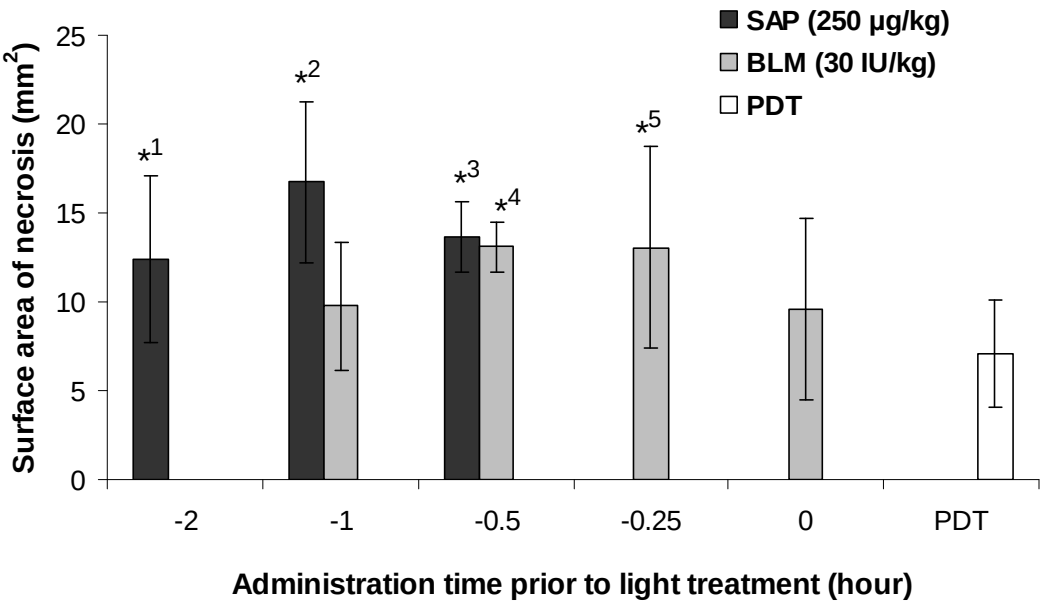

Figure 7.7 Mean surface area of necrotic lesions in liver at three days after light treatment in animals given 0.25 mg/kg Amphinex (i.v.) 24 hrs before light against the administration time of saporin (250 μg/kg) or bleomycin (30 IU/kg) prior to light treatment (hour). A minimum of 3 animals was involved in each experiment group. ($*^1$: $p<0.05$; $*^2$: $p<0.01$; $*^3$: $p=0.02$; $*^4$: $p<0.01$; $*^5$: $p=0.03$)

No macroscopic necrosis in liver was observed in any control animal. Rats which received saporin or bleomycin (either sensitised with Amphinex or treated with light) had about 15 g weight loss but were all in healthy condition.

7.3.3 Amphinex PCI in rat colon

PCI effects combining saporin or bleomycin on different organs were estimated using the rat colon model. The necrosis induced by PCI treatments in combination with saporin (250 μg/kg, i.v. 1 hour before light delivery) was increased but not significantly compared to the PDT treatments alone (Figure 7.8).

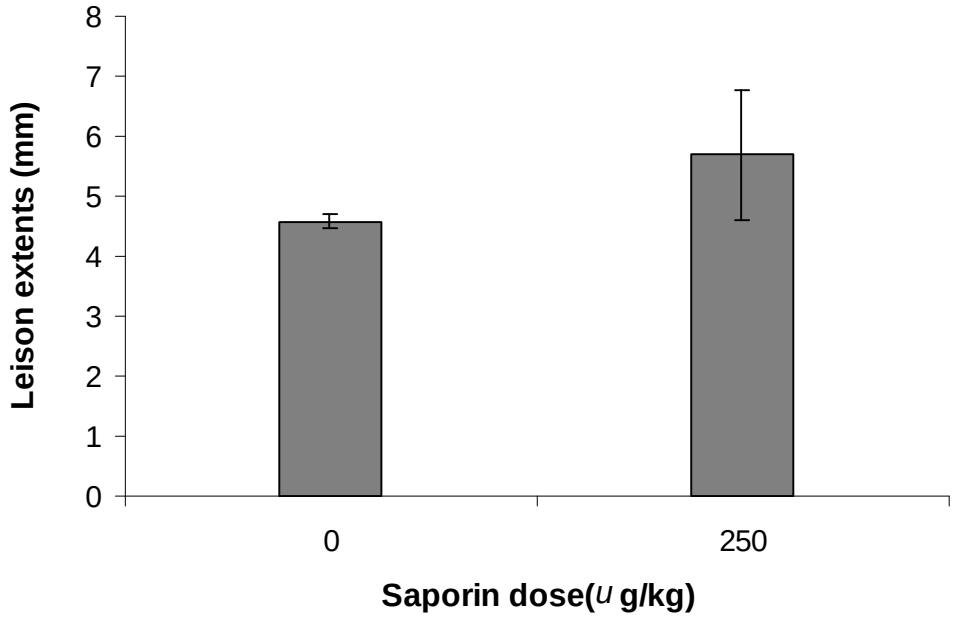

Figure 7.8 Extents of necrotic lesions in colon at three days after light treatment in animals given 0.25 mg/kg Amphinex (i.v.) 24 hrs before light against two doses of saporin given 1 hour before light treatment. Four animals were involved in each experiment group.

Following the same protocols, the effects of Amphinex PCI in combination with bleomycin (15 IU/kg) was also investigated using the rat colon model. As shown in Figure 7.9, PCI of bleomycin induced enhanced necrotic damage in colon significantly in all animals either receiving bleomycin before or after light treatments. The mean longest length of the necrosis was found when bleomycin was given 15 min before the light treatment. The diameter of the lesion was increased by more than a factor of 2 compared to PDT treatment alone ($p<0.01$). The second longest length of the necrotic lesions was observed when applying bleomycin to rats 1hr before light.

Giving double dose of bleomycin (30 IU/kg) 30 min before light induced larger necrotic damage to colon but with a wide variation. The minimum increase of necrosis using 15 IU/kg was observed when bleomycin was administered 30 minutes before light.

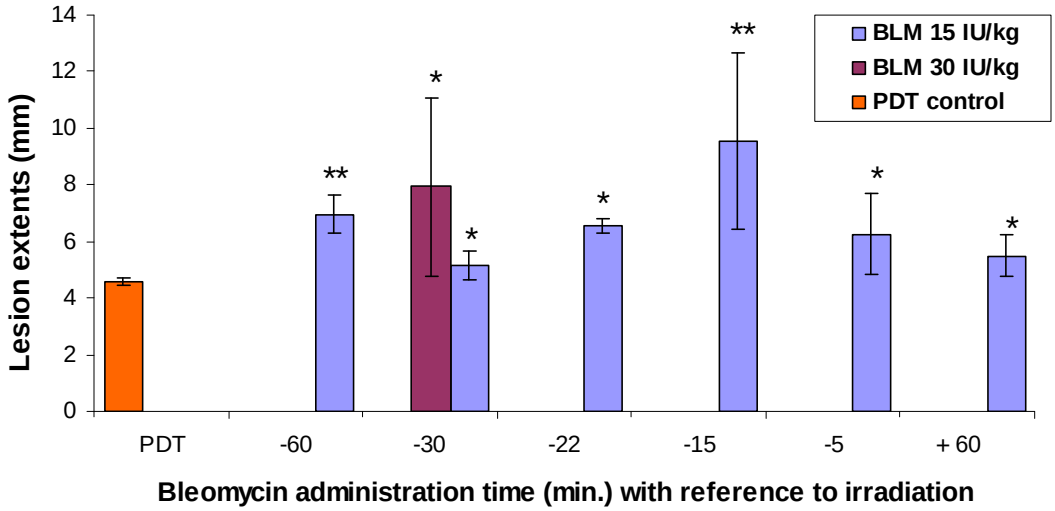

Figure 7.9 Mean surface area of necrotic lesions in colon at three days after light treatment in animals given 0.25mg/kg Amphinex (i.v.) 24 hrs before light against bleomycin administration time prior to light treatment (minutes). A minimum of 3 animals was involved in each experiment group. (*p=0.02~0.04; **p<0.01)

An example of the corresponding H&E stained histology results of Amphinex PDT in rat colon is shown in Figure 7.14.

7.3.4 $AlPcS_{2a}$ PCI in combination with saporin in rat liver

Similar experiments were carried out to investigate the $AlPcS_{2a}$ PCI effects combining different saporin doses and light doses on normal rat liver.

In the previous study, animals receiving 50 μg/kg gelonin prior to AlS_2Pc PDT (1 mg/kg, 24hrs drug light interval) had significantly increased necrotic lesions after 3 days compared to treatments in the absence of gelonin [Woodhams et al., 2009]. In the present studies, enhancement of PDT in combination with saporin (50 μg/kg and 250 μg/kg) did not appear after 10J and 25J light treatments (Figure 8.10). Increased mean surface area of necrotic lesions in liver was only observed from the animals treated with 5J light irradiation in combination with 250 μg/kg saporin. When 25J light was delivered 1 hour before saporin injection, the size of necrosis was similar to the light after saporin strategy. Two out of three and one out of four rats receiving 50 μg/kg and 250 μg/kg respectively 1hr before irradiation were observed full thickness necrosis in the livers after 25J light treatment.

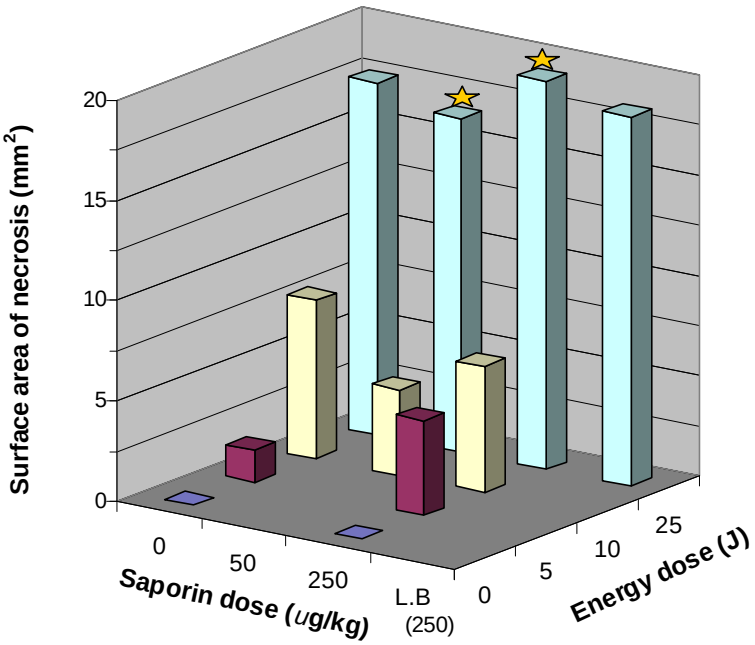

Figure 7.10 Mean surface area of necrosis induced by $AlPcS_{2a}$ PDT and PCI of saporin in rat liver. Stars mark the groups with the involvement of full thickness necrosis in liver induced after light treatments. L.B.: light before; 250 μg/kg saporin was given after light.

7.3.5 Macroscopic examination and histology

No macroscopic and histological changes could be detected in any control animals which received toxins or photosensitisers separately with no exposure to light. Sections from the animals receiving light treatments alone without any drug administration also showed normal tissue architecture.

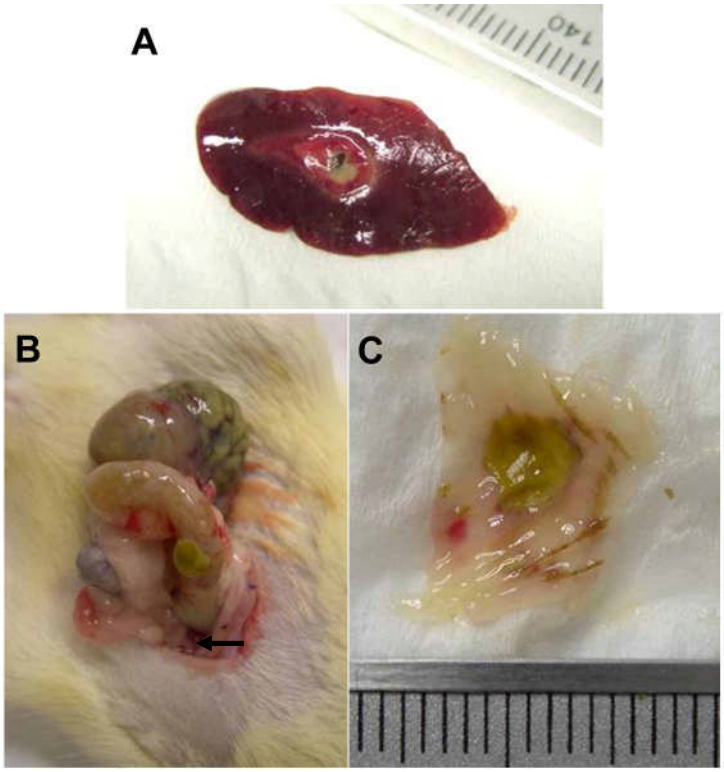

Figure 7.11 Photographs of examples of the macroscopic damage in normal rat liver (A) and colon (B and C) after PDT or PCI treatments.

The macroscopic damage induced after PDT and PCI treatments was observed to be similar despite the size differences in the necrotic lesions. Figure 7.11A is an example of the typical appearance of treated liver. The necrotic lesion was observed of oval shape and clearly distinguishable from the normal area. An example of the necrosis seen on colon was shown in Figure 7.11B and C. A sharply defined ulcer in colon was observed at post mortem (arrow, Figure 7.11B) and the necrotic lesion in yellow colour could be seen after the colon was opened up (Figure 7.11C). No obstruction or perforation was observed after either treatment but diarrhoea sometime could be seen in the harshest treatments in which higher drug and light doses were involved. Detailed histological studies are shown below.

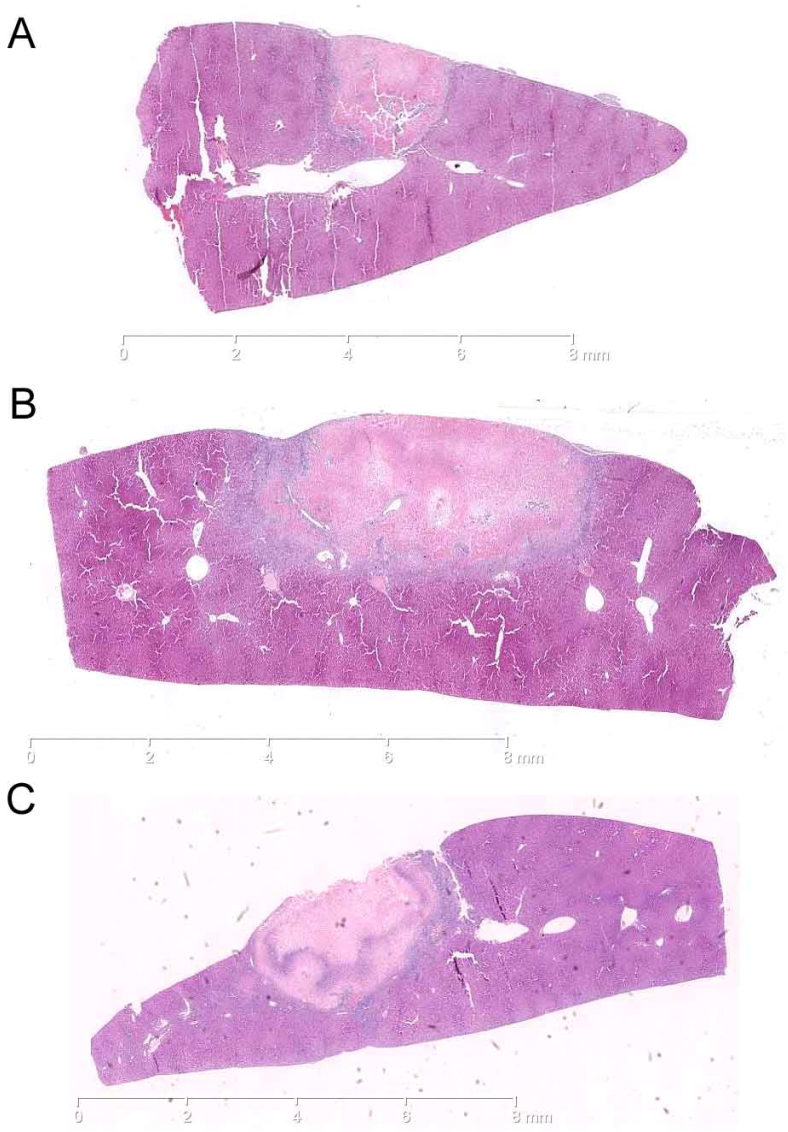

Figure 7.12 H&E stained histology sections of rat liver 3 days after Amphinex PDT (A) and PCI treatments in combination with 250 μg/kg saporin given 1 hour before light (B) or with 30 IU/kg bleomycin given 30 minutes before light (C).

Liver sections from animals receiving Amphinex PDT or PCI treatments in combination with saporin or bleomycin are shown in Figure 7.12. There was a well-defined zone of necrosis with inflammatory cells and early signs of healing with many fibroblasts in the region adjacent to untreated liver in each experimental group. The central area of the zone of necrosis induced by PCI treatments in combination with saporin and bleomycin are similar.

Histological results indicated the possible participation of the vasicular system in PDT or PCI treatments according to the surroundings of blood vessels by well-formed fibroblasts. Images with higher magnification are shown in Figure 7.13.

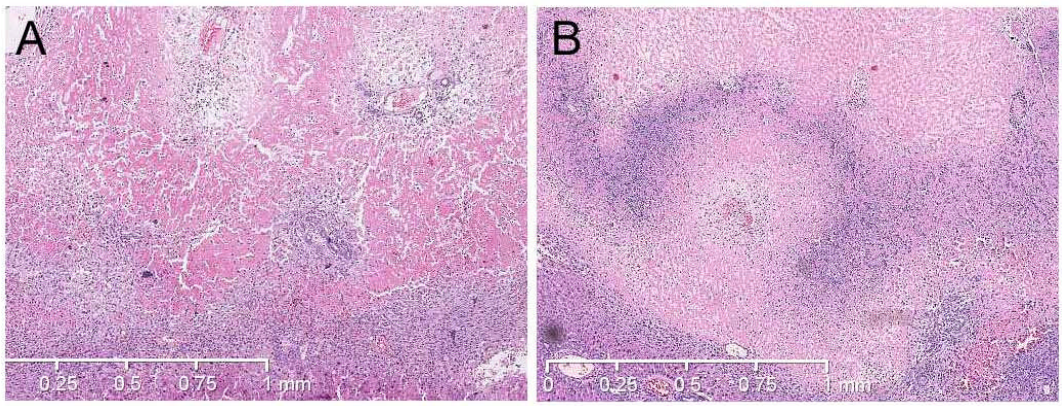

Figure 7.13 H&E stained histology sections of rat liver after PCI treatments at higher magnification. A: Amphinex PCI of 250 μg/kg saporin; B: Amphinex PCI of 30 IU/kg bleomycin.

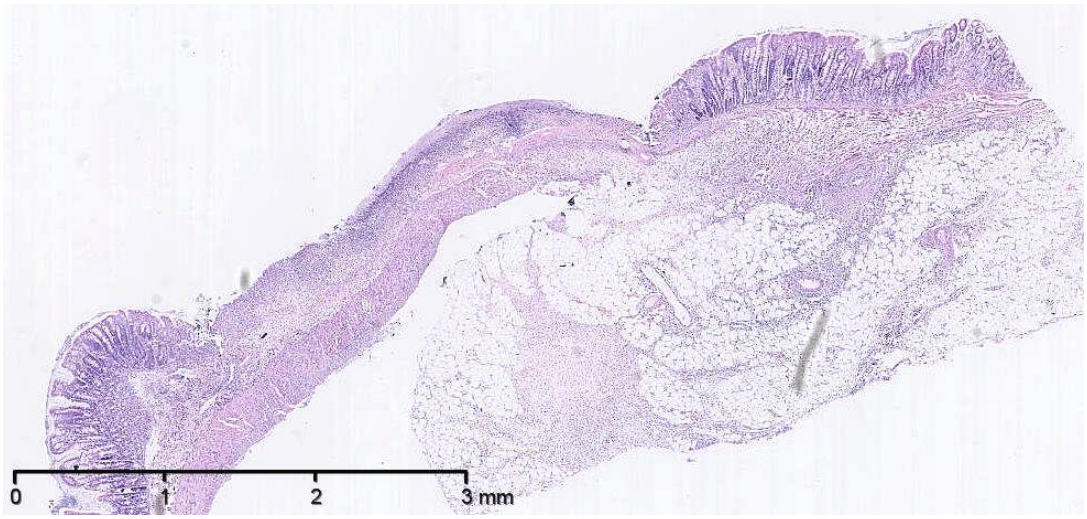

Figure 7.14 H&E stained histology sections of rat colon 3 days after Amphinex PDT treatments.

The histological changes induced by Amphinex PDT in normal rat colon are shown in Figure 7.14. A comparison of the colon wall in the light treated and untreated area with higher magnification are shown in Figure 7.15. The absence of the mucosal structure in the treated area indicated severe damage caused by the treatment. The submucosal layer was also affected and replaced by necrotic cells.

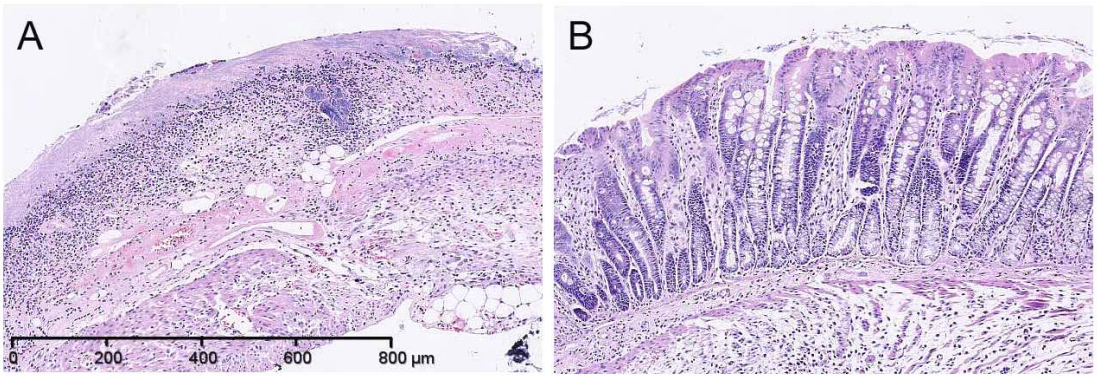

Figure 7.15 H&E stained histology sections of rat colon at higher magnification. A: treated area; B: untreated area. Both figures are in the same magnification.

7.4 Discussion

The present study has demonstrated the comparisons between PDT and PCI treatment using a new chlorin-based sensitiser, Amphinex, on the rat normal liver and colon.

Meso-tetra(3-hydroxyphenyl)chlorin (m-THPC) is a clinically approved photosensitiser in the European Union for treating head and neck cancers. Chlorin e6 (Ce6) is in the stage of completing its first clinical trial in Russia. In comparison with its chlorin-based analogues, Amphinex exhibits a similar quantum yield for singlet oxygen production and induces comparable lipid peroxidation in homogenous isotropic conditions [Mojzisova et al., 2009]. It is assumed that Amphinex is not only capable of inducing efficient photochemical reactions but also suitable for PCI treatment due to the amphiphilic property resulting in its membrane affinity.

The *in vivo* Amphinex PDT effect was investigated using the liver model in this chapter. Liver is a convenient organ which facilitates the quantitative measurement in three dimensions [Woodhams et al., 2009]. The size of the necrotic lesions induced after light treatment increased using higher drug or energy doses. In the previous study, the mean volume of necrosis induced by AlS_2Pc PDT (1mg/kg, 24 hours drug light interval and 25J light) was measured as 41 ± 8 mm^3 three days after light delivery. Similar results were obtained using Amphinex PDT in the present study. As shown in Figure 8.5, the mean volume of necrotic lesions was measured as 50mm^3 after Amphinex PDT using the same drug and light dose in spite of the half laser power (50mW) used for the current study. Because full thickness necrosis was found in some of the Amphinex PDT treatments using higher light or drug doses (Figure 7.5), a reduced combination of light and photosensitiser dose (0.25 mg/kg Amphinex and 10J light) was chosen for further PCI treatments which is different from the previous study.

PCI of saporin enhanced the PDT damage to liver. The maximum enhancement was found when saporin was given 1 hour before light delivery. This is consistent with the results of the previous study using gelonin [Woodhams et al., 2009]. The mean size of necrosis was increased by a factor of 2.4 in surface area and was 2.8 in volume (data not shown) in combination with saporin (250 μg/kg) compared to the PDT treatment. However, the enhancement was moderate in the treatments in colon.

Liver is known as one of the main organs for the uptake of type I RIP [Battelli et al., 1990]. It was found in mice that Type I RIPs were cleared rapidly with a blood half-life 4-8min and 0.4-23% of toxin was detected in liver 30min after i.v. injection [Barbieri et al., 1990]. The kinetics of gelonin in mice liver was reported with the highest concentration at 10 min, a decrease observed onwards and a retention between 1 and 2 hours after administration [Colaco et al., 2004]. It is not surprising that saporin markedly enhance the PDT effect in liver but not in colon. As type I RIPs are mainly concentrated in kidney, liver and spleen [Battelli, 2004], the saporin concentration in colon might be too low to induce an efficient PCI effect.

In contrast to saporin, PCI of bleomycin induced a significant increase of necrosis in both liver and colon (Figure 7.7 and 7.9). The maximum effects were found when bleomycin was given 30min before irradiation, a drug light interval shorter than saporin (Table 7.1). The enhancements in liver is by a factor of 1.8 in the surface area and is more than a factor of 2 in diameter in colon using half of the drug dose (15 IU/kg). Moreover, significant enhancements of the necrotic lesions in colon were observed in all PCI of bleomycin treatments regardless of the bleomycin administration timing. The results indicate a greater PCI effect using bleomycin in colon than in liver. The biodistribution of bleomycin may explain this as ^{67}Gallium-labelled bleomycin was found accumulated on average 1.2-1.9 times more in mice colon than in liver during the first 4 hours after i.v. injection [Tabeie et al., 2003].

Drug\ Treatment site	**liver**	**Colon**
Saporin	1h	No significant enhancement
Bleomycin	15-30min	15min

Table 7.1 Optimal administration time of saporin and bleomycin for Amphinex PCI treatments in rat liver and colon. Animals were injected with 0.25 mg/kg Amphinex 24 hrs before irradiation. Toxins were administered before light.

In Figure 7.6, no significant enhancement of necrosis was induced in liver when a range of doses of bleomycin was given 1 hour before illumination. Whereas, marked enhancement of necrosis can be seen when bleomycin was injected within 30 min (Figure 7.7). It is suggested that the administration time of bleomycin may play a more important role than the given dose in PCI treatment.

Although the results from the previous study show that AlS_2Pc PCI of gelonin is superior to PDT [Woodhams et al., 2009], the present study using pure $AlPcS_{2a}$ displayed a different picture. No significant enhancement in the necrosis size was observed in the liver treated with $AlPcS_{2a}$ PCI using saporin (50 and 250 μg/kg). The reason for the different results compared with the previous study is not fully understood. However, the direct comparison is not appropriate as AlS_2Pc is a mixture not a pure compound. Although the $AlPcS_{2a}$ dose used in this study was 10 times lower than the AlS_2Pc in the previous study, full thickness necrosis was measured in the PCI treatment using 25 J. This much more efficient therapeutic efficacy of the pure $AlPcS_{2a}$ PDT may therefore hinder the PCI effect in combination with saporin although the enhancement of PCI effect can not be seen using lower PDT dose. Multiple mechanisms may be involved in the $AlPcS_{2a}$ PDT and PCI treatments and require further investigation.

The toxicity of anti-cancer drugs is another thing that needs to be noted. Animals with PCI treatments were measured to have an average of 15g weight loss which was to be assumed a result from treatment. However, the same physiological changes were also observed in the control animals receiving only toxins (250 μg/kg saporin or 30 IU/kg bleomycin), suggesting the possibility of drug toxicity. The LD_{50} of saporin in mice is 4-8 mg/kg and is 358 IU/kg in the case of bleomycin (bleomycin sulphate) in rats by i.p. injection (from the safety data sheet of the manufacturers). The current study is a pioneering investigation using Amphinex PCI in combination with these two anti-cancer agents. The drug doses were chosen less than one tenth of the sub-lethal doses in order to obtain a rough idea of their therapeutic efficacy of this PCI strategy *in vivo*. Although animals behaved normally in terms of the activity, appearance and food and water uptake, the toxicity of drugs themselves should be taken into account regardless of the applied dose as unexpected side-effects may affect the treatment results as well as the animal welfare.

PDT is a treatment with the combination of photosensitisers and light. PCI is a modality based on PDT but with the additional application of other drugs. The study in this chapter focused on the influence of several parameters of PCI treatment and aimed to optimise the treatment conditions. PDT using Amphinex was shown to be favourable for PDT and PCI. The consistent results from both *in vitro* and *in vivo* experiments indicate the benefits of the Amphinex PCI approach which enhanced its PDT treatment and displayed synergistic effects in combination with cytotoxic drugs.

Further studies to investigate the PDT/PCI effects on a syngeneic rat fibrosarcoma tumour model will be shown in the next chapter. Mechanistic studies of *in vivo* Amphinex PDT and PCI in terms of the redistribution of Amphinex and saporin after illumination and the possible involvement of apoptosis after treatments will be addressed in Chapter 9.

Chapter 8: Amphinex PDT and PCI in a Transplanted Syngeneic Rat Fibrosarcoma Tumour Model

8.1 Introduction

The previous chapter has established that Amphinex PCI can enhance the biological effect of saporin and bleomycin using normal rat liver and colon models. However, as tumours often present altered biological and biochemical properties compared to normal tissues, the therapeutic effect of Amphinex PCI on tumours remains to be investigated. The detailed PCI applications *in vivo* for cancer treatment have been discussed in Chapter 2. In this chapter, the effects of Amphinex PDT and PCI would be examined using a syngeneic rat fibrosarcoma tumour model.

This tumour model is a fibrosarcoma cell line, MC28, which is syngeneic for the Hooded Lister rat. As a result, the advantages such as the same genetic background hold by the inbred animal and derived cell line and the occurrence of metastasis would make this model closer to the natural circumstances of human neoplastic diseases [Khanna and Hunter, 2005;Talmadge et al., 2007]. This tumour model has already been established in our lab to investigate the PDT effects of m-THPC and WST09 [Tsutsui et al., 2002;Woodhams et al., 2006].

In the present study, experimental protocols in terms of the drug dose, light dose and drug light interval were planned based on the experiences in the treatments on normal tissues from the previous chapter. All the drugs including Amphinex, saporin and bleomycin were systemically administered by intravenous (i.v.) injection. This is different from other *in vivo* PCI studies in which either direct injection of drugs to tumour (i.t.) or i.p. application was used mostly. Although, theoretically, i.t. injection of anti-cancer agents should lead to higher local drug concentration in the target tumour and lower systemic toxicity, the undesirable increased drug concentration in the surrounding normal tissues observed in some experimental and clinical studies should be taken into account [Brincker, 1993]. Moreover, the invasive nature of i.t. injection and the question of whether drug could distribute homogeneously within the target tumour after direct injection also needs to be addressed. In this regard, intravenous injection is still a preferable administration method, especially for new drug investigation. Intravenously injecting drugs to rats was performed in the previous chapters and would also be used in this section.

In the previous chapter, Amphinex PCI was shown to be able to enhance the therapeutic efficacy of saporin and bleomycin treating normal rat liver and colon while the treatment effects were observed under the influences of the administration timing of these two anti-cancer drugs. The maximum necrotic lesions in liver were achieved when saporin and bleomycin were given 1hr and 30min before light delivery respectively (Table 7.1). Therefore, the same administration timings of these two drugs were adopted for the experiments in this chapter.

The kinetics of Amphinex in normal Wistar rats has been studied in Chapter 6. The Amphinex level in liver displayed a rapid decrease after the peak uptake at 6 hrs after injection and a retention phase between 24hrs and 48 hrs with a much lower drug level (Figure 6.1). On the other hand, the drug level in colon mucosa reached the highest amount at 24hrs post i.v. (Figure 6.2). Although the kinetics results provide the information of the biodistribution of Amphinex in rats, the data for its tumour uptake is unavailable. Therefore, prior to PDT and PCI treatments, experiments to quantify the Amphinex level in tumour at the time of light delivery (24 hrs post injection) were carried out using chemical extraction and quantitative fluorescence microscopy. The photosensitiser levels in other normal tissues including liver, colon, skin and muscle at the same time point were also estimated and compared with the uptake in tumours. These experiments were to assess the biodistribution of Amphinex in tumour-bearing rats and the drug level in tumour in comparison with other organs at the time of illumination. The information of the cellular localisation of Amphinex in tumours could also be obtained from the fluorescence imaging results.

As mentioned before, PCI using $AlPcS_{2a}$ has demonstrated its potential for treating cancers significant tumour growth inhibition was reported in several pre-clinical studies. It was also hoped that PCI might have further clinical utilisation as an adjunct to surgery and radiotherapy [Norum et al., 2009c]. This chapter continued the previous research to investigate Amphinex PDT and PCI in combination with two potent anti-cancer drugs, saporin and bleomycin, on tumour eradication. This is also the first attempt to compare PDT and PCI by quantifying the extent of necrosis induced in tumours. Biodistribution of Amphinex at the time of light delivery were analysed by chemical extraction and quantitative fluorescence microscopy. The cellular localisation in tumours and other tissues was identified using fluorescence microscopy.

8.2 Materials and Methods

Chemicals

Amphinex in Cremophor (10 mg/ml) was kindly donated by PCI Biotech (Norway). Amphinex was diluted in phosphate-buffered saline (PBS) to a concentration of 0.25 mg/ml for intravenous (i.v.) injection. Saporin was purchased from Sigma-Aldrich (USA). Stock solution of saporin (1mg/ml) was prepared by dissolving the drug powder in sterile water. Aliquotes of saporin stock solution were kept at -20ºC until use. The saporin solution for injection (0.5 mg/ml) was prepared by diluting the stock solution with PBS. Bleomycin (Kyowa Hakko, Mayne) was provided as powder (15 IU per vial according to the U.S. standard equivalent to 15,000 IU according to the European Pharmacopeia. 5.1), and was then dissolved in 0.9% NaCl which is ready for injection. Solvable^{TM}, a solubilizer containing dodecyldimethylamine oxide, secondary alcohol ethoxylate and sodium hydroxide, was purchased from Perkin-Elmer (UK).

Animals and tumour models

Experiments were performed using a well-established subcutaneous transplanted syngeneic rat fibrosarcoma tumour model [Amirkhosravi and Francis, 1993;Tsutsui et al., 2002;Woodhams et al., 2006]. Female Hooded Lister rats (180-220g) were used through out. All animal experiments were conducted under the authority of project and personal licences granted by the Home Office and the UKCCCR Guidelines. Inhaled Halothane or Isoflurane was used to maintain a state of general anaesthesia for drug administration. For PDT and PCI experiments, animals were given analgesia subcutaneously 30 minutes before surgery.

MC28 cells, a methylcholanthrene-induced fibrosacoma cell line [Murphy et al., 1986], were cultured cultured in Dulbecco's Modified Eagle's medium containing 10% FCS (Invitrogen, UK), 2mM Glutamine (GIBCO BRL, UK) and 500µg/ml Gentamicin (GIBCO BRL, UK). All cells were incubated at 37 °C in a humidified atmosphere containing 5% CO_2. When exponential cell growth was reached, cells were washed twice with Ca^{++} and Mg^{++} free PBS and detached from the culture flask by incubating with 1x trypsin solution (Sigma, UK) at 37ºC for 30 second. Trypsinization process was neutralised by adding serum containing medium and cell solution was then centrifuged at 1500 rpm for 3min.Cells were re-suspended and re-centrifuged using Ca^{++} and Mg^{++}

free PBS. For the subcutaneous tumours, $2.5x10^6$ cells in 0.1ml PBS were inoculated subcutaneously into the lower flanks of each rat. Approximately after 10-12 days, tumours would reach about 10mm in diameter, which is a suitable size for PDT and PCI treatment. No evidence of spontaneous necrosis in tumours was observed from our previous experience when the tumour size is smaller than this.

In vivo localisation and quantification of Amphinex in rat tumours

Amphinex (2.5 mg/kg) was injected to rats (animal number = 3) intravenously via tail vein. After 24 hrs, animals were killed and tissues from tumour, liver, colon, muscle (thigh and under tumour) and skin (abdominal) were removed. Fresh surgical specimens were cut into suitable sizes. Half of the samples were directly frozen into liquid nitrogen and stored at -80 ºC for chemical extraction study. Half of the samples prepared for fluorescence microscopy were snapped into cooled isopentane for 10 sec, wiped out extra liquid with paper tissue, and placed into vials in a liquid nitrogen container. Frozen tissues were stored at -80 ºC until sectioning.

The protocol for fluorescence microscopy was almost the same as what has been stated in Chapter 6. The laser activation and detection system was changed to a 405 nm laser (3 mW) and the fluorescence was detected at 660 nm using a 35 nm bandpass filter. Sections were also stained with H&E. The procedure for chemical extraction was also described previously. The mean fluorescence intensity from tissue solution in Solvable was measured at 655nm and the corresponding concentrations of Amphinex in each sample could thereby be calculated. Emission spectra of Amphinex in different tissue Solvable solutions measured with the excitation wavelength at 420 nm and with a cut-off filter at 515nm using a LS50B Perkin-Elmer Spectrofluorimeter (Perkin-Elmer, UK).

Light source

The light source used for Amphinex PDT and PCI treatments was a diode laser emitting at 652 nm (Diomed Ltd, UK). An attenuator (FVA-UV fibreoptic variable attenuator, World Precision Instruments Ltd, UK) was used to reduce the laser power to 50mW. Lasers were calibrated and the power at the tip of the fibre was measured using a wavelength-independent pyroelectric power meter (TPM-300, Gentec Inc, Canada) before each treatment.

PDT and PCI treatments on tumours

For PDT experiments, 0.25 mg/kg Amphinex was administered via tail vein 24 hrs before light delivery. The area of subcutaneous tumour was shaved and exposed by a small incision in the overlying skin. The capsule of the tumour was pierced with a 21G needle and a cleaved tip 400 μm laser fibre was placed by inserting perpendicularly just into the top of the tumour. The laser power was 50 mW for providing the light doses of 10J. Photographs of the light treatment on tumours are shown in Figure 8.1.

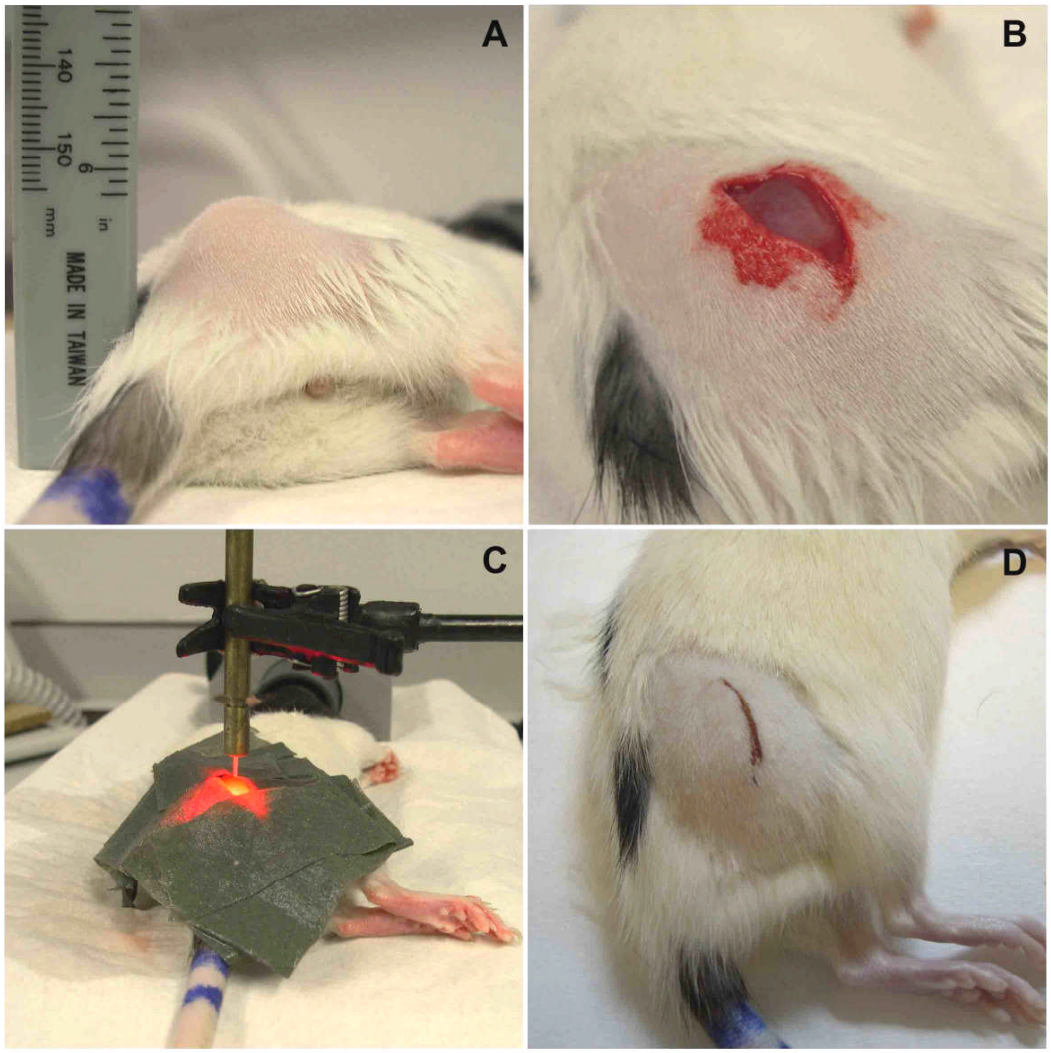

Figure 8.1 Photographs of the procedures of PDT and PCI treatments on the rat tumour. A: The subcutaneous transplanted tumour model growing on the lower flank 10-12 days after tumour cell injection. B: Skin incision and tumour exposure. C: Light delivery. D: Tumour at 24hr after light treatment.

For PCI treatment, animals were also sensitised with 0.25 mg/kg Amphinex via tail vein for 24 hrs before illumination. Saporin (250 μg/kg) and bleomycin (30 IU/kg) was injected to animals 1hr and 30min before light respectively.

Animals from each treatment group were killed by cervical dislocation at 24 hrs (six rats of each group) after surgery. The tumours were removed and fixed immediately in 4% formalin for 24 hrs. The tumours were sliced at 2mm intervals in the plane containing the line of fibre. Samples were wax-embedded and sectioned at 4 μm thickness onto poly-lysine coated slides after being placed in a tissue processing machine for further fixation. Sample slides were stained with H&E for histological examination.

The detail of PDT and PCI treatment schedule is shown below in Figure 8.2.

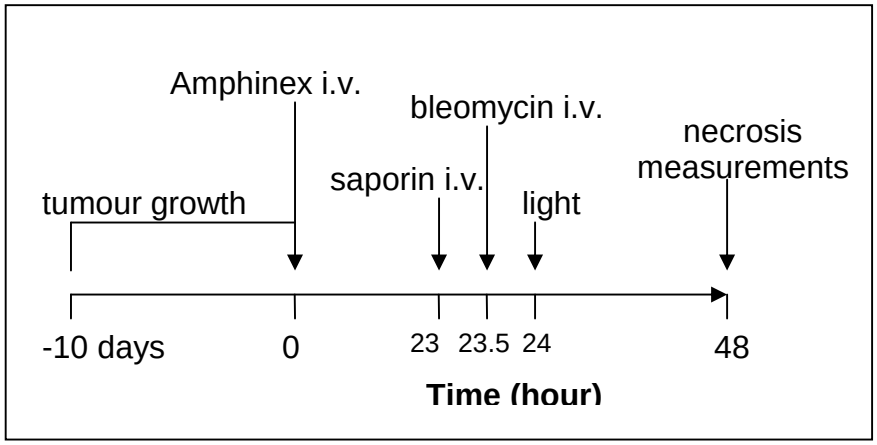

Figure 8.2 The scheme of PDT and PCI treatments on rat tumours.

H&E stained sections were examined using the Hamamatsu Nanozoomer Digital Pathology (NDP) scanner (Hamamatsu Photonics Ltd, UK) where digital images of the whole section were recorded. The PDT or PCI treatment response was examined by pathologically measuring the mean maximum area of necrosis (the plane extended from the line of fibre and perpendicular to the tumour surface) using the NDP server software.

Statistical analysis

All data were presented as mean ± SD. Significant differences between PDT and PCI treatments were assessed by one tailed Student's t-test analysis. $P \leq 0.05$ was considered statistically significant.

8.3 Results

8.3.1 Quantification and *in vivo* localisation of Amphinex in tumour-bearing rats

The biodistribution of Amphinex in tumour-bearing rats at 24hrs after i.v. injection was analysed by chemical extraction (Figure 8.3) and quantitative fluorescence microscopy (Figure 8.5). As shown in Figure 8.3, Amphinex displayed the highest concentration in liver and then tumour, colon, and skin at the time of light delivery. The concentration in muscle was the lowest and either from the thigh or the muscle under tumour was similar. The drug concentrations in the liver and colon of Hooded Lister rats 24hr after injection are consistent with the result of Wistar rats which is shown in Chapter 6 (Figure 6.5).

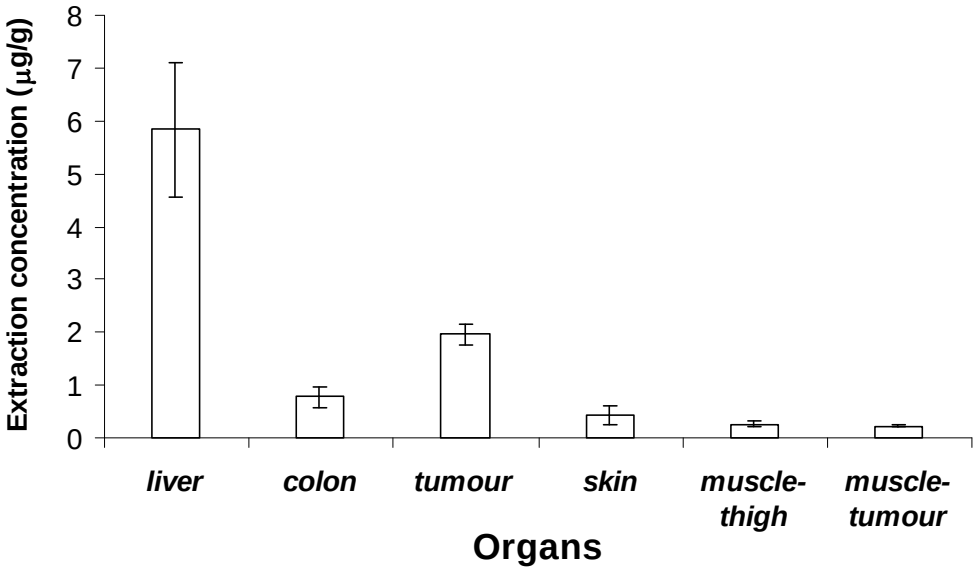

Figure 8.3 The concentration of Amphinex extracted from liver, colon, tumour, skin and muscle (thigh and under tumour) in Hooded Lister rats bearing tumours 24hrs after i.v. injection of 2.5 mg/kg Amphinex. Bars (SD) are based on three individual animals.

The fluorescence emission spectra of Amphinex in Solvable solution containing different tissues were shown in Figure 8.4. No shift was observed in different tissue solutions and all spectra display typical emission spectrum of Amphinex with the peak emission at 655 nm.

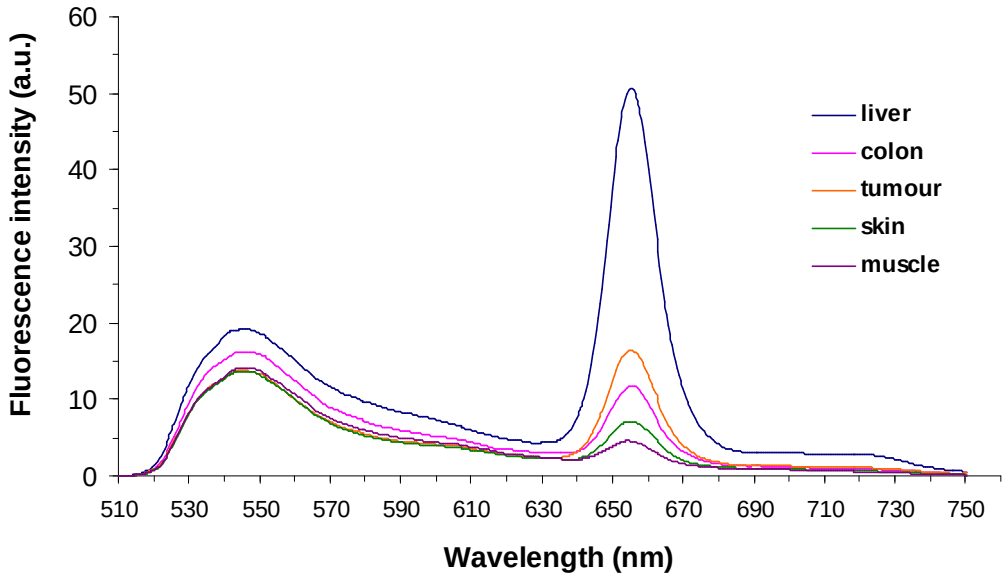

Figure 8.4 Representative fluorescence emission spectra (excitation wavelength 420nm) of Amphinex in different tissue solvable solutions. A cut-off filter at 515nm was used to remove the scatter light of shorter wavelength.

Half of the samples, originated from the same animals were used for fluorescence microscopic analysis. Similar results were obtained compared to chemical extraction where liver exhibited the highest Amphinex level among all tissues and tumour displayed higher drug uptake than colon mucosa (Figure 8.5). The fluorescence signal in the colon mucosa was measured significantly higher than the underlying muscle ($p<0.01$) by more than a factor of 2. The drug level in the muscle under tumour was estimated similar to the muscle in the colon wall but was slightly higher than in the muscle from thigh.

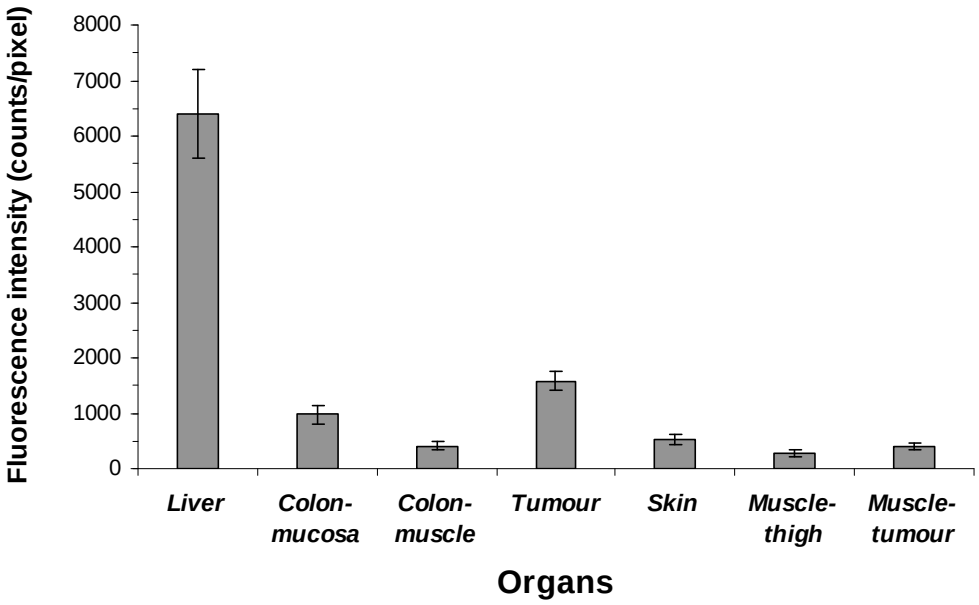

Figure 8.5 Fluorescence photometry of Amphinex in liver, colon, tumour, skin and muscle (thigh and under tumour) of Hooded Lister rats bearing tumours 24hrs after i.v. injection of 2.5 mg/kg Amphinex. Bars (SD) are based on three individual animals.

The comparison of the biodistribution of Amphinex examined between two different methods is showed in Figure 8.6. The value presents the normalised drug level to tumour. The drug uptake in colon by fluorescence microscopy is the average of the fluorescence intensity from colon mucosa and muscle. In general, the tissue-to-tumour ratios were measured in a good correlation between these two methods. The drug level measured in tumour was approximately 3-4 times lower than in liver and 2 times higher than in colon by two methods.

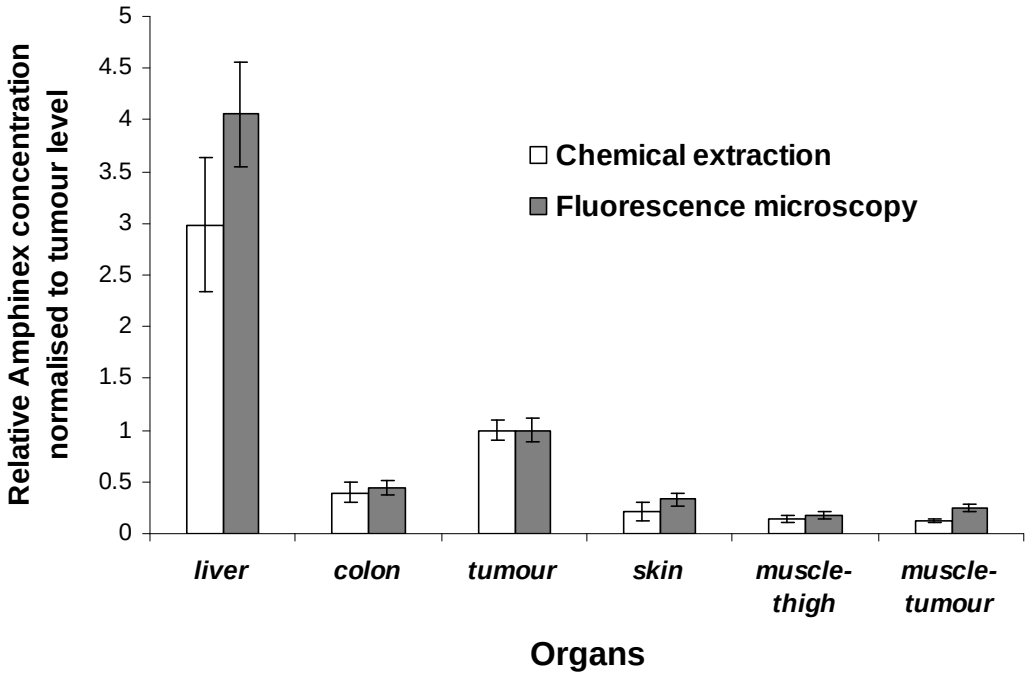

Figure 8.6 Comparison of the relative Amphinex concentration in different tissues determined by chemical extraction and fluorescence microscopy. Hooded Lister rats were sensitised with 2.5 mg/kg Amphinex for 24 hrs after i.v. injection. Bars (SD) are based on three individual animals.

The spatial distribution of Amphinex in tumour was analyzed by imaging the fluorescence signals of the frozen sections. A representative set of fluorescence images of tumour sections can be seen in Figure 8.7. Amphinex was homogeneously distributed in tumour 24 hrs after i.v. injection.

The fluorescence images of Amphinex in tumour with higher magnification are shown in Figure 8.8. Amphinex was accumulated inside tumour cells but not localised in the nuclei which are the shadow areas in the images (white arrows).

The endothelial localisation of Amphinex can be seen in Figure 8.9. The blood vessel in tumour is shown in the rectangles and the one in muscle is pointed out by the white arrows. The rectangle area is magnified in Figure 8.9a and b. These imaging results indicate that Amphinex accumulated in the endothelium at 24 hrs after i.v. administration. As shown in Figure 8.9C and D, Amphinex was found accumulated in the extracellular matrix of muscle tissues rather than the muscular cells.

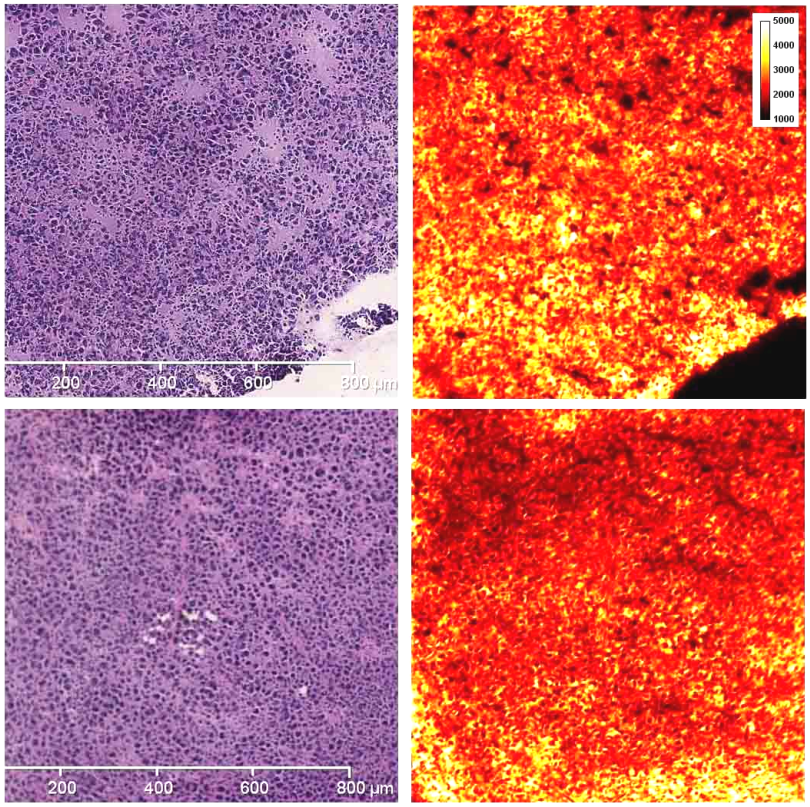

Figure 8.7 Fluorescence (right) and corresponding H&E stained (left) micrographs of frozen sections of fibrosarcoma tumour in Hooded Lister sampled 24h after i.v. injection of 2.5mg/kg Amphinex. The inset colour scale bar refers to the relative fluorescence intensity applied to all fluorescence images.

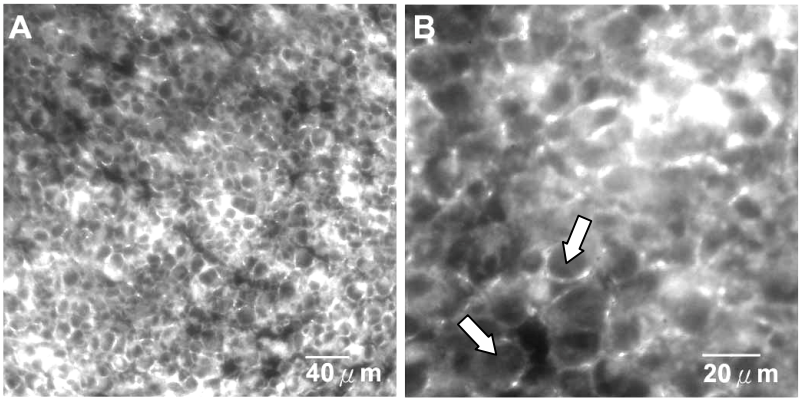

Figure 8.8 Fluorescence micrographs of the intracellular distribution of Amphinex in tumour with higher magnifications. Images were taken from frozen sections of the tumour tissue sampled 24h after i.v. injection of 2.5mg/kg Amphinex. The arrows indicate the cell nuclei.

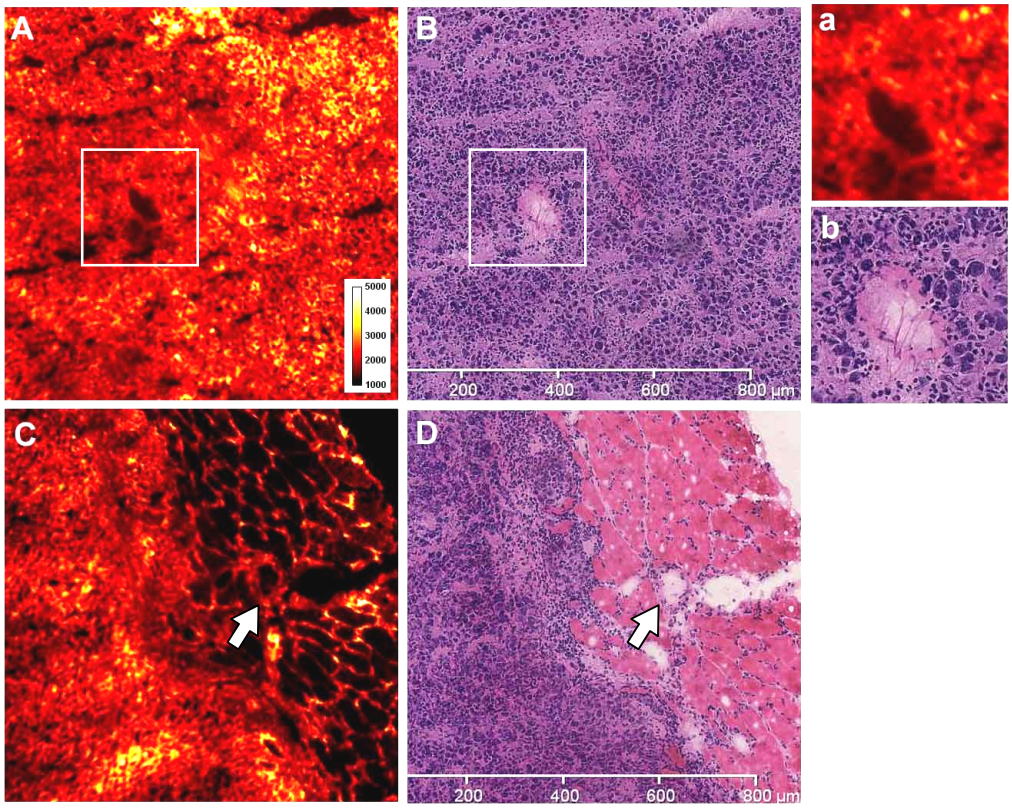

Figure 8.9 Distribution of Amphinex in tumour, muscle and vascular endothelium. Amphinex fluorescence micrographs (A, C and a) were from frozen sections of fibrosarcoma tumour sampled 24h after i.v. injection of 2.5mg/kg Amphinex. The corresponding H&E staining of the same sections are shown in B, D and b. The blood vessel in tumour is pointed out in the inset rectangle in (A) whose higher magnification image is in (a). The white arrow indicates the blood vessel in muscle.

Figure 8.10 illustrates the Amphinex localisation in rat liver 24hr after injection. Amphinex is evenly localised in liver cells with much higher fluorescence intensity compared to other tissues. The drug uptake in the endothelial cells (pointed by white arrows) of the blood vessel is lower than in the liver cells.

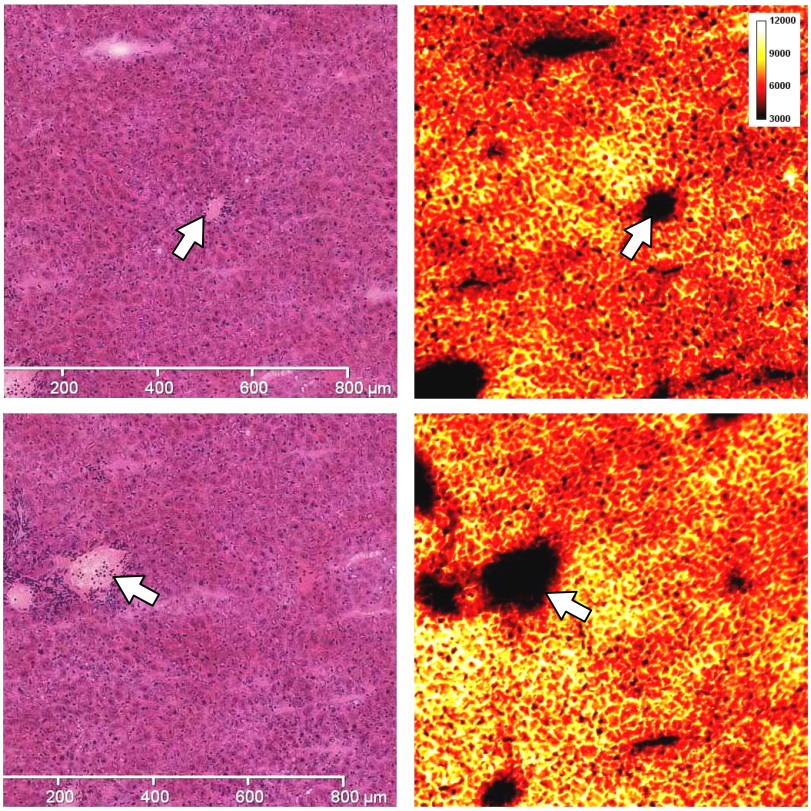

Figure 8.10 Fluorescence (right) and corresponding H&E stained (left) micrographs of frozen sections of liver in Hooded Lister sampled 24h after i.v. injection of 2.5mg/kg Amphinex. The inset colour scale bar refers to the relative fluorescence intensity applied to both fluorescence images. Arrows point out the identical blood vessels in the paired images.

According to the imaging results in Chapter 6, Amphinex is spread throughout colon mucosa 24hr after drug administration in Wistar rats (Figure 6.4). The distribution of Amphinex in colon in this tumour-bearing rat also shows the same pattern at this time point (Figure 8.11). A great drug uptake can be seen in the blood vessel in the submucosa (arrows). The distinct difference in the drug level between the colon muscle and mucosa was found.

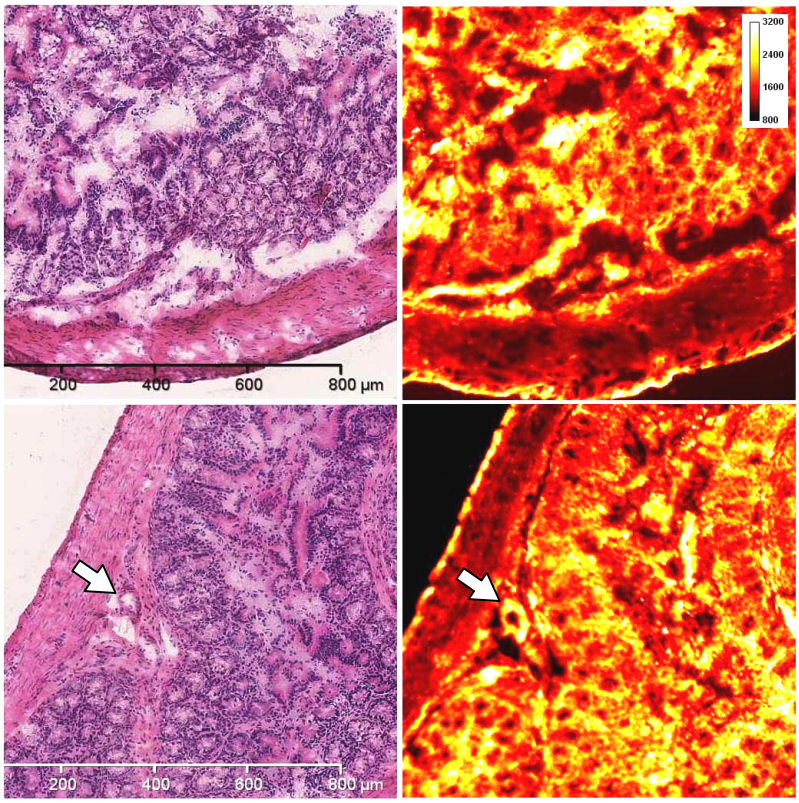

Figure 8.11 Fluorescence (right) and corresponding H&E stained (left) micrographs of frozen sections of colon in Hooded Lister sampled 24h after i.v. injection of 2.5mg/kg Amphinex. The inset colour scale bar refers to the relative fluorescence intensity applied to both fluorescence images. The arrows indicate a large blood vessel.

8.3.2 Amphinex PDT and PCI effects on a transplanted rat fibrosarcoma tumour model

Animals were sensitised with 0.25 mg/kg Amphinex for 24hrs before light delivery. For PCI treatment, the dose and administration timing of saporin and bleomycin was chosen based on the results of the treatments on liver, i.e 250 μg/kg saporin and 30 IU/kg bleomycin given 1hr and 30min prior to illumination respectively. The responses of treatments were evaluated by measuring the necrotic lesions at 24hrs after light treatment.

Tumour damage was found after Amphinex PDT and PCI treatments. As shown in Figure 8.12, the mean maximum necrotic area extended from the line of fibre induced after PDT treatments is about 7.6 mm^2. PCI in combination with either saporin or bleomycin significantly increased the necrotic area by a factor of 2 compared to PDT alone.

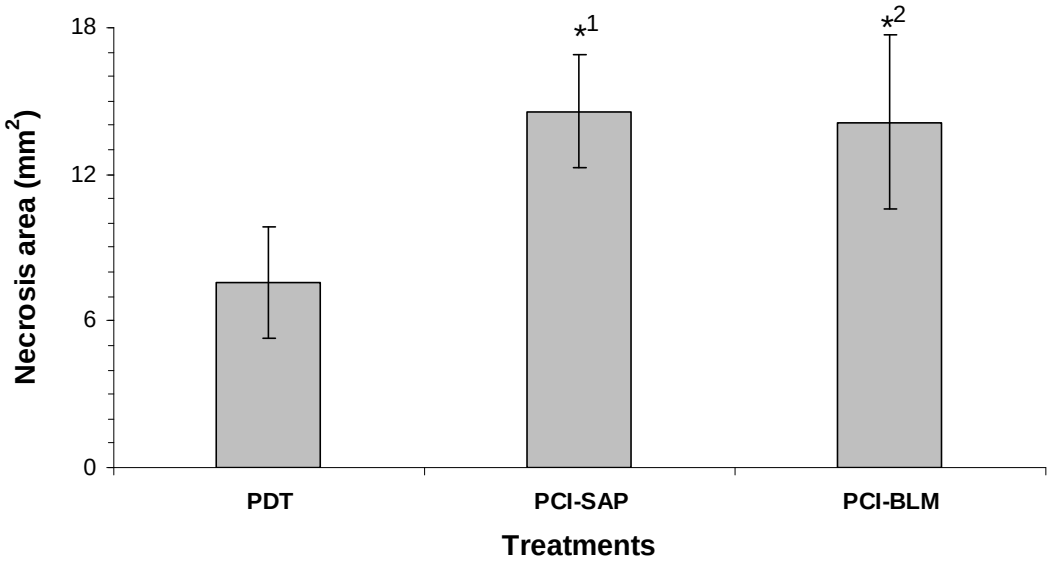

Figure 8.12 Mean maximum area of necrosis induced 24hrs after PDT/PCI treatments. There were six animals for each group. Saporin (250 μg/kg) and bleomycin (30 IU/kg) were given 1hr and 30min prior to illumination respectively. (*1: $p<0.001$; *2: $p=0.002$)

All animals were in healthy conditions after light treatments without any weight loss.

8.3.3 Macroscopic examination and histology

Figure 8.13A demonstrates the tumour growing on the lower flank of rats. Unlike the PDT damage on liver and colon, it is not easy to differentiate between the necrotic tumour and viable tumour. Tumour tissues, together with the attached muscles, were removed (Figure 8.13B) and fixed in 4% formalin for 24hrs (Figure 8.13C). The fixation time was kept constant to 24hr to minimise the variation of shrinkage between samples. The section cut through the plane extended from the line of fibre is displayed in Figure 8.13D). It is still difficult to recognise the difference between damaged lesions and viable tumours in this stage.

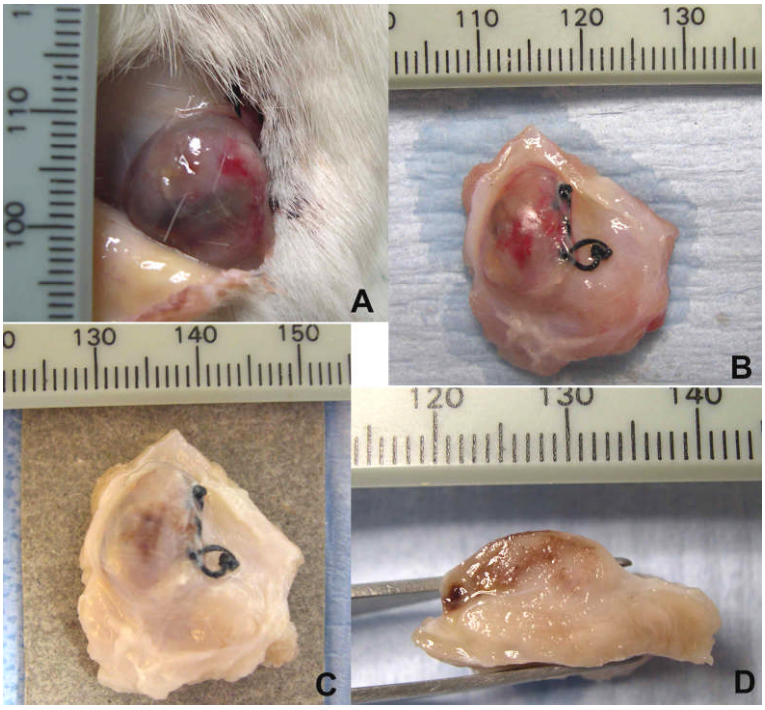

Figure 8.13 Photographs of representative MC28 subcutaneous tumours treated with 0.25μg/kg Amphinex PDT with a drug light interval of 24hrs. A: A tumour on the lower flank 24hr after PDT treatment. B: A freshly removed tumour. C: A tumour after the 24hr-fixation in 4% formalin. D: A 2mm thick section cut through the plane extend from the line of fibre and perpendicular to the tumour surface.

Histological examination was carried out on the H&E stained paraffin tumour sections. The non-treated MC28 fibrosarcoma was presented a monotonous hypercellular look after H&E stain (Figure 8.14A). Cells are closely packed with a high degree of nuclear pleomorphism and variation in cell shape and size. These are typical characteristics of poorly differentiated tumours. There is usually a fibrous capsule layer surrounding the tumour (Figure 8.14B, arrow). However, sometimes tumours could be highly malignant when tumour cells have infiltrated muscle tissues without the tumour capsule surrounded in the transitional zone on the border between tumour and muscle tissue (Figure 8.14C).

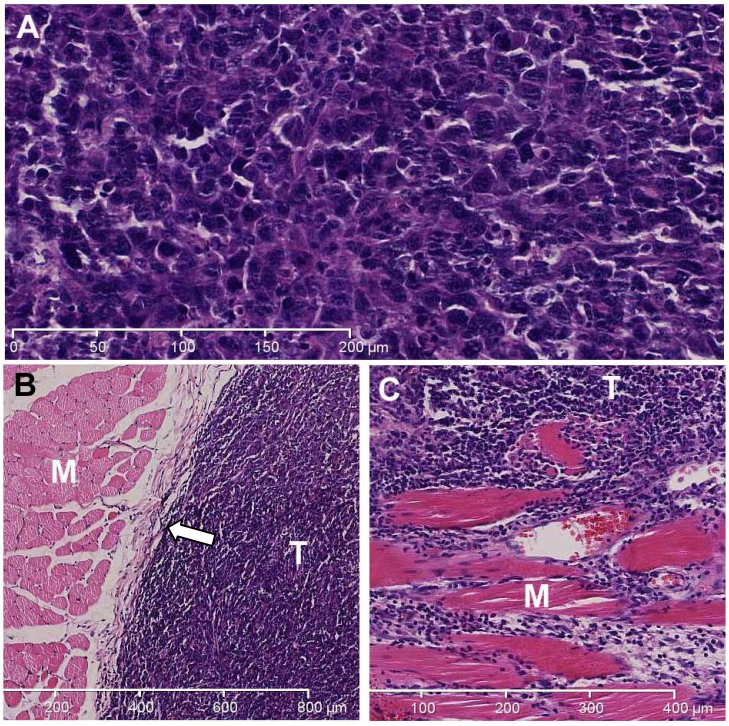

Figure 8.14 The MC28 fibrosarcoma tumour model. A: Tumour cells. B: The transitional zone between tumour (T) and muscle (M) without tumour infiltration. The fibrous tumour capsule was surrounding the tumour (arrow pointed). C: The transitional zone between tumour (T) and muscle (M) with tumour infiltration.

24hrs after PDT treatment, necrosis was observed from the top to the centre of tumour and viable tumour cells were found in the tumour periphery (Figure 8.15A). As shown in Figure 8.15B, the zone of necrosis is irregular. The areas in the green and yellow rectangles are highlighted in C and D. Figure 8.15C displays the region of the green rectangle at higher magnification. This is the transition zone between necrotic and viable tumour area. Half of the cells were damaged and fragmented nucleus was formed in some cells. Some dilated blood vessels could be found in this region. Figure 8.15D is a highlight of the yellow rectangle. Few viable tumour cells can be seen in the central necrotic area where necrotic cells with absence of nuclei were dominating. Moreover, the appearance of red blood cells scattered in this area indicated the blood vessels have become leaky due to the damage from treatments.

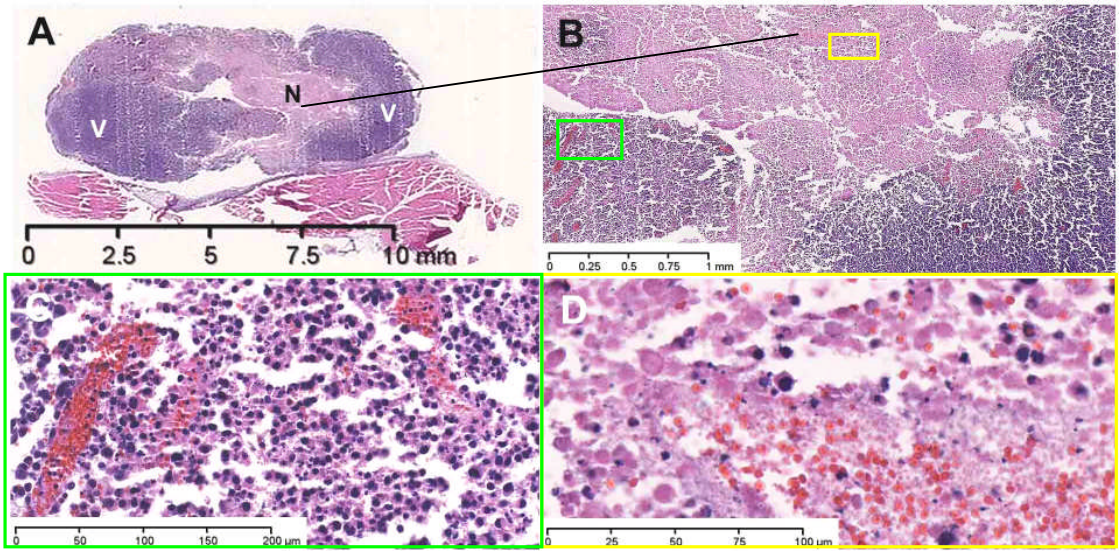

Figure 8.15 H&E stained histology section of transplanted rat sarcoma tumour one day after Amphinex PDT treatment. A: The whole tumour section. N: necrosis; V: viable tumour cells. B: The transition zone between necrosis and viable tumour area. The areas in the green and yellow rectangles are magnified in C and D. C: The region adjacent to necrotic area. D: The region in the necrosis centre.

Examples of the histological sections of tumours after PCI treatments combining saporin or bleomycin are shown in Figure 8.16 and 8.17. The areas of necrosis were found to be notably larger than the ones induced by PDT. The depths of necrosis between PDT and PCI treatments are similar since all treatments induced considerable depth of necrosis (close to the muscle layer). However, much wider necrotic lesions were observed in the tumour after either PCI treatment.

Severe extravasation with blood cells leaking out from blood vessels into the surrounding tissue was observed after both PCI treatments (Figure 8.16B and 17B). Like PDT treatment, transition zones with tumour cells containing fragmented nuclei could be found in between necrotic region and viable tumour area after PCI treatments (Figure 8.16C and 17C). Dilated blood vessels were also abounded in these areas. Compared to PDT, PCI treatments were shown to induce greater transition areas, resulting smaller area of viable tumour cells in the periphery.

Moreover, perivascular survival of tumour cells was more obvious in the tumours after PCI treatments, particularly in the transition region (Figure 8.16C and 17C). Nevertheless, as mentioned before, most of the viable cell here were apoptotic with fragmented nuclei.

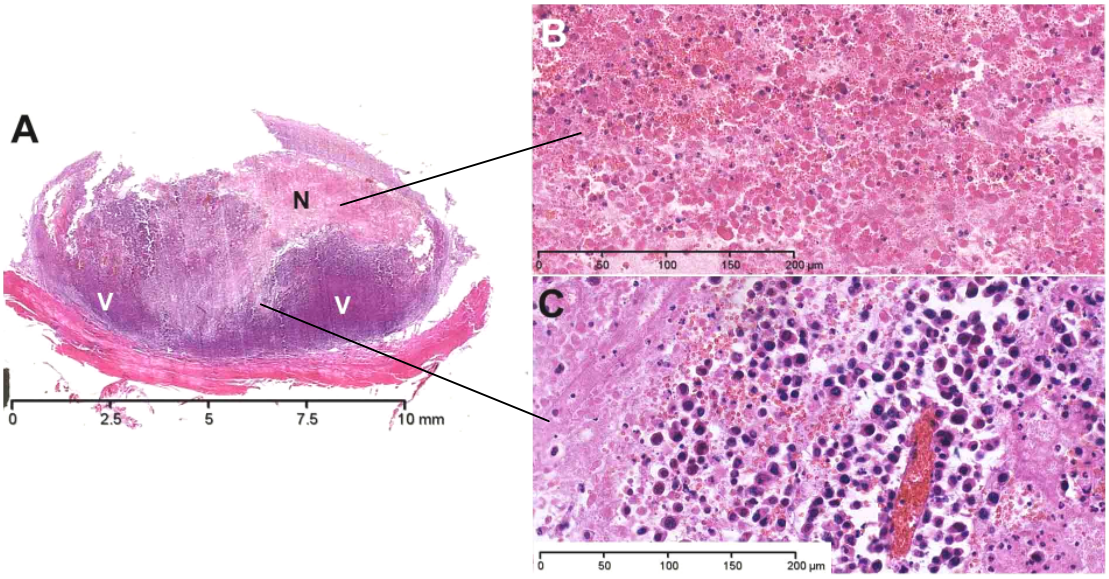

Figure 8.16 H&E stained histology section of transplanted rat sarcoma tumour one day after Amphinex PCI of saporin. A: The whole tumour section. N: necrosis; V: viable tumour cells. B: The region in the necrosis centre. C: The transition zone between necrosis and viable tumour area.

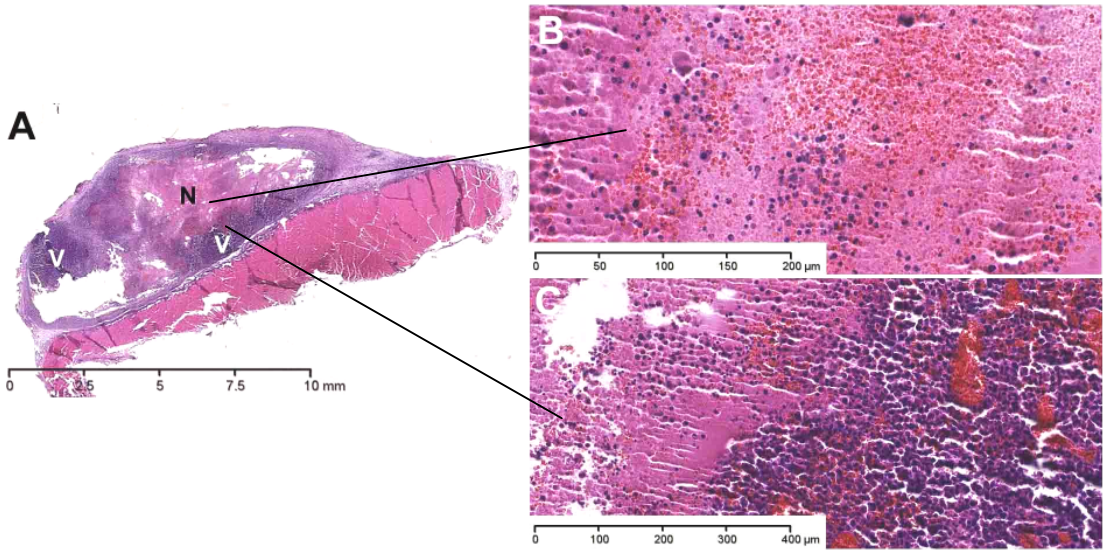

Figure 8.17 H&E stained histology section of transplanted rat sarcoma tumour one day after Amphinex PCI of bleomycin. A: The whole tumour section. N: necrosis; V: viable tumour cells. B: The region in the necrosis centre. C: The transition zone between necrosis and viable tumour area.

8.4 Discussion

This is the first study to investigate the Amphinex PDT and PCI effect using a syngeneic rat fibrosarcoma tumour model. Quantification of the Amphinex uptake in different tissues including tumour was carried out in tumour-bearing rats at the time of light delivery. Samples from the same animal (three animals in total) were divided into two groups for chemical extraction and quantitative fluorescence microscopy separately. According to the results of chemical extraction, the drug level in the liver and colon of Hooded Lister rats at 24hr after drug application was measured consistent with the data obtained from Wistar rats shown in Chapter 6 (Figure 8.3 and 6.5). This indicates that the uptake of Amphinex between this two species is similar.

The biodistribution of Amphinex in different tissues by chemical extraction was found in agreement with the results estimated by fluorescence microscopy (Figure 8.5) although the tissue-to-tumour ratios were slightly higher using fluorescence microscopy, particularly in liver.

According to the results of chemical extraction (Figure 8.3), Amphinex displayed a comparable tumour uptake compared to other water soluble porphyrin sensitisers e.g. $TPPS_4$ and m-THPP. The tumour accumulation of these two sensitisers has been investigated in a nude mice tumour model [Peng, 1987;Peng et al., 1995]. Much higher tumour-to-skin and tumour-to-muscle ratios of Amphinex uptake were obtained than the values for $TPPS_4$ and m-THPP. The results show that Amphinex has an efficient tumour uptake and the concentration in other normal tissue such as skin and muscle is much lower than other water soluble sensitisers, $TPPS_4$ and m-THPP.

The information of the drug distribution at the cellular level was also obtained from the fluorescence images. In Figure 8.7, Amphinex was observed homogenously distributed in the tumour cells apart from the absence of nuclear localisation. The same phenomenon has been reported in $AlPcS_{2a}$ using HT1080 xenograft tumour models 48hr after i.p. injection [Dietze et al., 2005;Norum et al., 2009a]. Norum et al. additionally pointed out that the fluorescence intensity of $AlPcS_{2a}$ was measured higher in the centre of tumour and declined towards the tumour border but with intense fluorescence signals in the transitional zone between tumour and muscle [Norum et al., 2009a]. These

findings were not shown in our results; constant uptake of Amphinex was detected throughout the whole tumour. This discrepancy may be due to the differences in the biological nature between different tumours. The HT1080 tumour model is rather aggressive with the absence of tumour capsule compared to our MC28 tumour models as tumour capsule often remains and no spontaneous necrosis is observed with the size less than 1cm in diameter. It was also suggested by the authors that neovascularisation is particularly active in periphery of HT1080 tumour model which may explain the higher uptake of $AlPcS_{2a}$ in some areas in this region.

Amphinex was also observed localised in blood vessel walls in different tissues. The fluorescence intensity in endothelial cells was measured lower than in liver cells (Figure 8.10), similar to or slightly lower than the signals from tumour cells (Figure 8.9A and C) and higher than the signals from colon mucosa and colon muscle layer (Figure 8.11). The drug localisation in the endothelium of blood vessels gives the implication of the possible photochemical damages to the vascular system after light treatment.

Amphinex PCI showed a significant enhancement in inducing necrosis in tumour. The mean maximum extent of necrotic lesions after PCI in combination with either saporin or bleomycin appeared to be significantly increased by a factor of 2 compared to PDT treatment (Figure 8.11). Measurements were based on the histological examination. It should be noted that some tumours were excluded when haemorrhage or cavities were observed (data not shown). As tumour cells grow aggressively, the above features can occur naturally, especially when the tumour size is too big. In this case, spontaneous necrosis may also occur in the centre of large tumours due to hypoxia. Other situations such as multiple tumours grown together are not suitable for measurements either. Hence, it is important to carry out experiments on the tumours with appropriate size to avoid misinterpreting the treatment responses.

Figure 8.18A and B show a tumour slice before and after fixation. The tumour flesh was often found amorphous before fixation (Figure 8.18A). Together with Figure 8.13, it is difficult to differentiate the damaged area by the appearance without further processesing. A direct macroscopic examination was not feasible in practice.

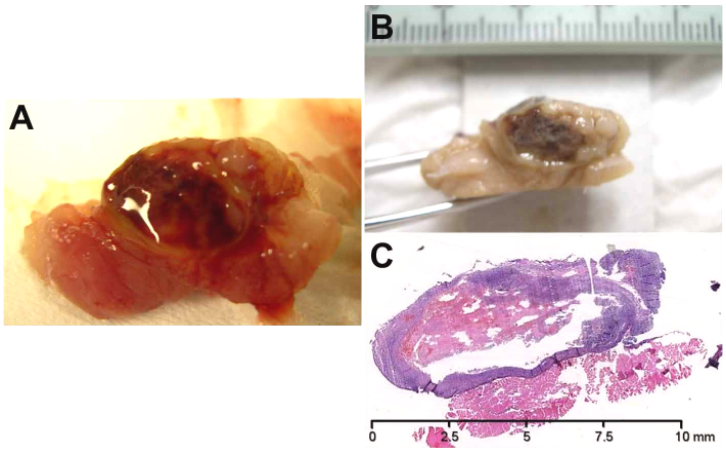

Figure 8.18 An example of tumour sections preparation. A and B: tumour slice before and after fixation. C: the corresponding H&E stained section. This is a tumour treated with PCI of bleomycin.

In the previous studies in our lab, the necrotic lesions induced after treatment were identified macroscopically after a staining procedure with Evans Blue dye [Tsutsui et al., 2002;Woodhams et al., 2006]. Evans Blue is a di-azo compound which binds firmly with the plasma albumin after injection intravenously. The viable tissues are stained with the dye but the necrotic areas remain unstained due to the lack of blood circulation. However, the margin might be ambiguous as the staining mainly relies on the blood supply which is not an absolute difference between necrotic and viable tissues. Moreover, Evans Blue dye may interfere the results of the following H&E stain and hinder other possible histological stains. Taking this into account, it was decided to carry out the measurement by histological examination based on the H&E stained tumour sections.

An early attempt to measure the depth of necrosis induced after PDT and PCI treatment was reported by Dietze and his colleagues in which the PDT effect resulted in 3-4mm deep necrotic lesions compared with the depth of 6-7 mm in the PCI group [Dietze et al., 2005]. However, as shown in the histological examination results in our tumour model (Figure 8.15-17), the necrosis areas often had irregular and asymmetric shapes which make it difficult to define the depth or width of the necrotic lesion. Therefore, instead of measuring the extent of necrotic lesion in one dimension, the measurement of the necrotic area, in the plane extended from the line of fibre and perpendicular to the tumour surface, was performed to evaluate and compare the treatment response between PDT and PCI quantitatively in this study.

The histological results show that necrotic lesions were induced after PDT and PCI treatments and the regions were observed from the tumour surface to deeper locations. The central areas of necrosis were observed to be similar with either treatment, i.e. most cells were necrotic and some cells were apoptotic.

Extravasation of blood can be seen in the centre of the necrosis zone and is particularly exaggerated in the tumour after PCI treatments (Figure 8.15D, 16B and 17B). The photodynamic effect on the vasculature in the PDT treatment of solid tumours has been recognized since early 1980s [Star et al., 1984]. The vascular damage acts as an additional therapeutic effect to the direct cytotoxicity of PDT. It causes blood flow stasis and the consequent reduced perfusion, resulting in the ischaemic death of tumour cells [Fingar, 1996]. The accumulation of Amphinex in the blood vessel wall was observed by fluorescence microscopy. The presence of the large number of blood cells in the centre of necrosis area (Figure 8.15D, 16B and 17B) again emphasises the vascular damage after Amphinex PDT and PCI treatments.

Dilated blood vessels were found in the transition area (Figure 8.15C, 16C and 17C). This appearance was caused by the inflammation reactions induced after PDT and PCI treatments. The occurrence of perivascular survival of tumour cells in this area is more noticeable in the tumours receiving PCI treatments. These results are consistent with the results of PDT and PCI treatment in normal rat liver in the previous chapter, as well as the results using AlS_2Pc PCI of gelonin in normal rat liver in the previous study [Woodhams et al., 2009]. Viable liver cells were observed surrounding blood vessels in the area near the border of necrotic regions (Figure 7.13).

The central necrosis is induced by PDT treatment and the outer area, the transition zone is thought to be due to PCI effects. Although oxygen should be favourable for PDT, photochemical reactions may be inefficient in this area as the light fluence rate is already low here. Tumour cells localised in perivascular areas (oxygenated region) often have higher survival rates after treatments compared to the cells in the remote area. Due to the benefits of a higher oxygen and nutrient supply from the microcirculation, perivascular tumour cells have potential protection against the harmful damage from treatment.

Although the lack of control studies on animals that are only given anti-cancer agents can not estimate the influence of the cytotoxicity from saporin and bleomycin alone in our study, evidence has been showed in other studies that toxins alone had no contribution to tumour growth retardation [Berg et al., 2005a;Dietze et al., 2005;Norum et al., 2009a;Selbo et al., 2001b]. The enlarged necrosis lesion induced by PCI of saporin and bleomycin compared with PDT in this study has demonstrated the benefit of this combined modality. Further studies to assess the mechanism of the therapeutic effect of PDT and PCI will be presented in Chapter 9.

The model used in this study is a syngeneic rat fibrosarcoma which is different from the xenograft models in immunodeficiency mice used in other *in vivo* PCI studies. As mentioned before, a syngeneic tumour model could naturally metastasize with less immune response expected and this is therefore of benefit for new drug investigation in cancer [Khanna and Hunter, 2005;Talmadge et al., 2007].

Amphinex PCI in combination with saporin and bleomycin has demonstrated a significant enhancement in inducing tumour destruction. PCI has recently started its first clinical trial using Amphinex PCI of bleomycin in head and neck cancers in the University College London Hospital. The results in this chapter show that Amphinex has the potential for further clinical utilization by enhancing the delivery of co-administered anti-cancer drugs.

Chapter 9: Mechanistic Studies of *In Vivo* Amphinex PDT and PCI

9.1 Introduction

The concept of PCI is based on photo-induced membrane rupture followed by cytosolic release of anti-cancer agents entrapped in the vesicles of endocytotic systems. The results from the previous chapters have shown that Amphinex PCI is a novel technology to enhance the cytotoxicity of saporin and bleomycin *in vitro* and *in vivo*. The mechanisms of the killing effects from PDT has been studied extensively as described in Chapter 1, whereas there are rare studies to investigate the mechanisms behind the enhanced cytotoxicity using PCI in combination with anti-cancer drugs. For this reason, the aims of this chapter are to examine the cell death induced by PCI and to monitor the photosensitisation and the consequent redistribution of macromolecules *in vivo*.

Firstly, as discussed before in Chapter 1, PDT is known to be able to induce apoptosis or necrosis or a combination of both pathways. It is generally considered that cells undergo apoptosis when treated with lower doses while cells can die through necrosis when receiving higher doses [Oleinick and Evans, 1998]. Many studies have documented the cell death triggered by PDT using different cell lines and photosensitisers; however, the cell death in response to PCI is not understood. According to the results shown in Chapter 7 and 8, necrosis was observed in the liver and tumour treated with Amphinex PDT and PCI of saporin or bleomycin. However, there is an observation of fragmented nuclei in some cells remaining in the central necrotic area, as well as the cells in the adjacent regions of tumours treated with Amphinex PDT and PCI. Because PCI is a drug delivery technology based on the use of a sub-lethal PDT dose, it is possible that apoptosis is also involved in Amphinex PDT and PCI.

To investigate the involvement of apoptosis in Amphinex PDT and PCI, a terminal deoxynucleotidyl transferse (TdT)-mediated dUTP nick-end labelling (TUNEL) assay was performed. TUNEL assay is used to detect apoptotic cells by measuring the nuclear DNA fragmentation, one of the biochemical hallmarks of apoptosis. The principle of this method is to target the break 3'-OH DNA end with fluorescein labelled dUTP in the presence of the recombinant enzyme TdT. Cells are often further stained with propidium iodide in their whole DNA and can therefore be visualised by fluorescence microscopy or quantified by flow cytometry.

In this section, TUNEL assay was used to stain the paraffin-embedded sections of liver and tumour treated with Amphinex PDT and PCI of saporin or bleomycin. The results were analysed using confocal microscopy with parallel H&E stained micrographs.

The following two sections of this chapter describe mechanistic studies of PCI action in tissue. The first describes the use of the TUNEL assay as detailed above, and the second section describes using confocal microscopy to image the distribution of Amphinex using the rat liver model. Confocal microscopy has been shown to be able to provide microscopic imaging of tissues *in vivo* or in human at high resolution [Goetz et al., 2008b;Rajadhyaksha et al., 1995]. For skin samples, melanin can be a natural contrast agent but for other tissues like liver, an additional administration of fluorescent agents such as fluorescein sodium or FITC-labelled dextran is necessary. Because the required benchtop device still limits its *in vivo* utilisation, a recent development of a miniaturised confocal scanner integrated into a flexible endoscope, named confocal laser endomicroscope (CLE), has made it possible to be used for clinic practice in gastroenterology [Hurlstone et al., 2008]. Combined with minilaparoscopy, CLE also can be used for imaging some interstitial organs like liver [Goetz et al., 2008a].

Since photosensitisers are fluorescent, *in vivo* imaging of the uptake of photosensitisers in tissue has been applied clinically (Table 1.1) for diagnosis purpose which is known as photodynamic diagnosis (PDD). Apart from this aspect, since confocal microscopy provides high-resolution subsurface imaging, it may be able to detect the distribution of photosensitisers on the cellular scale. In this regard, the experiment in this section was designed to show the feasibility of using such confocal microscopy to image the distribution and redistribution of Amphinex after illumination using intact freshly excised liver samples *ex vivo*.

The last section of this chapter examines the redistribution of saporin after light exposure using rat liver model. Amphinex PCI-induced redistribution of saporin in cells was demonstrated in chapter 4 of this thesis. Other examples of *in vitro* $AlPcS_{2a}$ PCI-mediated endo-lysosomal release of macromolecules also have been shown elsewhere [Selbo et al., 2000a;Selbo et al., 2009]. In a previous study from our laboratory, using immunohistochemistry, *in vivo* redistribution of gelonin was observed after $AlPcS_{2a}$ PCI in rat liver model [Woodhams et al., 2009]. In the present study, changes of the

distribution of saporin in liver after Amphinex PCI was investigated based on the same method but using a commercial available antibody against saporin.

9.2 Materials and Methods

Chemicals

Amphinex, in Cremophor (10 mg/ml) was kindly donated by PCI Biotech (Norway). Saporin was purchased from Sigma-Aldrich (USA). Bleomycin (Kyowa Hakko, Mayne) was provided as a powder (15 IU per vial according to the U.S. standard equivalent to 15,000 IU according to the European Pharmacopeia. 5.1). Detailed formulation and drug preparation for *in vivo* experiments has been mentioned in the previous chapters.

Animals and tumour models

All animal experiments were conducted under the authority of project and personal licences granted by the Home Office and the UKCCCR Guidelines. Inhaled Halothane or Isoflurane was used to maintain a state of general anaesthesia for drug administration. For PDT and PCI experiments, animals were given analgesia subcutaneously 30 minutes before surgery.

Female Hooded Lister rats (180-220g) were subcutaneously transplanted with MC28 cells in the lower flank to establish the transplanted syngeneic rat fibrosarcoma tumour model. The protocols for cell cultivation and the tumour model have been stated in the previous chapter. The experiments of Amphinex and saporin redistribution in liver were carried out using female Wistar rats (180-200g, Harlan, Oxon, UK).

Light source

The light source used for Amphinex PDT and PCI treatments was a diode laser emitting at 652nm (Diomed Ltd, UK). An attenuator (FVA-UV fibreoptic variable attenuator, World Precision Instruments Ltd, UK) was used to reduce the laser power to 50mW. Lasers were calibrated and the power at the tip of the fibre was measured using a wavelength-independent pyroelectric power meter (TPM-300, Gentec Inc, Canada) before each treatment.

Detection of apoptosis in liver and tumour after PDT and PCI treatments

TUNEL assay (DeadEnd^{TM} Fluorometric TUNEL System, Promega, UK) was used for the detection of fragmented DNA in apoptotic cells. The assay was carried out using paraffin liver and tumour sections. PDT and PCI treatments on liver and tumour have

been described in the previous chapters. Liver sections after PDT and PCI of saporin (250μg/kg, i.v. 1hr before light) or bleomycin (30 IU/kg, i.v. 30 min before light) were obtained from the samples of the experiments in Chapter 8. Tumour sections were collected from the tumours sampled 4 hrs after light treatments. Paraffin sections of liver and tumour were stained with the commercial apoptosis detection kit according to the manufacturer's instructions. Propidium iodide (PI) solution (Sigma-Aldrich, UK) in PBS (1 μg/ml) was used to stain nuclei. Sections were examined using confocal microscopy (FLUOVIEW FV1000, 60x magnification, NA 1.20, Olympus, Japan). The apoptotic bodies will be stained with fluorescein (green) and also PI (red), resulting in a yellow colour when the two images are merged.

Adjacent sections were stained with H&E and scanned using the Hamamatsu Nanozoomer Digital Pathology (NDP) scanner (Hamamatsu Photonics, UK).

Ex vivo observation of the redistribution of Amphinex after light in fresh rat liver

Animals were sensitised with Amphinex (i.v. 2.5 mg/kg) 24hrs before irradiation. A 652 nm laser was used for irradiation with the power of 50 mW for providing the light dose of 5J. One control animal, animals without light and with light treatments (N=2 each) were killed by cervical dislocation. Livers were removed and kept in vials with PBS on ice and immediately studied using confocal microscopy (FLUOVIEW FV1000, 60x magnification, NA 1.20, Olympus, Japan). In the light-treated liver, the area of irradiation was marked in the margin of tissue and thus can the position be identified. With a few drops of PBS, liver samples (approx. 1 cm^2) were 'face-down' placed on the centre of FluoroDish (WPI, UK), in full contact with the glass coverslip bottom of the dish and imaged using a 543 nm laser (Figure 9.1). All confocal microscopic studies were carried out using fresh liver samples taken within 1hr of the animal sacrifice.

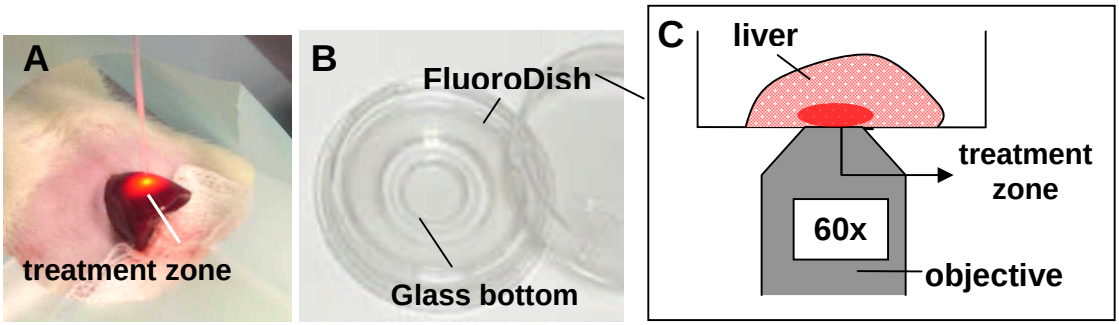

Figure 9.1 Micrographs of light treatment on liver (A), FluoroDish (B) and the imaging setup for confocal microscopy (C).

Immunnohistochemistry of saporin distribution in liver before and after light treatment

5 Wistar rats were sensitised with 0.25 mg/kg Amphinex for a 24hr drug light interval. One rat was used for control study, 2 rats were injected with 250μg/kg saporin 1hr before light and 2 rats were given 250μg/kg saporin but with no light treatment. Light treatments were carried out following the same protocol as mentioned before using a 50mW laser power for providing the light dose of 10J. 30 min after irradiation, all rats were killed and the livers were dissected. The livers from all rats were fixed in formalin, dehydrated and mounted in paraffin. The sectioning procedure of paraffin-embedded samples has been described in previous chapters.

Sections were then de-waxed (immersed in xylene solution three times), rehydrated (through graded ethanol washes- 100%, 95%, 85%, 70% and 50%) and rinsed in running water. For antigen retrieval, sections were placed in boiling citrate buffer (10mM, pH 6) in a pressure-cooker, cooked under full pressure for 2 min and cooled with running water. Sections were then incubated with 3% H_2O_2 in Methanol for 15min before the application of primary antibodies to quench the endogenous peroxidise. Saporin was detected by incubating with polyclonal goat anti-saporin (1:350 dilution, Advanced Targeting System, USA), the primary antibody, for 1hr at room temperature. Sections were then rinsed thoroughly with Tris Buffer Saline Tween-20 (TBST) and blocked with rabbit serum (Sigma-Aldrich, UK) for 20min to prevent non-specific binding. After rinsing with TBST three times, sections were incubated with secondary antibodies which are conjugated with horse radish peroxidise (rabbit anti-goat antibodies HRP conjugated, 1:1500 dilution, abcam, UK). After 40min incubation, antibodies were washed off with TBST and subtract solution containing diaminobenzidine (DAB) was added a few drops to sections. The colour development procedure (2-5min) was stopped by immersing sections in water. Counterstaining with haematoxylin was carried out followed by dehydration in graded ethanol solutions and section mounting.

Sections without primary or secondary antibodies were also prepared for control tests. All sections were scanned using the Hamamatsu Nanozoomer Digital Pathology (NDP) scanner (Hamamatsu Photonics Ltd, UK).

9.3 Results

9.3.1 Detection of apoptosis induced by Amphinex PDT and PCI in rat liver and tumour

PDT- or PCI-induced apoptosis was examined in rat MC28 sarcoma 4hrs after light treatment by TUNEL assay using confocal microscopy. Figure 9.2 shows the results of control untreated tumours in which TUNEL stained nuclei (merged in yellow colour) were nearly absent.

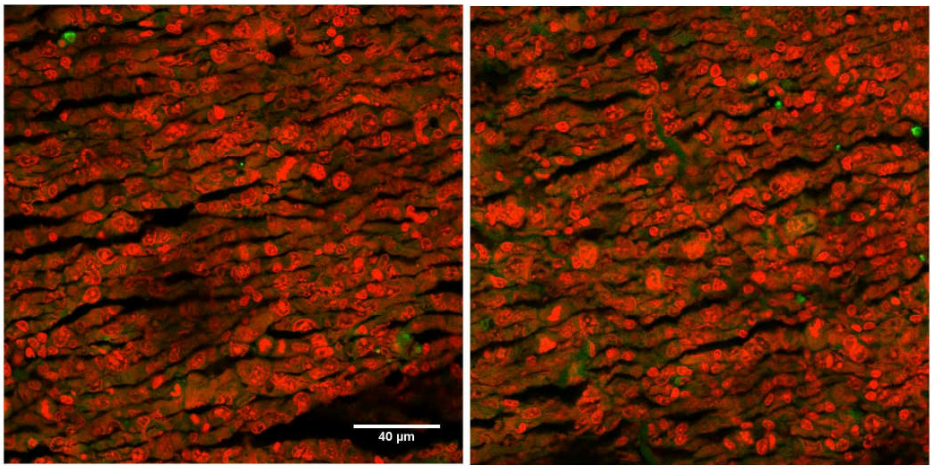

Figure 9.2 TUNEL staining of MC28 sarcomas without treatment. Tumour sections were obtained from control animals and stained with TUNEL assay and analysed using confocal microscopy. The green fluorescence maps the nuclei of apoptotic cells, opposed to the red fluorescence from propidium iodide which stains normal nuclei, resulting in yellow colour.

In contrast, TUNEL positive tumour cells were detected in the tumours treated with Amphinex PDT or PCI. Figure 9.3 shows the tumour after Amphinex PDT treatment. Figure 9.4 and Figure 9.5 are examples of PCI treatments in combination with saporin and bleomycin. Figure 9.3A, 4A and 5A are the whole H&E stained tumour section. Other subfigures are the confocal images and their corresponding H&E stained micrographs from nearby areas which are presented together.

As shown in Figure 9.3, Amphinex PDT induced apoptosis in MC28 sarcoma. Apoptotic tumour cells (Figure 9.3b, nucleus stained yellow) were particularly observed in the transition area between necrosis region (N) and viable tumour cells (V). In the

case of this tumour, many tumour cells infiltrated into muscle layers which are far away from the tumour surface where irradiation began, were also detected to be apoptotic (c), suggesting the tumour cells in this area were under the influence of PDT treatment as well. Muscle cells (c) and fibrous tumour capsule (d), on the other hand, were not observed to be apoptotic after PDT treatment. The information of the cells in the necrotic region is unfortunately not available. Necrotic tissues usually can not attach slides firmly and therefore these tissues are easily washed off during the staining procedure.

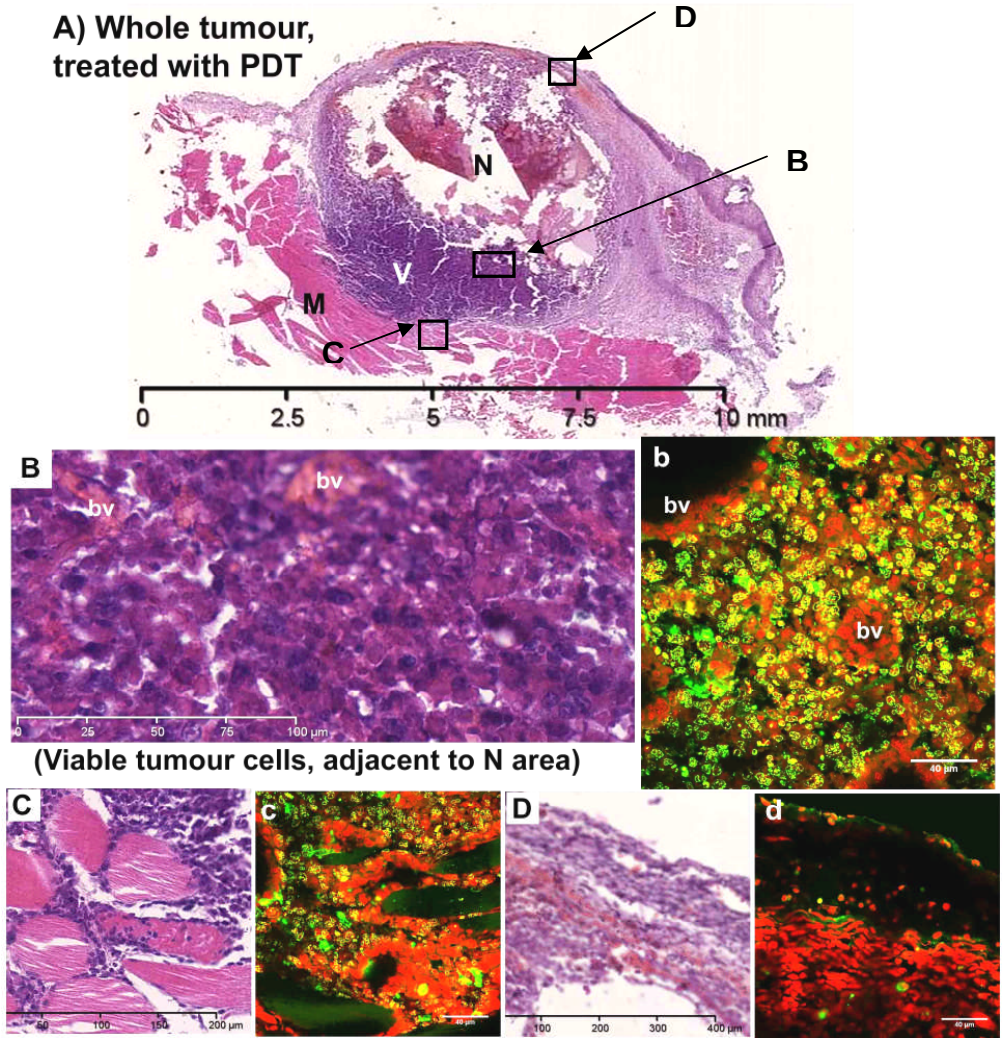

Figure 9.3 Histopathological analysis and TUNEL staining of MC28 sarcomas treated with Amphinex PDT. Hooded Lister rats bearing tumour were sensitised with 2.5 mg/kg Amphinex for 24 hrs. Tumour sections were obtained 4 hrs after light treatment (10J light dose using a 652nm laser). (A)-(D) are H&E stained and (b)-(d) are TUNEL stained fluorescence micrographs taken from nearby regions. A: the whole image of treated tumour with a scale on the bottom; B and b: the areas with viable tumour cells (V) adjacent to necrotic region (N); C and c: the transition zone between tumour and muscle (M); D and d: Tumour capsule. bv: blood vessels.

The TUNEL assay results of the tumour treated with Amphinex PCI of saporin is shown in Figure 9.4, presented together with the H&E stained sections from nearby regions. As shown in Figure 9.4C, the number of viable cells in the necrotic area (N) is low and some of the cells remaining were apoptotic with the whole nuclei stained TUNEL positive (c2). An increase of apoptotic cells was observed in the area (V) adjacent to the necrotic region (c1); however, the number of the apoptotic cells (presented in yellow) was not as many as the case from the same area treated with PDT alone (Figure 9.3b). Viable tumour cells located near muscle were rarely observed apoptotic (Figure 9.4d). Muscle cells and fibrous tumour capsule (Figure 9.4e and b) were not observed to be apoptotic after PCI of saporin treatment, either.

After the PCI of bleomycin, tumour cells in the necrotic area (Figure 9.5B and b) displayed similar pattern to the ones after treated with PCI of saporin: some cells were apoptotic with the whole nuclei stained TUNEL positive. Muscle cells (e) and fibrous tumour capsule (d) here were not apoptotic as well. However, less TUNEL positive cells were shown in the area adjacent to necrotic region (5c) compared to the ones treated with PDT or PCI of saporin.

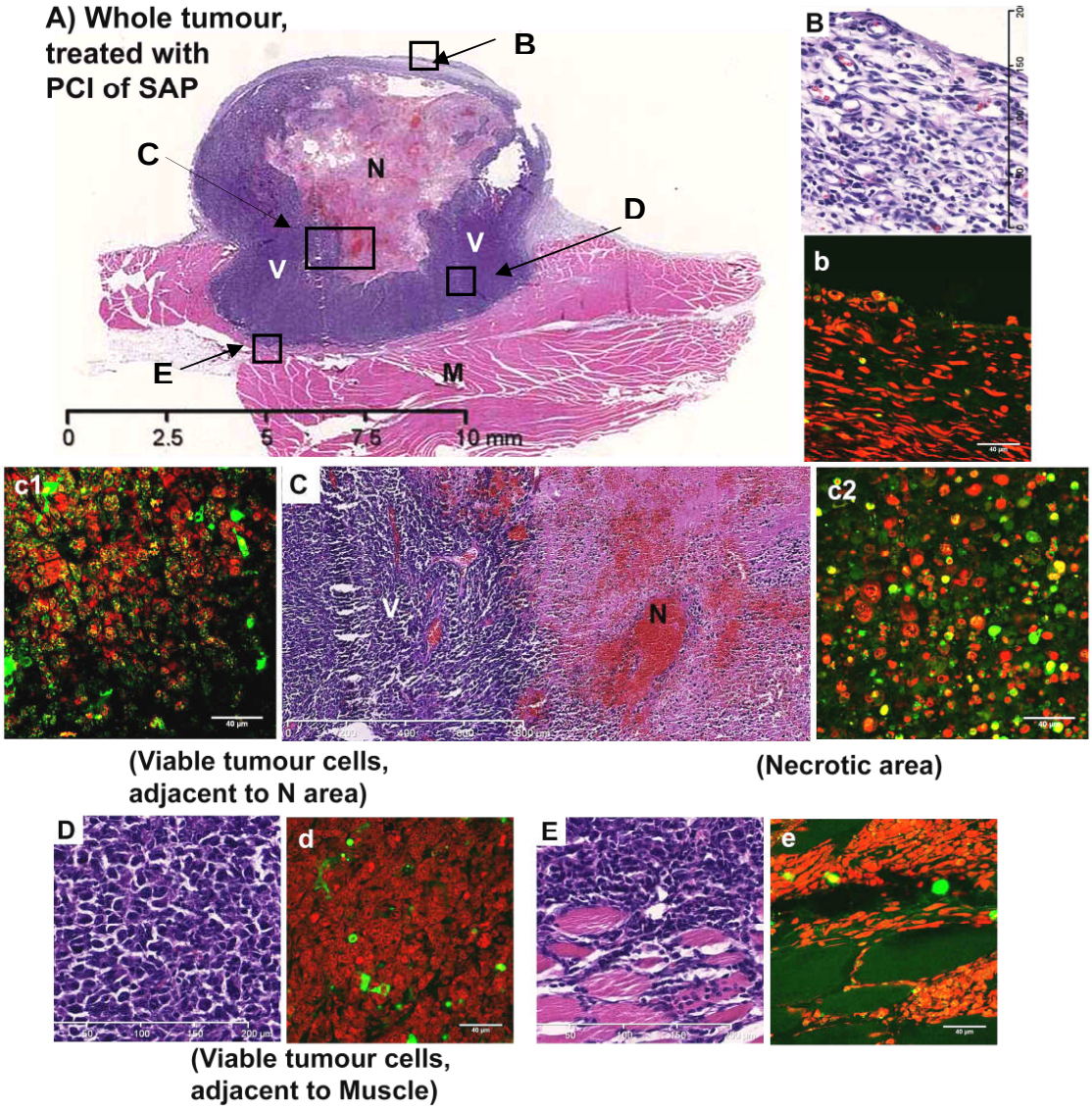

Figure 9.4 Histopathological analysis and TUNEL staining of MC28 sarcomas treated with Amphinex PCI of saporin (SAP). Hooded Lister rats bearing tumour were sensitised with 2.5 mg/kg Amphinex for 24 hrs and saporin (250 μg/kg) was injected to rats (i.v.) 1h before irradiation. Tumour sections were obtained 4 hrs after light treatment (10J light dose using a 652nm laser). (A)-(E) are H&E stained and (b)-(e) are TUNEL stained fluorescence micrographs taken from nearby regions. A and a: the whole image of treated tumour with a scale on the bottom; B: tumour capsule; C: the transition zone between necrotic (N) and viable tumour (V) regions; c1: the area with viable tumour cells adjacent to necrotic region; c2: necrotic area; D and d: the area with viable tumour cells (M); E and e: the transition zone between tumour and muscle.

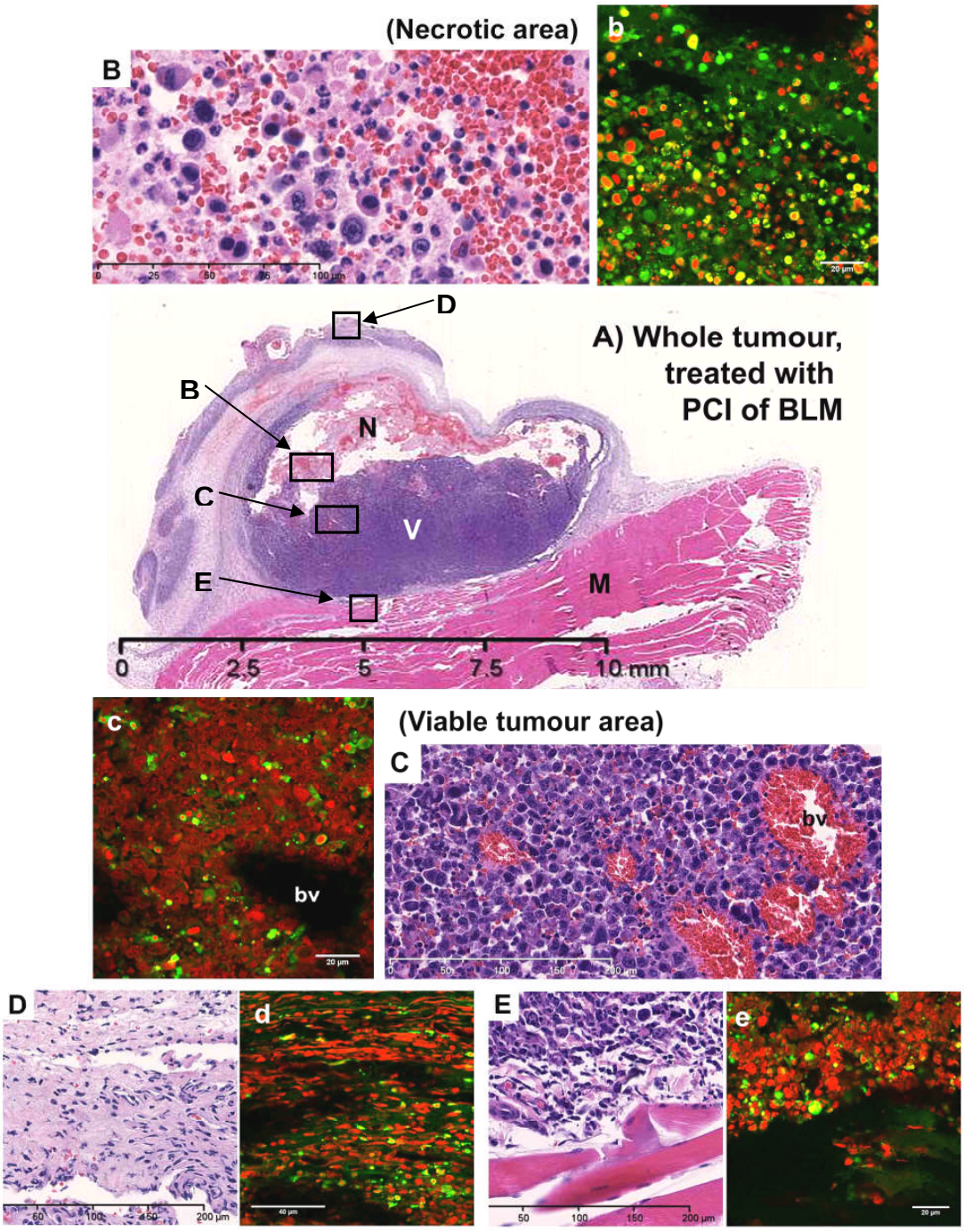

Figure 9.5 Histopathological analysis and TUNEL staining of MC28 sarcomas treated with Amphinex PCI of bleomycin (BLM). Hooded Lister rats bearing tumour were sensitised with 2.5 mg/kg Amphinex for 24 hrs and bleomycin (30 IU/kg) was injected to rats (i.v.) 30 min before irradiation. Tumour sections were obtained 4 hrs after light treatment (10J light dose using a 652nm laser). (A)-(E) are H&E stained and (b)-(e) are TUNEL stained fluorescence micrographs taken from nearby regions. A: the whole image of treated tumour with a scale on the bottom; B and b: necrotic area (N); C and c: the areas with viable tumour cells adjacent to necrotic region; D and d: Tumour capsule; E and e: the transition zone between tumour and muscle (M). bv: blood vessel.

TUNEL assay was also used to detect apoptosis in the rat liver treated with Amphinex PDT and PCI of saporin or bleomycin. Liver sections were obtained from the same liver tissues used for the studies in Chapter 7 which were collected 3 days after light treatment. The sections were from the samples with maximum necrosis whose treatment conditions are- PCI of saporin: 250 μg/kg saporin given 1 hr before light and PCI of bleomycin: 30 IU/kg bleomycin given 30 min before light. Each experiment contains 3 individual liver samples. The results were consistent and one of them was chosen to be presented here.

Figure 9.6 shows the results of untreated liver and the liver treated with PDT or PCI with the confocal images of TUNEL stained liver sections and the H&E stained micrographs from nearby regions. Images were chosen from the necrotic zone.

No apoptotic nuclei were detected in the control untreated liver (Figure 9.6A). On the other hand, apoptotic liver cells were found in the sample treated with PDT or PCI (nuclei in yellow, Figure 9.6B, D and F). However, there is an interesting finding that not all cells in the necrotic zone of treated liver presented the same results after TUNEL assay. It was observed that some cells were TUNEL positive but some were negative. The differences are consistent with the H&E stained sections that some cells were necrotic with the absence of nuclei (Figure 9.6c, e and g) and some cells have apoptotic nuclei (pointed with arrows, Figure 9.6b, d and f). These cells were randomly distributed and their locations were not related to the distance to the laser fibre.

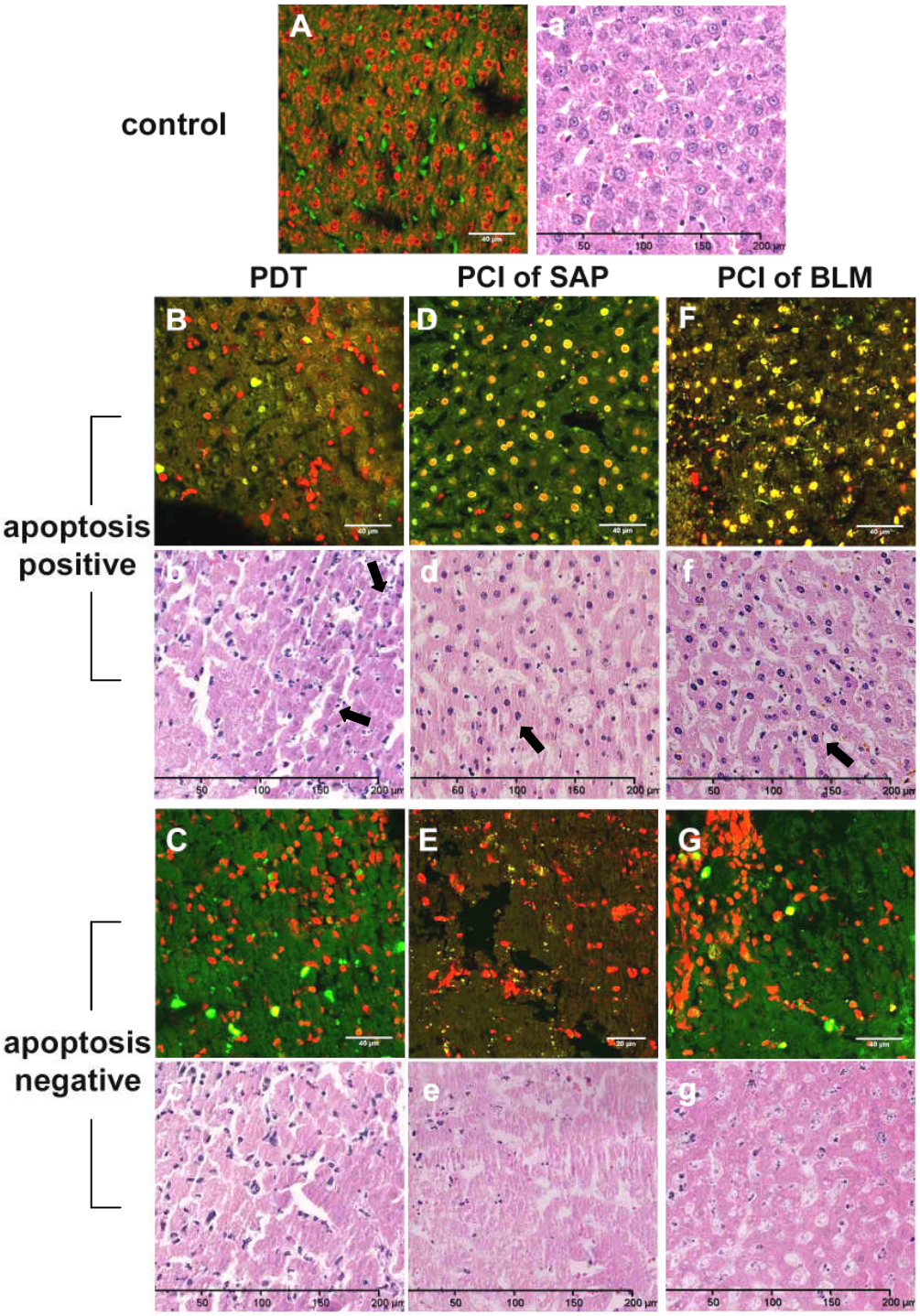

Figure 9.6 Histopathological analysis and TUNEL staining of rat liver treated with Amphinex PDT or PCI of saporin (SAP) or bleomycin (BLM). Wistar rats were sensitised with 2.5 mg/kg Amphinex for 24 hrs. Liver sections were obtained 3 days after light treatment (10J light dose using a 652nm laser). For PCI treatment, saporin (250 μg/kg) and bleomycin (30 IU/kg) was injected to rats (i.v.) 1 hr and 30 min before irradiation respectively. All micrographs (except control groups) are the areas in the central necrotic region. (a)-(g) are H&E stained and (A)-(G) are TUNEL stained fluorescence images taken from nearby region. A: untreated liver. B and C: PDT treated liver. D and E: PCI of SAP treated liver. F and G: PCI of BLM treated liver.

9.3.2 *Ex vivo* observation of the distribution of Amphinex and redistribution after illumination in rat liver using confocal microscopy

The studies of this section are to observe the distribution of Amphinex and its redistribution after light using intact liver samples by confocal microscopy *ex vivo*. The detailed protocols are described in Materials and Methods. After removal of the liver samples (approx. 1 cm^2) from untreated or light-treated animals sensitised with 2.5 mg/kg Amphinex for 24 hrs, samples were kept on ice and imaged using confocal microscopy immediately (within 1hr). The sample from the control animal was also prepared with the same procedure.

Before carrying out these exeriments the distribution of Amphinex in liver was investigated using frozen liver sections. Sections were obtained from liver samples with or without light treatment and were attached to large coverslips instead of conventional slides whose thickness is not ideal for imaging using the available inverted confocal microscope. Therefore CCD camera imaging was used but it was found that the lower resolution from the relatively thick frozen sections prevented reliable detection of intracellular distribution. Moreover fine details are not well preserved using frozen section preparation. Consequently, the next series of experiments as described here were carried out using fresh unfrozen liver samples under confocal imaging.

The results demonstrated that most images were of excellent quality in which nuclei and individual hepatocytes can be easily identified without using contrast agents. Nevertheless, images from the control animal exhibited negligible fluorescence signal (data not shown).

As shown in Figure 9.7A and B, a clear granular distribution of Amphinex in untreated liver was observed, whereas Amphinex appeared to be diffuse in light-treated livers (Figure 9.7C and D). Under higher magnifications, it is clearer that the granular distribution of Amphinex in liver is well distributed in the cytosol (Figure 9.8A and B).

Although the detection depth is unknown, the detectable distance was about 50 μm which covers more than 2 layers of cells.

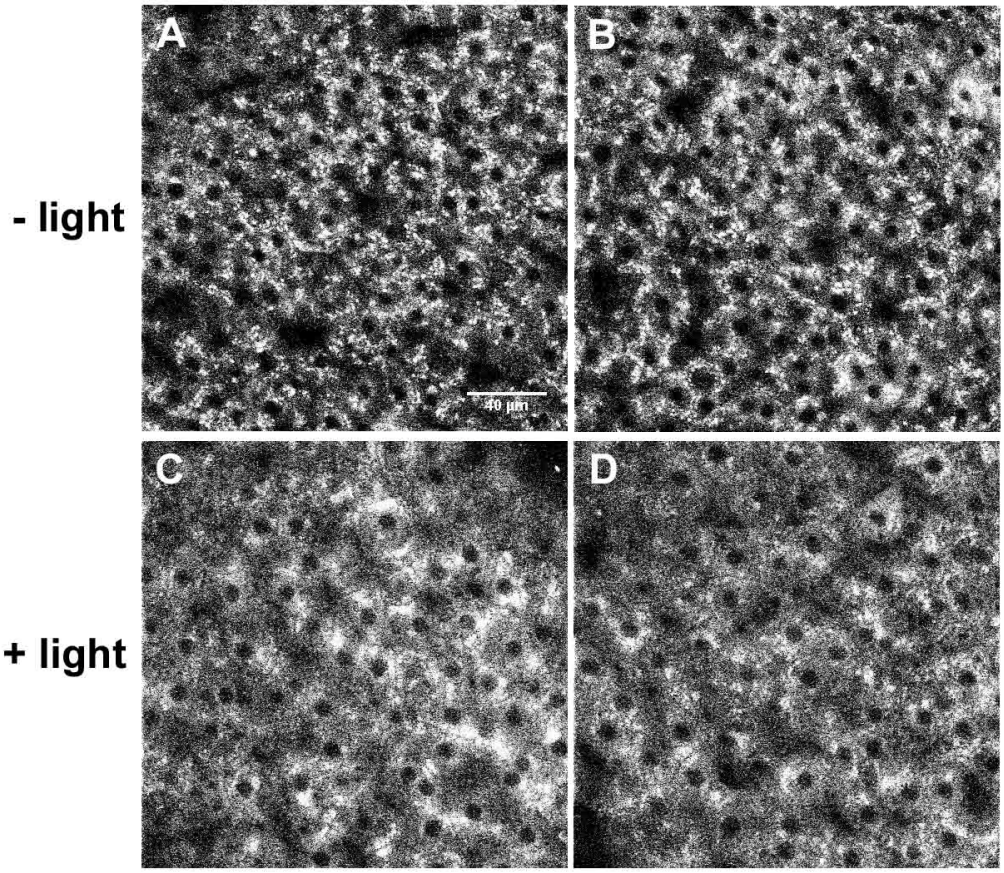

Figure 9.7 Ex vivo confocal images of Amphinex in fresh Wistar rat liver without or with illumination. Animals were sensitised with 2.5 mg/kg Amphinex for 24 hrs. A and B: liver samples without light treatment. C and D: liver samples after light treatment using a 652 nm laser with a dose of 10J (laser power: 50mW; irradiation time: 200 sec). Liver samples were placed on the FluoroDish (WPI, UK) and imagined using a 543 nm laser.

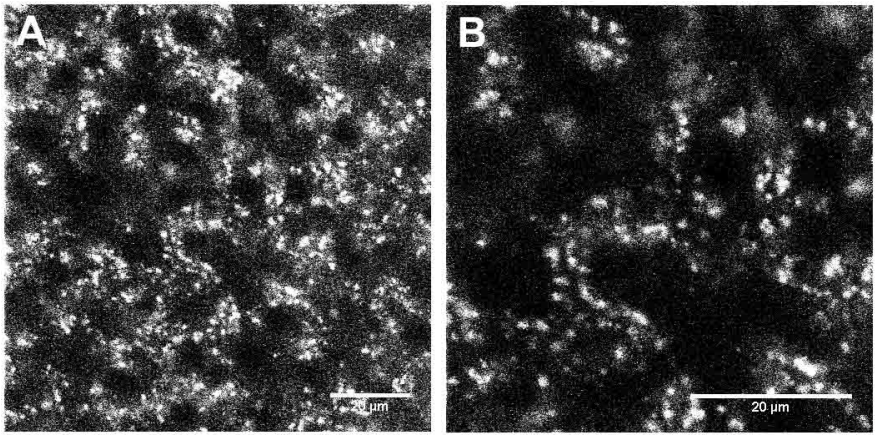

Figure 9.8 *Ex vivo* confocal images of Amphinex in fresh Wistar rat liver under higher magnifications without light. Animals were sensitised with 2.5 mg/kg Amphinex for 24 hrs. Liver samples were placed on the FluoroDish (WPI, UK) and imaged using a 543 nm laser. A: zoom in 2x. B: zoom in 4x. Scale bars: 20 µm.

9.3.3 Immunohistochemistry of saporin distribution in liver before and after Amphinex PCI

To observe the distribution of saporin and the redistribution after illumination in liver, saporin was stained by immunohistochemistry and the images were scanned using NDP microscopy. The results are shown in Figure 9.9; saporin was observed to be mainly localised in the kupffer cells (resident macrophages of the liver, the inset white arrows in Figure 9.9A) throughout the whole liver section. The granular pattern in the cytosol suggests that the intracellular localisation of saporin is in the endocytotic vesicles. In the liver 30min after light exposure, less kupffer cells with granularly distributed saporin were observed and the relocalisation of saporin can be seen in some cells that their cytosols were stained with diffused brown colour (the inset red star in Figure 9.9B). Some debris from lysed cells can be found in the sinusoid space (the inset black arrow in Figure 9.9B). Most of the hepatocytes appeared to be damaged with some large vesicles in the cytosol (the inset white arrow in Figure 9.9B).

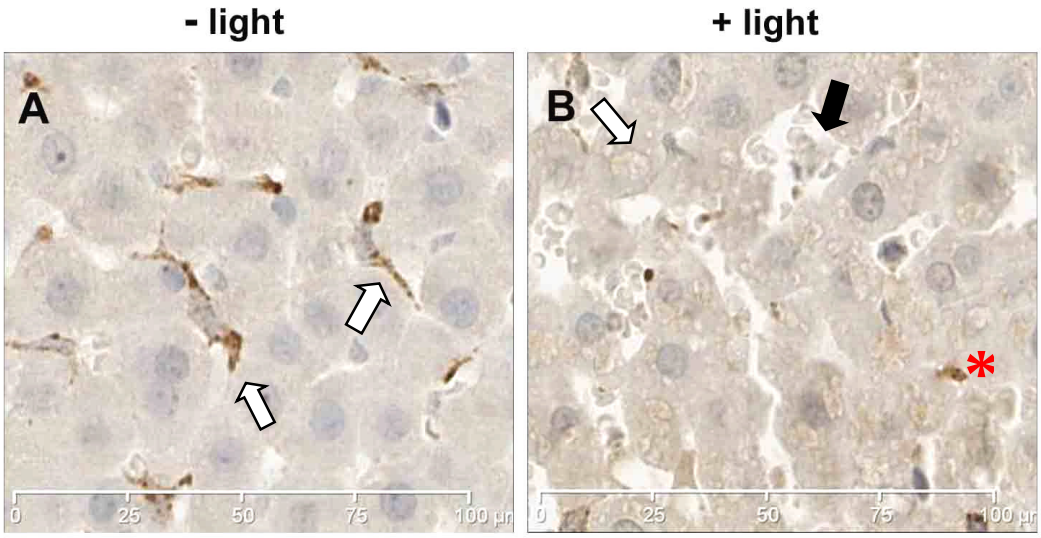

Figure 9.9 Photochemical-induced redistribution of saporin in Wistar rat liver by immunohistochemical staining. Animals were sensitised with 0.25 mg/kg Amphinex for 24 hrs. Saporin (250 µg/kg) was injected (i.v.) to rats 1hr before light treatment. A: Untreated liver. B: Liver examined 30 min after treated with 10J light using a 652 nm laser. Liver samples then fixed and stained with antibodies against saporin with details described in the Materials and Methods section.

9.4 Discussion

The results of the histological examination in this section show that necrosis can be detected 4hr after Amphinex PDT or PCI in combination with saporin or bleomycin in the MC28 rat sarcoma tumour model (Figure 9.3A-5A). This is consistent with the results shown in Chapter 8 in which tumours were sampled 24hr after light treatment (Figure 8.15-17). The experiment here further proved that apoptosis can be induced by Amphinex PDT and PCI. It should be noted that the sampling time point of the study here was earlier than the study in the previous section. The reason for this is that early PDT-induced apoptosis (within 24hr) was reported by many groups using different photosensitisers and tumour models [Fantini et al., 2008;Frank et al., 2003;Jalili et al., 2004]. Because this is the first study to examine apoptosis induced by PCI, a separate experiment where tumour-treated with Amphinex PDT or PCI was collected 4 hr after light exposure for TUNEL assay analysis.

Although apoptosis was detected in either Amphinex PDT or PCI of saporin and bleomycin, the distribution of apoptotic cells was observed to be different. In all cases, tumour cells in the necrotic area mainly die necrotically but with some apoptotic cells scattered (Figure 9.4c2, and 5b). However, the cells in the area adjacent to necrosis appeared to be different between these three treatments after TUNEL assay. The number of apoptotic cells in this region after PDT (Figure 9.3b) was higher than the one after PCI of saporin treatment (Figure 9.4c1). Few apoptotic cells can be seen in the tumour treated with PCI in combination with bleomycin (Figure 9.5c). Moreover, in the case of Amphinex PDT-treated tumour, the tumour cells in the area near muscle layer or already infiltrated into muscle were found to be apoptotic as well which was not observed in the tumours treated with Amphinex PCI in combination of saporin or bleomycin.

There is another interesting finding shown in Figure 9.3b that the endothelial cells of the blood vessels remain non-apoptotic while most of the surrounding tumours were stained TUNEL positive. There might be a selectivity of the photochemical effects on the tumour cells and the vasculature or a different mechanism for the endothelial cells in response to Amphinex PDT which needs further investigations.

The results of the Amphinex PDT and PCI treated livers show no differences after TUNEL assay analysis (Figure 9.6). Within the same liver, some cells in the treated area were stained TUNEL positive but some appeared to be negative. This was observed in all liver samples treated with either Amphinex PDT or PCI. A possible explanation is the time point of sample collection. The liver samples were the ones used for the studies in Chapter 7 for investigating the treatment efficacy which were sampled 3 days after illumination. It is possible that the same final outcomes maybe be obtained although cells actually die through different pathways.

As described in Chapter 1, PDT can induce necrotic and/or apoptotic cell death, which is likely to be dependent on the treatment dose (drugs and light). For PCI, the principal therapeutic effect may come from the employed anti-cancer drugs. The primary toxicity of saporin is due to the inhibition of protein synthesis, but it was also reported that apoptosis was observed from the cells treated with many ribosome-inactivating proteins, as well as antibody-conjugated saporin [Bolognesi et al., 2000;Narayanan et al., 2005]. Likewise, bleomycin mainly causes DNA breakage but cells were also found to die by apoptosis when using high drug concentrations [Tounekti et al., 2001]. In this regard, apoptosis is a reasonable assumption of the treatment response of Amphinex PDT/PCI.

The histological and the TUNEL assay results together indicate both necrosis and apoptosis can be induced in Amphinex PDT- and PCI- treated rat liver and tumour. However, TUNEL assay is a method to detect fragmented DNA, a common outcome of all the apoptosis pathways, so that it is not specific; the results based on the microscopic examination are not quantitative. As apoptosis is a dynamic process, further studies choosing different end points are important to monitor the changes during this biological process. Also, because several pathways are involved in apoptosis and the enzymatic steps employed are different (see Figure 1.4), examining the participation of different enzymes will be useful to determine the exact mechanisms undertaken in response to Amphinex PDT and PCI treatments.

The later two sections were aimed to observe *in vivo* PCI actions using *ex vivo* experiments: to observe the distribution of photosensitisers and the relocalisation of both photosensitisers and the employed anti-cancer drugs in tissues. Because photosensitisers are fluorescent, confocal microscopy was used to image Amphinex in liver (the organ with the highest drug uptake) at high resolution. For detecting the

redistribution of employed macromolecules, saporin was chosen as the target because proteins can be approached easily by immunostaining method in use of their antibodies.

Confocal laser laparoscopy and near-infrared reflectance confocal microscopy have been used for diagnosis purpose using normal and abnormal liver samples *ex vivo* and *in vivo* [Campo-Ruiz et al., 2005;Goetz et al., 2008b]. The results in section 9.2 demonstrate for the first time the use of confocal microscopic imaging technique to visualise the distribution and the redistribution of photosensitiser in intact tissue *ex vivo*.

Through the intact surface of liver, confocal microscopy imaging of freshly excised livers allowed a clear observation of the liver architecture with the presentation of parenchyma and vascular structure. Detailed cellular information such as individual hepatocytes and their nuclei were also visualised without the use of contrast agents (Figure 9.7A and B). The granular distribution of Amphinex was depicted, indicating that using confocal microscopy to observe the intracellular distribution of photosensitiser in tissues is feasible (Figure 9.7AB and Figure 9.8). Moreover, the distinct difference in the distribution of Amphinex before and after illumination also implies that a further use of confocal laser endomicroscopy may be a feasible technique for *in vivo* observation of photosensitisers. This is particularly beneficial to PCI mechanism studies where the redistribution of photosensitisers can therefore be monitored real time *in vivo*.

Using immunohistochemistry (IHC), the present study continued the previous work [Woodhams et al., 2009] and demonstrated the relocalisation of saporin in liver after Amphinex PCI treatment (Figure 9.9). Attempts have been made to detect the changes of saporin distribution in MC28 tumours after illumination using the same method but the results were not convincing (data not shown). It may be because the staining protocols have to be adjusted when applied to different tissues. The successful detection of the distribution of saporin in kidney (data not shown) gives another implication that the uptake of saporin in tumour may be never high enough for IHC staining since kidney and liver are known as the two organs with higher type I RIPs accumulation [Battelli, 2004]. It is also possible that the time point chosen for examination (4 hrs after irradiation, in this case) was not appropriate. Since the relocalisation of saporin in rat liver was observed using the liver sampled 30min after exposure to light, experiments choosing earlier sampling time points should be considered for future studies.

Together with the presented studies, other experiments also have been attempted for the aims of this chapter but with less success. In the experiment using the immunofluorescence (IF) staining method (using fluorescence labelled second antibodies) to detect saporin in liver, it was found that the resolution was insufficient to draw conclusions. In general, owing to the specific detection wavelength used, IF staining should give better specificity than IHC method. However, optimal staining protocols and the imaging setup were difficult to establish using either frozen or paraffin embedded liver sections. Therefore, satisfactory results were not obtained.

To summarise, the studies of this chapter have attempted to approach the *in vivo* mechanism of PCI. Using TUNEL assay, the results show that apoptosis can be induced by Amphinex PDT and PCI where cells with fragmented DNA were observed in treated liver and tumour samples. The distribution and relocalisation of Amphinex and saporin in liver before and after PCI were demonstrated using confocal microscopy and immunohistochemistry respectively. Further studies are required to understand the *in vivo* PCI mechanisms in details which will provide relevant information for clinical applications.

Section D: Discussion

General Discussion

Photochemical internalisation is attracting interest as a novel technology for improving macromolecular drug delivery to cells. It is a technique based on photodynamic therapy but in combination with membrane-associated photochemical reactions that enable site-specific light-induced drug delivery. Amphinex, a disulfonated chlorin ($TPCS_{2a}$), is a new photosensitiser designed for PCI. Investigations of the PCI effects using Amphinex in combination with saporin or bleomycin, two anti-cancer agents, were carried out *in vitro* and *in vivo* in this thesis. Using bioconjugates for their uses for PDT and PCI was studied in a separate chapter. Below is the general discussion of the studies in this thesis.

PCI with Amphinex vs $TPPS_{2a}$ and $AlPcS_{2a}$ in vitro and in vivo

Because $TPPS_{2a}$ and $AlPcS_{2a}$ are the most common photosensitisers for PCI, *in vitro* studies of Amphinex were compared to the results using these two sensitisers. It was found that Amphinex displayed the same efficient and concentration-dependent cellular uptake as $TPPS_{2a}$. In combination with saporin or bleomycin, enhanced cytotoxicity was found after PCI using these three photosensitisers in either A431 or HN5 cells although the synergistic killing effect was not obvious using bleomycin. For instance, Amphinex PCI of saporin induced the greatest cell kill by a factor of 29 compared to saporin alone in HN5 cells, whereas the cell viability only reduced by a factor of 3 compared to bleomycin alone.

For *in vivo* studies, the treatment efficacy of Amphinex PCI was investigated by measuring the extent of necrotic lesions induced in normal rat liver/colon and transplantable sarcoma tumour models. Although PCI treatments on normal tissues were designed to look at the influence of different treatment parameters (e.g. the dose of saporin/bleomycin and their administration time points) and the comparison of treatment responses between these two anti-cancer drugs in two tissues, the results also point out another important fact that Amphinex PCI in combination with bleomycin induced significantly larger necrotic lesions compared to PDT alone in both liver and colon. Using certain concentrations of bleomycin, the increased size of lesions was comparable to PCI of saporin. The results of treatments on tumours are consistent with the ones on normal tissues that Amphinex PCI of bleomycin can induce analogous enhancement in tumour destruction to the treatment using saporin.

Altogether, Amphinex PCI in combination with bleomycin seems to induce more pronounced cytotoxicity *in vivo* than *in vitro*. Similar findings were reported by Berg et al. (personal communication). The well-known selective toxicity of bleomycin towards different cells, different tumours and organs may explain this, since bleomycin causes DNA damage through multiple mechanisms and the consequent cellular response and repair pathways vary between cells as well [Chen and Stubbe, 2005].

Treatment responses of Amphinex PDT and PCI in vivo: normal vs tumour tissues

The pharmacokinetics of Amphinex in Wistar rats and the drug accumulation between normal and tumour tissues of Hooded Lister rats at the time of light delivery was studied in Chapter 6 and 8. The selectivity of Amphinex in terms of the response to its treatments in normal and tumour tissues can also be examined by comparing the depth of necrosis induced after treatments, although two tissues were derived from different animals. Figure D.1 shows a comparison of the depth of necrosis induced in rat liver and transplanted MC28 tumours between PDT and PCI treatment. The measurement was based on the H&E stained tissue sections and the data presented here was collected from the same sections used for other measurements described in the chapters.

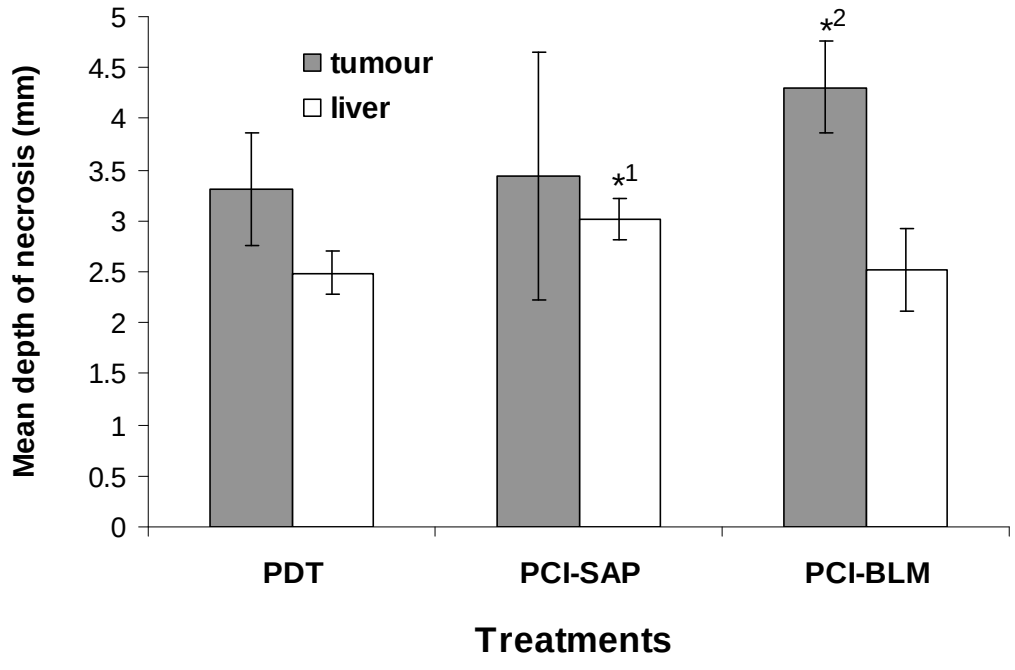

Figure D.1 Mean depth of necrosis induced after Amphinex PDT and PCI treatments in normal rat liver and transplanted MC28 tumours. PDT treatment: 0.25 mg/kg Amphinex, 652nm laser 10J (50mW x 200s), 24hrs drug light interval. Saporin (250 μg/kg) was administered (i.v.) 1h before light; bleomycin (30 IU/kg) was administed (i.v.) 30min before light. (*1: $p < 0.01$; *2: $p = 0.02$)

The depth of necrosis in tissues induced after treatment is an indicator of treatment efficacy and deeper necrosis would certainly benefit the treatment of large tumours. As shown in Figure D.1, tumour tissues are more susceptible to Amphinex PDT and PCI treatments in which deeper necrosis on average was measured compared to the value for liver. This might be due the different optical properties between tissues since more light will be absorbed by liver rather than tumour and results in shorter light penetration depth in treatments in liver. The variation of the necrosis depth in tumour was found to be larger than in liver which was due to the difficulty in the measurement as the necrotic lesions were often observed to be irregular as described in Chapter 8.

In comparison between PDT and PCI treatments, significant enhancements in the depth of necrotic lesions were only observed in PCI of saporin in liver and PCI of bleomycin in tumour. This may be due to the amount of anti-cancer agents in these two tissues that saporin accumulates more in liver than tumour and bleomycin displays the opposite biodistribution. It should also be noted that the treatment on liver was optimised after varying several treatment parameters whereas the protocols for tumour treatments were adopted from the above. In other words, it is possible that the mean depth of necrosis in tumour after Amphinex PDT or PCI can be larger than the present results under optimal treatment conditions. Nevertheless, the enhancement by PCI would reduce the required PDT dose to achieve the same therapeutic effect which is indeed the original concept of PCI treatment.

Clinically, the important selectivity is the difference of the drug uptake and/or the treatment responses between tumour and the tissue of origin of the tumour. Using models such as hamster cheek pouch tumour model can provide a more suitable platform for a direct comparison.

Amphinex vs m-THPC PDT

m-THPC is a clinical approved photosensitiser which is one of the most powerful sensitisers used for PDT. The similarities in the optical characteristics (e.g. strong absorption at 649 nm) of Amphinex and m-THPC, as well as their singlet oxygen quantum yields [Mojzisova et al., 2009], indicate the potential of Amphinex being an effective photosensitising agent. Studies of PDT using m-THPC in normal rat colon and MC28 tumours have been published from our laboratory [Tsutsui et al., 2002]. The laser powers used in the previous study were 20 mW and 100mW for treatment in colon and

were 5 mW and 100mW in the cases of tumour treatments which are different from present study (50 mW), but information still can be obtained from the value in between. Other treatment parameters such as the light dose (10 J), the light source (a 652 nm laser) and the drug-light-interval (24 hr) were the same, and the dose of photosensitiser were also similar (0.3 mg/kg for m-THPC and 0.25 mg/kg for Amphinex). The results in the previous study showed that the mean diameter of necrosis in colon induced by m-THPC PDT was less than 4 mm which is similar to the results in present study (Figure 8.9). However, PDT using m-THPC can induce necrosis in tumour about 4-6 mm in depth which was deeper than the treatment response of Amphinex PDT (Figure D.1). In this regard, m-THPC PDT is more effective in inducing damage to tumour.

Mechanistic studies and treatment monitoring

According to the results of histological examination and TUNEL assay on liver and tumour samples, both necrosis and apoptosis can be induced by Amphinex PDT and PCI. The distribution of Amphinex and the relocalisation of Amphinex and saporin were imaged by *ex vivo* confocal microscopy and immunohistochemistry.

The results together point out the importance of timing for mechanistic studies since the light-induced drug delivery process and consequent treatment responses are dynamic. Different photosensitisers, drugs and target tissues employed may lead to distinct results. The gathered information from different time points will be useful for the understanding of treatments and beneficial to treatment optimisation.

Light delivery

The light delivery system in the *in vivo* experiments in this thesis was using a laser with a bare tip fibre. Light treatments were carried out by perpendicularly placing the fibre against the surface of liver/colon or inserting the fibre just into the top of tumours. By using a point source of light on the tissue, measurement of the macroscopic dimensions of the zone of necrosis produced is a convenient way of comparing the effect of different treatment parameters, a technique we have used successfully for many years in a range of organs. One advantage of this technique is that all the light from the fibre is delivered directly into the tissue, like the system used for interstitial PDT treatment in clinic, whereas using external illumination results in reflection losses. The difference in the light delivery may be the reason for the diverse histological results between the tumours treated with Amphinex PDT in this study and the tumours treated with $AlPcS_{2a}$

PDT from another group [Norum et al., 2009a]. In their study, a rim of viable tumour cells was observed to be on the top of the subcutaneous tumour 5 days after treatment. Although the samples in our study were collected 24 hrs after light delivery, a more light-dependent distribution of necrosis was found to be from the top to the centre of tumours.

Conclusions and Future Work

This thesis is a study of photochemical internalisation and aimed to investigate the PCI effects induced by a new photosensitiser, Amphinex, in combination with two anti-cancer agents, saporin and bleomycin, both *in vitro* and *in vivo*.

Prior to the introduction to cells, the photophysical properties of Amphinex were examined and the results show that Amphinex has favourable photophysical properties as an efficient photosensitiser including the strong absorption in red region and photostable (less photobleaching). In combination with saporin, Amphinex PCI displayed a synergistic inhibition of cell growth with two cell lines, and an increased cytotoxicity was also measured in combination with bleomycin.

In the *in vivo* studies, pharmacokinetic studies using quantitative fluorescence microscopy showed highest-uptake of Amphinex in liver at 6hrs after drug administration. The amounts in other organs were lower and a clear decrease was observed in skin up to 8 days after injection. In addition, considerable drug concentration ratios of tumour to normal tissues (e.g. skin and muscle) were measured at 24hr after administration, which indicate the selectivity of Amphinex in normal and tumour tissues. Significant enhancement in inducing the necrosis was observed by Amphinex PCI compared to PDT treatment on normal rat liver/colon and transplanted sarcoma models.

In Chapter 9, experiments focused on looking at several *in vivo* Amphinex PCI mechanisms. The PCI effect, the redistribution of Amphinex and saporin after illumination was observed in liver. In addition, similar treatment responses (i.e. necrosis and apoptosis) were found between Amphinex PDT and PCI.

Bioconjugation was also applied to PCI strategy in this thesis in which a bioconjugate Tat-TPP (a cell penetrating peptide, Tat peptide conjugated with tetraphenylporphine) and an $AlPcS_{2a}$-saporin conjugate were synthesized. In the former study, unlike non-water soluble TPP, the Tat-TPP conjugate became bioavailable and amphiphilic. The results show that the Tat-TPP conjugate exhibited a high cellular accumulation and lysosomal localisation, resulting in synergistic cell kill effects in combination with

saporin in HN5 cells upon irradiation. In the later study, the $AlPcS_{2a}$-saporin conjugate was designed to combine the photosensitiser and the delivered macromolecule. The conjugate demonstrate a comparable PCI effect, inducing a similar cytotoxicity to the results using unconjugated $AlPcS_{2a}$ and saporin in HN5 cells after exposure to light.

The overall results in this thesis have established that Amphinex is an efficient photosensitiser for PCI. The consistency between *in vitro* and *in vivo* experiments indicates that Amphinex has the potential for clinical utilization by enhancing the delivery of co-administered anti-caner drugs.

The first clinical trial of Amphinex PCI of bleomycin is currently being undertaken for head and neck cancers in University College London Hospital. The preliminary results from the first few patients are encouraging. A short description is given in Appendix II.

Like PDT, the key advantage of PCI is the site specificity due to the light-dependent activation of photosensitisers which are co-administered with the macromolecule. The photochemical effect therefore only takes place in areas under light exposure. With this localized treatment effect and the use of sub-lethal PDT dose, PCI should result in lower side-effects.

Future work is firstly aimed to optimise the treatment parameters (i.e. the lowest drug and light dose enables the maximum therapeutic efficacy) under the safety guidelines obtained from the current trial. Different illumination regimes (i.e. light fractionation and low fluence rate) may provide options for enhancing the therapeutic effect of Amphinex PCI since these strategies are beneficial to PDT with ALA and m-THPC [Curnow et al., 1999;de Haas et al., 2008;Robinson et al., 1998;Tsutsui et al., 2002].

Studies on the skin phototoxicity of Amphinex PCI are also essential. Although the pharmacokinetics results in this thesis showed a clear decrease of Amphinex level in rat skin up to 8 days after administration, skin photosensitivity may be minimal but needs further solid investigation. Other experiments such as using confocal endomicroscopy to monitor PCI in real time *in vivo* and further investigations of the cell death in response to treatment can be of benefit to the understanding of Amphinex PCI.

The combination with targeted drugs such as immunotoxins is another future study of interest which could enhance treatment selectivity. A recently published study demonstrated the use of a fusion toxin for PCI which was composed of gelonin and a recombinant single-chain antibody against a marker protein associated with a large number of cancer cells [Selbo et al., 2009]. This construct was able to inhibit tumour growth significantly. The results indicated the potential using targeted anti-cancer drugs for PCI application *in vivo* in which improved therapeutic efficacy can be achieved by increasing the specificity of drug uptake to target tissues.

Appendix I

The synthesis of conjugates of Tat-TPP and $AlPcS_{2a}$-saporin

- **Tat-TPP Conjugate**

General Remarks

This work was carried out at the department of Pharmacy and Pharmacology, University of Bath. Chemical reagents were purchased from Sigma-Aldrich, Fluka, Acros, Lancaster and Novabiochem. All other solvents were purchased from Fisher Scientific and used as received. Peptide grade dimethylformamide was purchased from Rathburn Chemicals Ltd. Preparative RP-HPLC was performed on a Dionex HPLC system consisting of an Ultimate 3000 WPS autosampler, a P680 preparative pump (HPG), a UVD 170U multiwavelength detector, and a Foxy Jr fraction collector. The purifications were performed on a Phenomenex Gemini 5 μm C-18 (250 x 30 mm) column with a flow rate of 22.5 mL/min. Mobile phase A was 0.1% TFA in water, mobile phase B was 0.1% TFA in acetonitrile. High resolution mass spectrometry was performed using a Bruker MicroTOF autospec ESI mass spectrometer.

Synthesis

Porphyrin **1**[Sibrian-Vazquez et al., 2007] was prepared from **2** by acylation with maleimidopropionic acid (F. Giuntini and I. M. Eggleston, unpublished). The peptide sequence GRKKRRGRRRGYKC was assembled on an Activo P11 automated peptide synthesizer (Activotec, Cambridge, UK) on a 0.32 mmol scale on Rink Amide MBHA resin (Novabiochem), according to Fmoc-SPPS strategy. The resin was loaded using a 5-fold excess of Fmoc-protected aminoacid, using HOBt/DIC as the activating agents (5 cycles). The chain-elongation couplings were performed using a 3-fold excess of the protected amino acid, using PyBOP as the activating agent (double coupling). Deprotections were accomplished by washing the resin with 20% piperidine in DMF (3 x 3 min). Cleavage from the resin and deprotection was performed by treatment with TFA/water/TIS/EDT (94/2.5/2.5/1 volume ratio) during 3 hours. The peptide was purified by semi-preparative RP-HPLC (mobile phase A: 0.1% aq TFA, mobile phase B: 0.1% TFA in MeCN). Conjugate **3** was obtained as follows: 5 mg of peptide were dissolved in DMSO (200 μL), and the resulting solution was added to a solution of **2** (6 mg) in DMSO (200 μL), containing pyridine (3 μL). The mixture was shielded from light, and was allowed to stand overnight at room temperature. The mixture was then

partitioned between ethyl acetate and deionised 0.1% aq TFA. The aqueous layer was evaporated to a small volume, and applied to a Discovery DSC-18 solid phase extraction cartridge (Supelco). The desired compound was eluted with (5% MeCN-0.1% aq TFA) mobile phase: and lyophilised to give 9 mg of **3**, which was characterised by high resolution mass spectrometry.

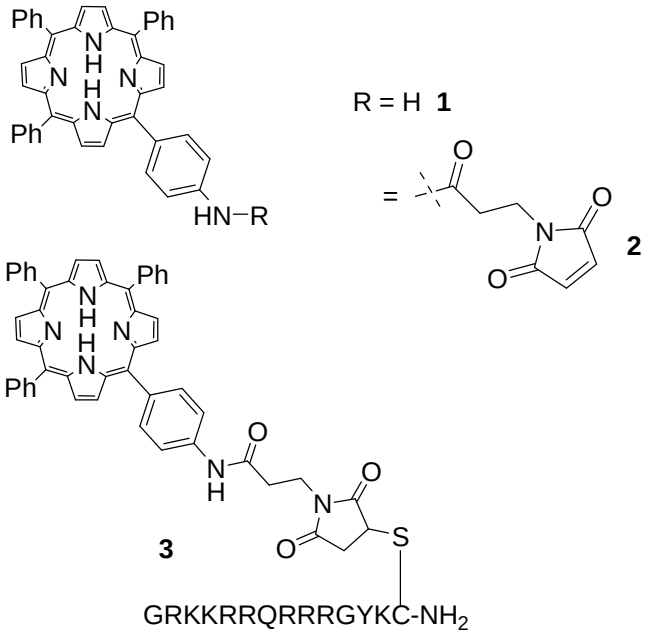

Abbreviations:

DIC: diisopropyl carbodiimide

DMF: dimethylformamide

DMSO: dimethylsulfoxide

EDT: ethanedithiol

HOBt: 1-hydroxybenzotriazole

PyBOP: benzotriazol-1-yl-oxytripyrrolidinophosphonium hexafluorophosphate

PyBrOP: Bromo-*tris*-pyrrolidino phosphoniumhexafluorophosphate

SPE: solid phase extraction

TFA: trifluoroacetic acid

TIS: triisopropylsilane

- **$AlPcS_{2a}$-saporin Conjugate**

Materials and Methods

The materials utilized in the conjugation methods were purchased from Sigma-Aldrich (Sigma-Aldrich, UK) otherwise stated: *N*-succinimidyl 3-(2-pyridyldithio) propionate (SPDP) reagent, dimethylsulfoxide (DMSO), Phosphate buffered saline with EDTA (PBS-EDTA): 100 mM sodium phosphate, 150 mM NaCl, 1 mM EDTA, 0.02%, sodium azide, pH 7.5. Dithiothreitol (DTT), Desalting column (Zeba™ Desalt Spin Columns). Dialysis tubing (Tubing Specta/Por Biotech dialysis membrane, Fisherscientific) 500 molecular weight cut off (MWCO). Sephadex G-50 Fine GE Healthcare. This work was carried out at School of Biological Science, University of Essex.

Synthesis of $AlPcS_{2a}$-SPDP linker (1-4)

$AlPcS_{2a}$ **1** (50mg, 63.6 µM) was dissolved in thionyl chloride (5 ml); the mixture was refluxed for 8 h. The excess of thionyl chloride was evaporated under vacuum and the residue was washed with dichloromethane (DCM) several times, and then evaporated to obtain pure dichlorosulfonyl phthalocyanine **2.** β-Alanine hydrazine (32 mg, 159 µM) was dissolved in dimethylformamide (DMF, 5 ml) under Argon. $AlPcS_{2a}$ dichloride, Compound **2** was dissolved in 5 ml of DMF and added to the above solution. The mixture was heated to 50ºC and stirred for 12 h. The excess of solvent was evaporated under high vacuum to dryness, and the residue was dissolved in DCM and washed with water. The organic layer was dried with $MgCl_2$ and then the solvent was evaporated. The residue was purified on silica gel using 20% methanol and DCM, the layer of Phthalocyanin-alanin **3** with R_f 0.2 was collected. Compound **3** was dissolved in DCM 10 ml under Argon and 1 ml of trifluoroacetic acid (TFA) was added to remove BOC group. The mixture was stirred for 2h, and then solvents were evaporated in vacuum.

Compound 5

SPDP Reagent (20 mM solution) was prepared in DMSO (2 mg reagent in 320 µl of DMSO). SPDP solution (25 µl of the 20 mM) was added to 2-5 mg of $AlPcS_{2a}$ dissolved in 1.0 ml of PBS-EDTA. The reaction mixture was incubated overnight at room temperature. SPDP-$AlPcS_{2a}$-ß-alanine was dialyzed in 2L of ultrapure water using dialysis membrane 500 MWCO to remove byproducts and excess non-reacted SPDP reagent. DTT (23 mg) was dissolved in 1 ml PBS-EDTA. DTT solution and was added

0.5 ml per 1 ml of SPDP-$AlPcS_{2a}$ (results in 50 mM DTT) to reduce the disulfide bridge and prepare sulfhydryl terminal group for conjugating with saporin. The solution was kept stirring overnight, then dialyzed again using 500 MWCO dialysis membranes for one day.

Compound 6

The above procedure for solution A was repeated using saporin instead of $AlPcS_{2a}$ without reducing the disulfide bridge of SPDP linker. The reaction mixture was kept stirring gently overnight at 4ºC. The solution of saporin was eluted on desalting column, which was previously equilibrated with PBS-EDTA, to remove the DTT. Solution A ($AlPcS_{2a}$-SPDP) with free sulfhydryl terminal was stirred with solution B (saporin-SPDP) in (20mM PBS-EDTA at pH 7.5) over for 18 h at 4C. The reaction mixture was dialyzed in 2L of pure water for 6h at 4C. The $AlPcS_{2a}$-saporin was purified on Sephadex and eluted with PBS. The first band, which contains $AlPcS_{2a}$-saporin was collected.

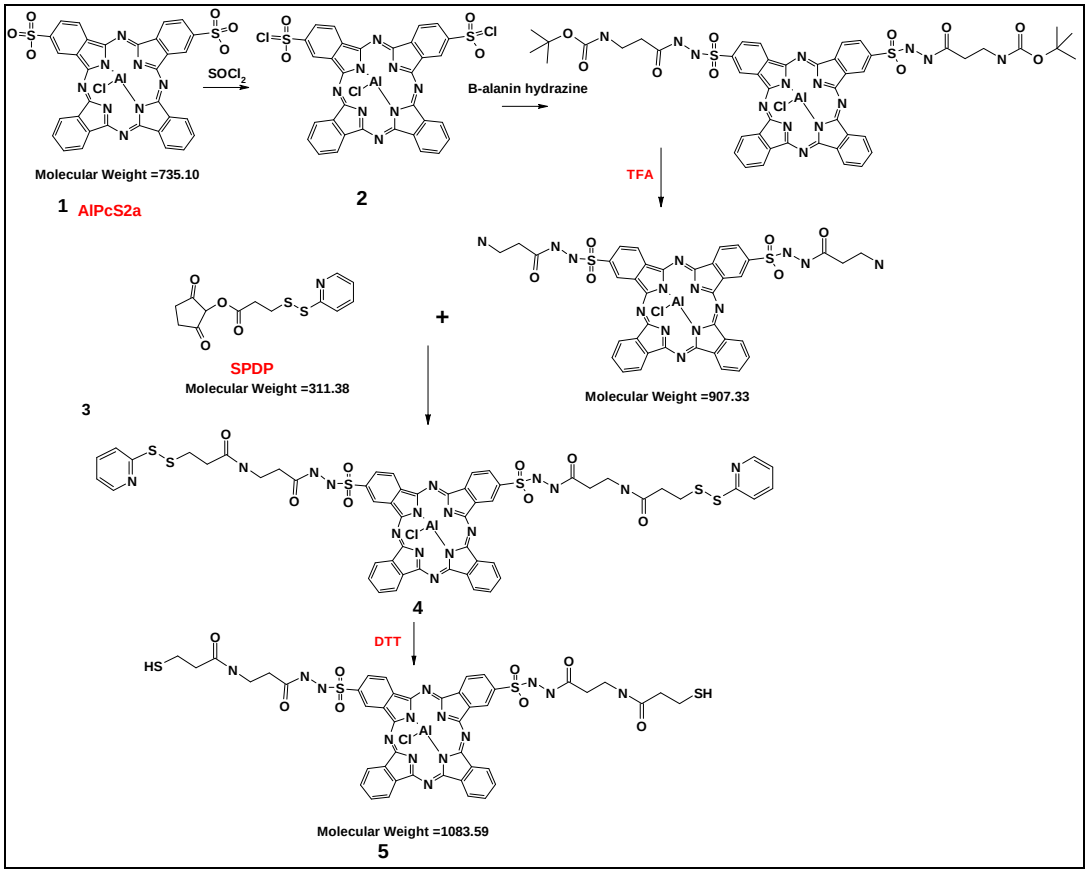

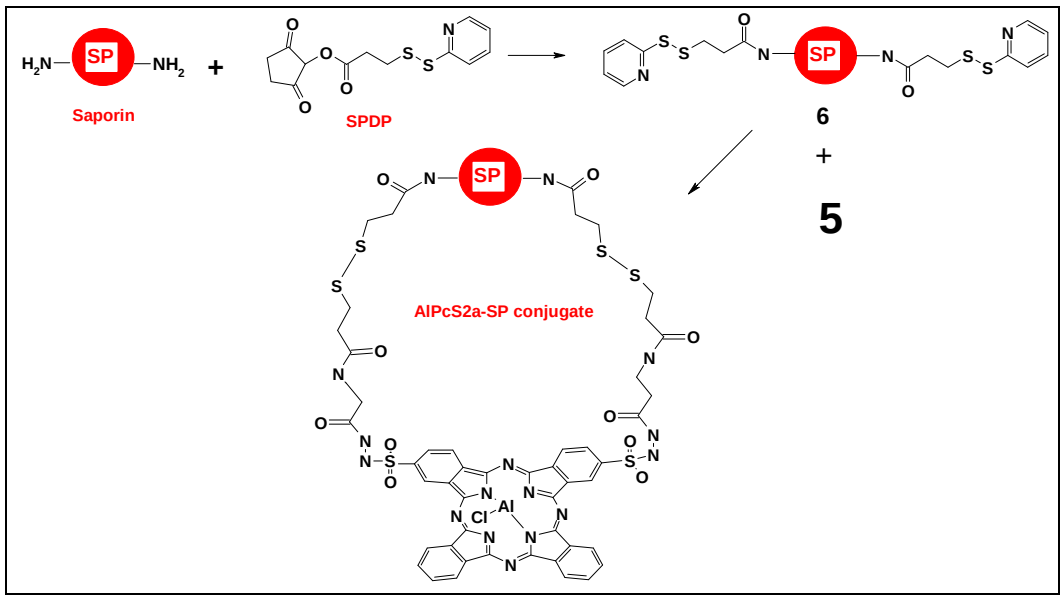
Saporin
SPDP
6
+
5
AlPcS2a-SP conjugate

Appendix II PCI “First in man”

Based at least partly on the results described in this thesis, the first trial of PCI in man has recently started in University College London Hospital. The first patient was a 56 year old man with a chondroblasticosteosarcoma of the jaw which had failed to respond satisfactorily to surgery, radiotherapy and chemotherapy. No further conventional treatments were possible for him. The tumour had destroyed much of the right side of the face and a metal plate had been inserted to close the hole between the mouth and the skin, caused by the cancer. The prominent nodule at the front of the cancer, marked with an arrow in Figure 1 (shown on day 0, the day Amphinex was given) was chosen as the “target” lesion for PCI as it was the easiest area to document the extent of the PDT effect. Four days later, bleomycin was given, followed 3 hours after this by light delivery to the entire tumour surface. Darkening of the target lesion was seen almost as soon as light delivery was completed. Changes to the less vascular parts of the tumour back as far as the ear were less obvious at this stage (Figure 2). By 7 days (Figure 3), changes were apparent over the whole tumour area and by day 14 (Figure 4) the target lesion was black and completely necrotic with considerable loss of volume. Some other parts of the tumour had also sloughed. The metal plate, previously hidden by tumour, had become partly visible (arrow inset).

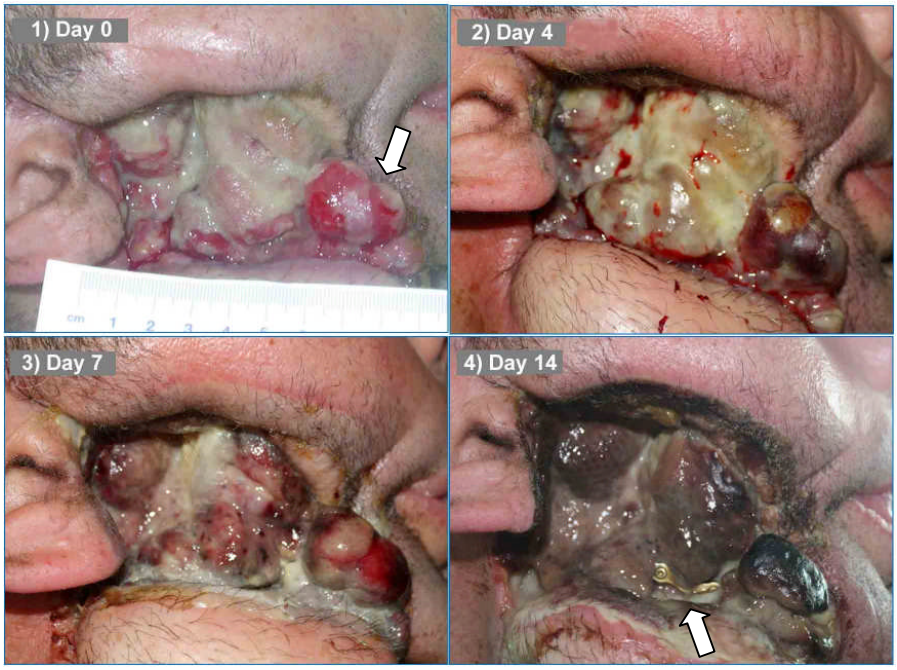

Figure Chondroblasticosteosarcoma of jaw. (1) Day 0, administration of Amphinex, (2) Day 4 Immediately after light delivery, (3) Day 7, 3days after light delivery, (4) Day 14, 10 days after light delivery.

Although the patient had moderate pain in the first 24 hours after treatment, this soon settled. Tests of skin sensitivity to simulated sunlight showed no evidence of any effect.

As a “first in man” procedure, the treatment conditions had been chosen to be gentle, so it was a surprise to see such a dramatic and beneficial effect on the tumour with minimal effect on normal skin. This trial is on-going, but augurs well for the future of PCI as a clinical therapy.

I thank Dr Waseem Jerjes and Mr Colin Hopper from the Department of Oral & Maxillo-Facial Surgery, UCH, for permission to include this brief report in my thesis.

Appendix III Conference Presentations

13th Congress of the European Society of Photobiology, Wroclaw, Poland (September 5th-10th ,2009)

- **Tzu-wen** (**Julie) Wang**, Alexander J. MacRobert, Kristian Berg, Anders Høgset, Stephen G. Bown. Photodynamic therapy and photochemical internalisation on a transplanted rat fibrosarcoma using $TPCS_{2a}$ (Oral presentation)

12th World Congress of the International Photodynamic Association, Seattle, USA (June 11th-15th, 2009)

- **Tzu-wen (Julie) Wang,** Josephine Woodhams, Alexander J. MacRobert, Kristian Berg, Anders Høgset, Stephen G. Bown. Investigation of PDT and photochemical internalisation using a sulfonated chlorin $TPCS_{2a}$ photosensitiser in combination with anti-cancer drugs *in vivo* (Oral presentation)

- **Tzu-wen (Julie) Wang,** Francesca Giuntini, Ian M. Eggleston, Stephen G. Bown, Alexander J. MacRobert. Investigation of a Tat peptide-photosensitiser bioconjugate for photodynamic therapy and photochemical internalisation. (Oral presentation)

1st Scientific Meeting of Head and Neck Optical Diagnosis Society, London, UK (March 14th, 2009)

- **Tzu-wen** (**Julie) Wang**, Alexander J. MacRobert, Stephen G. Bown. Investigation of photochemical internalisation in HN5 head and neck carcinoma cells and in an *in vivo* rat model. (Poster presentation)

7th International Symposium on Photodynamic Therapy and Photodiagnosis in Clinical Practice, Brixen, Italy (October 7th-11th, 2008)

- **Tzu-wen** (**Julie) Wang**, Alexander J. MacRobert, Stephen G. Bown. Investigation of the effect of $TPCS_{2a}$ PCI in combination with saporin *in vitro* and *in vivo*. (Poster presentation)

12th Congress of the European Society of Photobiology, Bath, UK (September 1st-6th,2007)

- **Tzu-wen** (**Julie) Wang**, Stephen G. Bown, Alexander J. MacRobert. Photochemical internalisation can enhance the cytotoxicity of bleomycin and saporin in the A431 cell line. (Oral presentation)

11th World Congress of the International Photodynamic Association, Shanghai, China (March 28th-31rd, 2007)

- **Tzu-wen (Julie) Wang,** Kristian Berg, Stephen G. Bown, Alexander. J MacRobert. Enhanced cytotoxicity of bleomycin and saporin in the A431 cell line using photochemical internalisation (PCI) (Oral presentation)

Tetrapyrrole Disscussion Group Meeting, London, UK (January 5th 2007)

- **Tzu-wen** (**Julie) Wang**, Stephen G. Bown, Alexander J. MacRobert. Enhanced cytotoxicity of bleomycin and saporin using photochemical internalization with a phthalocyanine sensitiser. (Poster presentation)

Appendix IV Publications

Papers have been submitted:

- Julie T-W Wang, Francesca Giuntini, Ian M. Eggleston, Stephen G. Bown, Alexander J. MacRobert. Investigation of a Tat peptide-photosensitiser bioconjugate for Photodynamic therapy and photochemical internalisation.

Articles currently being prepared for submission:

- Julie T-W Wang, Alexander J. MacRobert, Stephen G. Bown, Kristian Berg. Review of PCI. The 3rd issue of the CRC Handbook of Organic Photochemistry and Photobiology.

- Julie T-W Wang, Anders Høgset, Kristian Berg, Stephen G. Bown, Alexander. J MacRobert. Investigation of the effect of PCI using a sulfonated chlorin photosensitiser Amphinex in combination with saporin *in vitro*.

- Julie T-W Wang**,** Kristian Berg, Anders Høgset, Alexander J. MacRobert, Stephen G. Bown. Investigation of PDT and photochemical internalisation using a sulfonated chlorin photosensitiser Amphinex in combination with anti-cancer drugs *in vivo*.

- Julie T-W Wang, Kristian Berg, Anders Høgset, Alexander J. MacRobert, Stephen G. Bown. Photodynamic therapy and photochemical internalisation on a transplanted rat fibrosarcoma using a sulfonated chlorin photosensitiser Amphinex.

References

Adigbli DK, Wilson DG, Farooqui N, Sousi E, Risley P, Taylor I, Macrobert AJ, Loizidou M (2007) Photochemical internalisation of chemotherapy potentiates killing of multidrug-resistant breast and bladder cancer cells. *Br J Cancer* **97**: 502-512

Agarwal ML, Clay ME, Harvey EJ, Evans HH, Antunez AR, Oleinick NL (1991) Photodynamic therapy induces rapid cell death by apoptosis in L5178Y mouse lymphoma cells. *Cancer Res* **51**: 5993-5996

Allen CM, Langlois R, Sharman WM, La MC, van Lier JE (2002) Photodynamic properties of amphiphilic derivatives of aluminum tetrasulfophthalocyanine. *Photochem Photobiol* **76**: 208-216

Amano T, Prout GR, Jr., Lin CW (1988) Intratumor injection as a more effective means of porphyrin administration for photodynamic therapy. *J Urol* **139**: 392-395

Amirkhosravi M, Francis JL (1993) Procoagulant activity of the MC28 fibrosarcoma cell line in vitro and in vivo. *Br J Haematol* **85**: 736-744

Anderson WF (1998) Human gene therapy. *Nature* **392**: 25-30

Austwick MR, Woodhams JH, Chalau V., Mosse CA, Eliot C, Lovat LB, Macrobert AJ, Bigio IJ, Bown S (2009) Optical pharmacokinetics for drug dosimetry in photodynamic therapy. Submitted for publications.

Baas P, Michielsen C, Oppelaar H, van ZN, Stewart FA (1994) Enhancement of interstitial photodynamic therapy by mitomycin C and EO9 in a mouse tumour model. *Int J Cancer* **56**: 880-885

Barbieri L, Battelli MG, Stirpe F (1990) Blood clearance and organ distribution and tissue concentration of native, homopolymerized and IgG-conjugated ribosome-inactivating proteins. *Xenobiotica* **20**: 1331-1341

Barbieri L, Battelli MG, Stirpe F (1993) Ribosome-inactivating proteins from plants. *Biochim Biophys Acta* **1154**: 237-282

Bareford LM, Swaan PW (2007) Endocytic mechanisms for targeted drug delivery. *Adv Drug Deliv Rev* **59**: 748-758

Barel A, Jori G, Perin A, Romandini P, Pagnan A, Biffanti S (1986) Role of high-, low- and very low-density lipoproteins in the transport and tumor-delivery of hematoporphyrin in vivo. *Cancer Lett* **32**: 145-150

Barr H, Chatlani P, Tralau CJ, Macrobert AJ, Boulos PB, Bown SG (1991) Local eradication of rat colon cancer with photodynamic therapy: correlation of distribution of photosensitiser with biological effects in normal and tumour tissue. *Gut* **32**: 517-523

Barr H, Macrobert AJ, Tralau CJ, Boulos PB, Bown SG (1990) The significance of the nature of the photosensitizer for photodynamic therapy: quantitative and biological studies in the colon. *Br J Cancer* **62**: 730-735

Bastogne T, Tirand L, Bechet D, Barberi-Heyob M, Richard A (2007) System identification of photosensitiser uptake kinetics in photodynamic therapy. *Biomedical Signal Processing and Control* **2**: 217-225

Battelli MG (2004) Cytotoxicity and toxicity to animals and humans of ribosome-inactivating proteins. *Mini Rev Med Chem* **4**: 513-521

Battelli MG, Barbieri L, Stirpe F (1990) Toxicity of, and histological lesions caused by, ribosome-inactivating proteins, their IgG-conjugates, and their homopolymers. *APMIS* **98**: 585-593

Bellnier DA, Ho YK, Pandey RK, Missert JR, Dougherty TJ (1989) Distribution and elimination of Photofrin II in mice. *Photochem Photobiol* **50**: 221-228

Belzacq AS, Jacotot E, Vieira HL, Mistro D, Granville DJ, Xie Z, Reed JC, Kroemer G, Brenner C (2001) Apoptosis induction by the photosensitizer verteporfin: identification of mitochondrial adenine nucleotide translocator as a critical target. *Cancer Res* **61**: 1260-1264

Berg K, Bommer JC, Moan J (1989a) Evaluation of sulfonated aluminum phthalocyanines for use in photochemotherapy. A study on the relative efficiencies of photoinactivation. *Photochem Photobiol* **49**: 587-594

Berg K, Bommer JC, Moan J (1989b) Evaluation of sulfonated aluminum phthalocyanines for use in photochemotherapy. Cellular uptake studies. *Cancer Lett* **44**: 7-15

Berg K, Bommer JC, Winkelman JW, Moan J (1990) Cellular uptake and relative efficiency in cell inactivation by photoactivated sulfonated meso-tetraphenylporphines. *Photochem Photobiol* **52**: 775-781

Berg K, Dietze A, Kaalhus O, Hogset A (2005a) Site-specific drug delivery by photochemical internalization enhances the antitumor effect of bleomycin. *Clin Cancer Res* **11**: 8476-8485

Berg K, Moan J (1994) Lysosomes As Photochemical Targets. *International Journal of Cancer* **59**: 814-822

Berg K, Prasmickaite L, Selbo PK, Hellum M, Bonsted A, Hogset A (2003) Photochemical internalization (PCI)--a novel technology for release of macromolecules from endocytic vesicles. *Oftalmologia* **56**: 67-71

Berg, K., Sandvig, K., and Moan, J. Transfer of molecules into the cytosol of cells. [PCT/NO95/00149]. 1996.

Berg K, Selbo PK, Prasmickaite L, Tjelle TE, Sandvig K, Moan J, Gaudernack G, Fodstad O, Kjolsrud S, Anholt H, Rodal GH, Rodal SK, Hogset A (1999) Photochemical internalization: a novel technology for delivery of macromolecules into cytosol. *Cancer Res* **59**: 1180-1183

Berg K, Selbo PK, Weyergang A, Dietze A, Prasmickaite L, Bonsted A, Engesaeter BO, ngell-Petersen E, Warloe T, Frandsen N, Hogset A (2005b) Porphyrin-related photosensitizers for cancer imaging and therapeutic applications. *J Microsc* **218**: 133-147

Berg K, Hogset A, Prasmickaite L, Weyergang A, Bonsted A, Dietze A, Lou PJ, Bown S, Norum OJ, Mollergard HMT, Selbo PK (2006) Photochemical internalization (PCI): A novel technology for activation of endocytosed therapeutic agents. *Medical Laser Application* **21**: 239-250

Bisland SK, Lilge L, Lin A, Rusnov R, Wilson BC (2004) Metronomic photodynamic therapy as a new paradigm for photodynamic therapy: Rationale and preclinical evaluation of technical feasibility for treating malignant brain tumors. *Photochemistry and Photobiology* **80**: 22-30

Blant SA, Glanzmann TM, Ballini JP, Wagnieres G, van den BH, Monnier P (2002) Uptake and localisation of mTHPC (Foscan) and its 14C-labelled form in normal and tumour tissues of the hamster squamous cell carcinoma model: a comparative study. *Br J Cancer* **87**: 1470-1478

Boe S, Longva AS, Hovig E (2007) Photochemically induced gene silencing using small interfering RNA molecules in combination with lipid carriers. *Oligonucleotides* **17**: 166-173

Bogoyevitch MA, Kendrick TS, Ng DC, Barr RK (2002) Taking the cell by stealth or storm? Protein transduction domains (PTDs) as versatile vectors for delivery. *DNA Cell Biol* **21**: 879-894

Bohmer RM, Morstyn G (1985) Uptake of hematoporphyrin derivative by normal and malignant cells: effect of serum, pH, temperature, and cell size. *Cancer Res* **45**: 5328-5334

Bolognesi A, Polito L, Tazzari PL, Lemoli RM, Lubelli C, Fogli M, Boon L, de BM, Stirpe F (2000) In vitro anti-tumour activity of anti-CD80 and anti-CD86 immunotoxins containing type 1 ribosome-inactivating proteins. *Br J Haematol* **110**: 351-361

Bonnett R, Charlesworth P, Djelal BD, Foley S, McGarvey DJ, Truscott TG (1999) Photophysical properties of 5,10,15,20-tetrakis(m-hydroxyphenyl)porphyrin-(m-THPP), 5,10,15,20-tetrakis(m-hydroxyphenyl)chlorin (m-THPC) and 5,10,15,20-tetrakis(m-hydroxyphenyl)bacteriochlorin (m-THPBC): a comparative study. *Journal of the Chemical Society-Perkin Transactions 2* 325-328

Bonnett R, Martinez G (2001) Photobleaching of sensitisers used in photodynamic therapy. *Tetrahedron* **57**: 9513-9547

Bonsted A, Engesaeter BO, Hogset A, Maelandsmo GM, Prasmickaite L, Kaalhus O, Berg K (2004) Transgene expression is increased by photochemically mediated transduction of polycation-complexed adenoviruses. *Gene Ther* **11**: 152-160

Bown SG, Tralau CJ, Smith PD, Akdemir D, Wieman TJ (1986) Photodynamic therapy with porphyrin and phthalocyanine sensitisation: quantitative studies in normal rat liver. *Br J Cancer* **54**: 43-52

Boyle RW, Dolphin D (1996) Structure and biodistribution relationships of photodynamic sensitizers. *Photochem Photobiol* **64**: 469-485

Brancaleon L, Moseley H (2002) Laser and non-laser light sources for photodynamic therapy. *Lasers Med Sci* **17**: 173-186

Brand E, Choi HS, Karalis K, Papaioannou T, Fishbein MC, Braunstein G, Wade ME, Lagasse LD, Grundfest WS (1990) Photodynamic therapy of choriocarcinoma transplanted to the hamster cheek pouch. I. Intraperitoneal photosensitization. *Gynecol Oncol* **36**: 200-206

Brasseur N, Ouellet R, La MC, van Lier JE (1999) Water-soluble aluminium phthalocyanine-polymer conjugates for PDT: photodynamic activities and pharmacokinetics in tumour-bearing mice. *Br J Cancer* **80**: 1533-1541

Bremner JC, Adams GE, Pearson JK, Sansom JM, Stratford IJ, Bedwell J, Bown SG, Macrobert AJ, Phillips D (1992) Increasing the effect of photodynamic therapy on the RIF-1 murine sarcoma, using the bioreductive drugs RSU1069 and RB6145. *Br J Cancer* **66**: 1070-1076

Brincker H (1993) Direct intratumoral chemotherapy. *Crit Rev Oncol Hematol* **15**: 91-98

Brooks H, Lebleu B, Vives E (2005) Tat peptide-mediated cellular delivery: back to basics. *Adv Drug Deliv Rev* **57**: 559-577

Brown SB, Brown EA, Walker I (2004) The present and future role of photodynamic therapy in cancer treatment. *Lancet Oncol* **5**: 497-508

Busch TM (2006) Local physiological changes during photodynamic therapy. *Lasers Surg Med* **38**: 494-499

Buytaert E, Callewaert G, Hendrickx N, Scorrano L, Hartmann D, Missiaen L, Vandenheede JR, Heirman I, Grooten J, Agostinis P (2006) Role of endoplasmic reticulum depletion and multidomain proapoptotic BAX and BAK proteins in shaping cell death after hypericin-mediated photodynamic therapy. *FASEB J* **20**: 756-758

Byrne CJ, Marshallsay LV, Ward AD (1990) The composition of Photofrin II. *Journal of Photochemistry and Photobiology B: Biology* **6**: 13-27

Campo-Ruiz V, Lauwers GY, Anderson RR, gado-Baeza E, Gonzalez S (2005) In vivo and ex vivo virtual biopsy of the liver with near-infrared, reflectance confocal microscopy. *Mod Pathol* **18**: 290-300

Cantau C, Pigot T, Manoi N, Oliveros E, Lacombe S (2007) Singlet oxygen in microporous silica xerogel: Quantum yield and oxidation at the gas-solid interface. *Chemphyschem* **8**: 2344-2353

Canti G, Lattuada D, Nicolin A, Taroni P, Valentini G, Cubeddu R (1994) Antitumor immunity induced by photodynamic therapy with aluminum disulfonated phthalocyanines and laser light. *Anticancer Drugs* **5**: 443-447

Canti G, Nicolin A, Cubeddu R, Taroni P, Bandieramonte G, Valentini G (1998) Antitumor efficacy of the combination of photodynamic therapy and chemotherapy in murine tumors. *Cancer Lett* **125**: 39-44

Caron NJ, Torrente Y, Camirand G, Bujold M, Chapdelaine P, Leriche K, Bresolin N, Tremblay JP (2001) Intracellular Delivery of a Tat-eGFP Fusion Protein into Muscle Cells. *Mol Ther* **3**: 310-318

Castano AP, Mroz P, Hamblin MR (2006) Photodynamic therapy and anti-tumour immunity. *Nature Reviews Cancer* **6**: 535-545

Castriciano MA, Donato MG, Villari V, Micali N, Romeo A, Scolaro LM (2009) Surfactant-like behavior of short-chain alcohols in porphyrin aggregation. *J Phys Chem B* **113**: 11173-11178

Chaloin L, Bigey P, Loup C, Marin M, Galeotti N, Piechaczyk M, Heitz F, Meunier B (2001) Improvement of porphyrin cellular delivery and activity by conjugation to a carrier peptide. *Bioconjug Chem* **12**: 691-700

Chang SC, Buonaccorsi GA, Macrobert AJ, Bown SG (1997) Interstitial photodynamic therapy in the canine prostate with disulfonated aluminum phthalocyanine and 5-aminolevulinic acid-induced protoporphyrin IX. *Prostate* **32**: 89-98

Chatlani PT, Bedwell J, Macrobert AJ, Barr H, Boulos PB, Krasner N, Phillips D, Bown SG (1991) Comparison of Distribution and Photodynamic Effects of Di-Sulfonated and Tetra-Sulfonated Aluminum Phthalocyanines in Normal Rat Colon. *Photochemistry and Photobiology* **53**: 745-751

Chen J, Stubbe J (2005) Bleomycins: towards better therapeutics. *Nat Rev Cancer* **5**: 102-112

Colaco M, Misquith S, Bapat MM, Wattiaux-De CS, Wattiaux R (2004) A comparative study of the subcellular distribution of native and deglycosylated gelonin in rat liver and kidney. *Biochem Biophys Res Commun* **319**: 1299-1306

Colussi VC, Feyes DK, Mulvihill JW, Li YS, Kenney ME, Elmets CA, Oleinick NL, Mukhtar H (1999) Phthalocyanine 4 (Pc 4) photodynamic therapy of human OVCAR-3 tumor xenografts. *Photochem Photobiol* **69**: 236-241

Console S, Marty C, Garcia-Echeverria C, Schwendener R, Ballmer-Hofer K (2003) Antennapedia and HIV Transactivator of Transcription (TAT) "Protein Transduction Domains" Promote Endocytosis of High Molecular Weight Cargo upon Binding to Cell Surface Glycosaminoglycans. *J Biol Chem* **278**: 35109-35114

Crum ED (1993) Effect of cisplatin upon expression of in vivo immune tumor resistance. *Cancer Immunol Immunother* **36**: 18-24

Curnow A, McIlroy BW, Postle-Hacon MJ, Macrobert AJ, Bown SG (1999) Light dose fractionation to enhance photodynamic therapy using 5-aminolevulinic acid in the normal rat colon. *Photochem Photobiol* **69**: 71-76

de Duve C (1969) The lysosome in retrospect. In *Lysosome in Biology and Pathology*, Dingle JT, Fell HB (eds) pp 3-40. North-Holland: Amsterdam

de Haas ER, de Vijlder HC, Sterenborg HJ, Neumann HA, Robinson DJ (2008) Fractionated aminolevulinic acid-photodynamic therapy provides additional evidence for the use of PDT for non-melanoma skin cancer. *J Eur Acad Dermatol Venereol* **22**: 426-430

del Carmen MG, Rizvi I, Chang Y, Moor AC, Oliva E, Sherwood M, Pogue B, Hasan T (2005) Synergism of epidermal growth factor receptor-targeted immunotherapy with photodynamic treatment of ovarian cancer in vivo. *J Natl Cancer Inst* **97**: 1516-1524

Delius M, Adams G (1999) Shock wave permeabilization with ribosome inactivating proteins: a new approach to tumor therapy. *Cancer Res* **59**: 5227-5232

Dellinger M (1996) Apoptosis or necrosis following Photofrin photosensitization: influence of the incubation protocol. *Photochem Photobiol* **64**: 182-187

Dhami S, Rumbles G, Macrobert AJ, Phillips D (1997) Comparative photophysical study of disulfonated aluminum phthalocyanine in unilamellar vesicles and leukemic K562 cells. *Photochem Photobiol* **65**: 85-90

Dietz GP, Bahr M (2004) Delivery of bioactive molecules into the cell: the Trojan horse approach. *Mol Cell Neurosci* **27**: 85-131

Dietze A, Peng Q, Selbo PK, Kaalhus O, Muller C, Bown S, Berg K (2005) Enhanced photodynamic destruction of a transplantable fibrosarcoma using photochemical internalisation of gelonin. *Br J Cancer* **92**: 2004-2009

Dixon MJ, Bourrθ L, MacRobert AJ, Eggleston IM (2007) Novel prodrug approach to photodynamic therapy: Fmoc solid-phase synthesis of a cell permeable peptide incorporating 5-aminolaevulinic acid. *Bioorganic & Medicinal Chemistry Letters* **17**: 4518-4522

Dolmans DE, Fukumura D, Jain RK (2003) Photodynamic therapy for cancer. *Nat Rev Cancer* **3**: 380-387

Donnelly RF, McCarron PA, Morrow DI, Sibani SpA, Woolfson AD (2008) Photosensitiser delivery for photodynamic therapy. Part 1: Topical carrier platforms. *Expert Opinion on Drug Delivery* **5**: 757-766

Dougherty TJ, Grindey GB, Fiel R, Weishaupt KR, Boyle DG (1975) Photoradiation Therapy .2. Cure of Animal Tumors with Hematoporphyrin and Light. *Journal of the National Cancer Institute* **55**: 115-121

Du H, Fuh RCA, Li JZ, Corkan LA, Lindsey JS (1998) PhotochemCAD: A computer-aided design and research tool in photochemistry. *Photochemistry and Photobiology* **68**: 141-142

Dykxhoorn DM, Novina CD, Sharp PA (2003) Killing the messenger: short RNAs that silence gene expression. *Nat Rev Mol Cell Biol* **4**: 457-467

Egorov SY, Kamalov VF, Koroteev NI, Krasnovsky AA, Toleutaev BN, Zinukov SV (1989) Rise and Decay Kinetics of Photosensitized Singlet Oxygen Luminescence in Water - Measurements with Nanosecond Time-Correlated Single Photon-Counting Technique. *Chemical Physics Letters* **163**: 421-424

El-Rayes BF, LoRusso PM (2004) Targeting the epidermal growth factor receptor. *Br J Cancer* **91**: 418-424

Elliott G, O'Hare P (1997) Intercellular trafficking and protein delivery by a herpesvirus structural protein. *Cell* **88**: 223-233

Elmquist A, Lindgren M, Bartfai T, Langel U (2001) VE-cadherin-derived cell-penetrating peptide, pVEC, with carrier functions. *Exp Cell Res* **269**: 237-244

Endo Y, Mitsui K, Motizuki M, Tsurugi K (1987) The mechanism of action of ricin and related toxic lectins on eukaryotic ribosomes. The site and the characteristics of the modification in 28 S ribosomal RNA caused by the toxins. *J Biol Chem* **262**: 5908-5912

Evans HH, Horng MF, Ricanati M, Deahl JT, Oleinick NL (1997) Mutagenicity of photodynamic therapy as compared to UVC and ionizing radiation in human and murine lymphoblast cell lines. *Photochem Photobiol* **66**: 690-696

Fantini F, Greco A, Cesinaro AM, Surrenti T, Peris K, Vaschieri C, Marconi A, Giannetti A, Pincelli C (2008) Pathologic changes after photodynamic therapy for Basal cell carcinoma and Bowen disease: a histologic and immunohistochemical investigation. *Arch Dermatol* **144**: 186-194

Figge FH, Weiland GS, Manganiello LO (1948) Cancer detection and therapy; affinity of neoplastic, embryonic, and traumatized tissues for porphyrins and metalloporphyrins. *Proc Soc Exp Biol Med* **68**: 640

Fingar VH (1996) Vascular effects of photodynamic therapy. *J Clin Laser Med Surg* **14**: 323-328

Fingar VH, Wieman TJ, Wiehle SA, Cerrito PB (1992) The role of microvascular damage in photodynamic therapy: the effect of treatment on vessel constriction, permeability, and leukocyte adhesion. *Cancer Res* **52**: 4914-4921

Finsen NR (1901) *Phototherapy*. Edward Arnold: London

Fisher AM, Ferrario A, Rucker N, Zhang S, Gomer CJ (1999) Photodynamic therapy sensitivity is not altered in human tumor cells after abrogation of p53 function. *Cancer Res* **59**: 331-335

Fittipaldi A, Ferrari A, Zoppe M, Arcangeli C, Pellegrini V, Beltram F, Giacca M (2003) Cell membrane lipid rafts mediate caveolar endocytosis of HIV-1 Tat fusion proteins. *J Biol Chem* **278**: 34141-34149

Folini M, Berg K, Millo E, Villa R, Prasmickaite L, Daidone MG, Benatti U, Zaffaroni N (2003) Photochemical internalization of a peptide nucleic acid targeting the catalytic subunit of human telomerase. *Cancer Res* **63**: 3490-3494

Foster TH, Murant RS, Bryant RG, Knox RS, Gibson SL, Hilf R (1991) Oxygen consumption and diffusion effects in photodynamic therapy. *Radiat Res* **126**: 296-303

Frank J, Lambert C, Biesalski HK, Thews O, Vaupel P, Kelleher DK (2003) Intensified oxidative and nitrosative stress following combined ALA-based photodynamic therapy and local hyperthermia in rat tumors. *Int J Cancer* **107**: 941-948

Frankel AD, Pabo CO (1988) Cellular uptake of the tat protein from human immunodeficiency virus. *Cell* **55**: 1189-1193

Friberg EG, Cunderlikova B, Pettersen EO, Moan J (2003) pH effects on the cellular uptake of four photosensitizing drugs evaluated for use in photodynamic therapy of cancer. *Cancer Lett* **195**: 73-80

Futaki S, Suzuki T, Ohashi W, Yagami T, Tanaka S, Ueda K, Sugiura Y (2001) Arginine-rich peptides. An abundant source of membrane-permeable peptides having potential as carriers for intracellular protein delivery. *J Biol Chem* **276**: 5836-5840

Gerweck LE, Seetharaman K (1996) Cellular pH gradient in tumor versus normal tissue: potential exploitation for the treatment of cancer. *Cancer Res* **56**: 1194-1198

Geze M, Morliere P, Maziere JC, Smith KM, Santus R (1993) Lysosomes, A Key Target of Hydrophobic Photosensitizers Proposed for Photochemotherapeutic Applications. *Journal of Photochemistry and Photobiology B-Biology* **20**: 23-35

Gibson SL, van der Meid KR, Murant RS, Hilf R (1990a) Increased efficacy of photodynamic therapy of R3230AC mammary adenocarcinoma by intratumoral injection of Photofrin II. *Br J Cancer* **61**: 553-557

Gibson SL, VanDerMeid KR, Murant RS, Raubertas RF, Hilf R (1990b) Effects of various photoradiation regimens on the antitumor efficacy of photodynamic therapy for R3230AC mammary carcinomas. *Cancer Res* **50**: 7236-7241

Gius DR, Ezhevsky SA, Becker-Hapak M, Nagahara H, Wei MC, Dowdy SF (1999) Transduced p16INK4a Peptides Inhibit Hypophosphorylation of the Retinoblastoma Protein and Cell Cycle Progression Prior to Activation of Cdk2 Complexes in Late G1. *Cancer Res* **59**: 2577-2580

Glanzmann T, Forrer M, Blant SA, Woodtli A, Grosjean P, Braichotte D, van den BH, Monnier P, Wagnieres G (2000) Pharmacokinetics and pharmacodynamics of tetra(m-hydroxyphenyl)chlorin in the hamster cheek pouch tumor model: comparison with clinical measurements. *J Photochem Photobiol B* **57**: 22-32

Goetz M, Kiesslich R, Dienes HP, Drebber U, Murr E, Hoffman A, Kanzler S, Galle PR, Delaney P, Neurath MF (2008a) In vivo confocal laser endomicroscopy of the human liver: a novel method for assessing liver microarchitecture in real time. *Endoscopy* **40**: 554-562

Goetz M, Vieth M, Kanzler S, Galle PR, Delaney P, Neurath MF, Kiesslich R (2008b) In vivo confocal laser laparoscopy allows real time subsurface microscopy in animal models of liver disease. *J Hepatol* **48**: 91-97

Golab J, Wilczynski G, Zagozdzon R, Stoklosa T, Dabrowska A, Rybczynska J, Wasik M, Machaj E, Olda T, Kozar K, Kaminski R, Giermasz A, Czajka A, Lasek W, Feleszko W, Jakobisiak M (2000) Potentiation of the anti-tumour effects of Photofrin-based photodynamic therapy by localized treatment with G-CSF. *Br J Cancer* **82**: 1485-1491

Gollnick SO, Evans SS, Baumann H, Owczarczak B, Maier P, Vaughan L, Wang WC, Unger E, Henderson BW (2003) Role of cytokines in photodynamic therapy-induced local and systemic inflammation. *Br J Cancer* **88**: 1772-1779

Gollnick SO, Vaughan L, Henderson BW (2002) Generation of effective antitumor vaccines using photodynamic therapy. *Cancer Res* **62**: 1604-1608

Gomer CJ (1991) Preclinical examination of first and second generation photosensitizers used in photodynamic therapy. *Photochem Photobiol* **54**: 1093-1107

Gorman AM, McGowan A, ONeill C, Cotter T (1996) Oxidative stress and apoptosis in neurodegeneration. *Journal of the Neurological Sciences* **139**: 45-52

Gottesman MM, Fojo T, Bates SE (2002) Multidrug resistance in cancer: role of ATP-dependent transporters. *Nat Rev Cancer* **2**: 48-58

Granville DJ, Carthy CM, Jiang H, Shore GC, McManus BM, Hunt DW (1998) Rapid cytochrome c release, activation of caspases 3, 6, 7 and 8 followed by Bap31 cleavage in HeLa cells treated with photodynamic therapy. *FEBS Lett* **437**: 5-10

Granville DJ, Shaw JR, Leong S, Carthy CM, Margaron P, Hunt DW, McManus BM (1999) Release of cytochrome c, Bax migration, Bid cleavage, and activation of caspases 2, 3, 6, 7, 8, and 9 during endothelial cell apoptosis. *Am J Pathol* **155**: 1021-1025

Greber UF, Willetts M, Webster P, Helenius A (1993) Stepwise dismantling of adenovirus 2 during entry into cells. *Cell* **75**: 477-486

Green DR, Reed JC (1998) Mitochondria and apoptosis. *Science* **281**: 1309-1312

Green M, Loewenstein PM (1988) Autonomous functional domains of chemically synthesized human immunodeficiency virus tat trans-activator protein. *Cell* **55**: 1179-1188

Guchelaar HJ, Vermes A, Vermes I, Haanen C (1997) Apoptosis: molecular mechanisms and implications for cancer chemotherapy (vol 19, pg 119, 1997). *Pharmacy World & Science* **19**: 253

Hamblin MR, Newman EL (1994) Photosensitizer targeting in photodynamic therapy I. Conjugates of haematoporphyrin with albumin and transferrin. *Journal of Photochemistry and Photobiology B: Biology* **26**: 45-56

Hansen J, Qing K, Kwon HJ, Mah C, Srivastava A (2000) Impaired intracellular trafficking of adeno-associated virus type 2 vectors limits efficient transduction of murine fibroblasts. *J Virol* **74**: 992-996

He C, Agharkar P, Chen B (2008) Intravital microscopic analysis of vascular perfusion and macromolecule extravasation after photodynamic vascular targeting therapy. *Pharm Res* **25**: 1873-1880

He J, Agarwal ML, Larkin HE, Friedman LR, Xue LY, Oleinick NL (1996) The induction of partial resistance to photodynamic therapy by the protooncogene BCL-2. *Photochem Photobiol* **64**: 845-852

Hecht SM (2000) Bleomycin: new perspectives on the mechanism of action. *J Nat Prod* **63**: 158-168

Henderson BW, Fingar VH (1987) Relationship of tumor hypoxia and response to photodynamic treatment in an experimental mouse tumor. *Cancer Res* **47**: 3110-3114

Henderson BW, Waldow SM, Potter WR, Dougherty TJ (1985) Interaction of photodynamic therapy and hyperthermia: tumor response and cell survival studies after treatment of mice in vivo. *Cancer Res* **45**: 6071-6077

Hogset A, Engesaeter BO, Prasmickaite L, Berg K, Fodstad O, Maelandsmo GM (2002) Light-induced adenovirus gene transfer, an efficient and specific gene delivery technology for cancer gene therapy. *Cancer Gene Ther* **9**: 365-371

Hogset A, Prasmickaite L, Selbo PK, Hellum M, Engesaeter BO, Bonsted A, Berg K (2004) Photochemical internalisation in drug and gene delivery. *Adv Drug Deliv Rev* **56**: 95-115

Hogset A, Prasmickaite L, Tjelle TE, Berg K (2000) Photochemical transfection: a new technology for light-induced, site-directed gene delivery. *Hum Gene Ther* **11**: 869-880

Hope MJ, Nayar R, Mayer LD, Cullis PR (1992) Reduction of liposome size and preparation of unilamellar vesicles by extrusion techniques. In *Liposome Technology*, Gregoriadis G (ed) pp 123-139. CRC Press: Boca Raton, FL

Hopper C (2000) Photodynamic therapy: a clinical reality in the treatment of cancer. *Lancet Oncol* **1**: 212-219

Huang Z, Xu H, Meyers AD, Musani AI, Wang L, Tagg R, Barqawi AB, Chen YK (2008) Photodynamic therapy for treatment of solid tumors--potential and technical challenges. *Technol Cancer Res Treat* **7**: 309-320

Hurlstone DP, Baraza W, Brown S, Thomson M, Tiffin N, Cross SS (2008) In vivo real-time confocal laser scanning endomicroscopic colonoscopy for the detection and characterization of colorectal neoplasia. *Br J Surg* **95**: 636-645

Iyer AK, Khaled G, Fang J, Maeda H (2006) Exploiting the enhanced permeability and retention effect for tumor targeting. *Drug Discovery Today* **11**: 812-818

Jager HR, Taylor MN, Theodossy T, Hopper C (2005) MR imaging-guided interstitial photodynamic laser therapy for advanced head and neck tumors. *AJNR Am J Neuroradiol* **26**: 1193-1200

Jalili A, Makowski M, Switaj T, Nowis D, Wilczynski GM, Wilczek E, Chorazy-Massalska M, Radzikowska A, Maslinski W, Bialy L, Sienko J, Sieron A, Adamek M, Basak G, Mroz P, Krasnodebski IW, Jakobisiak M, Golab J (2004) Effective photoimmunotherapy of murine colon carcinoma induced by the combination of photodynamic therapy and dendritic cells. *Clin Cancer Res* **10**: 4498-4508

Jarvi MT, Niedre MJ, Patterson MS, Wilson BC (2006) Singlet oxygen luminescence dosimetry (SOLD) for photodynamic therapy: current status, challenges and future prospects. *Photochem Photobiol* **82**: 1198-1210

Johannes L, Decaudin D (2005) Protein toxins: intracellular trafficking for targeted therapy. *Gene Ther* **12**: 1360-1368

Johansson A, Svensson J, Bendsoe N, Svanberg K, Alexandratou E, Kyriazi M, Yova D, Grafe S, Trebst T, ndersson-Engels S (2007) Fluorescence and absorption assessment of a lipid mTHPC formulation following topical application in a non-melanotic skin tumor model. *Journal of Biomedical Optics* **12**:

Joliot A, Pernelle C, agostini-Bazin H, Prochiantz A (1991) Antennapedia homeobox peptide regulates neural morphogenesis. *Proc Natl Acad Sci U S A* **88**: 1864-1868

Jones HJ, Vernon DI, Brown SB (2003) Photodynamic therapy effect of m-THPC (Foscan) in vivo: correlation with pharmacokinetics. *Br J Cancer* **89**: 398-404

Jori G (1996) Tumour photosensitizers: approaches to enhance the selectivity and efficiency of photodynamic therapy. *J Photochem Photobiol B* **36**: 87-93

Jori G, Reddi E (1993) The role of lipoproteins in the delivery of tumour-targeting photosensitizers. *Int J Biochem* **25**: 1369-1375

Juliano RL, striab-Fisher A, Falke D (2001) Macromolecular therapeutics: emerging strategies for drug discovery in the postgenome era. *Mol Interv* **1**: 40-53

Juzenas P, Moan J (2006) Singlet oxygen in photosensitization. *Journal of Environmental Pathology Toxicology and Oncology* **25**: 29-50

Juzeniene A, Peng Q, Moan J (2007) Milestones in the development of photodynamic therapy and fluorescence diagnosis. *Photochem Photobiol Sci* **6**: 1234-1245

Kascakova S, Kruijt B, de Bruijn HS, van der Ploeg-van den Heuvel, Robinson DJ, Sterenborg HJ, Amelink A (2008) Ex vivo quantification of mTHPC concentration in tissue: influence of chemical extraction on the optical properties. *J Photochem Photobiol B* **91**: 99-107

Kelbauskas L, Dietel W (2002) Internalization of aggregated photosensitizers by tumor cells: subcellular time-resolved fluorescence spectroscopy on derivatives of pyropheophorbide-a ethers and chlorin e6 under femtosecond one- and two-photon excitations. *Photochem Photobiol* **76**: 686-694

Kelly JF, Snell ME (1976) Hematoporphyrin Derivative - Possible Aid in Diagnosis and Therapy of Carcinoma of Bladder. *Journal of Urology* **115**: 150-151

Kelly JF, Snell ME, Berenbaum MC (1975) Photodynamic Destruction of Human Bladder Carcinoma. *British Journal of Cancer* **31**: 237-244

Kerr JF, Wyllie AH, Currie AR (1972) Apoptosis: a basic biological phenomenon with wide-ranging implications in tissue kinetics. *Br J Cancer* **26**: 239-257

Kessel D (1981) Transport and binding of hematoporphyrin derivative and related porphyrins by murine leukemia L1210 cells. *Cancer Res* **41**: 1318-1323

Kessel D (1986) Porphyrin-lipoprotein association as a factor in porphyrin localization. *Cancer Lett* **33**: 183-188

Kessel D, Luo Y (1998) Mitochondrial photodamage and PDT-induced apoptosis. *Journal of Photochemistry and Photobiology B-Biology* **42**: 89-95

Kessel D, Luo Y (1999) Photodynamic therapy: a mitochondrial inducer of apoptosis. *Cell Death Differ* **6**: 28-35

Kessel D, Luo Y, Deng YQ, Chang CK (1997) The role of subcellular localization in initiation of apoptosis by photodynamic therapy. *Photochemistry and Photobiology* **65**: 422-426

Kessel D, Reiners JJ, Jr. (2007) Apoptosis and autophagy after mitochondrial or endoplasmic reticulum photodamage. *Photochem Photobiol* **83**: 1024-1028

Kessel D, Rossi E (1982) Determinants of Porphyrin-Sensitized Photo-Oxidation Characterized by Fluorescence and Absorption-Spectra. *Photochemistry and Photobiology* **35**: 37-41

Kessel D, Vicente MG, Reiners JJ, Jr. (2006) Initiation of apoptosis and autophagy by photodynamic therapy. *Autophagy* **2**: 289-290

Kessel D, Whitcomb KL, Schulz V (1992) Lipoprotein-mediated distribution of N-aspartyl chlorin-E6 in the mouse. *Photochem Photobiol* **56**: 51-56

Kessel D, Woodburn K (1993) Biodistribution of photosensitizing agents. *Int J Biochem* **25**: 1377-1383

Khanna C, Hunter K (2005) Modeling metastasis in vivo. *Carcinogenesis* **26**: 513-523

Kim HR, Luo Y, Li G, Kessel D (1999) Enhanced apoptotic response to photodynamic therapy after bcl-2 transfection. *Cancer Res* **59**: 3429-3432

Kirveliene V, Grazeliene G, Dabkeviciene D, Micke I, Kirvelis D, Juodka B, Didziapetriene J (2006) Schedule-dependent interaction between Doxorubicin and mTHPC-mediated photodynamic therapy in murine hepatoma in vitro and in vivo. *Cancer Chemother Pharmacol* **57**: 65-72

Kongshaug M (1992) Distribution of tetrapyrrole photosensitizers among human plasma proteins. *Int J Biochem* **24**: 1239-1265

Koppelhus U, Awasthi SK, Zachar V, Holst HU, Ebbesen P, Nielsen PE (2002) Cell-dependent differential cellular uptake of PNA, peptides, and PNA-peptide conjugates. *Antisense Nucleic Acid Drug Dev* **12**: 51-63

Korbelik M (1996) Induction of tumor immunity by photodynamic therapy. *J Clin Laser Med Surg* **14**: 329-334

Korbelik M, Krosl G, Krosl J, Dougherty GJ (1996) The role of host lymphoid populations in the response of mouse EMT6 tumor to photodynamic therapy. *Cancer Res* **56**: 5647-5652

Korbelik M, Sun J (2006) Photodynamic therapy-generated vaccine for cancer therapy. *Cancer Immunol Immunother* **55**: 900-909

Kramer SD, Wunderli-Allenspach H (2003) No entry for TAT(44-57) into liposomes and intact MDCK cells: novel approach to study membrane permeation of cell-penetrating peptides. *Biochim Biophys Acta* **1609**: 161-169

Kubler A, Haase T, Rheinwald M, Barth T, Muhling J (1998) Treatment of oral leukoplakia by topical application of 5-aminolevulinic acid. *Int J Oral Maxillofac Surg* **27**: 466-469

Kubler AC, Scheer M, Zoller JE (2001) Photodynamic therapy of head and neck cancer. *Onkologie* **24**: 230-237

Kunz L, Connelly JP, Woodhams JH, Macrobert AJ (2007) Photodynamic modification of disulfonated aluminium phthalocyanine fluorescence in a macrophage cell line. *Photochem Photobiol Sci* **6**: 940-948

Kuppuswamy M, Subramanian T, Srinivasan A, Chinnadurai G (1989) Multiple functional domains of Tat, the trans-activator of HIV-1, defined by mutational analysis. *Nucleic Acids Res* **17**: 3551-3561

Kwitniewski M, Juzeniene A, Glosnicka R, Moan J (2008) Immunotherapy: a way to improve the therapeutic outcome of photodynamic therapy? *Photochem Photobiol Sci* **7**: 1011-1017

Lai PS, Pai CL, Peng CL, Shieh MJ, Berg K, Lou PJ (2008) Enhanced cytotoxicity of saporin by polyamidoamine dendrimer conjugation and photochemical internalization. *J Biomed Mater Res A* **87**: 147-155

Lavie G, Kaplinsky C, Toren A, Aizman I, Meruelo D, Mazur Y, Mandel M (1999) A photodynamic pathway to apoptosis and necrosis induced by dimethyl tetrahydroxyhelianthrone and hypericin in leukaemic cells: possible relevance to photodynamic therapy. *Br J Cancer* **79**: 423-432

Lee CC, Pouge BW, Strawbridge RR, Moodie KL, Bartholomew LR, Burke GC, Hoopes PJ (2001) Comparison of photosensitizer (AIPcS2) quantification techniques: in situ fluorescence microsampling versus tissue chemical extraction. *Photochem Photobiol* **74**: 453-460

Lee LK, Whitehurst C, Pantelides ML, Moore JV (1995) In situ comparison of 665 nm and 633 nm wavelength light penetration in the human prostate gland. *Photochem Photobiol* **62**: 882-886

Lipson RL, Baldes EJ, Olsen AM (1961) The use of a derivative of hematoporhyrin in tumor detection. *J Natl Cancer Inst* **26**: 1-11

Lloyd JB (2000) Lysosome membrane permeability: implications for drug delivery. *Advanced Drug Delivery Reviews* **41**: 189-200

Lou PJ, Lai PS, Shieh MJ, Macrobert AJ, Berg K, Bown SG (2006) Reversal of doxorubicin resistance in breast cancer cells by photochemical internalization. *Int J Cancer* **119**: 2692-2698

Lugade AA, Moran JP, Gerber SA, Rose RC, Frelinger JG, Lord EM (2005) Local radiation therapy of B16 melanoma tumors increases the generation of tumor antigen-specific effector cells that traffic to the tumor. *J Immunol* **174**: 7516-7523

Luksiene Z, Kalvelyte A, Supino R (1999) On the combination of photodynamic therapy with ionizing radiation. *J Photochem Photobiol B* **52**: 35-42

Luo Y, Kessel D (1997) Initiation of apoptosis versus necrosis by photodynamic therapy with chloroaluminum phthalocyanine. *Photochemistry and Photobiology* **66**: 479-483

MacDonald IJ, Dougherty TJ (2001) Basic principles of photodynamic therapy. *Journal of Porphyrins and Phthalocyanines* **5**: 105-129

Maiolo JR, Ferrer M, Ottinger EA (2005) Effects of cargo molecules on the cellular uptake of arginine-rich cell-penetrating peptides. *Biochimica et Biophysica Acta (BBA) - Biomembranes* **1712**: 161-172

Margaron P, Gregoire MJ, Scasnar V, Ali H, van Lier JE (1996) Structure-photodynamic activity relationships of a series of 4-substituted zinc phthalocyanines. *Photochem Photobiol* **63**: 217-223

Maziere JC, Morliere P, Santus R (1991) The role of the low density lipoprotein receptor pathway in the delivery of lipophilic photosensitizers in the photodynamic therapy of tumours. *J Photochem Photobiol B* **8**: 351-360

Messmann H, Mlkvy P, Buonaccorsi G, Davies CL, Macrobert AJ, Bown SG (1995) Enhancement of photodynamic therapy with 5-aminolaevulinic acid-induced porphyrin photosensitisation in normal rat colon by threshold and light fractionation studies. *Br J Cancer* **72**: 589-594

Meyer-Betz F (1913) Untersuchung uber die biologische (photodynamische) Wirkung des Hamatoporphyrins und anderer Derivate des Blutund Gallenfarbstoffs. *Dtsch Arch Klin Med* **112**: 476-503

Mlkvy P, Messmann H, Regula J, Conio M, Pauer M, Millson CE, Macrobert AJ, Bown SG (1998) Photodynamic therapy for gastrointestinal tumors using three photosensitizers--ALA induced PPIX, Photofrin and MTHPC. A pilot study. *Neoplasma* **45**: 157-161

Moan J (1986) Porphyrin photosensitization and phototherapy. *Photochem Photobiol* **43**: 681-690

Moan J, Berg K (1991) The Photodegradation of Porphyrins in Cells Can be Used to Estimate the Lifetime of Singlet Oxygen. *Photochemistry and Photobiology* **53**: 549-553

Moan J, Berg K, Anholt H, Madslien K (1994) Sulfonated Aluminum Phthalocyanines As Sensitizers for Photochemotherapy - Effects of Small Light Doses on Localization, Dye Fluorescence and Photosensitivity in V79 Cells. *International Journal of Cancer* **58**: 865-870

Moan J, Berg K, Bommer JC, Western A (1992) Action spectra of phthalocyanines with respect to photosensitization of cells. *Photochem Photobiol* **56**: 171-175

Moan J, Berg K, Kvam E, Western A, Malik Z, Ruck A, Schneckenburger H (1989) Intracellular localization of photosensitizers. *Ciba Found Symp* **146**: 95-107

Moan J (1990) On the diffusion length of singlet oxygen in cells and tissues. *Journal of Photochemistry and Photobiology B: Biology* **6**: 343-344

Mojzisova H, Bonneau S, Maillard P, Berg K, Brault D (2009) Photosensitizing properties of chlorins in solution and in membrane-mimicking systems. *Photochem Photobiol Sci* **8**: 778-787

Montanaro L, Sperti S, Mattioli A, Testoni G, Stirpe F (1975) Inhibition by ricin of protein synthesis in vitro. Inhibition of the binding of elongation factor 2 and of

adenosine diphosphate-ribosylated elongation factor 2 to ribosomes. *Biochem J* **146**: 127-131

Montanaro L, Sperti S, Stirpe F (1973) Inhibition by ricin of protein synthesis in vitro. Ribosomes as the target of the toxin. *Biochem J* **136**: 677-683

Moor AC (2000) Signaling pathways in cell death and survival after photodynamic therapy. *J Photochem Photobiol B* **57**: 1-13

Moser J.G. (1998) *Photodynamic tumor therapy: 2nd and 3rd generation photosensitizers*. Harwood Academic Publishers: New Delhi

Mourant JR, Johnson TM, Los G, Bigio LJ (1999) Non-invasive measurement of chemotherapy drug concentrations in tissue: preliminary demonstrations of in vivo measurements. *Physics in Medicine and Biology* **44**: 1397-1417

Murphy P, Alexander P, Kirkham N, Fleming J, Taylor I (1986) Pattern of spread of bloodborne tumour. *Br J Surg* **73**: 829-834

Nahabedian MY, Cohen RA, Contino MF, Terem TM, Wright WH, Berns MW, Wile AG (1988) Combination cytotoxic chemotherapy with cisplatin or doxorubicin and photodynamic therapy in murine tumors. *J Natl Cancer Inst* **80**: 739-743

Narayanan S, Surendranath K, Bora N, Surolia A, Karande AA (2005) Ribosome inactivating proteins and apoptosis. *FEBS Lett* **579**: 1324-1331

Niedre M, Patterson MS, Wilson BC (2002) Direct near-infrared luminescence detection of singlet oxygen generated by photodynamic therapy in cells in vitro and tissues in vivo. *Photochemistry and Photobiology* **75**: 382-391

Niedre MJ, Patterson MS, Giles A, Wilson BC (2005) Imaging of photodynamically generated singlet oxygen luminescence in vivo. *Photochem Photobiol* **81**: 941-943

Niesner U, Halin C, Lozzi L, Gunthert M, Neri P, Wunderli-Allenspach H, Zardi L, Neri D (2002) Quantitation of the tumor-targeting properties of antibody fragments conjugated to cell-permeating HIV-1 TAT peptides. *Bioconjugate Chemistry* **13**: 729-736

Nishiyama N, Iriyama A, Jang WD, Miyata K, Itaka K, Inoue Y, Takahashi H, Yanagi Y, Tamaki Y, Koyama H, Kataoka K (2005) Light-induced gene transfer from packaged DNA enveloped in a dendrimeric photosensitizer. *Nat Mater* **4**: 934-941

Noodt BB, Berg K, Stokke T, Peng Q, Nesland JM (1999) Different apoptotic pathways are induced from various intracellular sites by tetraphenylporphyrins and light. *Br J Cancer* **79**: 72-81

Norata G, Canti G, Ricci L, Nicolin A, Trezzi E, Catapano AL (1984) In vivo assimilation of low density lipoproteins by a fibrosarcoma tumour line in mice. *Cancer Lett* **25**: 203-208

Norum OJ, Gaustad JV, ngell-Petersen E, Rofstad EK, Peng Q, Giercksky KE, Berg K (2009a) Photochemical internalization of bleomycin is superior to photodynamic therapy due to the therapeutic effect in the tumor periphery. *Photochem Photobiol* **85**: 740-749

Norum OJ, Giercksky KE, Berg K (2009b) Photochemical internalization as an adjunct to marginal surgery in a human sarcoma model. *Photochem Photobiol Sci* **8**: 758-762

Norum OJ, Selbo PK, Weyergang A, Giercksky KE, Berg K (2009c) Photochemical internalization (PCI) in cancer therapy: From bench towards bedside medicine. *J Photochem Photobiol B*

Nowis D, Makowski M, Stoklosa T, Legat M, Issat T, Golab J (2005) Direct tumor damage mechanisms of photodynamic therapy. *Acta Biochim Pol* **52**: 339-352

Oenbrink G, Jurgenlimke P, Gabel D (1988) Accumulation of porphyrins in cells: influence of hydrophobicity aggregation and protein binding. *Photochem Photobiol* **48**: 451-456

Oleinick NL, Evans HH (1998) The photobiology of photodynamic therapy: Cellular targets and mechanisms. *Radiation Research* **150**: S146-S156

Oleinick NL, Morris RL, Belichenko I (2002) The role of apoptosis in response to photodynamic therapy: what, where, why, and how. *Photochem Photobiol Sci* **1**: 1-21

Panjehpour M, Sneed RE, Frazier DL, Barnhill MA, O'Brien SF, Harb W, Overholt BF (1993) Quantification of phthalocyanine concentration in rat tissue using laser-induced fluorescence spectroscopy. *Lasers Surg Med* **13**: 23-30

Pantelides ML, Whitehurst C, Moore JV, King TA, Blacklock NJ (1990) Photodynamic therapy for localised prostatic cancer: light penetration in the human prostate gland. *J Urol* **143**: 398-401

Paquette B, Ali H, Langlois R, van Lier JE (1988) Biological activities of phthalocyanines--VIII. Cellular distribution in V-79 Chinese hamster cells and phototoxicity of selectively sulfonated aluminum phthalocyanines. *Photochem Photobiol* **47**: 215-220

Patterson MS, Madsen SJ, Wilson BC (1990) Experimental tests of the feasibility of singlet oxygen luminescence monitoring in vivo during photodynamic therapy. *J Photochem Photobiol B* **5**: 69-84

Pavlova I, Weber CR, Schwarz RA, Williams M, El-Naggar A, Gillenwater A, Richards-Kortum R (2008) Monte Carlo model to describe depth selective fluorescence spectra of epithelial tissue: applications for diagnosis of oral precancer. *J Biomed Opt* **13**: 064012

Peng Q (1987) [A comparative study between ultrastructural changes of the photodynamic effect of photocarcinorin in killing human liver cancer cells]. *Zhonghua Bing Li Xue Za Zhi* **16**: 292-4, 52

Peng Q, Moan J, Cheng LS (1991) The effect of glucose administration on the uptake of photofrin II in a human tumor xenograft. *Cancer Lett* **58**: 29-35

Peng Q, Moan J, Ma LW, Nesland JM (1995) Uptake, localization, and photodynamic effect of meso-tetra(hydroxyphenyl)porphine and its corresponding chlorin in normal and tumor tissues of mice bearing mammary carcinoma. *Cancer Res* **55**: 2620-2626

Peterson CM, Shiah JG, Sun Y, Kopeckova P, Minko T, Straight RC, Kopecek J (2003) HPMA copolymer delivery of chemotherapy and photodynamic therapy in ovarian cancer. *Adv Exp Med Biol* **519**: 101-123

Poddevin B, Orlowski S, Belehradek J, Jr., Mir LM (1991) Very high cytotoxicity of bleomycin introduced into the cytosol of cells in culture. *Biochem Pharmacol* **42 Suppl**: S67-S75

Pooga M, Hallbrink M, Zorko M, Langel U (1998) Cell penetration by transportan. *FASEB J* **12**: 67-77

Pooga M, Land T, Bartfai T, Langel U (2001) PNA oligomers as tools for specific modulation of gene expression. *Biomol Eng* **17**: 183-192

Postigo F, Mora M, De Madariaga MA, Nonell S, Sagrista ML (2004) Incorporation of hydrophobic porphyrins into liposomes: characterization and structural requirements. *Int J Pharm* **278**: 239-254

Pottier R, Kennedy JC (1990) The possible role of ionic species in selective biodistribution of photochemotherapeutic agents toward neoplastic tissue. *J Photochem Photobiol B* **8**: 1-16

Prasmickaite L, Hogset A, Berg K (2001) Evaluation of different photosensitizers for use in photochemical gene transfection. *Photochem Photobiol* **73**: 388-395

Prasmickaite L, Hogset A, Selbo PK, Engesaeter BO, Hellum M, Berg K (2002) Photochemical disruption of endocytic vesicles before delivery of drugs: a new strategy for cancer therapy. *Br J Cancer* **86**: 652-657

Prasmickaite L, Hogset A, Tjelle TE, Olsen VM, Berg K (2000) Role of endosomes in gene transfection mediated by photochemical internalisation (PCI). *J Gene Med* **2**: 477-488

Pron G, Mahrour N, Orlowski S, Tounekti O, Poddevin B, Belehradek J, Jr., Mir LM (1999) Internalisation of the bleomycin molecules responsible for bleomycin toxicity: a receptor-mediated endocytosis mechanism. *Biochem Pharmacol* **57**: 45-56

Raab O (1900) Ueber die wirkung fluoreszierender stoffe auf infusorien. *Zeitung Biol* **39**: 524-546

Rajadhyaksha M, Grossman M, Esterowitz D, Webb RH, Anderson RR (1995) In vivo confocal scanning laser microscopy of human skin: melanin provides strong contrast. *J Invest Dermatol* **104**: 946-952

Redmond RW, Gamlin JN (1999) A compilation of singlet oxygen yields from biologically relevant molecules. *Photochem Photobiol* **70**: 391-475

Ricchelli F (1995) Photophysical properties of porphyrins in biological membranes. *Journal of Photochemistry and Photobiology B: Biology* **29**: 109-118

Richard JP, Melikov K, Vives E, Ramos C, Verbeure B, Gait MJ, Chernomordik LV, Lebleu B (2003) Cell-penetrating Peptides. A revaluation of the mechanism of cellular uptake. *J Biol Chem* **278**: 585-590

Robertson JD, Orrenius S (2000) Molecular mechanisms of apoptosis induced by cytotoxic chemicals. *Critical Reviews in Toxicology* **30**: 609-627

Robinson DJ, de Bruijn HS, van d, V, Stringer MR, Brown SB, Star WM (1998) Fluorescence photobleaching of ALA-induced protoporphyrin IX during photodynamic therapy of normal hairless mouse skin: the effect of light dose and irradiance and the resulting biological effect. *Photochem Photobiol* **67**: 140-149

Roby A, Erdogan S, Torchilin VP (2006) Solubilization of poorly soluble PDT agent, meso-tetraphenylporphin, in plain or immunotargeted PEG-PE micelles results in dramatically improved cancer cell killing in vitro. *Eur J Pharm Biopharm* **62**: 235-240

Rovers JP, Saarnak AE, de JM, Sterenborg HJ, Terpstra OT, Grahn MF (2000) Biodistribution and bioactivity of tetra-pegylated meta-tetra(hydroxyphenyl)chlorin compared to native meta-tetra(hydroxyphenyl)chlorin in a rat liver tumor model. *Photochem Photobiol* **71**: 211-217

Rovers JP, Saarnak AE, Molina A, Schuitmaker JJ, Sterenborg HJ, Terpstra OT (1999) Effective treatment of liver metastases with photodynamic therapy, using the second-generation photosensitizer meta-tetra(hydroxyphenyl)chlorin (mTHPC), in a rat model. *Br J Cancer* **81**: 600-608

Ruben S, Perkins A, Purcell R, Joung K, Sia R, Burghoff R, Haseltine WA, Rosen CA (1989) Structural and functional characterization of human immunodeficiency virus tat protein. *J Virol* **63**: 1-8

Sandgren S, Cheng F, Belting M (2002) Nuclear Targeting of Macromolecular Polyanions by an HIV-Tat Derived Peptide. ROLE FOR CELL-SURFACE PROTEOGLYCANS. *J Biol Chem* **277**: 38877-38883

Schneider R, Tirand L, Frochot C, Vanderesse R, Thomas N, Gravier J, Guillemin F, Barberi-Heyob M (2006) Recent improvements in the use of synthetic peptides for a selective photodynamic therapy. *Anticancer Agents Med Chem* **6**: 469-488

Schwartz SK, Absolon K, Vermund H (1955) Some relationships of porphyrins, X-rays and tumours. *Univ Minn Med Bull* **27**: 7-8

Schwarze SR, Ho A, Vocero-Akbani A, Dowdy SF (1999) In Vivo Protein Transduction: Delivery of a Biologically Active Protein into the Mouse. *Science* **285**: 1569-1572

Schwarze SR, Hruska KA, Dowdy SF (2000) Protein transduction: unrestricted delivery into all cells? *Trends in Cell Biology* **10**: 290-295

Sehgal I, Sibrian-Vazquez M, Vicente MG (2008) Photoinduced cytotoxicity and biodistribution of prostate cancer cell-targeted porphyrins. *J Med Chem* **51**: 6014-6020

Selbo PK, Kaalhus O, Sivam G, Berg K (2001a) 5-Aminolevulinic acid-based photochemical internalization of the immunotoxin MOC31-gelonin generates synergistic cytotoxic effects in vitro. *Photochem Photobiol* **74**: 303-310

Selbo PK, Rosenblum MG, Cheung LH, Zhang W, Berg K (2009) Multi-modality therapeutics with potent anti-tumor effects: photochemical internalization enhances delivery of the fusion toxin scFvMEL/rGel. *PLoS One* **4**: e6691

Selbo PK, Sandvig K, Kirveliene V, Berg K (2000a) Release of gelonin from endosomes and lysosomes to cytosol by photochemical internalization. *Biochim Biophys Acta* **1475**: 307-313

Selbo PK, Sivam G, Fodstad O, Sandvig K, Berg K (2000b) Photochemical internalisation increases the cytotoxic effect of the immunotoxin MOC31-gelonin. *Int J Cancer* **87**: 853-859

Selbo PK, Sivam G, Fodstad O, Sandvig K, Berg K (2001b) In vivo documentation of photochemical internalization, a novel approach to site specific cancer therapy. *Int J Cancer* **92**: 761-766

Selbo PK, Weyergang A, Bonsted A, Bown SG, Berg K (2006) Photochemical internalization of therapeutic macromolecular agents: a novel strategy to kill multidrug-resistant cancer cells. *J Pharmacol Exp Ther* **319**: 604-612

Separovic D, He J, Oleinick NL (1997) Ceramide generation in response to photodynamic treatment of L5178Y mouse lymphoma cells. *Cancer Res* **57**: 1717-1721

Separovic D, Mann KJ, Oleinick NL (1998) Association of ceramide accumulation with photodynamic treatment-induced cell death. *Photochem Photobiol* **68**: 101-109

Shiraishi T, Nielsen PE (2006) Photochemically enhanced cellular delivery of cell penetrating peptide-PNA conjugates. *FEBS Lett* **580**: 1451-1456

Sibani SpA, McCarron PA, Woolfson AD, Donnelly RF (2008) Photosensitiser delivery for photodynamic therapy. Part 2: systemic carrier platforms. *Expert Opinion on Drug Delivery* **5**: 1241

Siboni G, Weitman H, Freeman D, Mazur Y, Malik Z, Ehrenberg B (2002) The correlation between hydrophilicity of hypericins and helianthrone: internalization mechanisms, subcellular distribution and photodynamic action in colon carcinoma cells. *Photochem Photobiol Sci* **1**: 483-491

Sibrian-Vazquez M, Jensen TJ, Hammer RP, Vicente MG (2006) Peptide-mediated cell transport of water soluble porphyrin conjugates. *J Med Chem* **49**: 1364-1372

Sibrian-Vazquez M, Jensen TJ, Vicente MG (2008) Synthesis, characterization, and metabolic stability of porphyrin-peptide conjugates bearing bifunctional signaling sequences. *J Med Chem* **51**: 2915-2923

Sibrian-Vazquez M, Ortiz J, Nesterova IV, Fernandez-Lazaro F, Sastre-Santos A, Soper SA, Vicente MG (2007) Synthesis and properties of cell-targeted Zn(II)-phthalocyanine-peptide conjugates. *Bioconjug Chem* **18**: 410-420

Siemann DW, Horsman MR (2009) Vascular targeted therapies in oncology. *Cell Tissue Res* **335**: 241-248

Sikic BI, Rozencweig M, Carter SK (1985) *Bleomycin Chemotherapy*. Academic Press: Orlando FL

Sitnik TM, Hampton JA, Henderson BW (1998) Reduction of tumour oxygenation during and after photodynamic therapy in vivo: effects of fluence rate. *Br J Cancer* **77**: 1386-1394

Spikes JD (1986) Phthalocyanines as photosensitizers in biological systems and for the photodynamic therapy of tumors. *Photochem Photobiol* **43**: 691-699

Star WM, Marijnissen JP, van den Berg-Blok AE, Reinhold HS (1984) Destructive effect of photoradiation on the microcirculation of a rat mammary tumor growing in "sandwich" observation chambers. *Prog Clin Biol Res* **170**: 637-645

Stirpe F (2004) Ribosome-inactivating proteins. *Toxicon* **44**: 371-383

Stirpe F, Bailey S, Miller SP, Bodley JW (1988) Modification of ribosomal RNA by ribosome-inactivating proteins from plants. *Nucleic Acids Res* **16**: 1349-1357

Stirpe F, Battelli MG (2006) Ribosome-inactivating proteins: progress and problems. *Cell Mol Life Sci* **63**: 1850-1866

Tabeie F, Bolouri B, Jalilian AR, Mossaffa N, Rajabi H, Asli EN, Labibi F, Karimian AR, Shirazi B (2003) Dynamic distribution of 67Ga-bleomycin complex and carrier free 67Gallium in normal mice. *Iranian Journal of Pharmacology and Theraperutics* **1**: 24-29

Talmadge JE, Singh RK, Fidler IJ, Raz A (2007) Murine models to evaluate novel and conventional therapeutic strategies for cancer. *Am J Pathol* **170**: 793-804

Tanielian C, Wolff C, Esch M (1996) Singlet oxygen production in water: Aggregation and charge-transfer effects. *Journal of Physical Chemistry* **100**: 6555-6560

Thomas JP, Girotti AW (1989) Glucose administration augments in vivo uptake and phototoxicity of the tumor-localizing fraction of hematoporphyrin derivative. *Photochem Photobiol* **49**: 241-247

Thorpe PE, Brown AN, Bremner JA, Jr., Foxwell BM, Stirpe F (1985) An immunotoxin composed of monoclonal anti-Thy 1.1 antibody and a ribosome-inactivating protein from Saponaria officinalis: potent antitumor effects in vitro and in vivo. *J Natl Cancer Inst* **75**: 151-159

Torchilin VP, Rammohan R, Weissig V, Levchenko TS (2001) TAT peptide on the surface of liposomes affords their efficient intracellular delivery even at low temperature and in the presence of metabolic inhibitors. *Proc Natl Acad Sci U S A* **98**: 8786-8791

Tounekti O, Kenani A, Foray N, Orlowski S, Mir LM (2001) The ratio of single- to double-strand DNA breaks and their absolute values determine cell death pathway. *Br J Cancer* **84**: 1272-1279

Trehin R, Krauss U, Muff R, Meinecke M, Beck-Sickinger AG, Merkle HP (2004) Cellular internalization of human calcitonin derived peptides in MDCK monolayers: a comparative study with Tat(47-57) and penetratin(43-58). *Pharm Res* **21**: 33-42

Trivedi NS, Wang HW, Nieminen AL, Oleinick NL, Izatt JA (2000) Quantitative analysis of Pc 4 localization in mouse lymphoma (LY-R) cells via double-label confocal fluorescence microscopy. *Photochemistry and Photobiology* **71**: 634-639

Tsujimoto Y, Shimizu S (2005) Another way to die: autophagic programmed cell death. *Cell Death Differ* **12 Suppl 2**: 1528-1534

Tsutsui H, Macrobert AJ, Curnow A, Rogowska A, Buonaccorsi G, Kato H, Bown SG (2002) Optimisation of illumination for photodynamic therapy with mTHPC on normal colon and a transplantable tumour in rats. *Lasers Med Sci* **17**: 101-109

Uehara M, Inokuchi T, Ikeda H (2006) Enhanced susceptibility of mouse squamous cell carcinoma to photodynamic therapy combined with low-dose administration of cisplatin. *J Oral Maxillofac Surg* **64**: 390-396

van Dongen GAMS, Visser GW, Vrouenraets MB (2004) Photosensitizer-antibody conjugates for detection and therapy of cancer. *Advanced Drug Delivery Reviews* **56**: 31-52

van Geel IP, Oppelaar H, Oussoren YG, Schuitmaker JJ, Stewart FA (1995) Mechanisms for optimising photodynamic therapy: second-generation photosensitisers in combination with mitomycin C. *Br J Cancer* **72**: 344-350

Vantieghem A, Assefa Z, Vandenabeele P, Declercq W, Courtois S, Vandenheede JR, Merlevede W, de WP, Agostinis P (1998) Hypericin-induced photosensitization of HeLa cells leads to apoptosis or necrosis. Involvement of cytochrome c and procaspase-3 activation in the mechanism of apoptosis. *FEBS Lett* **440**: 19-24

Vendeville A, Rayne F, Bonhoure A, Bettache N, Montcourrier P, Beaumelle B (2004) HIV-1 Tat Enters T Cells Using Coated Pits before Translocating from Acidified Endosomes and Eliciting Biological Responses. *Mol Biol Cell* **15**: 2347-2360

Verheij M, Bartelink H (2000) Radiation-induced apoptosis. *Cell and Tissue Research* **301**: 133-142

Verma IM, Somia N (1997) Gene therapy -- promises, problems and prospects. *Nature* **389**: 239-242

Violini S, Sharma V, Prior JL, Dyszlewski M, Piwnica-Worms D (2002) Evidence for a plasma membrane-mediated permeability barrier to Tat basic domain in well-differentiated epithelial cells: lack of correlation with heparan sulfate. *Biochemistry* **41**: 12652-12661

Vives E (2003) Cellular uptake [correction of utake] of the Tat peptide: an endocytosis mechanism following ionic interactions. *J Mol Recognit* **16**: 265-271

Vives E (2005) Present and future of cell-penetrating peptide mediated delivery systems: "is the Trojan horse too wild to go only to Troy?". *J Control Release* **109**: 77-85

Vives E, Brodin P, Lebleu B (1997a) A truncated HIV-1 Tat protein basic domain rapidly translocates through the plasma membrane and accumulates in the cell nucleus. *J Biol Chem* **272**: 16010-16017

Vives E, Granier C, Prevot P, Lebleu B (1997b) Structure-activity relationship study of the plasma membrane translocating potential of a short peptide from HIV-1 Tat protein. *Letters in Peptide Science* **4**: 429-436

von Tappeiner H, Jesionek A (1903) Therapeutische versuche mit fluoreszierenden stoffen. *Muench Med Wochenschr* **47**: 2042-2044

von Tappeiner, H. and Jodlbauer, A. (1907) Die sensiblilisierende Wirkung fluoreszierender Substanzer Gesammte Untersuchungen uber die photodynamische Erscheinerung. (Report, Voger, F.C., Leipzig.)

Wadia JS, Stan RV, Dowdy SF (2004) Transducible TAT-HA fusogenic peptide enhances escape of TAT-fusion proteins after lipid raft macropinocytosis. *Nat Med* **10**: 310-315

Wagnieres G, Hadjur C, Grosjean P, Braichotte D, Savary JF, Monnier P, van den BH (1998) Clinical evaluation of the cutaneous phototoxicity of 5,10,15,20-tetra(m-hydroxyphenyl)chlorin. *Photochem Photobiol* **68**: 382-387

Weishaupt KR, Gomer CJ, Dougherty TJ (1976) Identification of Singlet Oxygen As Cytotoxic Agent in Photo-Inactivation of A Murine Tumor. *Cancer Res* **36**: 2326-2329

Wender PA, Mitchell DJ, Pattabiraman K, Pelkey ET, Steinman L, Rothbard JB (2000) The design, synthesis, and evaluation of molecules that enable or enhance cellular uptake: peptoid molecular transporters. *Proc Natl Acad Sci U S A* **97**: 13003-13008

Weyergang A, Selbo PK, Berg K (2006) Photochemically stimulated drug delivery increases the cytotoxicity and specificity of EGF-saporin. *J Control Release* **111**: 165-173

Whitacre CM, Feyes DK, Satoh T, Grossmann J, Mulvihill JW, Mukhtar H, Oleinick NL (2000) Photodynamic therapy with the phthalocyanine photosensitizer Pc 4 of SW480 human colon cancer xenografts in athymic mice. *Clin Cancer Res* **6**: 2021-2027

Whitacre CM, Satoh TH, Xue L, Gordon NH, Oleinick NL (2002) Photodynamic therapy of human breast cancer xenografts lacking caspase-3. *Cancer Lett* **179**: 43-49

Wilson BC, Olivo M, Singh G (1997) Subcellular localization of Photofrin(R) and aminolevulinic acid and photodynamic cross-resistance in vitro in radiation-induced fibrosarcoma cells sensitive or resistant to photofrin-mediated photodynamic therapy. *Photochemistry and Photobiology* **65**: 166-176

Woodhams JH, Kunz L, Bown SG, Macrobert AJ (2004) Correlation of real-time haemoglobin oxygen saturation monitoring during photodynamic therapy with microvascular effects and tissue necrosis in normal rat liver. *Br J Cancer* **91**: 788-794

Woodhams, J. H., Lou, P. J., Selbo, P. K., Mosse, C. A., Oukrif, D., Macrobert, A. J., Novelli, M., Peng, Q., Berg, K., and Bown, S. (2010) Intracellular relocalisation by photochemical internalisation enhances the cytotoxic effect of gelonin - quantitative studies in normal rat liver. *Journal of Controlled Release*. (In press)

Woodhams JH, Macrobert AJ, Novelli M, Bown SG (2006) Photodynamic therapy with WST09 (Tookad): quantitative studies in normal colon and transplanted tumours. *Int J Cancer* **118**: 477-482

Xue LY, Chiu SM, Azizuddin K, Joseph S, Oleinick NL (2007) The death of human cancer cells following photodynamic therapy: apoptosis competence is necessary for Bcl-2 protection but not for induction of autophagy. *Photochem Photobiol* **83**: 1016-1023

Xue LY, Chiu SM, Azizuddin K, Joseph S, Oleinick NL (2008) Protection by Bcl-2 against apoptotic but not autophagic cell death after photodynamic therapy. *Autophagy* **4**: 125-127

Yip WL, Weyergang A, Berg K, Tonnesen HH, Selbo PK (2007) Targeted delivery and enhanced cytotoxicity of cetuximab-saporin by photochemical internalization in EGFR-positive cancer cells. *Mol Pharm* **4**: 241-251

Zavodnik IB, Zavodnik LB, Bryszewska MJ (2002) The mechanism of Zn-phthalocyanine photosensitized lysis of human erythrocytes. *J Photochem Photobiol B* **67**: 1-10

Zhang X, Wan L, Pooyan S, Su Y, Gardner CR, Leibowitz MJ, Stein S, Sinko PJ (2004) Quantitative assessment of the cell penetrating properties of RI-Tat-9: evidence for a cell type-specific barrier at the plasma membrane of epithelial cells. *Mol Pharm* **1**: 145-155

Zhu TC, Finlay JC (2008) The role of photodynamic therapy (PDT) physics. *Med Phys* **35**: 3127-3136

Zhuang LH, Wang BH, Sauder DN (2000) Molecular mechanism of ultraviolet-induced keratinocyte apoptosis. *Journal of Interferon and Cytokine Research* **20**: 445-454

Zhuang S, Lynch MC, Kochevar IE (1999) Caspase-8 mediates caspase-3 activation and cytochrome c release during singlet oxygen-induced apoptosis of HL-60 cells. *Exp Cell Res* **250**: 203-212

Zilberstein J, Schreiber S, Bloemers MC, Bendel P, Neeman M, Schechtman E, Kohen F, Scherz A, Salomon Y (2001) Antivascular treatment of solid melanoma tumors with bacteriochlorophyll-serine-based photodynamic therapy. *Photochem Photobiol* **73**: 257-266

Zuluaga MF, Lange N (2008) Combination of photodynamic therapy with anti-cancer agents. *Curr Med Chem* **15**: 1655-1673